

VOLUME 78

JUNE 20, 1974

NUMBER 13

JPCHA x

THE JOURNAL OF

PHYSICAL
CHEMISTRY

PUBLISHED BIWEEKLY BY THE AMERICAN CHEMICAL SOCIETY

THE JOURNAL OF PHYSICAL CHEMISTRY

BRYCE CRAWFORD, Jr., *Editor*

WILMER G. MILLER, *Associate Editor*

ROBERT W. CARR, Jr., **FREDERIC A. VAN-CATLEDGE**, *Assistant Editors*

EDITORIAL BOARD: A. O. ALLEN (1970-1974), C. A. ANGELL (1973-1977), F. C. ANSON (1974-1978), V. A. BLOOMFIELD (1974-1978), J. R. BOLTON (1971-1975), L. M. DORFMAN (1974-1978), M. FIXMAN (1970-1974), H. S. FRANK (1970-1974), R. R. HENTZ (1972-1976), W. J. KAUZMANN (1974-1978), R. L. KAY (1972-1976), D. W. McCLURE (1974-1978), R. M. NOYES (1973-1977), J. A. POPLER (1971-1975), B. S. RABINOVITCH (1971-1975), H. REISS (1970-1974), S. A. RICE (1969-1975), F. S. ROWLAND (1973-1977), R. L. SCOTT (1973-1977), A. SILBERBERG (1971-1975), J. B. STOTHERS (1974-1978), W. A. ZISMAN (1972-1976)

AMERICAN CHEMICAL SOCIETY, 1155 Sixteenth St., N.W., Washington, D. C. 20036

Books and Journals Division

JOHN K CRUM, *Director*

RUTH REYNARD, *Assistant to the Director*

CHARLES R. BERTSCH, *Head, Editorial Processing Department*

D. H. MICHAEL BOWEN, *Head, Journals Department*

BACIL GUILLEY, *Head, Graphics and Production Department*

SELDON W. TERRANT, *Head, Research and Development Department*

©Copyright, 1974, by the American Chemical Society. Published biweekly by the American Chemical Society at 20th and Northampton Sts., Easton, Pa. 18042. Second-class postage paid at Washington, D. C., and at additional mailing offices.

All manuscripts should be sent to *The Journal of Physical Chemistry*, Department of Chemistry, University of Minnesota, Minneapolis, Minn. 55455.

Additions and Corrections are published once yearly in the final issue. See Volume 77, Number 26 for the proper form.

Extensive or unusual alterations in an article after it has been set in type are made at the author's expense, and it is understood that by requesting such alterations the author agrees to defray the cost thereof.

The American Chemical Society and the Editor of *The Journal of Physical Chemistry* assume no responsibility for the statements and opinions advanced by contributors.

Correspondence regarding accepted copy, proofs, and reprints should be directed to Editorial Processing Department, American Chemical Society, 20th and Northampton Sts., Easton, Pa. 18042. Head: **CHARLES R. BERTSCH**. Editorial Assistant: **JOSEPH E. YURVATI**.

Advertising Office: Centcom, Ltd., 50 W. State St., Westport, Conn. 06880.

Business and Subscription Information

Send all new and renewal subscriptions *with payment* to: Office of the Controller, 1155 16th Street, N.W., Washington, D. C. 20036. Subscriptions should be renewed promptly to avoid a break in your series. All correspondence and telephone calls regarding changes of

address, claims for missing issues, subscription service, the status of records, and accounts should be directed to Manager, Membership and Subscription Services, American Chemical Society, P.O. Box 3337, Columbus, Ohio 43210. Telephone (614) 421-7230.

On changes of address, include both old and new addresses with ZIP code numbers, accompanied by mailing label from a recent issue. Allow four weeks for change to become effective.

Claims for missing numbers will not be allowed (1) if loss was due to failure of notice of change in address to be received before the date specified, (2) if received more than sixty days from date of issue plus time normally required for postal delivery of journal and claim, or (3) if the reason for the claim is "issue missing from files."

Subscription rates (1974): members of the American Chemical Society, \$20.00 for 1 year; to nonmembers, \$60.00 for 1 year. Those interested in becoming members should write to the Admissions Department, American Chemical Society, 1155 Sixteenth St., N.W., Washington, D. C. 20036. Postage to Canada and countries in the Pan-American Union, \$5.00; all other countries, \$6.00. Air freight rates available on request. Single copies for current year: \$3.00. Rates for back issues from Volume 56 to date are available from the Special Issues Sales Department, 1155 Sixteenth St., N.W., Washington, D. C. 20036.

Subscriptions to this and the other ACS periodical publications are available on microfilm. Supplementary material not printed in this journal is now available in microfiche form on a current subscription basis. For information on microfilm or microfiche subscriptions, write Special Issues Sales Department at the address above.

THE JOURNAL OF
PHYSICAL CHEMISTRY

Volume 78, Number 13 June 20, 1974

JPCHAx 78(13) 1245-1338 (1974)

ISSN 0022-3654

- Homoallylic Isomerization of 1-Penten-4-yl and the Critical Energy for Methyl + 1,3-Butadiene
..... **W. P. L. Carter and D. C. Tardy*** 1245
- Chemiluminescent Reactions of Disulfur Monoxide
..... **D. H. Stedman,* H. Alvord, and A. Baker-Blocker** 1248
- Chemiluminescent Reactions after Pulse Radiolysis of Aqueous Dye Solutions. Absolute Yields
..... **W. A. Prütz and E. J. Land*** 1251
- Photolysis of Liquid and Solid Ethylene at 184.9 nm
..... **Shun-ichi Hirokami and R. J. Cvetanović*** 1254
- Positron Annihilation in Amino Acids and Proteins **S. Y. Chuang and S. J. Tao*** 1261
- The Rate of the Photochemical Reaction of a Thin Powdered Layer **E. L. Simmons** 1265
- Energetics of Formation of Some Structural Isomers of Gaseous $C_2H_5O^+$ and $C_2H_6N^+$ Ions
..... **B. H. Solka and M. E. Russell*** 1268
- Mechanism of Hydroxyapatite Dissolution. The Synergistic Effects of Solution Fluoride,
Strontium, and Phosphate
..... **Mahendra G. Dedhiya, Fudah Young, and William I. Higuchi*** 1273
- Kinetics of Surface Reactions from Nuclear Magnetic Resonance Relaxation Times
..... **H. A. Resing** 1279
- Volume Change for the Formation of Magnesium Sulfate Ion Pairs at Various Temperatures
..... **Frank J. Millero* and William L. Masterton** 1287 ■
- Electron Paramagnetic Resonance Identification of Molten Salt Produced Superoxide Ions
..... **Pier Giorgio Zambonin** 1294
- Transition State Theory for Vaporization and Condensation
..... **Alan W. Searcy* and Dario Beruto** 1298
- Raman Spectra and Structure of Water from -10 to 90°
..... **James R. Scherer,* Man K. Go, and Saima Kint** 1304 ■
- Nitrogen-14 and Oxygen-17 Hyperfine Interactions in Perturbed Nitroxides
..... **Allan H. Cohen and Brian M. Hoffman*** 1313
- Estimating Microsecond Rotational Correlation Times from Lifetime Broadening of Nitroxide
Electron Spin Resonance Spectra Near the Rigid Limit
..... **Ronald Paul Mason and Jack H. Freed*** 1321
- Comments on the Interpretation of Electron Spin Resonance Spectra of Spin Labels Undergoing
Very Anisotropic Rotational Reorientation
..... **Ronald Paul Mason, Carl F. Polnaszek, and Jack H. Freed*** 1324
- Proton Magnetic Resonance Study of Molecular Interactions in Solutions of Fluoranthene in
Carbon Tetrachloride and Cyclohexane
..... **K. D. Bartle, R. B. Mallion, D. W. Jones,* and C. K. Pickles** 1330

26 2. 2517

COMMUNICATIONS TO THE EDITOR

Singlet-Triplet Separation in Helium	Richard L. Snow* and James L. Bills	1334
Low-Temperature Studies of Photolyses of Transition-Metal Complexes. The Ferricyanide Ion	Martyn C. R. Symons,* Douglas X. West, and James G. Wilkinson	1335
Electron Spin Polarization Effects in a Study of Transient Hydrogen Atoms in Acidic Ices under Electron Irradiation	Hirotsugu Shiraishi, Hajime Kadoi, Yosuke Katsumura, Yoneho Tabata,* and Keichi Oshima	1336
Reaction of the Nitrate Radical with Acetaldehyde and Propylene	E. D. Morris, Jr., and H. Niki*	1337

■ Supplementary material for this paper is available separately, in photocopy or microfiche form. Ordering information is given in the paper.

* In papers with more than one author, the asterisk indicates the name of the author to whom inquiries about the paper should be addressed.

AUTHOR INDEX

Alvord, H., 1248	Higuchi, W. I., 1273	Morris, E. D., Jr., 1337	Simmons, E. L., 1265
	Hirokami, S., 1254		Snow, R. L., 1334
Baker-Blocker, A., 1248	Hoffman, B. M., 1313	Niki, H., 1337	Solka, B. H., 1268
Bartle, K. D., 1330			Stedman, D. H., 1248
Beruto, D., 1298	Jones, D. W., 1330	Oshima, K., 1336	Symons, M. C. R., 1335
Bills, J. L., 1334			
	Kadoi, H., 1336	Pickles, C. K., 1330	Tabata, Y., 1336
Carter, W. P. L., 1245	Katsumura, Y., 1336	Polnaszek, C. F., 1324	Tao, S. J., 1261
Chuang, S. Y., 1261	Kint, S., 1304	Prütz, W. A., 1251	Tardy, D. C., 1245
Cohen, A. H., 1313			
Cvetanović, R. J., 1254	Land, E. J., 1251	Resing, H. A., 1279	West, D. X., 1335
		Russell, M. E., 1268	Wilkinson, J. G., 1335
Dedhiya, M. G., 1273	Mallion, R. B., 1330		
	Mason, R. P., 1321, 1324	Scherer, J. R., 1304	Young, F., 1273
Freed, J. H., 1321, 1324	Masterton, W. L., 1287	Searcy, A. W., 1298	
	Millero, F. J., 1287	Shiraishi, H., 1336	Zambonin, P. G., 1294
Go, M. K., 1304			

THE JOURNAL OF PHYSICAL CHEMISTRY

Registered in U. S. Patent Office © Copyright, 1974, by the American Chemical Society

VOLUME 78, NUMBER 13 JUNE 20, 1974

Homoallylic Isomerization of 1-Penten-4-yl and the Critical Energy for Methyl + 1,3-Butadiene¹

W. P. L. Carter and D. C. Tardy*

Department of Chemistry, University of Iowa, Iowa City, Iowa 52242 (Received December 7, 1973)

The homoallylic radicals, 1-penten-4-yl and 3-methyl-1-buten-4-yl, were generated in the gas phase by adding H to 1,4-pentadiene. Evidence is given that they are in equilibrium even when thermalized at 0°, and that the isomerization critical energy is less than 15 kcal/mol. The decomposition of 3-methyl-1-buten-4-yl to 1,3-butadiene was studied, and a critical energy of 12 ± 1 kcal/mol for the addition of methyl to the 2 position of 1,3-butadiene was obtained. This is around 3 to 4 kcal/mol higher than the usual alkyl radical plus olefin critical energy; the extra energy is explained as being due to the effect of the conjugation stabilization of 1,3-butadiene being destroyed in the activated complex.

Introduction

Vibrationally excited free radicals have been observed to undergo a variety of unimolecular isomerizations and decompositions.²⁻⁶ Among the fastest of the several possible isomerizations is the so-called homoallylic rearrangement, an example of which is the interconversion of 1-penten-4-yl (I) and 3-methyl-1-buten-4-yl (II) shown in Figure 1. Evidence that this reaction proceeds *via* a cyclopropyl form such as III was obtained in liquid-phase studies^{2a} where it was observed that the *cis-trans* isomerization of several homoallylic radicals occurred at rates similar to the skeletal rearrangement. This is supported by recent gas-phase work where it appears that the 2-penten-5-yl radical undergoes a *trans* to *cis* isomerization with a critical energy of approximately 22 kcal/mol,^{2b} much less than the expected 60 kcal/mol³ for *cis-trans* isomerizations of olefins. It would be useful to obtain a quantitative estimate of the critical energy of the skeletal rearrangement so comparisons with the *cis-trans* isomerization critical energy can be made. In addition, calculations suggesting that the skeletal rearrangement occurs with about 17 kcal/mol⁷ critical energy can be tested.

Although no quantitative determination of the skeletal homoallylic rearrangement critical energy has been made, it is possible to estimate its maximum value. Two studies of the chemical activation system generated by the addition of isopropyl radicals to acetylene are useful in this regard.^{4,8} The initially formed 3-methyl-1-buten-1-yl can undergo a 1,4 H shift isomerization to II which in turn isomerizes to I, where I and II have minimum vibrational excitation energies of 41.3 and 39.7 kcal/mol, respectively.

(These energies are calculated using primary and secondary C-H bond dissociation energies of 96.2 and 92.8 kcal/mol, respectively,⁹ a H + olefin addition critical energy of 1.6 kcal/mol,⁹ and the heats of formation given in the API tables.¹⁰) The rate constant for the overall isomerization of 3-methyl-1-buten-1-yl to I at 127° was estimated to be $2 \times 10^8 \text{ sec}^{-1}$,⁴ while for the 1,4 H shift alone a rate constant of $4.1 \times 10^8 \text{ sec}^{-1}$ at 53° was measured.⁸ Clearly, the isomerization of II to I must go with a rate constant faster than about $4 \times 10^8 \text{ sec}^{-1}$ in this system. Using an activated complex model which resembles III and gives a 300°K thermal A factor of $10^{13.3} \text{ sec}^{-1}$ for the II to I isomerization, RRKM¹¹ theory is used to estimate that a minimum rate constant of $4 \times 10^8 \text{ sec}^{-1}$ corresponds to a maximum critical energy of 18.5 kcal/mol for II to I, or 17 kcal/mol for I to II. The results of the study of the H + 1,4-pentadiene system reported here indicate that this maximum can be reduced to 14-15 kcal/mol.

Additional information obtained from the H + 1,4-pentadiene system is the rate constant for the decomposition of II to 1,3-butadiene. From that rate constant, RRKM theory¹¹ can be used to obtain estimates for the critical energy of the reverse reaction, the anti-Markonikov addition of methyl to the 2 position of 1,3-butadiene. In thermal studies of the reaction of methyl + 1,3-butadiene, methyl adds predominately to the 1 position with an activation energy of 4-5 kcal/mol.¹² This is significantly less than the usual 7-9 kcal/mol for radical + olefin,¹² allenic diene,¹³ or alkyne⁴ addition reactions; presumably some of the 10 kcal/mol stabilization of the allylic radical¹² formed is reflected in the activated complex of the methyl

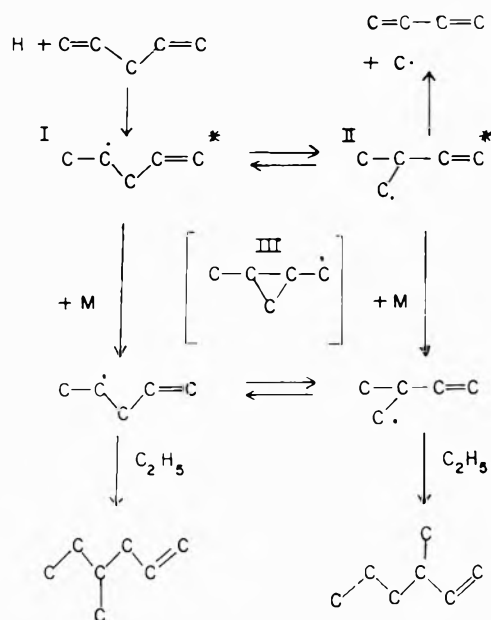


Figure 1. Reaction scheme for $H + 1,4$ -pentadiene. Isomers I and II contain a minimum of 40.4 and 38.8 kcal/mol of vibration excitation, respectively.

+ 1,3-butadiene Markonikov addition reaction. However, if methyl adds to the 2 position, an allylic radical is not formed, so that activated complex should not be stabilized. In addition, we would expect the 3-4 kcal/mol conjugation stabilization of 1,3-butadiene^{14,15} to be at least partially destroyed in the addition complex, causing the critical energy to be higher than the usual radical + olefin values. This is what is observed in this study.

Experimental Section

Hydrogen atoms were generated by Hg (³P₁) photo-sensitized decomposition of hydrogen molecules¹⁶ resulting from irradiation (through a 90-99% opaque filter) by a G8T5 germicidal lamp in a quartz well in a reaction vessel attached to a standard, mercury-saturated, vacuum system with grease-free stopcocks and a Barocel electronic manometer.

Two series of runs were performed. (1) High-pressure runs were done at 100 to 5×10^4 mm (1000 psi above atmospheric) in a 1-l. cylindrical stainless steel vessel. The reaction mixtures consisted of 0.07-0.15 mm of 1,4-pentadiene and 0.13-0.26 mm of ethylene with hydrogen added to obtain the desired pressure. The 1,4-pentadiene-ethylene ratio was held constant at 0.56. Runs were done at room temperatures and also while the reaction vessel was surrounded by melting ice. (2) Reaction mixtures consisting of 0.063-0.24% 1,4-pentadiene, 0.023-0.88% 2-methyl-1-butene in hydrogen were photolyzed in a 20-l. Pyrex vessel at room temperatures. The 1,4-pentadiene-2-methyl-1-butene ratio was held constant at 0.271 ($\pm 2\%$).

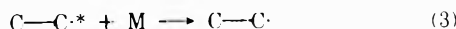
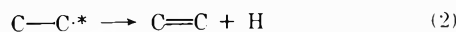
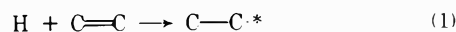
Hydrogen was purified by being passed through a liquid nitrogen cooled silica gel trap before use. 1,4-Pentadiene (Chemical Samples Co., 99%) and 2-methyl-1-butene (Aldrich, 99+%) were purified by preparative vapor phase chromatography (vpc). Ethylene (Matheson, CP) was taken from the tank without further purification.

After each run, condensable products were trapped by pumping out the reaction vessel through a liquid nitrogen cooled, glass wool filled trap, and transferred in a similar way to the vpc injection system, and analyzed by vpc

using a flame ionization detector. The C₇ products of the 1,4-pentadiene-ethylene runs were analyzed using a 29-ft squalane column, while the C₂-C₄ products of the 1,4-pentadiene-2-methyl-1-butene runs were analyzed using a 17-ft hexamethylphosphoramide column in series with an ice-cooled 35-ft squalane column.

Results and Discussion

1,4-Pentadiene-Ethylene-Hydrogen Runs. The presence of ethylene in the reaction mixture was to generate ethyl radicals used to trap the stabilized forms of radicals I and II. Ethyl is produced by the reactions



As the rate of reaction 2 is approximately $4 \times 10^7 \text{ sec}^{-1}$,¹⁷ it is not important compared to reaction 3 at the pressures employed here.

1,4-Pentadiene-hydrogen mixtures, upon photolysis, give a number of C₃-C₅ products, but no C₇ products were observed. When ethylene was present in the reaction mixture, two new high boiling products were observed. These were identified as 4-methyl-1-hexene, believed to result from the ethyl trapping of I, and 3-methyl-1-hexene, from the ethyl trapping of II. Identifications were made by comparison of product vpc retention times with those of known samples.

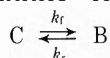
In runs done at room temperatures with pressures ranging from 100 to 5×10^4 mm, the 4-methyl-1-hexene-3-methyl-1-hexene ratio varied from 51.3 to 69.2 in a seemingly random manner with no apparent pressure dependence. Runs done at 0° and 100 mm pressure were more reproducible and gave a significantly different ratio of 81.4.

The fact that the ice-cooled runs gave such a different ratio indicates that the irreproducibility of the room temperature ratios was probably due to the lack of temperature control. These observations are difficult to explain if it is believed that I and II interconvert only when highly vibrationally excited, as in that case the ratio should be much more sensitive to pressure than temperature. The fact that the opposite is true makes sense only if it is assumed that I and II interconvert rapidly even after they are thermalized, and that they are in thermal equilibrium. Indeed, if one assumes that the II to I interconversion is fast and thus has an equilibrium constant of 57 ± 6 at 300°K and of 81 ± 8 at 273°K, it can be calculated¹⁸ that the heat of formation of II is about 2.1 ± 1 kcal/mol higher than that of I, which compares well with the expected value of 1.6 kcal/mol. (The "expected" value is obtained using primary and secondary C-H bond dissociation energies of 96.2 and 92.8 kcal/mol, respectively, and using hydrocarbon heats of formation given in the API tables.¹⁰) Thus it appears that the homoallylic rearrangement is so rapid that I and II are in thermal equilibrium even at 0°.

It is possible to estimate a maximum activation energy from the assumption of equilibrium at 0°. If the thermalized radicals are in equilibrium, they must isomerize faster than they are destroyed by disproportionation-combination reactions with other radicals. The total radical concentration can be estimated from the light intensity. From a rough knowledge of the approximate photolysis times required to obtain 10% reaction with known pressures of reactants in our reaction system, we can estimate that the light input is about 3×10^{-13} einsteins/cc sec.

Assuming a radical + radical bimolecular rate constant of about 10^{13} cc/molecule sec,³ the total radical concentration is about 5×10^{-13} molecule/cc, giving a pseudounimolecular radical destruction rate of 5 sec^{-1} . The estimation is probably only good to an order of magnitude, but the radical destruction rate should not be slower than 1 sec^{-1} . This gives a minimum rate of about 5 sec^{-1} for the thermal isomerization of I to II (the slower of the two). Assuming the thermal *A* factor for the isomerization is about $10^{12.9} \text{ sec}^{-1}$ (calculated from activated complex frequencies appropriate to III, with a C-C stretch taken as the reaction coordinate), this minimum rate constant corresponds to a *maximum* activation energy of 15.4 kcal/mol. This also corresponds to a maximum activation energy of 13.8 kcal/mol for II to I.

As pointed out by one of the referees the isomerization of cyclopropylcarbinyl (C) to butene-4-yl (B) has been reported by Sheldon and Kochi¹⁹ to have a rate constant, k_r , greater than $1 \times 10^8 \text{ sec}^{-1}$ at 25°. Using the appropriate thermochemical quantities²⁰ for



$\Delta S^\circ = 6.6 \text{ eu}$ and $\Delta H^\circ = -5.2 \text{ kcal/mol}$ and estimating $A_f \approx 10^{14.5} \text{ sec}^{-1}$ and thus $E_a(f) \geq 9.0 \text{ kcal/mol}$ $E_a(r)$ is found to be $\geq 14.2 \text{ kcal/mol}$. This activation energy is in agreement with the value reported here for the analogous reaction.

Recently Lee and coworkers²¹ have studied the reaction $F + 1,4\text{-pentadiene}$ *via* molecular beam techniques to obtain information on the energy distribution of unimolecular decompositions. In their studies the excited radicals had approximately 10 kcal/mol more vibrational energy than in our experiments. In their system one would also expect a very rapid homoallylic isomerization so that the initially formed 5-fluoro-1-penten-3-yl would be in equilibrium with 2-fluoromethylpropen-3-yl; the former would decompose to give allylfluoride + vinyl while the latter would competitively decompose at a faster rate to give predominantly 1,3-butadiene + fluoromethyl and allyl fluoride + vinyl. They only reported the presence of mass 85, corresponding to the H atom split off reaction; according to our calculations the process producing 1,3-butadiene should predominate. Their findings are not in agreement with ours, however, it should be pointed out that our work deals primarily with delineating the mechanism and the unimolecular rate constants for each process and is supported with complete product analysis by vpc. The purpose of their work was to obtain energy distributions *assuming* a simple mechanism which included only β scission reactions and ignored the possibilities of other unimolecular reactions such as homoallylic isomerization, H atom migrations, etc. Consequently, it should be pointed out that these radical systems should be understood at the pseudomacroscopic level before microscopic information can be extracted.

1,4-Pentadiene-2-Methyl-1-butene-Hydrogen System. The rate of decomposition of II to 1,3-butadiene was measured using the previously characterized²² decomposition of 2-methylbutyl-2 generated by the $H + 2\text{-methyl-1-butene}$ reaction, as an internal standard. The $C_3\text{-}C_4$ products resulting from the photolysis of 1,4-pentadiene-hydrogen mixtures were primarily propylene (and perhaps propane) and 1,3-butadiene. The 1,3-butadiene was identified using vpc retention times of known samples. The C_3 yield was about 1/5 that of 1,3-butadiene. The only product in the $C_3\text{-}C_4$ range resulting from the photolysis of 2-

methyl-1-butene-hydrogen mixtures was identified as isobutene. Identification was made by comparison of vpc retention times with those of authentic samples. When 1,4-pentadiene-2-methyl-1-butene-hydrogen mixtures were photolyzed, no new products were observed, but the C_3 yield was equal to the 1,3-butadiene yield. The 1,3-butadiene-isobutene ratio was measured to be 0.113 ± 0.006 in the pressure range of 0.915 to 50.0 mm.

From this ratio a rate constant for the decomposition to 1,3-butadiene can be estimated. The rate constant for the decomposition of 2-methylbutyl-2 with hydrogen as the bath gas is $1.75 \times 10^7 (\pm 5\%) \text{ sec}^{-1}$.²² The ratio of 2-methyl-1-butene-1,4-pentadiene in these mixtures was 3.69. Assuming that hydrogen atoms add to the 1 position of 1,4-pentadiene twice as fast as it adds to the 1 position of 2-methyl-1-butene (because 1,4-pentadiene has two double bonds to which the H can add), one obtains the rate constant for the decomposition of I and II to 1,3-butadiene in hydrogen to be $3.6 \times 10^6 (\pm 10\%) \text{ sec}^{-1}$.

The overall rate constant can be calculated using the critical energy for the decomposition; the details of such calculations on systems where only decompositions or collisional stabilizations are important have been given previously.^{22,23} In addition to the energies, vibrational frequency assignments of the reactants and the decomposition and formation activated complexes^{11,22} and energy transfer models for collisional deactivation of the excited radicals in hydrogen^{22,23} are required for calculation of the rate constants. The vibrational frequencies used are listed elsewhere,²⁴ and were obtained using previously described techniques.^{2,6,24,25} Collisional deactivation in hydrogen was assumed to be described by a step ladder model with step size of 400 cm^{-1} (1.144 kcal/mol).²³

Because radicals I and II interconvert so rapidly, they could be treated as a single species for the purpose of the calculation. At each energy level, the density of vibrational states used in the RRKM calculation¹¹ was then the density of I plus the density of II at that energy.

The calculated overall rate constant fits the observed rate constant when a critical energy for the decomposition of II is taken as $34.8 \pm 0.1 \text{ kcal/mol}$. This corresponds to a methyl + 1,3-butadiene anti-Markonikov addition energy of $12.4 \pm 0.1 \text{ kcal/mol}$.

The uncertainties in the critical energies cited above are those which are propagated from the experimental uncertainties. Additional error may be introduced from the calculational procedure, in particular the calculational parameters such as collisional efficiency, structural factors and geometries, vibrational frequency assignments (probably the largest uncertainty), etc. In general all of these parameters would contribute a factor in the *absolute* rate constants between 0.33 and 3. For this particular system the rate constant *increases* by a factor of 5.6 for a 1 kcal/mol *decrease* in the critical energy. Thus the critical energy for decomposition is encompassed by the value $34 \pm 1 \text{ kcal/mol}$ while the anti-Markonikov addition critical energy by the value $12 \pm 1 \text{ kcal/mol}$.

Conclusion

It is determined that the homoallylic skeletal rearrangement is much too fast for it to be studied by usual chemical activation means. Consequently, it has not been possible to use this study to obtain a quantitative estimate of the rate constant for, and thus the critical energy of, the isomerization of the homoallylic radicals 1-penten-4-yl (I) and 3-methyl-1-buten-4-yl (II). However, it has been pos-

sible to use this study to estimate that the critical energy should be less than about 15.4 kcal/mol. This is somewhat less than calculations suggest,⁷ and much less than the estimated 22 kcal/mol^{2b} for cis-trans isomerizations of homoallylic radicals. More work is needed if a more quantitative characterization of this reaction is desired.

The H + 1,4-pentadiene system has been also used to obtain a critical energy of 12 ± 1 kcal/mol for the anti-Markonikov addition of methyl to the 2 position of 1,3-butadiene. This is significantly higher than the usual 7-9 kcal/mol^{4,12,13} for radical + olefin reactions, and contrasts markedly with the 4-5 kcal/mol activation energy for the Markonikov addition of methyl to the 1 position of 1,3-butadiene.¹² In one case, allylic stabilization¹² of the forming radical stabilizes the addition transition state, while in the other, conjugation stabilization¹⁵ previously available in 1,3-butadiene is partially lost to the transition state.

Acknowledgment. Acknowledgment is made to the Research Corporation for a grant which was used for the purchase of equipment and summer support of W. P. L. C. Funds from the University of Iowa Graduate College used at the University Computer Center were greatly appreciated.

References and Notes

- (1) Taken in part from the Ph.D. Thesis of W. P. L. Carter, University of Iowa, 1973.
- (2) (a) L. K. Montgomery, J. W. Matt, and J. K. Webster, *J. Amer. Chem. Soc.*, **89**, 923 (1967); L. K. Montgomery and J. W. Matt, *J. Amer. Chem. Soc.*, **89**, 934 (1967); (b) W. P. L. Carter and D. C. Tardy, manuscript in preparation.
- (3) S. W. Benson and H. E. O'Neal, *Nat. Stand. Ref. Data Ser., Nat. Bur. Stand.*, No. 21 (1970).
- (4) R. R. Getty, J. A. Kerr, and A. F. Trotman-Dickenson, *J. Chem. Soc. A*, 1360 (1967); J. A. Dominguez and A. F. Trotman-Dickenson, *J. Chem. Soc.*, 940 (1962).
- (5) R. Walsh, *Int. J. Chem. Kinet.*, **2**, 71 (1970).
- (6) C. W. Larson, P. T. Chua, and B. S. Rabinovitch, *J. Phys. Chem.*, **76**, 2507 (1972).
- (7) W. J. Heare, *J. Amer. Chem. Soc.*, **95**, 2643 (1973).
- (8) K. W. Watkins and L. A. O'Deen, *J. Phys. Chem.*, **75**, 2265 (1971).
- (9) C. W. Larson and B. S. Rabinovitch, *J. Chem. Phys.*, **50**, 871 (1969).
- (10) F. D. Rossini, "Selected Values of Physical and Thermodynamic Properties of Hydrocarbons and Related Compounds," Carnegie Press, Pittsburgh, Pa., 1953.
- (11) R. A. Marcus and O. K. Rice, *J. Phys. Colloid Chem.*, **55**, 894 (1951); R. A. Marcus, *J. Chem. Phys.*, **20**, 359 (1952).
- (12) R. J. Cvetanovic and R. S. Irwin, *J. Chem. Phys.*, **46**, 1694 (1967).
- (13) R. R. Getty, J. A. Kerr, and A. F. Trotman-Dickenson, *J. Chem. Soc. A*, 979 (1967).
- (14) D. M. Golden and S. W. Benson, *Chem. Rev.*, **69**, 125 (1969).
- (15) J. D. Cox and G. Pilcher, "Thermochemistry of Organic and Organometallic Compounds," Academic Press, London, 1970.
- (16) R. J. Cvetanovic, *Progr. React. Kinet.*, **2**, 39 (1964).
- (17) M. J. Pearson and B. S. Rabinovitch, *J. Chem. Phys.*, **42**, 1624 (1965).
- (18) D. F. Eggers, L. W. Gregory, G. D. Halsey, and B. S. Rabinovitch, "Physical Chemistry," Wiley, New York, N. Y., 1964, p. 313.
- (19) R. A. Sheldon and J. K. Kochi, *J. Amer. Chem. Soc.*, **92**, 4395 (1970).
- (20) (a) D. F. McMillan, D. M. Golden, and S. W. Benson, *Int. J. Chem. Kinet.*, **3**, 359 (1971); (b) S. W. Benson, F. R. Crvickshank, D. M. Golden, G. R. Haugen, H. E. O'Neal, A. S. Rcdgers, R. Shaw, and R. Walsh, *Chem. Rev.*, **69**, 279 (1969); (c) H. E. O'Neal and S. W. Benson, *Int. J. Chem. Kinet.*, **1**, 221 (1969).
- (21) K. Shobatake, J. M. Parson, Y. T. Lee, and S. A. Rice, *J. Chem. Phys.*, **59**, 1416 (1973).
- (22) D. C. Tardy and B. S. Rabinovitch, *J. Chem. Phys.*, **48**, 5194 (1968).
- (23) D. C. Tardy and B. S. Rabinovitch, *J. Chem. Phys.*, **45**, 3720 (1966).
- (24) W. P. L. Carter, Ph.D. Thesis, University of Iowa, Iowa City, Iowa, 1973.
- (25) C. W. Larson, B. S. Rabinovitch, and D. C. Tardy, *J. Chem. Phys.*, **47**, 4570 (1967).

Chemiluminescent Reactions of Disulfur Monoxide¹

D. H. Stedman,* H. Alvord, and A. Baker-Blocker

Chemistry Department and Department of Atmospheric and Oceanic Science, University of Michigan, Ann Arbor, Michigan 48104
(Received December 27, 1973)

Publication costs assisted by The University of Michigan

The gas-phase reactions of S₂O with O, H, N, Ar(³P_{0,2}), Cl, and O₃ were studied using a flow system. No chemiluminescence is reported from O₃; spectra from H, N, Ar* were obtained, but do not help to elucidate the heat of formation of S₂O. The reaction O + S₂O → SO + SO provides a clean flow system source of SO radicals and strong SO₂* chemiluminescence. An estimate of the rate constant is $1.5 \times 10^{-12} \text{ cm}^3 \text{ molecule}^{-1} \text{ sec}^{-1}$ at 298°K.

Introduction

Disulfur monoxide is an unstable gas, whose properties have been reviewed by Murthy, *et al.*^{2a} It condenses to a red solid at low temperature and cannot be reevaporated, the products being a sulfuroxy polymer and SO₂. In the gas phase it is also unstable with respect to a slow, surface-dependent disproportionation to sulfur and SO₂.

The thermodynamic properties of S₂O are uncertain. Blukis and Meyers^{2b} estimate $\Delta H^\circ_f > -34 \text{ kcal mol}^{-1}$

from bond energy considerations, $<2 \text{ kcal mol}^{-1}$ from Schenk's preparation technique,³ and $> -13 \text{ kcal mol}^{-1}$ from a consideration of Dewing and Richardson's work.⁴

This study was prompted by the lack of knowledge of S₂O gas-phase reactions, uncertain thermodynamics, and a suggestion by Clyne, *et al.*⁵ that the reaction O + S₂O → SO + SO would be fast. If so, this would then provide a simple flow system source for the SO radical. Another reason for interest in S₂O stems from the report by Iversen⁶ that it is a biological intermediate in the metabolism

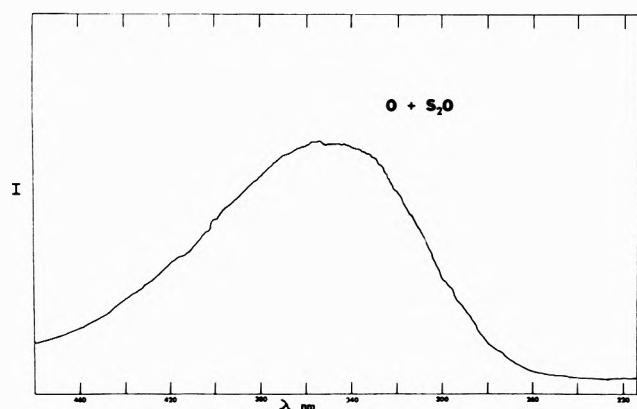


Figure 1. An uncorrected photoelectric scan of the blue afterglow from the reaction $O + S_2O$ at 0.8 Torr in 95% argon.

of a sulfate reducing bacterium *Desulfovibrio desulfuricans*.

Experimental Section

S_2O was prepared by the method of Genz and Schenk^{3b} by passing $SOCl_2$ in N_2 , over CuS at 150° and a pressures of 0.5-1.5 Torr. It was transferred directly into the Pyrex flow system. Other reagents were taken from standard tank gases, dried by passage through 5A molecular sieve traps at liquid N_2 temperature. Oxygen, nitrogen, hydrogen, and chlorine atoms were prepared in the flow system by microwave discharge of the parent gases in 95-99.5% argon carrier. Oxygen atoms were also prepared from N atoms by NO titration.⁵ Excited argon atoms ($^3P_{2,0}$) were produced by the method of Stedman and Setser.⁷ The reagents entered the atom stream just above a 30-mm diameter by 200-mm long cell. This cell was observed end-on by a 1-m Jarrell Ash spectrometer with photoelectric readout, or side-on with a moveable photomultiplier tube and filter assembly.

Results

Chemiluminescent spectra were observed from O, H, N, and Ar^* . Figures 1-3 show the spectra observed from O, H, and N with S_2O . $Cl + S_2O$ gave no apparent light emission, and only the addition of large flows of S_2O showed some reduction of the chlorine afterglow, possibly by enhancing the third-order Cl atom recombination rate. $Ar^* + S_2O$ gave a bright blue flame consisting apparently of many overlapping bands from systems of SO and S_2 between 240 and 500 nm.

The intense blue flame from $O + S_2O$ was visible in the ordinarily lit laboratory and showed a maximum intensity which decreased with increasing S_2O flow. This behavior is similar to $O + NO_2$ so the kinetics of the two systems were compared under otherwise identical conditions, switching directly from a flow of NO_2 to a flow of S_2O . The flow of S_2O was an estimate taken by measuring the flow of N_2 into an $SOCl_2$ saturator, assuming saturation, and 95% yield of S_2O from the CuS reactor.^{3b} The kinetics were determined with the moveable photometer, using a 450 ± 5 nm interference filter for both the S_2O and NO_2 afterglow. The intensity 13 msec downstream from the mixing point at a total pressure of 0.8 Torr is shown in Figure 4 for both S_2O and NO_2 . $O_3 + S_2O$ gave no chemiluminescent emission between 0.5 and 6 Torr.

Although the method of S_2O preparation is reported to have a purity of >98%,^{2a} we tested all systems with the

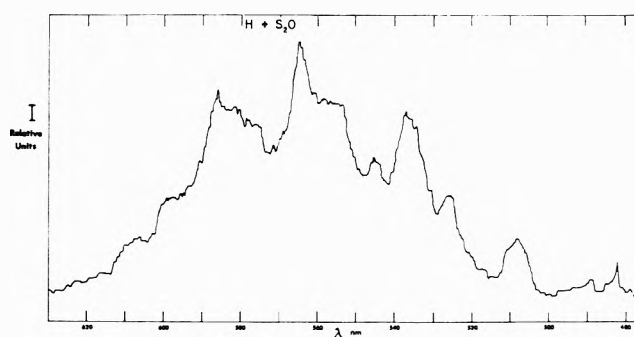


Figure 2. An uncorrected photoelectric scan of the orange afterglow from $H + S_2O$.

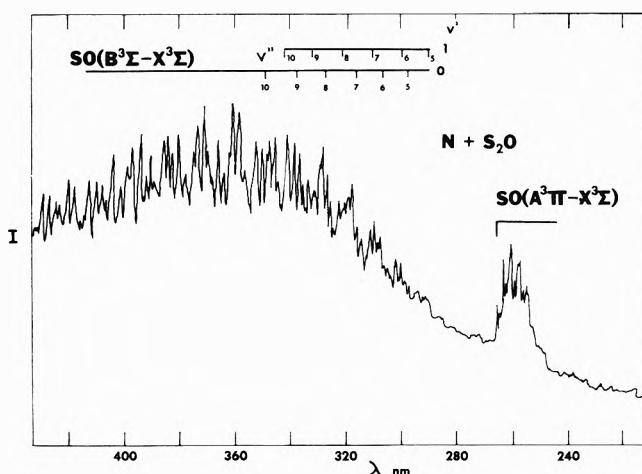


Figure 3. An uncorrected photoelectric scan of the blue afterglow from $N + S_2O$.

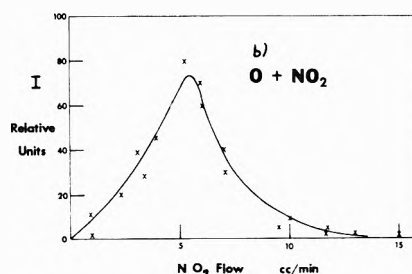
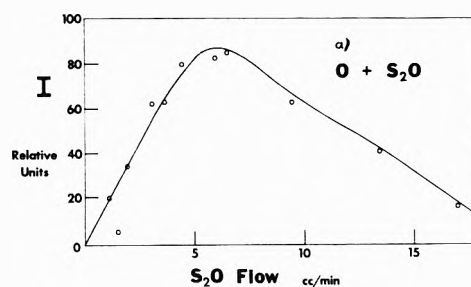


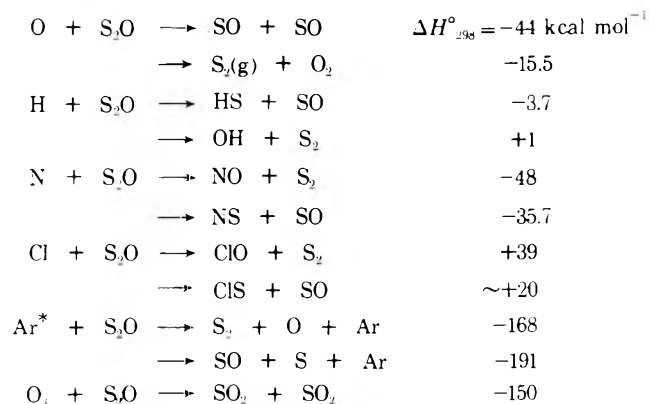
Figure 4. The dependence of light intensity at 450 nm, 13 msec after mixing in a mixture of 5 cc/min of O_2 in 200 cc/min of Ar^* at a reaction pressure of 0.8 Torr: (a) $O + S_2O$; (b) $O + NO_2$.

S_2O conversion oven inactive. Blank spectra were negligible except in the case of the Ar^* system in which the known strong emission from $Ar^* + SOCl_2$ ⁷ was observed. The absence of the uv end of this spectrum with the oven on indicated complete removal of $SOCl_2$. Possible spectral

contamination with the decomposition product SO_2 was also tested with negative results except for the Ar^* case. The $\text{O} + \text{SO}_2$ chemiluminescence being very weak compared to $\text{O} + \text{S}_2\text{O}$.

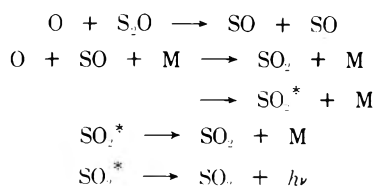
Discussion

Reactions of S_2O which might be expected in this system were



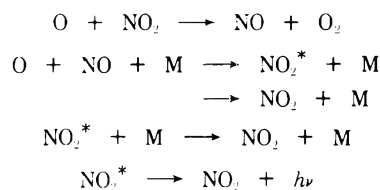
The heats of reaction were obtained assuming $-13 \text{ kcal mol}^{-1}$ for $\Delta H^\circ(\text{S}_2\text{O})$ and using Okabe's⁸ value of $\Delta H^\circ(\text{SO})$ of $+1.3 \text{ kcal mol}^{-1}$. Other values were from the JANAF tables.⁹ As explained these data may be uncertain by $\pm 15 \text{ kcal mol}^{-1}$ due to the uncertainty in S_2O thermodynamics.

The above heats of reaction explain the wealth of bands obtained from $\text{Ar}^* + \text{S}_2\text{O}$, and the apparent lack of reaction with chlorine atoms. They also show that there is insufficient energy release in the primary reactions with O, H, and N to account for the spectra of Figures 1-3. Thus these must result from secondary interactions. The details of these interactions have been studied only in the case of oxygen atoms. The postulated mechanism is



This is verified by three observations. (a) The observed spectrum in Figure 1 is identical with that from the reaction between O and SO. This was confirmed by a study of the SO_2 afterglow in our own system. In the SO_2 afterglow the emission is known to be from $\text{O} + \text{SO}$.⁵ (b) The peaked intensity vs. flow curve in Figure 4 shows that oxygen atoms are both consumed in the primary reaction and needed for the generation of the light emitter. (c) The maximum in the $\text{O} + \text{NO}_2$ curve occurs at a little over 5 cc/min of both NO_2 and S_2O . Since the unit stoichiometry of $\text{O} + \text{NO}_2$ has been confirmed in a number of studies, this observation shows that the reaction $\text{O} + \text{S}_2\text{O}$ also has a 1:1 stoichiometry. If the initial products were $\text{S}_2 + \text{O}_2$, the fast reactions $\text{O} + \text{S}_2 \rightarrow \text{SO} + \text{S}$ and $\text{S} + \text{O}_2 \rightarrow \text{SO} + \text{O}$ would lead to the same apparent reaction scheme.^{10a}

The mechanism of $\text{O} + \text{NO}_2$ chemiluminescence is somewhat different since the light emitter (NO_2) is recycled to NO



In this study we estimated the relative rate constants by measuring the decay along the tube of the intensity maxima shown in Figure 4. Using the above mechanisms and second-order rate constant theory, these data gave an estimate of the ratio of rate constants $k(\text{O} + \text{NO}_2)/k(\text{O} + \text{S}_2\text{O}) = 6.0 \pm 0.5$. Using $k(\text{O} + \text{NO}_2) = 9.1 \times 10^{-12} \text{ cm}^3 \text{ molecules}^{-1} \text{ sec}^{-1}$ this gives $k(\text{O} + \text{S}_2\text{O}) = 1.5 \pm 0.2 \times 10^{-12} \text{ cm}^3 \text{ molecule}^{-1} \text{ sec}^{-1}$.^{10b} Thus the original prediction of Clyne, *et al.*,⁵ is correct, and $\text{O} + \text{S}_2\text{O} \rightarrow 2\text{SO}$ is a fast stoichiometric reaction. It provides a good source of SO radicals in a flow system for further chemical studies.

The intense blue chemiluminescence from $\text{O} + \text{S}_2\text{O}$ may be useable as a detector for atmospheric S_2O , certainly down to parts per million, and probably parts per billion. Since S_2O is a biochemical intermediate,⁶ it may be observable in sulfurous bacterial environments. The relatively weak interference from SO_2 ¹¹ would have to be subtracted by appropriate calibration and a concurrent SO_2 monitor. Other routes to S_2O are electric discharge in SO_2 and heating a mixed sulfide and oxide.^{2a} These processes bear a marked resemblance to the industrial processes of electrostatic precipitation in flue gases and sulfide ore roasting, thus S_2O may be found more widely than one would initially expect.

Figure 2 shows the orange chemiluminescence with hydrogen atoms. The spectrum observed is not recognizable from among those tabulated by Pearse and Gaydon,¹² perhaps it is excited H_2S , similar to the known excited H_2O spectrum. The observation of this spectrum and a reaction at least as fast as the $\text{O} + \text{S}_2\text{O}$ reaction suggests that at least one of the bimolecular reactions $\text{H} + \text{S}_2\text{O}$ is exothermic, thus $\Delta H^\circ(\text{S}_2\text{O})$ must be greater than $-19 \text{ kcal mol}^{-1}$.

Figure 3 shows the blue spectrum observed in active nitrogen. From energy considerations these excited states cannot be formed directly, however, they could be the result of energy transfer from $\text{N}_2(\text{A}^3\Sigma_u^+)$ or higher excited states of N_2 known to be present.

References and Notes

- (1) First presented at the American Chemical Society Meeting, Chicago, Ill., Sept 1973.
- (2) (a) A. R. V. Murthy, T. R. N. Kutty, and D. K. Sharma, *Int. J. Sulfur Chem., B*, **6**, 161 (1971); part B, **6** (2), 161 (1971); (b) U. Blukis and R. J. Meyers, *J. Phys. Chem.*, **69**, 1154 (1965).
- (3) (a) P. W. Schenk, *Z. Anorg. Allg. Chem.*, **229**, 305 (1936); (b) Von W. Genz and P. W. Schenk, *Z. Anorg. Allg. Chem.*, **379**, 300 (1970).
- (4) E. W. Dewing and F. D. Richardson, *Trans. Faraday Soc.*, **54**, 679 (1958).
- (5) M. A. Clyne, C. J. Halstead, and B. A. Thrush, *Proc. Roy. Soc., Ser. A*, **295**, 355 (1966).
- (6) W. P. Iverson, *Science*, **156**, 1112 (1967).
- (7) D. H. Stedman and D. W. Setser, *Progr. React. Kinet.*, **6**, part 4 (1971).
- (8) H. Okabe, *J. Chem. Phys.*, **56**, 3378 (1972).
- (9) "JANAF Thermochemical Tables," D. R. Stull and H. Prophet, Ed., Dow Chemical Co., Midland, Mich., 1971.
- (10) (a) D. D. Davis, R. B. Klemm, and M. Pilling, *Int. J. Chem. Kinet.*, **4**, 367 (1973); (b) D. D. Davis, J. T. Herrold, and R. E. Huie, *J. Chem. Phys.*, **58**, 530 (1973).
- (11) M. F. R. Mulcahy and D. J. Williams, *Chem. Phys. Lett.*, **7**, 455 (1970).
- (12) R. W. B. Pearse and A. G. Gaydon, "The Identification of Molecular Spectra," Chapman and Hall, London, 1965.

Chemiluminescent Reactions after Pulse Radiolysis of Aqueous Dye Solutions. Absolute Yields

W. A. Prütz

Institut für Biophysik und Strahlenbiologie der Universität Freiburg, 7800 Freiburg, Germany

and E. J. Land*

Paterson Laboratories, Christie Hospital and Holt Radium Institute, Manchester M20 9BX, England (Received October 30, 1972; Revised Manuscript Received February 25, 1974)

The number of fluorescence quanta emitted per reaction [dye(oxidized by $\cdot\text{OH}$) + e_{aq}^-], denoted ϕ_{ch} , has been estimated for several dyes. Two standards were used involving high energy irradiation: (A) Cerenkov light induced fluorescence of the dye itself, (B) *p*-terphenyl fluorescence in benzene. Both methods agreed within experimental error and gave mean values of ϕ_{ch} for Acriflavin, Rhodamine B, Fluorescein (at pH 10), and anthranilic acid of 0.011, 0.018, 0.031, and 0.020, respectively.

Introduction

Oxidized intermediates of various dyes, formed after pulse radiolysis of aqueous dye solutions by the action of OH radicals, have been found to yield singlet excitation of these dyes by subsequent reaction with hydrated electrons.¹⁻³ Time dependencies of such chemiluminescences, which build up and decay over tens of microseconds after a single pulse, and the effect of dye concentration and of adding various radical scavengers to the solutions, have been described earlier.^{1,3} Possible chemiluminescent processes were also discussed in these papers. The present article reports determinations of the absolute yields of such emissions.

Experimental Section

Two different methods (A and B) were applied using 0.005-1- μsec pulses of 8-14-MeV electrons from a Vickers accelerator and the pulse radiolysis apparatus of Keene.⁴ Solutions were irradiated at room temperature in a black-quartz cell with Suprasil end windows (0.7-cm electron path and 2.5-cm optical path) and emissions observed at right angles to the electron beam. Commercial dyes were used as before^{1,3} without further purification, the extinction coefficient obtained at the absorption maximum was $\epsilon(452)$ $3.8 \times 10^4 \text{ M}^{-1} \text{ cm}^{-1}$ for Acriflavin (Fluka AG) at pH 7, $\epsilon(554)$ $1.1 \times 10^5 \text{ M}^{-1} \text{ cm}^{-1}$ for Rhodamine B (Merck AG) at pH 7, $\epsilon(491)$ $8.3 \times 10^4 \text{ M}^{-1} \text{ cm}^{-1}$ for Fluorescein (Merck AG) at pH 10, and $\epsilon(310)$ $2.8 \times 10^3 \text{ M}^{-1} \text{ cm}^{-1}$ for anthranilic acid (Merck AG) at pH 7.

Method A. During the electron pulse the dye solutions show a strong prompt emission which is assumed to be due predominantly to excitation of the dye by Cerenkov light. The number of dye molecules thus excited can be calculated from the theoretical yield of Cerenkov light and the geometry of its propagation (see, *e.g.*, ref 5). This fluorescence can be used as a reference for each particular dye for the determination of the chemiluminescence yield. Since these chemiluminescences actually involve the formation of the same singlet excited dye molecules^{1,3} this method avoids any spectroscopic correction.

According to Cerenkov light theory⁵ the number of photons (N) emitted per unit path within the spectral region λ to $\lambda + d\lambda$ is given by

$$d^2N/dx = 2\pi\alpha \sin^2 \theta (d\lambda/\lambda^2)$$

where α ($= 1/137$) is the fine structure constant and θ is the angle of light emission with respect to the electron path, which is connected to the refractive index $n(\lambda)$ and to β , the ratio of the electron velocity to that of light *in vacuo*, via the Cerenkov relation $\cos \theta = 1/n\beta$. The Cerenkov relation in this case ($\beta \approx 1$) ensures total light reflection at the side wall of the cell. Since the cell had black front and end walls, with respect to the electron beam, no Cerenkov light was generated in the entrance window and no light reflection occurred at the end surface. The Cerenkov light produced at any point with distance x from the inner entrance surface of the electron beam will be absorbed only along the light path $(l - x)/\cos \theta$, where l is the cell depth. Integrating the total absorption of light produced along the electron path l by the dye at concentration c we obtain

$$G_A = \phi_f \frac{200\pi\alpha}{(dE/dx)} \int \left(1 + \frac{e^{-r\lambda:2.3cl/\cos\theta} - 1}{\epsilon(\lambda)2.3cl/\cos\theta} \right) \frac{\sin^2 \theta}{\lambda^2} d\lambda$$

where G_A is the number of fluorescence quanta produced by Cerenkov light per 100 eV absorbed in the solution. The literature values used for the fluorescence quantum efficiencies, ϕ_f , which are independent of the excitation wavelength,^{6,7} are given in Table I. $(dE/dx) = 2.0 \times 10^6 \text{ eV/cm}^8$ was used for the mean differential energy loss of the electrons. Dye concentrations of around $5 \times 10^{-5} \text{ M}$ were used for the reference solutions, which ensured similar uniformity of excitation as occurs in the chemiluminescence situation. Calculated values of G_A at a dye concentration of $4 \times 10^{-5} \text{ M}$, for example, were of the order of 5×10^{-3} to 10^{-2} quanta per 100 eV for each dye. Direct excitation of the dye by electron impact can be neglected since it has been found to yield only about 2×10^{-5} quanta/100 eV at 10^{-4} M dye from low-energy X-irradiation experiments.⁹ Absolute chemiluminescence yields G_{ch} , in quanta/100 eV, were obtained using the integrated areas under the emission intensity *vs.* time curves for Cerenkov light induced fluorescence (10^{-5} to 10^{-4} M dye) and those for chemiluminescence (0.05 to $1 \times 10^{-5} \text{ M}$ dye) at a wavelength where no reabsorption takes place. A typical oscilloscope trace of such chemiluminescence is inserted in Figure 2. In the case of Cerenkov light induced

fluorescence the <10% background Cerenkov light at the wavelength of observation was subtracted.

Due to the low yield of Cerenkov light this method is sensitive to any unknown additional excitation process which might occur in the reference solution. The yields might therefore be underestimated to some extent.

Method B. An independent approach to the absolute chemiluminescence quantum yield was made by using 10^{-2} M *p*-terphenyl (T) in benzene (B) as a standard. A singlet excited benzene (mainly excimer) G value of 1.55^{10} was employed (this compares with other recent literature values of 1.45,¹¹ 1.4,¹² and 0.9¹³), and the fraction of energy transferred from benzene to *p*-terphenyl, $f_{TB} = 0.9$, was estimated from the singlet benzene half-life (18.2 nsec)¹⁴ and the singlet energy transfer rate for this system ($4.2 \times 10^{10} M^{-1} \text{sec}^{-1}$).¹⁵ Using the *p*-terphenyl fluorescence in benzene quantum efficiency, $\phi_f(T) = 0.75$,¹⁶ and taking into account both concentration quenching by a factor $q_T = 0.96$ ¹⁷ and the reduction of energy deposition in benzene relative to water by the density ratio $R = 0.88$, we obtain a reference yield of $G_B(T) = G(^1B)f_{TB}\phi_f(T)q_T R = 0.89$. Reabsorption of *p*-terphenyl fluorescence was taken into account by fitting the low concentration spectrum of *p*-terphenyl fluorescence in cyclohexane¹⁸ to the spectrum observed in our experiments. The spectral quantum sensitivity of the optical system was obtained from the photomultiplier response to Cerenkov light from pure water. Excitation of *p*-terphenyl and benzene by Cerenkov light was neglected since it was estimated as in method A to yield less than 10^{-2} quanta/100 eV.

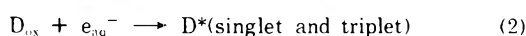
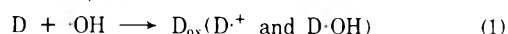
Use of anthracene (A) instead of *p*-terphenyl as reference and corresponding $f_{AB} = 0.9$ (from ref 14), $\phi_f(A) = 0.27$,⁶ and $q_A = 0.8$,¹⁹ i.e., $G_B(A) = 0.27$, revealed a discrepancy in the ratio of the (spectroscopically corrected) intensities: $I(A)/I(T) \approx 0.6G_B(A)/G_B(T)$. This discrepancy, which is not understood is being investigated. The values given in Table I relate to the *p*-terphenyl measurements since *p*-terphenyl was the scintillator used in the absolute determination of $G(^1B)$ by Skarstad, *et al.*¹⁰

The accuracy of method B ultimately depends upon the value of $G(^1B)$ taken. Since the recent literature values¹⁰⁻¹³ vary between 0.9 and 1.55 the yields calculated on basis of $G(^1B) = 1.55^{10}$ could be too high.

Results and Discussion

Concentration and dose dependencies of the total chemiluminescence yield after single pulse electron irradiation of aqueous dye solutions are shown in Figure 1. In Figure 2 are given results for anthranilic acid, which appears to exhibit the same type of chemiluminescence as previously^{1,3} detected with dyes. Absolute chemiluminescence quantum yields, G_{ch} , obtained from methods A and B at a particular dose and dye concentration, are collected in Table I. Individual values were reproducible to within $\pm 30\%$. Since the two sets of results (A and B) are consistent within the experimental error the mean values of G_{ch} given in Table I were used for the estimation of chemiluminescence efficiencies, ϕ_{ch} .

From reactions 1-3, proposed to be involved in these chemiluminescences,^{1,3} we have calculated the



total number of reactions 2 per 100 eV, G_{cald} , occurring after a single pulse of dose D in rads (see Table I and Fig-

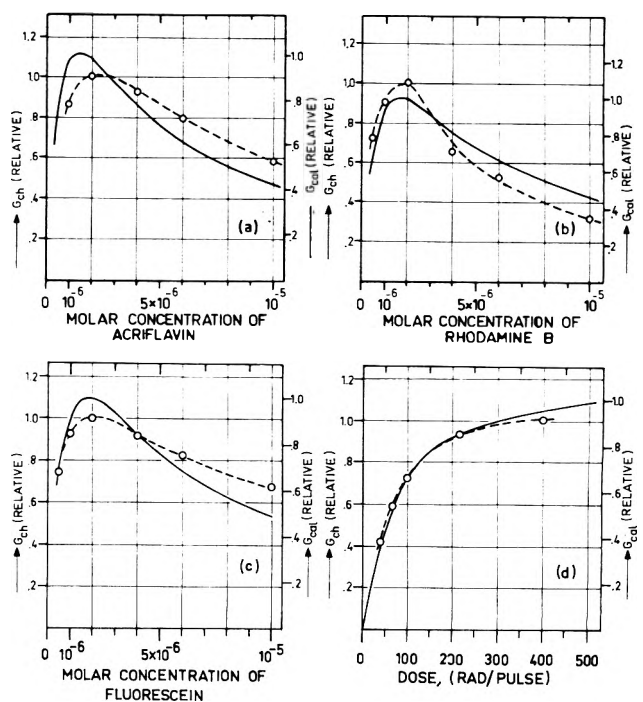


Figure 1. Concentration and dose dependencies of the observed chemiluminescence quantum yields, G_{ch} (dashed curves, left-hand ordinates), and of the calculated number of reactions 2, G_{cald} (continuous curves, right-hand ordinates), occurring on pulse radiolysis of deaerated aqueous solutions of various dyes: (a) Acriflavin, pH 6, concentration dependence at 200 rads/pulse; (b) Rhodamine B, pH 6, concentration dependence at 200 rads/pulse; (c) Fluorescein, pH 10, concentration dependence at 200 rads/pulse; (d) Fluorescein, pH 10, dose dependence at 4×10^{-6} M dye. Both G_{ch} and G_{cald} are plotted relative to their values at 2×10^{-6} M dye given in Table I.

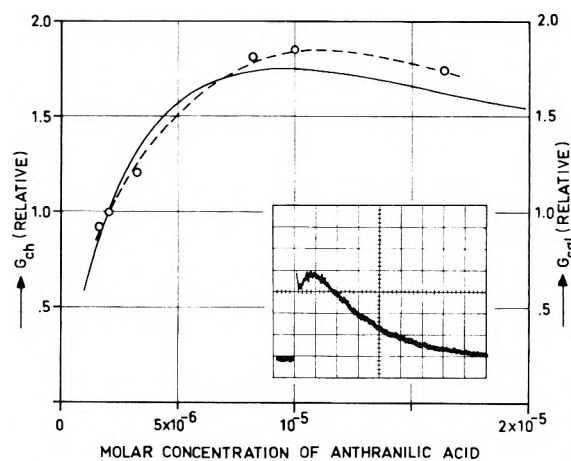


Figure 2. Concentration dependence of the observed chemiluminescence quantum yield, G_{ch} (dashed curve, left-hand ordinate), and of the calculated number of reactions 2, G_{cald} (continuous curve, right-hand ordinate), occurring after pulse radiolysis of deaerated aqueous anthranilic acid solutions at pH 6.2 (adjusted by adding KOH): dose 200 rads/pulse. Both G_{ch} and G_{cald} are plotted relative to their values at 2×10^{-6} M anthranilic acid given in Table I. Inset shows oscilloscope trace of the chemiluminescence from 1.64×10^{-6} M anthranilic acid after a $0.5\text{-}\mu\text{sec}$ pulse. Time base is $20\ \mu\text{sec}$ per large division.

ures 1 and 2)

$$G_{cald} = \frac{9.66 \times 10^8}{D} \int k_2 [D_{ox}](t) [e_{aq}^-](t) dt$$

$G(e_{aq}^-) = 2.722$ and $G(OH) = 2.7522$ and the rate con-

TABLE I: Quantum Efficiencies, G_{ch} , and Number of Reactions 2, G_{cald} , for the Chemiluminescence from Deaerated Aqueous Solutions of $2 \times 10^{-6} M$ Dye after Irradiation with 200-rad ($\pm 20\%$) Electron Pulses^a

Dye	ϕ_f	G_{ch}^b			G_{cald}^b	ϕ_{ch}
		Method A	Method B	Mean		
Acridflavin (neutral)	0.54 ^c	0.53	0.61	0.57	60	0.011
Rhodamine B (neutral)	0.30 ^d	1.01	0.54	0.77	40	0.018
Fluorescein (pH 10)	0.87 ^e	2.90	2.24	2.57	92	0.031
Anthranilic acid (pH 6.2)	0.51 ^f	0.28	0.33	0.30	15	0.020

^a Fluorescence quantum efficiencies, ϕ_f , and the mean number of quanta per reaction 2, ϕ_{ch} , obtained from the data at all concentrations (see Figures 1 and 2) are also given. ^b In units of 10^{-3} quanta per 100 eV. ^c Reference 20. ^d Reference 21. ^e Reference 6. ^f Estimated by comparing with aqueous salicylate ($\phi_f(\text{salicylate}) = 0.28$),²⁰ which has a very similar fluorescence spectrum, the integrated areas under the fluorescence spectra obtained for narrow bandwidth excitation at a wavelength where both solutions had equal optical densities.

TABLE II: Rate Constants ($10^{10} M^{-1} \text{sec}^{-1}$) for Reactions of e_{aq}^- (k_3) and $\cdot\text{OH}$ (k_1) with Various Dyes

Dye	k_3	k_1
Acridflavin	3.7 ^a	1.2 ^a
Rhodamine B	3.0 ^b	0.9 ^b
Fluorescein (pH 10)	1.4 ^c	1.2 ^d
Anthranilic acid	0.19 ^d	1.1 ^d

^a Reference 3. ^b Reference 1. ^c Reference 24. ^d This study.

stants given in Table II were used in these calculations.²³ The decay of e_{aq}^- and $\cdot\text{OH}$ in pure water was allowed for as previously³ and the unknown rate constant k_2 was assumed equal to k_3 . In the case of Fluorescein the rate constant k_1 was obtained from absorption changes, *i.e.*, dye bleaching and simultaneous product formation, after pulse radiolysis of N_2O -saturated solutions. (A value of $k_1 = 1.6 \times 10^9 M^{-1} \text{sec}^{-1}$ found in the literature²⁴ for Fluorescein is incompatible with our results.) For anthranilic acid the kinetics of OH-product formation in N_2O -saturated solutions and of e_{aq}^- decay in Ar-saturated solutions containing $10^{-1} M$ sodium formate were used to determine k_1 and k_3 , respectively.

The relative concentration dependencies of G_{cald} can be fitted by scale adjustment with the corresponding chemiluminescence results, as shown in Figures 1 and 2. By comparing the mean chemiluminescence yields G_{ch} (Table I) with the G_{cald} shown in Table I and Figures 1 and 2, we obtain the (quanta per reaction 2) efficiencies, ϕ_{ch} , given in the last column of Table I. The chemiluminescence efficiencies ϕ_{ch} which are much lower than the corresponding fluorescence quantum efficiencies ϕ_f might even be overestimations if $k_2 > k_3$. One reason for the lower quantum efficiencies in the chemical excitation of the dye may be that both singlet and triplet states are formed in reaction 2. Such possible triplet yields are too low to be observed by absorption spectroscopy at these concentrations. Another more important reason may be that both D^+ and $\text{D}\cdot\text{OH}$ adducts are probably formed^{3,24} in reaction 1 but only one of these leads to emission *via* reaction 2. Presumably the OH products which do not lead to luminescence are formed in large excess. The above effects may also explain why there is no apparent correlation between the changes in ϕ_{ch} and ϕ_f in going from one dye to another.

Previous attempts³ to identify D^+ and $\text{D}\cdot\text{OH}$ by absorption measurements on dyes, and hence to determine the $\text{D}^+/\text{D}\cdot\text{OH}$ ratio, were inconclusive. Anthranilic acid is however a simpler molecule and may allow resolution and positive identification of the corresponding D^+ and $\text{D}\cdot\text{OH}$. Additional studies using anthranilic acid, aimed at further understanding these chemiluminescent processes, are in progress.

Acknowledgments. This work was supported by grants from the Cancer Research Campaign and the Medical Research Council. Funds were also given by the Deutsche Forschungsgemeinschaft.

References and Notes

- (1) W. Prutz and E. J. Land, *Biophysik*, **3**, 349 (1967).
- (2) (a) L. I. Grossweiner and A. F. Rodde, Jr., *J. Phys. Chem.*, **72**, 756 (1968); (b) L. I. Grossweiner, *Radiat. Res. Rev.*, **2**, 345 (1970).
- (3) W. A. Prutz and E. J. Land, *J. Phys. Chem.*, **74**, 2107 (1970).
- (4) J. P. Keene, *J. Sci. Instrum.*, **41**, 493 (1964).
- (5) J. V. Jelly, "Cerenkov Radiation and Its Application," Pergamon Press, London, 1958.
- (6) W. R. Dawson and M. W. Windsor, *J. Phys. Chem.*, **72**, 3251 (1968).
- (7) A. Schmillen and R. Legler, "Landolt-Bornstein, New Series II/3," K. -H. Hellwege and A. M. Hellwege, Ed., Springer-Verlag, Berlin, 1967, p 270.
- (8) H. Bichsel, "Radiation Dosimetry, I," F. H. Attix and W. C. Roesch, Ed., Academic Press, New York, N. Y., 1968, p 157.
- (9) W. Prutz and K. Sommermeyer, *Biophysik*, **4**, 48 (1967).
- (10) P. Skarstad, R. Ma, and S. Lipsky, *Mol. Cryst.*, **4**, 3 (1968).
- (11) R. R. Hentz and L. M. Perkey, *J. Phys. Chem.*, **74**, 3047 (1970).
- (12) B. M. Zarnigar and D. G. Whitten, *J. Phys. Chem.*, **76**, 198 (1972).
- (13) C. Fuchs, F. Heisel, and R. Voltz, *J. Phys. Chem.*, **76**, 3867 (1972).
- (14) R. Cooper and J. K. Thomas, *J. Chem. Phys.*, **48**, 5097 (1968).
- (15) S. Lipsky, W. P. Helman, and J. F. Merklin, "Luminescence of Organic and Inorganic Materials," H. P. Kallmann, Ed., Wiley, New York, N. Y., 1962, p 83.
- (16) (a) W. P. Helman, Ph.D. Dissertation, University of Minnesota, 1964; (b) J. B. Birks, Proceedings of the University of New Mexico Conference on Organic Scintillation Detectors, G. Daub, F. M. Hayes, and E. Sullivan, Ed., U. S. Atomic Energy Commission Report No. TID-7612, 1960.
- (17) W. Stotz, *Acta Phys. Polon.*, **26**, 501 (1964).
- (18) I. B. Berlman, "Handbook of Fluorescence Spectra of Aromatic Molecules," Academic Press, New York, N. Y., 1971.
- (19) W. H. Melhuish, *J. Phys. Chem.*, **65**, 229 (1961).
- (20) G. Weber and F. W. J. Teale, *Trans. Faraday Soc.*, **53**, 646 (1957).
- (21) E. J. Bowen and F. Wokes, "Fluorescence of Solutions," Longmans, Green and Co., London, 1953, p 22.
- (22) M. S. Matheson and L. M. Dorfman, "Pulse Radiolysis," MIT Press, Cambridge, Mass., 1969, p 64.
- (23) The IBM-7040 computer of the Freiburg University Computer Center was used in these calculations.
- (24) P. Cordier and L. I. Grossweiner, *J. Phys. Chem.*, **72**, 2018 (1968).

Photolysis of Liquid and Solid Ethylene at 184.9 nm¹

Shun-ichi Hirokami and R. J. Cvetanovic*

Division of Chemistry, National Research Council of Canada, Ottawa, Canada (Received January 8, 1974)

Publication costs assisted by the National Research Council of Canada

Low-temperature photolysis of liquid, solid, and dissolved ethylene has been studied at 184.9 nm. The major products observed in the photolysis of liquid ethylene and of ethylene-ethane solutions at $-(160 \pm 1)^\circ$ are hydrogen and acetylene. The minor products are butene-1, *n*-butane, 1,3-butadiene, methylcyclopropane, cyclobutane, hexene-1, and 1,5-hexadiene. Methylcyclopropane, cyclobutane, and the greater part of butene-1 appear to result from direct addition of excited ethylene molecules to ethylene. In the photolysis of dideuterioethylene in liquid nitrogen solution at 77°K, *cis*-*trans* isomerization, H-atom scrambling, molecular decomposition into hydrogen and acetylene, and a much smaller decomposition into hydrogen atoms and vinyl radicals are observed. The photolysis of liquid and dissolved ethylene may be explained by a mechanism involving either a single or, somewhat more logically, two excited states of ethylene. The two-state mechanism is formally similar to the mechanism previously postulated for the mercury ($\text{Hg}(^3\text{P}_1)$) photosensitized reaction of ethylene. Addition of vinyl radicals (but not of ethyl radicals) to ethylene at $-(160 \pm 1)^\circ$ is observed. At this temperature the ratio $k(\text{C}_2\text{H}_3 + \text{C}_2\text{H}_4)/k(\text{H} + \text{C}_2\text{H}_4)$ is 0.24. Photochemically induced intermolecular hydrogen exchange at 184.9 nm between C_2H_4 and C_2D_4 in the solid phase at 77°K is at best only a very minor process. The ratio of the free radical to the molecular decomposition of liquid ethylene photolyzed at -160° is about 0.03.

Introduction

The kinetics of the mercury-sensitized photolysis of ethylene^{2a} was explained by Callear and Cvetanovic^{2b} in terms of a mechanism involving two excited state intermediates. Isomerization of dideuterioethylene photosensitized by $\text{Hg}(^3\text{P}_1)$, $\text{Cd}(^3\text{P}_1)$, benzene, and benzene derivatives has been similarly explained by a two excited state reaction mechanism.³⁻⁹ One of the two excited states is assumed to be a vibrationally excited triplet ethylene, capable of *cis*-*trans* isomerization (*i.e.*, interconversion of *cis*- and *trans*-1,2-dideuterioethylene) and of spontaneous conversion into the other excited state. The latter is assumed to be a vibrationally excited triplet ethylidene, capable of H-atom scrambling (formation of 1,1- from 1,2-dideuterioethylene and of *cis*- and *trans*-1,2-dideuterioethylene from 1,1-dideuterioethylene) or of dissociating into hydrogen and acetylene.^{2,4} Minor amounts of ethylene dimer and trimer olefinic products have also been observed in the mercury photosensitization of ethylene in the gas phase² and Chesick¹⁰ has detected traces of cyclobutane but no methylcyclopropane.

Reaction of short-lived intermediates (for example, ethylidene biradicals) with the reactant molecules to form molecular dimers could be expected to be favored in the liquid phase and, moreover, energy-rich intermediates formed by dimerization should be rapidly stabilized by transfer of excess energy to solvent molecules. With this prospect in mind, we have now investigated the photolysis at 184.9 nm of ethylene and dideuterioethylene in liquid nitrogen solution at 77°K, of liquid ethylene and ethylene-ethane solutions at $-(160 \pm 1)^\circ$, and of solid ethylene at 77°K.

Photolysis of ethylene has been recently studied in the gas phase at room temperature¹¹⁻¹⁴ and in the solid phase at 36¹⁴ and at 20°K.¹⁵ Cyclodimerization of *cis*- and *trans*-2-butene to give the four tetramethylcyclobutane isomers has been recently observed in the liquid phase.¹⁶

Experimental Section

The vacuum reaction system used was mercury free and the 184.9-nm radiation was obtained from a homemade, spiral low-pressure mercury lamp constructed of Suprasil quartz. The photolyses of ethylene in liquid nitrogen solution and of solid-phase ethylene were carried out using the Suprasil reaction vessel and dewar flask described in an earlier paper.¹⁷ The photolyses of liquid ethylene and of liquid ethylene-ethane solutions at $-(160 \pm 1)^\circ$ were carried out in a flat Suprasil reaction vessel connected to a dewar flask containing isopentane slush.

Matheson grade nitrogen (99.9995%) was used after passage through two spiral traps cooled with liquid oxygen. Matheson research grade ethylene and Phillips research grade ethane were used after thorough degassing and distillation from a trap at -160° . Merck Sharp and Dohme ethylene-*d*₄ and *trans*-1,2-, *cis*-1,2-, and 1,1-dideuterioethylene (asym- $\text{C}_2\text{H}_2\text{D}_2$) were used after degassing and distillation. Ethylene was found to contain a trace of ethane (0.0030%) and of propane (0.0004%). Ethane was found to contain a trace of propane (0.001%) and of propylene (0.0005%). Mass spectrometric analysis showed an isotopic impurity in ethylene-*d*₄ of 3.5% C_2HD_3 .

In the photolysis of ethylene in liquid nitrogen solutions at 77°K, reaction samples were prepared as described earlier.¹⁷ The total amount of liquid nitrogen solution used was either 10 or 20 ml. After irradiation, the nitrogen solvent was distilled off and the condensable products and excess ethylene were collected in a trap at 77°K.

In the photolysis of liquid ethylene and of ethylene-ethane solutions at $-(160 \pm 1)^\circ$, volumetrically measured amounts of ethylene and ethane were introduced into the reaction vessel at liquid nitrogen temperature. The liquid nitrogen in the dewar flask was replaced by an isopentane slush at $-(160 \pm 1)^\circ$. After irradiation, the isopentane slush was replaced by liquid nitrogen. In the photolysis of the solid-phase ethylene, a volumetrically measured

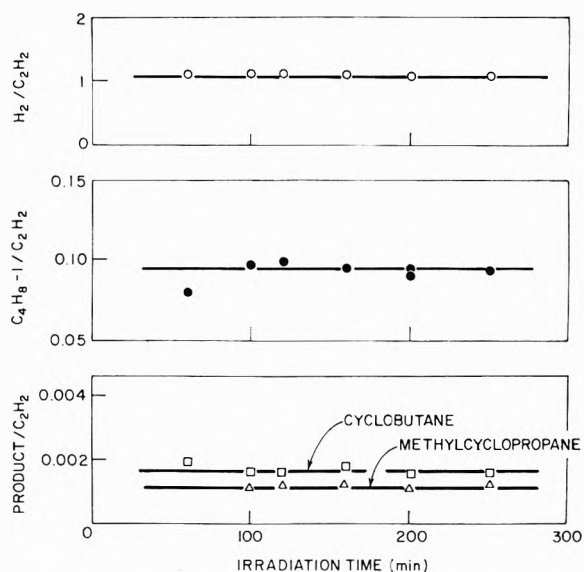


Figure 1. Relative yields of hydrogen, butene-1, and methylcyclopropane to acetylene in the 184.9-nm photolysis of liquid ethylene at $-(160 \pm 1)^\circ$

amount of ethylene was frozen onto the wall of the reaction vessel and was photolyzed after a 5-min thermal equilibration period.

The mercury-free reaction system was connected to the mercury containing analysis system through two protective spiral liquid nitrogen traps. The condensable gases, consisting of H_2 with at best only a trace of N_2 , were collected in a combined Toepler pump-gas buret and measured manometrically before and after the removal of H_2 in a copper oxide furnace at about 240° . The condensable products and excess reactant were analyzed by gas chromatography with flame ionization detectors. Ethane and ethylene were analyzed on a 1.5-m silica gel column at 75° . The C_2 , C_3 , and C_4 hydrocarbons were analyzed on a 12-m dimethylsulfolane (20% w/w on Chromosorb P) packed column at room temperature. The C_4 and C_6 hydrocarbons were analyzed on a 3-m dimethylsulfolane packed column at room temperature, on a 300-ft stainless steel capillary column at 0° coated with squalane, and on a 300-ft stainless steel capillary column at 0° coated with 1:1 squalane- β, β' -thiodipropionitrile (β, β' -TDPN) mixture.

The identification of C_2 , C_4 , and C_6 hydrocarbons was confirmed by seeding with authentic samples when available. Methylcyclopropane was synthesized by the mercury photosensitized reaction of butene-1.¹⁸ The identification of C_4 and C_6 hydrocarbons except for the minor products (methylcyclopropane and cyclobutane) was also confirmed by direct mass spectrometric analysis of peaks eluted at 0° from the 300-ft stainless steel capillary column coated with 1:1 squalane- β, β' -TDPN mixture.

Isotopic ethylenes produced from isomerization of deuterioethylene were analyzed by a Perkin-Elmer 621 grating infrared spectrophotometer. The absorption peaks used for the analysis were 987 and 725 cm^{-1} for *trans*-, 842 cm^{-1} for *cis*-, and 943 and 751 cm^{-1} for *asym*-dideuteroethylene.¹⁹ Calibration curves were made using the pure compounds. A small infrared cell was constructed with KBr windows in order to detect the isotopic acetylenes. An Atlas CH-4 mass spectrometer was used to determine the isotopic composition of the ethylenes by low-

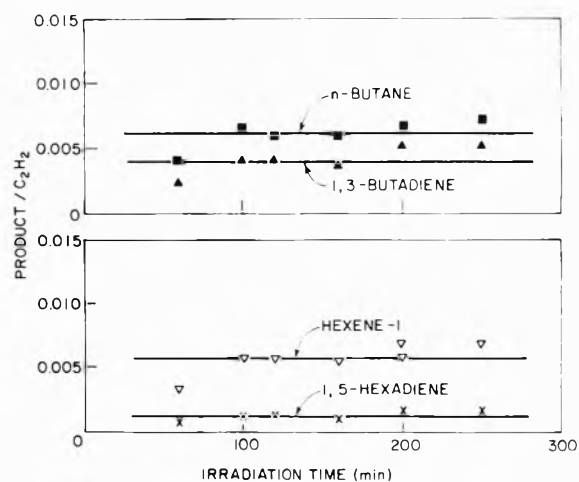


Figure 2. Relative yield of *n*-butane, 1,3-butadiene, hexene-1, and 1,5-hexadiene to acetylene in the 184.9-nm photolysis of liquid ethylene at $-(160 \pm 1)^\circ$.

voltage parent peak analysis and of the isotopic hydrogens at standard voltage (70 V).

The number of light quanta absorbed by ethylene was estimated from the amount of N_2 produced in the photolysis of N_2O and $N_2O-C_2H_6$ mixtures in the gas phase.

The flame ionization detector molar responses for the hydrocarbons were taken to be directly proportional to the number of carbon atoms.

The total amount of ethylene or ethylene-ethane solution used was about $(2.6-4.9) \times 10^{-2}$ mol, corresponding to a volume of about (1.1-2.2) cc at $-(160 \pm 1)^\circ$.

Results

Photolysis of Liquid Ethylene and of Ethylene-Ethane Solutions at $-(160 \pm 1)^\circ$. The main photolysis products observed are hydrogen and acetylene and the minor products are ethane, *n*-butane, butene-1, 1,3-butadiene, methylcyclopropane, cyclobutane, hexene-1, and 1,5-hexadiene. The effect of irradiation time on the yields relative to acetylene of all the observed products except ethane is shown in Figures 1 and 2. The yield of ethane relative to acetylene was only about 10^{-3} . The relative yields of the products are within the experimental error independent of irradiation time. The ratio of the yields of hydrogen and acetylene is very close to unity.

The effect of the concentration of ethylene diluted by ethane on the relative yields of products is shown in Figures 3-5. The yields of butene-1, methylcyclopropane, and cyclobutane relative to acetylene increase linearly with the mole fraction of ethylene. The relative yields of *n*-butane, 1,3-butadiene, hexene-1, and 1,5-hexadiene remain constant within the experimental error. Figure 6 shows that the yields of methylcyclopropane and cyclobutane relative to butene-1 are independent of ethylene concentration.

The quantum yield of products in typical runs is shown in Table I. The quantum yields of hydrogen and acetylene are constant at different concentrations of ethylene and are less than unity.

These results show that hydrogen and acetylene are formed by unimolecular decomposition of the photoexcited ethylene. Methylcyclopropane, cyclobutane, and the greater part of butene-1 are formed by direct addition of the excited ethylene molecules to ethylene. *n*-Butane,

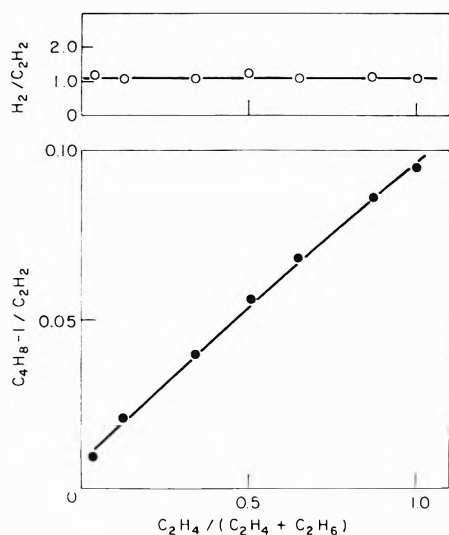


Figure 3. Dependence of the yields of hydrogen and butene-1 relative to acetylene on the mole fraction of ethylene in the 184.9-nm photolysis of liquid ethylene-ethane solutions at $-(160 \pm 1)^\circ$.

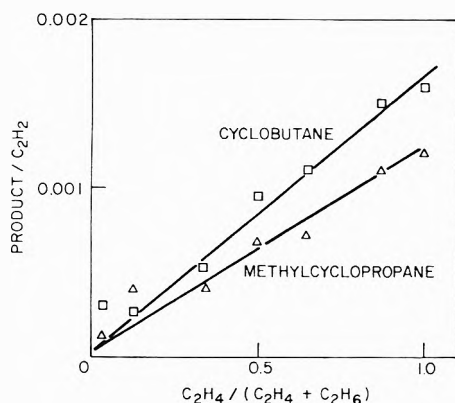


Figure 4. Dependence of the yields of methylcyclopropane and cyclobutane relative to acetylene on the mole fraction of ethylene in the 184.9-nm photolysis of liquid ethylene-ethane solution at $-(160 \pm 1)^\circ$.

1,3-butadiene, hexene-1, 1,5-hexadiene, and the smaller part of butene-1 are formed by recombination of the radicals produced in the primary and secondary processes. A quantum yield of all products of less than unity suggests that the excited ethylene molecules are partially stabilized to ground-state ethylene molecules.

Photolysis of C₂H₄ and Dideuterioethylene in Liquid Nitrogen Solutions at 77°K. The products observed in the photolysis of C₂H₄ in liquid nitrogen solution at 77°K are acetylene, 1,3-butadiene, and a trace of butene-1. (No measurements of hydrogen were possible in the presence of the huge excess of N₂.) Butane, hexene-1, and 1,5-hexadiene were not observed in this case. The effect of irradiation time on the main product, acetylene, is shown in Figure 7, for 8.15×10^{-4} , 7.70×10^{-3} , and 5.74×10^{-2} M ethylene solutions. The yield of acetylene increases linearly with the irradiation time. The yields of 1,3-butadiene and butene-1 relative to acetylene were about $(1-8) \times 10^{-3}$ and 10^{-4} , respectively (in the 7.70×10^{-3} M ethylene solution). Absence of *n*-butane and hexene-1 from the products shows that hydrogen atoms formed in the photolysis are apparently effectively scavenged by traces of O₂ present as impurity in the nitrogen.

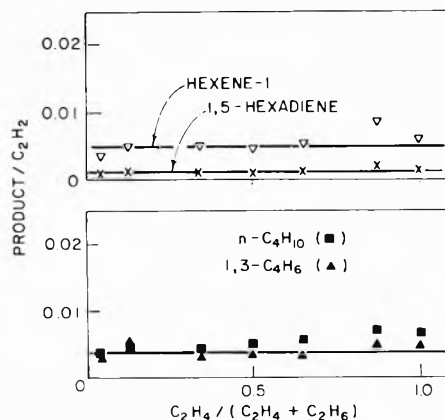


Figure 5. Dependence of the yields of *n*-butane, 1,3-butadiene, hexene-1, and 1,5-hexadiene relative to acetylene on the mole fraction of ethylene in the 184.9-nm photolysis of liquid ethylene-ethane solutions at $-(160 \pm 1)^\circ$.

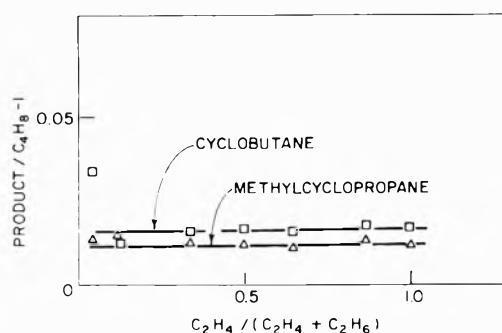


Figure 6. Dependence of the yields of cyclobutane and methylcyclopropane relative to butene-1 on the mole fraction of ethylene in the 184.9-nm photolysis of liquid ethylene-ethane solutions at $-(160 \pm 1)^\circ$.

TABLE I: Quantum Yields of Products in the 184.9-nm Photolysis of Liquid Ethylene and Ethylene Dissolved in Ethane at $-(160 \pm 1)^\circ$

Reaction products	Quantum yields of products	
	Ethylene ^a	Ethylene/ethane ^b
Hydrogen	0.74	0.71
Acetylene	0.71	0.63
Butene-1	0.066	0.0058
Methylcyclopropane	0.00077	0.000083
Cyclobutane	0.0011	0.00020
<i>n</i> -Butane	0.0049	0.0023
1,3-Butadiene	0.0038	0.0019
Hexene-1	0.0058	0.0024
1,5-Hexadiene	0.0013	0.00052

^a Liquid ethylene at $-(160 \pm 1)^\circ$. ^b Ethylene dissolved in ethane at $-(160 \pm 1)^\circ$, C₂H₄/(C₂H₄ + C₂H₆) = 0.0376.

The observed products in the photolysis of *trans*-, *cis*-, and *asym*-dideuterioethylene in liquid nitrogen solution at 77°K are the isomers of dideuterioethylene, the isotopic acetylenes (C₂H₂, C₂HD, C₂D₂), and a trace of 1,3-butadiene. The effect of dideuterioethylene concentration on product yields is shown in Table II. The yields of *trans*- and *cis*-C₂H₂D₂ in the photolysis of *asym*-C₂H₂D₂ are the same, within the experimental error. In the photolysis of *trans*- and *cis*-C₂H₂D₂, the yield of *asym*-C₂H₂D₂ (relative to acetylene) is approximately the same as that of *cis*- and *trans*-C₂H₂D₂ in the photolysis of *asym*-C₂H₂D₂. The relative yields of *cis*-C₂H₂D₂ from *trans*-C₂H₂D₂ and of

TABLE II: Photolysis of Dideuterioethylene in Liquid Nitrogen Solution at 77°K with the 184.9-nm Hg Resonance Line

Ethylene, μmol	Ethylene, $M \times 10^3$	Photolysis time, min	Total acetylene, μmol	Products			
				Relative yields of products, $r_{\text{acetylene}} = 1$			
				C ₂ H ₂ D ₂			1,3-Butadiene
Trans	Cis	Asym					
1. <i>asym</i> -C ₂ H ₂ D ₂							
105	5.02	50	12.0	0.35	0.36		0.011
155	7.77	35	11.8	0.32	0.36		0.011
201	10.0	25	11.5	0.34	0.28		0.005
201	20.1	20	9.07	0.37	0.36		0.005
412	41.2	50	28.5	0.36	0.36		0.003
2. <i>trans</i> -C ₂ H ₂ D ₂							
71.1	7.11	40	9.61		0.55	0.29	0.008
214	10.7	35	13.1		0.65	0.34	0.009
156	15.6	35	13.8		0.62	0.34	0.004
206	20.6	26	11.9		0.65	0.32	0.004
3. <i>cis</i> -C ₂ H ₂ D ₂							
171	8.55	45	14.0	0.70		0.36	nd ^a
162	16.2	45	20.5	0.60		0.27	0.004

^a nd = not determined.

TABLE III: Photolysis of Solid Ethylene at 184.9 nm and 77°K

Ethylene			Irradiation time, min	Hydrogen			Products						
Total amount, μmol	Relative amounts			Total amount, μmol	H ₂ , %	HD, %	D ₂ , %	Relative yield of products ($r_{\text{hydrogen}} = 1$)					
	C ₂ H ₄	C ₂ D ₄						Acetylene	Butene-1	MCP ^a	CB ^b	<i>n</i> -Butane	1,3-Butadiene
105	1.00	0	15	2.40			0.946	0.0317	0.0019	0.0002	0.0016	0.0125	
206	1.00	0	15	2.84			0.979	0.0311	0.0019	0.0001	0.0017	0.0130	
273	1.00	0	15	2.78			0.903	0.0303	0.0015	0.0001	0.0014	0.0103	
172	1.00	1.00	20	2.72	79	2	19	nd ^c	0.0311	nd	0.0004	0.0014	0.0166
171	1.00	1.00	20	3.58	79	2	19	nd	0.0321	0.0007	0.0004	0.0013	0.0191
181	1.00	1.03	18	2.82	79	2	19	0.926	0.0319	0.0010	0.0004	0.0014	0.017 _±
169	1.00	3.27	20	2.20	72	3	25	nd	0.0286	0.0010	0.0003	0.0010	0.0260
133	0	1.00	15	1.21	1	4	95	0.992	0.0214	0.0014	0.0009	0.0041	0.017 _±
174	0	1.00	15	1.19	1	3	96	0.941	0.0226	0.0012	0.0004	0.0079	0.0346
109	0	1.00	15	1.09	1	3	96	0.936	0.0217	0.0012	0.0007	0.0004	0.0356

^a MCP = methylcyclopropane. ^b CB = cyclobutane. ^c nd = not determined.

TABLE IV: Isotopic Composition of Hydrogen and Ethylene from the 184.9-nm Photolysis of Mixtures of C₂H₄ and C₂D₄ at 77°K

Ethylene			Irradiation time, min	Hydrogen			Ethylene (relative to C ₂ D ₄ = 100)		
C ₂ H ₄ , μmol	C ₂ D ₄ , μmol	Total amount, μmol		% of total hydrogen			C ₂ D ₄	C ₂ HD ₂	C ₂ H ₂ D ₂
				H ₂	HD	D ₂			
86.0	86.0	20	2.72	79	2	19	100	3.9	0.3
85.6	85.6	20	3.58	79	2	19	100	3.6	0.3
39.5	129	20	2.20	72	3	25	100	3.7	0
86.0	86.0	0					100	3.6	0

trans-C₂H₂D₂ from *cis*-C₂H₂D₂ are approximately the same. Furthermore, these relative yields are always larger than the yield of *asym*-C₂H₂D₂. The significance of these results will be discussed further below.

Photolysis of Ethylene in the Solid Phase at 77°K. The products observed in the photolysis of C₂H₄, C₂D₄, and C₂H₄-C₂D₄ mixtures in the solid phase at 77°K are hydrogen, acetylene, butene-1, methylcyclopropane, cyclobutane, *n*-butane, 1,3-butadiene, and perhaps a trace of cyclobutene. The C₆ hydrocarbons, for example hexene-1 and 1,5-hexadiene, were not found. The experimental results are shown in Tables III and IV. By far the major

products are hydrogen and acetylene. Formation of equal amounts of hydrogen and acetylene is in agreement with earlier findings in the photolysis of solid ethylene^{14,15} and indicates that these two compounds result from molecular elimination from excited ethylene molecules in the primary process. This explanation is confirmed by the earlier¹⁵ and present experimental observations that the isotopic hydrogen formed in the photolysis of an equimolar mixture of C₂H₄ and C₂D₄ is mainly composed of H₂ and D₂. The smaller amount of *n*-butane than of 1,3-butadiene observed in the present work and the presence of some HD in the photolysis of the equimolar mixture of C₂H₄

and C₂D₄ indicate that the greater part of the hydrogen atoms probably recombines in this system on the surface of the reaction vessel.

The very small amount of C₂H₂D₂ shown in Table IV for the photolysis of equimolar mixtures of C₂H₄ and C₂D₄ is close to analytical uncertainty and represents an upper limit. The relative yield of intermolecular hydrogen atom exchange between C₂H₄ and C₂D₄ to the total amount of hydrogen is therefore at best only about 0.10 and perhaps it may be much less.

The small amounts of ethylene dimer products, butene-1, methylcyclopropane, and cyclobutane, are probably formed by direct addition of the electronically excited ethylene molecules to ethylene. Cyclobutene is a very minor product and is perhaps formed by direct addition of the excited acetylene molecules (one of the primary products) to ethylene. The products of photolysis of solid ethylene observed in the present work (at 184.9 nm) are appreciably simpler than reported for more energetic photons ($\lambda \leq 147$ nm)^{14,15} although the main features are similar.

Photolysis of Ethylene in the Gas Phase. In view of the somewhat unexpected observation that vinyl radicals add to ethylene at cryogenic temperatures, several experiments have been carried out in the gas phase at room temperature (22°), in the hope that additional information may be obtained about the reaction of vinyl radicals with ethylene. Hg(³P₁) photosensitization of ethylene and direct photolysis of ethylene at 184.9 nm were used as the source of vinyl radicals.

The main products observed in Hg(³P₁) photosensitized reaction of ethylene at a pressure of 323 Torr are acetylene and hydrogen. The less important products and their relative yields are *n*-butane (1.0), butene-1 (0.1), 1,3-butadiene (0.26), *n*-hexane (0.12), hexene-1 (0.45), and 1,5-hexadiene (0.003). The results obtained are in fair agreement with the relative yields of products which have been previously reported by Chesick.¹⁰ Such products as 1-hexene and 1,5-hexadiene show that C₂H₃ adds readily to ethylene in this system but the reaction is very complex and it would be difficult to draw quantitative conclusions.

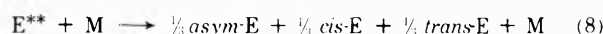
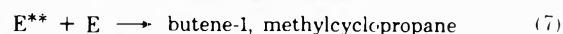
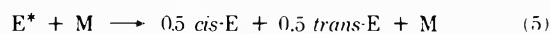
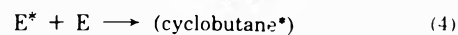
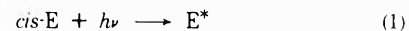
The direct photolysis of ethylene at 184.9 nm has been carried out at the following pressures of ethylene and CO₂: (1) C₂H₄ 10.3 Torr, CO₂ 783 Torr; (2) C₂H₄ 40.0 Torr, CO₂ 781 Torr; (3) C₂H₄ 478 Torr, CO₂ none (*i.e.*, no CO₂ was added). The main products observed and their relative yields are in 1 and 2, respectively, hydrogen (1.0), acetylene (0.60, 0.83), *n*-butane (0.30, 0.34), butene-1 (0.006, 0.009), 1,3-butadiene (0.002, 0.004), pentane (0.020, 0.023), pentene-1 (0.018, 0.034), *n*-hexane (0.0006, 0.004), and hexene-1 (0.002, 0.028), and in 3 hydrogen (1.0), acetylene (1.01), *n*-butane (0.26), butene-1 (0.031), and hexene-1 (0.21), although the reaction was quite complex, with many other products formed in smaller amounts. No conclusions could be drawn regarding the involvement of vinyl radicals in this system.

Discussion

The primary reactions of the photoexcited ethylene molecules formed in the photolysis of liquid and solid ethylene at 184.9 nm are (1) deexcitation (the stabilization), (2) addition, and (3) decomposition.

Stabilization of Photoexcited Ethylene. In the photolysis of dideuterioethylene in liquid nitrogen solution at 77°K, the following reactions are observed: (i) *cis*-*trans*

isomerization, (ii) internal H-atom scrambling, (iii) molecular decomposition into hydrogen and acetylene, and (iv) decomposition into hydrogen atoms and vinyl radicals. These observations can be explained, with some assumptions, by postulating a single photoexcited state of ethylene which can react along four different reaction channels: rotation around the CC bond (leading to *cis*-*trans* isomerization), internal migration of H and D atoms, molecular decomposition and free radical decomposition. An alternative, although kinetically very similar explanation, can be formulated by postulating involvement of two distinct excited states, the initially formed state (E*) is, perhaps, the first excited singlet (the V state²⁰) which can undergo easily *cis*-*trans* isomerization, cycloaddition to form cyclobutane, decomposition into H and C₂H₃, or spontaneous conversion into a second excited state (E**). The second excited state can be visualized perhaps as a (vibrationally) excited singlet ethylidene biradical, which can decompose into H₂ and C₂H₂, undergo internal H or D migration, add to ethylene (to form butene-1 or methylcyclopropane), or revert to ground state ethylene. This mechanism involves therefore the following reactions



E stands for ethylene. *cis*-E, *trans*-E, and *asym*-E apply to the reactions of dideuterioethylenes and represent *cis*-1,2-, *trans*-1,2-, and 1,1-dideuterioethylene.

This mechanism is somewhat similar to the two-state mechanism of the mercury-photosensitized reaction of ethylene,² although the latter process must involve, at least initially, a triplet species. Thus the analogy is only formal.

The present results do not distinguish clearly between the two alternative mechanisms, although the two-state mechanism is perhaps capable of explaining some of the observations in a somewhat more logical manner, for example, the ratios of the three isomers formed in the photolysis of dideuterioethylenes and the dimerization products (cyclobutane, methylcyclopropane, and butene-1). We shall, therefore, for the time being, discuss our results in terms of the two-state mechanism (reactions 1-8).

The yields of reactions 5 and 8 in the photolysis of dideuterioethylenes, relative to reaction 6, are summarized in the last two columns of Table V. The ratio of the rate of reaction 3 to that of reaction 6 is approximately 0.02. If the sum of the quantum yields of the four reactions 3, 5, 6, and 8 is unity, their respective quantum yields are approximately 0.01 (eq 3), 0.24 (eq 5), 0.37 (eq 6), and 0.38 (eq 8).

Steady-state treatment of E* and E** in the reactions 1-8 yields the following expressions (since reactions 4 and 7 are very minor processes in liquid nitrogen solutions)

$$\frac{R(\text{H-atom scrambling})}{R(\text{acetylene})} = \frac{k_2}{k_6} [M]$$

TABLE V: Relative Rates of the H-Atom Scrambling and of Cis-Trans Isomerization to the Decomposition (into Hydrogen and Acetylene) in the 184.9-nm Photolysis of Dideuterioethylene in Liquid Nitrogen Solution at 77°K

Ethylene, $M \times 10^3$	Time, min	Relative rates ^a	
		H-atom scrambling	Cis-trans isomerization
<i>asym</i> -C ₂ H ₂ D ₂			
5.02	50	1.1	
7.77	35	1.0	
10.0	25	0.93	
20.1	20	1.1	
41.2	50	1.1	
<i>trans</i> -C ₂ H ₂ D ₂			
7.11	40	0.87	0.52
10.7	35	1.0	0.61
15.6	35	1.0	0.57
20.6	26	0.96	0.66
<i>cis</i> -C ₂ H ₂ D ₂			
8.55	45	1.1	0.69
16.2	45	0.80	0.69
	Av	1.0	Av 0.62

^a Relative to acetylene taken as unity.

$$\frac{R(\text{cis-trans isomerization})}{R(\text{acetylene})} = \frac{k_2[M]}{k_2} \left(1 + \frac{k_2}{k_6[M]} \right)$$

Therefore, in view of the data in Table V

$$k_6 = k_2[M]$$

$$k_2 = 3.2k_5[M]$$

$k_5[M]$ and $k_8[M]$ represent here the collision frequency of solute molecules with solvent molecules. The collision frequency of solute-solvent molecules (Z) can be calculated from the following equation²¹

$$Z = 0.892 \times 3\pi\sigma\eta / \mu$$

σ is the diameter of solute molecules, μ the reduced mass of a solute-solvent pair, and η is the viscosity of the medium. At 77°K the value of η is²² 1.58×10^{-3} (cgs), and taking a collision diameter³ of 4.95 Å for C₂H₂D₂, both $k_5[M]$ and $k_8[M]$ are equal or less (depending on the efficiency of collisional deexcitation) than $2.7 \times 10^{13} \text{ sec}^{-1}$ and therefore $k_2 \leq 8.6 \times 10^{13} \text{ sec}^{-1}$ and $k_6 \leq 2.7 \times 10^{13} \text{ sec}^{-1}$. As expected, these rates are apparently very much greater than the corresponding rates⁴ in the mercury photosensitized reaction.

Addition Reactions of Photoexcited Ethylene. The trends in the yields of butene-1, methylcyclopropane, and cyclobutane relative to acetylene shown in Figures 3 and 4 and in the relative yield of methylcyclopropane to butene-1 shown in Figure 6 can be explained by the above mechanism. The relative yield of butene-1 to acetylene shown in Figure 3 does not approach zero at low mole fractions of ethylene, suggesting that butene-1 is not formed only in reaction 7 but also to some extent, at lower mole fractions of ethylene, by the combination of ethyl and vinyl radicals. If the relative yield of butene-1 formed by the combination of ethyl and vinyl radicals to acetylene is constant, the dependence of the total yield of butene-1 relative to acetylene on the mole fraction of ethylene may be expressed as

$$\phi(\text{C}_4\text{H}_8-1) / \phi(\text{C}_2\text{H}_2) = af + b$$

f represents the mole fraction of ethylene, a and b are, re-

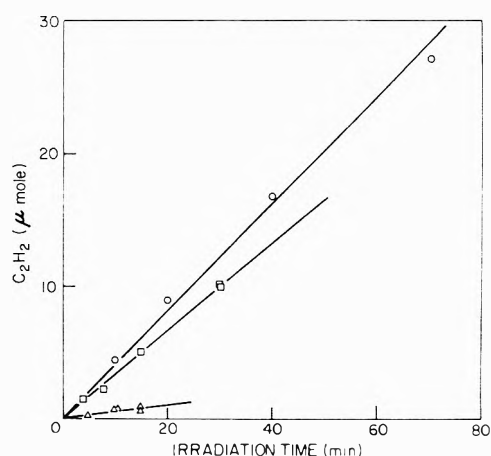


Figure 7. Effect of irradiation time at 184.9 nm on acetylene yield in liquid nitrogen solution at 77°K (ethylene concentration: O, $5.74 \times 10^{-2} M$; □, $7.70 \times 10^{-3} M$; Δ, $8.15 \times 10^{-4} M$).

spectively, the yields relative to acetylene of butene-1 formed from the direct addition of the excited ethylene to ethylene (a) and from the combination of ethyl and vinyl radicals (b). The least-squares values and standard deviations of a and b obtained from the plot in Figure 3 are $a = 0.0881 \pm 0.0027$ and $b = 0.0091 \pm 0.0016$, *i.e.*, free radical formation of butene-1 is only a relatively small fraction of the overall butene-1 yield.

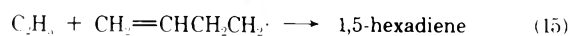
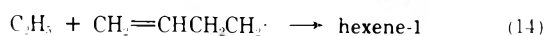
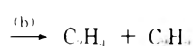
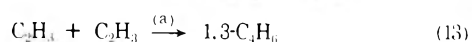
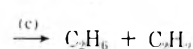
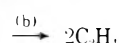
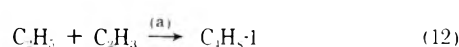
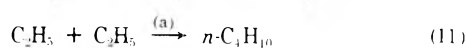
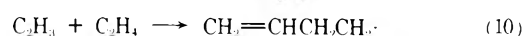
In the liquid-phase photolysis of 2-butene¹⁶ with the 213.9-nm zinc or the 228.8-nm cadmium resonance line, three main types of products are observed: (1) isomerization, (2) cyclodimerization, and (3) fragmentation products. If the basic reaction mechanism of the photoexcited ethylene is the same, both isomerization (of dideuterioethylene) and formation of cyclobutane would be expected in the liquid-phase photolysis of ethylene. The first expectation is borne out by the photolysis of dideuterioethylene in liquid nitrogen solution at 77°K. The second expectation seems to be fulfilled also, since some cyclobutane is found in the products (Figures 1 and 4), although its yield is very small.

H-atom scrambling in the photolysis of dideuterioethylene in liquid nitrogen solutions suggests strongly the presence of ethylenic biradicals as transient intermediates. Furthermore, molecular photodimerization of condensed ethylene into methylcyclopropane and, very selectively, into butene-1 is most logically explained by reactions of ethylidene with ethylene. For the selective formation of butene-1 two distinct reaction paths may be envisaged: (1) ethylidene addition to ethylene to form a 1,3 biradical which then rearranges to butene-1 by a readily occurring 1,4 H-atom shift or (2) direct insertion of ethylidene into the CH bonds of ethylene. The first path would perhaps involve vibrationally excited triplet ethylidene capable of adding to condensed ethylene but not of inserting into its CH bonds. The second reaction path could perhaps be expected for singlet ethylidene, at least by analogy with singlet methylene.²³⁻²⁵ Unfortunately, information on chemical behavior of ethylidene^{26,27} is still very incomplete. Frey^{26a} has observed in one instance its addition to propylene but not to 2-butene nor its insertion into the CH bonds of these olefins or of propane and butane. No reaction with several olefins (including one in the liquid phase) was observed by Frey and Stevens in another study.^{26b}

The possibility of occurrence of specific chemical reactions of ethylidene, in competition with its fragmentation and degradation to ethylene, evidently depends critically on its multiplicity and energy content and on experimental conditions. With increasing fraction of ethane in the present experiments with ethylene-ethane solutions there was, as expected, a decrease in the yields of butene-1, methylcyclopropane, and cyclobutane (Figures 3 and 4) but there was not an enhancement in *n*-butane (Figure 5). These results suggest qualitatively that under conditions of these experiments there was little or no ethylidene insertion into the CH bonds of ethane (to form *n*-butane). However, since there appears to be no positive evidence at present of ethylidene insertion into any paraffinic CH bonds, although it has been occasionally postulated, and in view of the still very limited knowledge of the chemical behavior of singlet and triplet ethylidene of varying energy content, further discussion of these observations would be unwarranted at this time.

It is of interest that under present reaction conditions the yield of butene-1 is about hundred times larger than the yield of methylcyclopropane. Qualitatively similar results were obtained in the solid state photolysis of ethylene at 36¹⁴ and 20°K.¹⁵

Decomposition of Photoexcited Ethylene. As mentioned earlier, photoexcited ethylene decomposes mainly into H₂ and C₂H₂ (reaction 6) and to a much smaller extent into H and C₂H₃ (reaction 3). In liquid ethylene and liquid ethylene-ethane solutions at $-(160 \pm 1)^\circ$, hydrogen atoms produced in (3) are rapidly scavenged by ethylene molecules to form ethyl radicals. The vibrationally excited vinyl radicals produced in (3) are probably stabilized in the liquid phase. The secondary reactions of ethyl and vinyl radicals may be described by the following reaction scheme



Addition of ethyl radicals to ethylene is ignored at these low temperatures because no *n*-hexane was observed in the products, although in the gas-phase photolysis of ethylene at room temperature, it is one of the major products. Addition of vinyl radicals to ethylene (reaction 10), on the other hand, has to be invoked to explain the formation of hexene-1 and 1,5-hexadiene. Little is known²⁸⁻³⁰ about reactions of vinyl radicals with hydrocarbons in the gas and liquid phase and their ability to add to ethylene at -160° is of interest; it indicates a very low activation energy for reaction 10. The relative rate constant k_{10}/k_9 can be roughly estimated from the relation

TABLE VI: Sums of the Yields of Ethyl and Vinyl Radicals Relative to the Acetylene Formed in the Photolysis of Liquid Ethylene and Ethylene-Ethane Solutions at $-(160 \pm 1)^\circ$

Mole fraction of ethylene	C ₂ H ₅ /C ₂ H ₃ ^a		Mole fraction of ethylene	C ₂ H ₅ /C ₂ H ₃ ^b	
	C ₂ H ₅ /C ₂ H ₃ ^a	C ₂ H ₅ /C ₂ H ₃ ^b		C ₂ H ₅ /C ₂ H ₃ ^a	C ₂ H ₅ /C ₂ H ₃ ^b
1.00	0.032	0.031	0.870	0.035	0.034
1.00	0.033	0.030	0.648	0.028	0.024
1.00	0.031	0.026	0.502	0.027	0.024
1.00	0.030	0.026	0.340	0.024	0.024
1.00	0.029	0.024	0.125	0.026	0.027
1.00	0.034	0.033	0.0376	0.022	0.021

^a Average C₂H₅/C₂H₃ = 0.029. ^b Average C₂H₅/C₂H₃ = 0.027.

$$\frac{k_{10}}{k_9} = \frac{R(\text{C}_4\text{H}_7\cdot)}{R(\text{C}_2\text{H}_5\cdot)} = \frac{R(\text{hexene-1}) + R(1,5\text{-hexadiene})}{2R(\text{C}_4\text{H}_{10})1.14 + R(\text{C}_4\text{H}_8\text{-1}^*)1.15 + R(\text{hexene-1})} \quad (I)$$

($R(\text{C}_4\text{H}_8\text{-1}^*)$ is the rate of C₄H₈-1 formation in reaction 12a.) This gives $k_{10}/k_9 \approx 0.24$ at $-(160 \pm 1)^\circ$. The rate of addition of vinyl radicals to ethylene at -160° is therefore only about four times slower than the addition of H atoms to ethylene.

The disproportionation to combination ratios of radical reactions 12-15 cannot be determined from the products obtained because either ethylene, ethane, or acetylene is the reactant, solvent, or one of the main products in this reaction system. The disproportionation to combination ratio for two ethyl radicals in liquid phase, k_{11b}/k_{11a} , is³¹ 0.12-0.15. The disproportionation to combination ratios for ethyl + vinyl and vinyl + vinyl radicals are not known in liquid phase but if they had the same values as in the gas phase, they would be 0.15 and 0.02, respectively.^{30,32} The disproportionation to combination ratios for ethyl + *n*-butenyl and vinyl + *n*-butenyl in the gas and liquid phase are not known.

If the proposed mechanism is correct, the relative quantum yield of reaction 3 to that of reaction 6 can be estimated from the following relations

$$\frac{\phi(\text{H})}{\phi(\text{C}_2\text{H}_2)} = \frac{\phi(\text{C}_2\text{H}_3)}{\phi(\text{C}_2\text{H}_2)} = \frac{1}{\phi(\text{C}_2\text{H}_2)} \times \{2\phi(n\text{-C}_4\text{H}_{10})1.14 + \phi(\text{C}_4\text{H}_8\text{-1}^*)1.15 + \phi(\text{hexene-1})\} \quad (II)$$

$$\frac{\phi(\text{C}_2\text{H}_3)}{\phi(\text{C}_2\text{H}_2)} = \frac{1}{\phi(\text{C}_2\text{H}_2)} \{2\phi(1,3\text{-C}_4\text{H}_6)1.02 + \phi(\text{C}_4\text{H}_8\text{-1}^*)1.15 + \phi(\text{hexene-1}) + 2\phi(1,5\text{-hexadiene})\} \quad (III)$$

Disproportionation in reactions 14 and 15 is ignored. The yield of butene-1 produced by the recombination of vinyl and ethyl radicals relative to acetylene, $\phi(\text{C}_4\text{H}_8\text{-1}^*)/\phi(\text{C}_2\text{H}_2)$, is obtained from the value of the intercept in Figure 3.

The values calculated from eq II and III are shown in Table VI. The relative yields obtained from the two expressions, $\phi(\text{C}_2\text{H}_5)/\phi(\text{C}_2\text{H}_2)$ and $\phi(\text{C}_2\text{H}_3)/\phi(\text{C}_2\text{H}_2)$, are the same within the experimental error. This indicates that no significant fraction of the vinyl radicals (*i.e.*, not more than 10%) could have been used up to form some other (unobserved) products. The ratio $\phi(\text{C}_2\text{H}_5)/\phi(\text{C}_2\text{H}_2) = 0.029$ represents the ratio of the quantum yield of reaction 3 to that of reaction 6, *i.e.*, of the free radical to the

molecular decomposition of liquid ethylene photolyzed at -160° .

In our gas-phase photolysis of ethylene at 184.9 nm, the ratio of the yield of reaction 3 to that of reaction 6 is estimated to be approximately unity. This value could be compared with 1.8, 1.0, and 0.97 obtained, respectively,¹¹⁻¹³ at 123.6 and 147.0 nm, and by flash photolysis in the 155–190-nm region.

The smaller ratio of the yields of reaction 3 to 6 in liquid phase than in the gas phase could be explained by assuming a more efficient dissipation of excess energy in the liquid phase.

Acknowledgment. The authors are grateful to R. F. Potte, R. Ironside, and R. S. Irwin for performing several mass spectrometric, infrared, and gas chromatographic analyses.

References and Notes

- Issued as NRCC No. 14024.
- (a) R. J. Cvetanović, *Progr. React. Kinet.*, **2**, 40 (1964); (b) R. J. Cvetanović and A. B. Callear, *J. Chem. Phys.*, **23**, 1182 (1955); A. B. Callear and R. J. Cvetanović, *ibid.*, **24**, 873 (1956).
- D. W. Setser, D. W. Placzek, R. J. Cvetanović, and B. S. Rabinovitch, *Can. J. Chem.*, **40**, 2179 (1962).
- D. W. Setser, B. S. Rabinovitch, and D. W. Placzek, *J. Amer. Chem. Soc.*, **85**, 862 (1963).
- S. Tsunashima, S. Hirokami, and S. Sato, *Can. J. Chem.*, **46**, 995 (1968).
- H. E. Hunziker, *J. Chem. Phys.*, **50**, 1288 (1969).
- T. Terao, S. Hirokami, S. Sato, and R. J. Cvetanović, *Can. J. Chem.*, **44**, 2173 (1966).
- S. Hirokami and S. Sato, *Can. J. Chem.*, **45**, 3181 (1967).
- R. B. Cundall and A. S. Davies, *Trans. Faraday Soc.*, **62**, 1151 (1966).
- J. P. Chesick, *J. Amer. Chem. Soc.*, **85**, 3718 (1963).
- M. C. Sauer and L. M. Dorfman, *J. Chem. Phys.*, **35**, 497 (1961).
- H. Okabe and J. R. McNesby, *J. Chem. Phys.*, **36**, 601 (1962).
- R. A. Back and D. W. L. Griffiths, *J. Chem. Phys.*, **46**, 4839 (1967).
- E. Tschuikow-Roux, J. R. McNesby, W. M. Jackson, and J. L. Faris, *J. Phys. Chem.*, **71**, 1531 (1967).
- R. Gordon, Jr., and P. Ausloos, *J. Res. Nat. Bur. Stand., Sect. A*, **75**, 141 (1971).
- H. Yamazaki and R. J. Cvetanović, *J. Amer. Chem. Soc.*, **91**, 520 (1969).
- S. Hirokami and R. J. Cvetanović, *Can. J. Chem.*, **51**, 373 (1973).
- R. J. Cvetanović and L. C. Doyle, *J. Chem. Phys.*, **37**, 543 (1962).
- R. L. Arnett and B. L. Crawford, Jr., *J. Chem. Phys.*, **18**, 118 (1950).
- P. G. Wilkinson and R. S. Muliken, *J. Chem. Phys.*, **23**, 1895 (1955).
- E. A. Moelwyn-Hughes, "Chemical Statics and Kinetics of Solutions," Academic Press, London, 1971, p. 118.
- N. S. Rudenko and L. W. Schubinikow, *Phys. Z. Sowjetunion*, **6**, 470 (1934).
- R. C. Woodworth and P. S. Skell, *J. Amer. Chem. Soc.*, **81**, 3383 (1959).
- W. von E. Doering and H. Prinzbach, *Tetrahedron*, **6**, 24 (1959).
- D. F. Ring and B. S. Rabinovitch, *Int. J. Chem. Kinet.*, **1**, 11 (1969).
- (a) H. M. Frey, *J. Chem. Soc.*, 2293 (1962); (b) H. M. Frey and I. D. R. Stevens, *J. Chem. Soc.*, 1700 (1965).
- D. P. Chong and G. B. Kistiakowsky, *J. Phys. Chem.*, **68**, 1793 (1964).
- A. W. Tickner and D. J. Le Roy, *J. Chem. Phys.*, **19**, 1247 (1951).
- N. A. Weir, *J. Chem. Soc.*, 6870 (1965).
- A. G. Sherwood and H. E. Gunning, *J. Phys. Chem.*, **69**, 2323 (1965).
- R. Sheldon and J. Kochi, *J. Amer. Chem. Soc.*, **92**, 4395 (1970).
- D. G. L. James and G. E. Troughton, *Trans. Faraday Soc.*, **62**, 145 (1966).

Positron Annihilation in Amino Acids and Proteins¹

S. Y. Chuang and S. J. Tao*

The New England Institute, Ridgefield, Connecticut 06877 (Received October 17, 1973;
Revised Manuscript Received April 10, 1974)

Publication costs assisted by the U. S. Atomic Energy Commission

The mean lives of positron annihilation in amino acids and proteins were carefully measured. The positron annihilation rate of the second (long) component λ_2 in an amino acid is found to be related to the number of strong polar groups or the number of oxygen atoms in its molecule. The nonpolar part of the molecule has less effect on the annihilation rate λ_2 than the polar part. This may roughly apply to proteins as well. The effect of the properties of amino acids and proteins on the values of I_2 and λ_1 is also discussed.

Introduction

When an energetic positron enters a medium, it will lose energy rapidly *via* collisions with the medium molecules. After the energy of the positron has reached the range of chemical energies, around 10 eV, it may capture an electron from a surrounding atom or molecule to form positronium (Ps), a bound state of the positron-electron pair, or it may annihilate directly with an electron in a free state. The positronium atom has two ground states. The singlet state with total spin zero is called *para*-positronium (*p*-Ps), and the triplet state with total spin one is

called *ortho*-positronium (*o*-Ps). In free space, *p*-Ps annihilates *via* 2γ decay with a mean life of 0.125 nsec while *o*-Ps undergoes 3γ annihilation with a mean life of 140 nsec. In common condensed media, the mean life of *o*-Ps is considerably reduced due to interaction with surrounding molecules since there is a chance for the positron in *o*-Ps to sense the electrons of opposite spin in the surrounding molecules and then annihilate *via* the faster 2γ annihilation. This is called pick-off quenching.

The two methods most often used in positron annihilation research are positron lifetime measurement and 2γ

TABLE I: Values of τ_1 , τ_2 , and I_2 for Common Amino Acids

Amino acids	τ_1 , nsec	τ_2 , nsec	I_2 , %
L-Alanine	0.300 ± 0.010	0.68 ± 0.03	30.3 ± 4.5
L-Arginine	0.331 ± 0.006	0.91 ± 0.02	43.2 ± 2.1
L-Aspartic acid	0.312 ± 0.004	1.12 ± 0.05	8.6 ± 1.0
L-Cysteine (HCl)	0.322 ± 0.004	1.07 ± 0.05	5.7 ± 0.9
L-Cystine	0.314 ± 0.004	1.15 ± 0.07	4.0 ± 0.8
L-Glutamic acid	0.294 ± 0.004	1.3 ± 0.1	3.3 ± 0.7
Glycine	0.271 ± 0.004	1.07 ± 0.05	5.3 ± 0.7
L-Histidine	0.356 ± 0.010	0.89 ± 0.04	27.6 ± 4.5
L-Hydroproline	0.285 ± 0.021	0.68 ± 0.03	41.6 ± 5.0
L-Isoleucine	0.324 ± 0.007	1.13 ± 0.03	25.3 ± 0.8
L-Leucine	0.300 ± 0.009	1.12 ± 0.02	41.7 ± 1.5
L-Lysine (HCl)	0.315 ± 0.004	0.99 ± 0.04	8.3 ± 1.1
L-Methionine	0.371 ± 0.004	1.42 ± 0.03	29.4 ± 1.2
L-Phenylalanine	0.338 ± 0.005	0.93 ± 0.02	22.0 ± 1.5
L-Proline	0.341 ± 0.006	0.86 ± 0.02	42.0 ± 2.0
L-Serine	0.240 ± 0.015	0.59 ± 0.02	57.0 ± 5.0
L-Threonine	0.322 ± 0.012	0.73 ± 0.03	26.2 ± 5.0
L-Tryptophan	0.363 ± 0.006	1.13 ± 0.02	24.4 ± 1.5
L-Tyrosine	0.367 ± 0.004	1.19 ± 0.02	13.8 ± 1.1
L-Valine	0.316 ± 0.006	0.98 ± 0.02	21.9 ± 1.6

angular correlation of annihilating positron-electron pairs. The annihilation rate or its inverse, the mean life, can be measured using ^{22}Na as the positron source. In general, the lifetime spectra of positrons in molecular substances consist of two lifetime components. The short mean life τ_1 is due to the self-annihilation of *p*-Ps and the direct annihilation of free positrons. The long mean life τ_2 with a relative intensity I_2 is attributed to the pick-off quenching annihilation of *o*-Ps. However, in certain molecular crystalline substances, the long lifetime component may be due to the annihilation of free positrons.²

From the angular correlation curve the momentum of the electrons annihilating with positrons can be determined. The annihilation of *p*-Ps atoms appears as a sharp narrow peak in the angular correlation curve on the top of the broader bell-type curve due to the annihilation of free positrons and pick-off of *o*-Ps.

For a general discussion of the annihilation of positrons and positronium and the techniques used, one is referred to some general review articles.^{3,4}

Recently, it has been shown that in organic liquid media the pick-off quenching rate is not only related to the properties, such as surface tension of the medium,⁵ but the pick-off quenching rate is also an additive property of the functional groups of the molecule of the medium⁶ and related to the value of "parachor" of the compound.⁷ These relationships clearly imply that the pick-off rate is related to the intermolecular forces exerted on the *o*-Ps. It is reasonable to infer that this also applies to the free-positron annihilation rate.

Positron and positronium annihilation has also been used to study the structure of macromolecular substances, such as the glass transition of polymers^{8,9} and other phase transitions.¹⁰ Even the possibility of investigating the structure of muscle has been explored.¹¹ This paper briefly reports our positron lifetime measurements of common amino acids and several common proteins.

Experimental Section

All the samples used in this experiment were obtained from Nutritional Biochemicals Corp. The purest possible forms of the compounds available at a reasonable price were used. L-Cysteine and L-lysine were obtained as HCl salts. No further purification was made. The samples were

degassed under 10^{-4} Torr for about 24 hr before the lifetime measurements were made. All the measurements were at room temperature 22°. All the samples were in solid form.

A conventional type of positron lifetime measuring apparatus was used for this work. A pair of RCA-8575 photomultipliers coupled with Naton 136 scintillators were employed as detectors. The resolution of the time-to-amplitude converter used for the lifetime measurement was 400 psec or slightly better. The positron source was approximately 10 μCi of ^{22}Na deposited on a very thin (<2 mg/cm²) sheet of mica.

Results

The positron annihilation lifetime spectra obtained were analyzed by our standard method.¹² A simple two-exponential component curve fit was used.

The annihilation mean life of the first component τ_1 , the annihilation mean life of the second component τ_2 , and the intensity of the second component I_2 are the resultant output after the data reduction. The values of τ_1 , τ_2 , and I_2 for common amino acids are summarized in Table I. The values of τ_1 , τ_2 , and I_2 for some DL-amino acids and a couple of other compounds are summarized in Table II. The values of τ_1 , τ_2 , and I_2 for some common proteins and a few other compounds such as RNA and DNA are summarized in Table III.

Discussion

A. Amino Acids. 1. τ_1 , τ_2 , and the Properties of Amino Acids. We shall disregard the common amino acids for which the intensity I_2 is less than 10% because of complications arising from the nature of the annihilation processes and data reduction. Then for the remaining 14 amino acids, the annihilation mean life of the second component τ_2 is found to be related to the number of strong polar groups in the molecule of the amino acid. Or quantitatively, the annihilation rate λ_2 ($1/\tau_2$) in these amino acids is found to follow roughly the simple relationship

$$\lambda_2 = 0.4 + 2.80(N_a/N_t) \quad (1)$$

as shown in Figure 1, where N_a is the number of oxygen

TABLE II: Values of τ_1 , τ_2 , and I_2 for Some DL-Amino Acids and Other Compounds

Compound	τ_1 , nsec	τ_2 , nsec	I_2 , %
DL-Alanine	0.317 ± 0.007	0.89 ± 0.03	23.2 ± 2.5
DL-Aspartic acid	0.324 ± 0.003	0.98 ± 0.03	9.9 ± 0.9
DL-Isoleucine	0.320 ± 0.010	1.18 ± 0.02	43.7 ± 2.0
DL-Leucine	0.347 ± 0.006	1.22 ± 0.01	42.3 ± 1.7
DL-Methionine	0.322 ± 0.003	1.34 ± 0.01	32.7 ± 0.6
DL-Phenylalanine	0.360 ± 0.004	1.05 ± 0.01	36.8 ± 1.2
DL-Serine	0.334 ± 0.005	0.92 ± 0.05	18.1 ± 3.6
DL-Threonine	0.336 ± 0.008	0.86 ± 0.03	27.1 ± 2.9
DL-Tryptophane	0.372 ± 0.005	1.32 ± 0.05	22.7 ± 1.5
DL-Valine	0.324 ± 0.006	0.95 ± 0.01	33.1 ± 1.5
β -Alanine	0.348 ± 0.005	1.00 ± 0.02	18.9 ± 1.5
Glycineglycine	0.340 ± 0.009	0.76 ± 0.02	22.3 ± 3.0
D-Ribose	0.330 ± 0.010	0.81 ± 0.03	34.9 ± 5.1

TABLE III: Values of τ_1 , τ_2 , and I_2 for Some Common Proteins^a

Protein	τ_1 , nsec (measured)	τ_2 , nsec		I_2 , %	
		Measured	Calcd	Measured	Calcd
Casein	0.354 ± 0.005	1.58 ± 0.02	0.96	28.4 ± 0.8	23.4
Collagin	0.354 ± 0.005	1.43 ± 0.02	0.89	25.9 ± 1.0	21.7
Fibrin (bovine)	0.357 ± 0.005	1.62 ± 0.02	0.87	24.4 ± 0.7	24.1
Gelatin	0.346 ± 0.006	1.33 ± 0.02	0.88	24.6 ± 1.3	22.0
Gluten	0.373 ± 0.004	1.61 ± 0.02	1.19	24.9 ± 0.7	19.8
Hemoglobin (bovine)	0.369 ± 0.004	1.57 ± 0.03	0.96	13.1 ± 0.8	24.7
Keratin	0.366 ± 0.004	1.66 ± 0.03	0.95	14.8 ± 0.6	21.3
Lactalbumin	0.365 ± 0.008	1.68 ± 0.03	0.98	23.1 ± 1.4	21.3
Pepsin (3X)	0.361 ± 0.005	1.58 ± 0.02	1.02	23.4 ± 0.9	13.2
Zein	0.379 ± 0.004	1.93 ± 0.02	0.92	25.7 ± 0.8	26.4
Trypsin (1:300)	0.348 ± 0.005	1.35 ± 0.02		20.7 ± 1.0	
Hensin	0.353 ± 0.005	1.4 ± 0.3		2.5 ± 1.2	
RNA	0.353 ± 0.005	1.26 ± 0.04		11.8 ± 1.9	
DNA	0.362 ± 0.004	1.34 ± 0.04		14.1 ± 1.3	

^a The amino acid compositions of the proteins for the calculation were obtained from ref 13. The values of τ_2 and I_2 for lysine (HCl) instead of pure lysine were used. The error involved from this substitution should be quite small.

atoms in molecules of neutral amino acids or the number of oxygen atoms in basic amino acids plus one, N_t is the total number of atoms except hydrogen in a molecule, and λ_2 is in units of nsec^{-1} .

We shall briefly show that the above relationship is due to the fact that the annihilation rate λ_2 is an additive property of the function groups of the molecule. If the annihilation rate λ_2 is an additive property of the function groups of the molecule, we have the general formula

$$\lambda_2 = \left(\sum_i \alpha_i n_i \right) / V_m \quad (2)$$

where n_i and α_i are the number and the reduced partial annihilation rate of the i th functional group in the molecule, respectively, and V_m is the molar volume of the compound. If we assume $V_m \propto N_t$, we obtain

$$\lambda_2 = \left(\sum_i \beta_i n_i \right) / N_t \quad (3)$$

where β is the partial annihilation rate. After an inspection of (3) one can easily see that eq 1 is a special case of (3).

Equation 1 indicates that the partial annihilation rates for CH_3 , $\text{CH}_2=$, $\text{CH}\equiv$, and nonbasic $\text{NH}=\text{}$ groups are approximately the same, 0.4 nsec^{-1} , and the partial annihilation rates for $\text{CO}=\text{}$ and $-\text{OH}$ are approximately 2.8 nsec^{-1} . This is quite different from the results for pick-off quenching of o -Ps in liquids where these partial quenching rates vary very little.⁶

Using a similar argument one can deduce that the partial annihilation rates for $\text{S}=\text{}$ or $\text{SH}=\text{}$ are much lower than the others. Since we have only the values of 14 amino

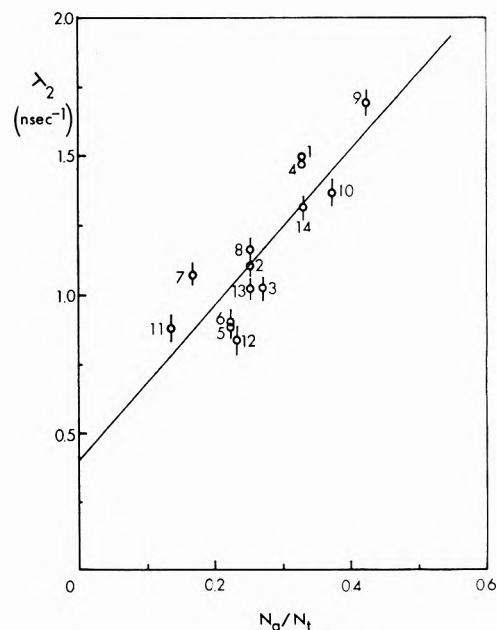


Figure 1. The relationship between the annihilation rate λ_2 and the ratio N_a/N_t for amino acids: 1, L-alanine; 2, L-arginine; 3, L-histidine; 4, L-hydroproline; 5, L-isoleucine; 6, L-leucine; 7, L-phenylalanine; 8, L-proline; 9, L-serine; 10, L-threonine; 11, L-tryptophan; 12, L-tyrosine; 13, L-valine; 14, glycylglycine.

acids we shall not attempt to calculate the partial annihilation rates for all the functional groups involved.

The values of the annihilation rates of the first component λ_1 are found to increase with the value of λ_2 . This re-

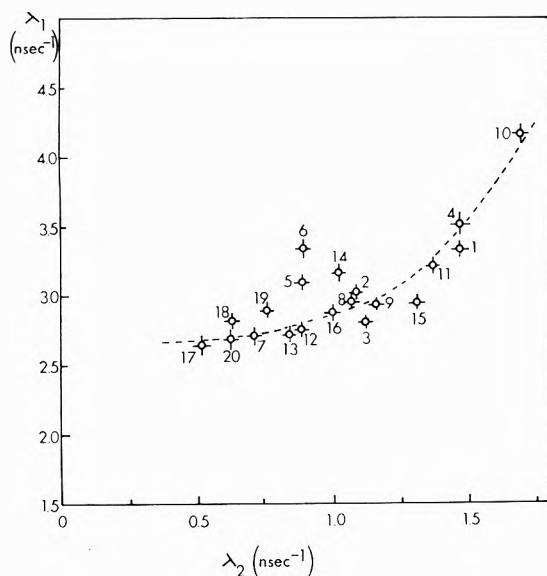


Figure 2. The relationship between the annihilation rates, λ_1 and λ_2 , for amino acids and proteins: 1, L-alanine; 2, L-arginine; 3, L-histidine; 4, L-hydroproline; 5, L-isoleucine; 6, L-leucine; 7, L-methionine; 8, L-phenylalanine; 9, L-proline; 10, L-serine; 11, L-threonine; 12, L-tryptophan; 13, L-tyrosine; 14, L-valine; 15, glycylglycine; 16, β -alanine; 17, zein; 18, casein; 19, gelatin; 20, gluten.

relationship can be easily visualized by inspecting Figure 2. It is interesting that in a substance where the annihilation rate λ_2 is low, the annihilation rate λ_1 approaches 2.5 nsec^{-1} . For DL-amino acids the values of τ_1 , τ_2 , and I_2 are found to be very close to the values of those for L-amino acids.

2. I_2 and the Properties of Amino Acids. After a thorough search no systematic relationship can be found between I_2 and many properties of amino acids. However, we have found some relationship between I_2 and the value of the isoelectric point, pI , as shown in Figure 3. For basic amino acids the values of I_2 are around 30%; for acidic amino acids the values of I_2 are very low, nearly negligible. For neutral amino acids, which have pI values in the range of 6 to 7, the values of I_2 scatter widely.

B. Proteins. The positron annihilation mean lives in common proteins vary within limited ranges. The values of τ_1 vary from 0.35 to 0.38 nsec and the values of τ_2 vary from 1.4 to 1.9 nsec . The values of the intensity I_2 range from 21 to 28% except for those of hemoglobin and keratin.

The values of τ_2 and I_2 as well as τ_1 for a protein are not found to be additive properties of individual amino acids in the protein. If we consider proteins as condensation polymers of amino acids, neglect the water produced during condensation, and treat the values of $\lambda_1 = 1/\tau_1$, $\lambda_2 = 1/\tau_2$, and I_2 as additive properties of the composition of proteins, the values of τ_1 , τ_2 , and I_2 for a protein can be calculated from the values of τ_1 , τ_2 , and I_2 for individual amino acids, provided the amino acid composition of the protein is known.

$$(1/\tau) = \frac{\sum_i (I_i P_i / \tau_i)}{\sum_i (I_i P_i)} \quad (4)$$

and

$$I = \frac{\sum_i (I_i P_i)}{\sum_i (P_i)} \quad (5)$$

where I_i is the intensity of the component for the i th

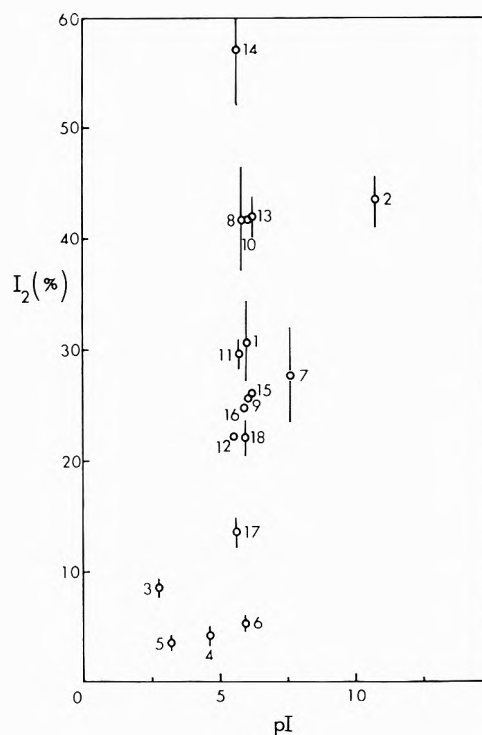


Figure 3. The relationship between the intensity I_2 and the pI value of amino acids: 1, L-alanine; 2, L-arginine; 3, L-aspartic acid; 4, L-cystine; 5, L-glutamic acid; 6, glycine; 7, L-histidine; 8, L-hydroxyproline; 9, L-isoleucine; 10, L-leucine; 11, L-methionine; 12, L-phenylalanine; 13, L-proline; 14, L-serine; 15, L-threonine; 16, L-tryptophan; 17, L-tyrosine; 18, L-valine.

amino acid, τ_1 is the mean life of the component for the i th amino acid and P_i is the fraction of the i th amino acid in the protein. Values of τ_2 and I_2 calculated in this manner are shown with the measured values in Table III. The calculated values are quite different from the measured values.

Actually, we should treat protein as a polymer or a macromolecule. As mentioned before, the positron annihilation rate λ_2 is related to the number of oxygen atoms in an amino acid molecule. The oxygen atoms form the polar part of the molecule of an amino acid. From eq 1 we can see that the nonpolar part of the molecule of an amino acid tends to have less effect on the pick-off quenching of o -Ps than that of the polar part. The peptide link, $-\text{C}-\text{N}-$, if it is not nonpolar, certainly is much less polar than the free amine and carboxyl groups in an amino acid. Besides, the solid structure of protein macromolecules certainly is different from the solid structure of short chain amino acids. Therefore, the mean life τ_2 and its intensity I_2 in a protein composed of common amino acids should be in the same range as those of a polymer with $-\text{C}-\text{N}-$ links, such as Nylon 6, which has a meanlife of 1.6 nsec .^{14,15} The values for the ratio N_a/N_l using eq 1 and the values of τ_2 are calculated to be between 0.05 and 0.15 for the proteins studied. The actual values of N_a/N_l for these proteins based on their composition are calculated to be between 0.17 and 0.20. A possible explanation for the difference may be that the polar groups in proteins are more or less neutralized by hydrogen bonding.

Conclusions

The annihilation rate of the second (long) component λ_2 in an amino acid is found to have an empirical relation-

ship with the number of atoms which form the strong polar groups or the number of oxygen atoms and carbon atoms in the molecule. This implies that the annihilation rate λ_2 is an additive property of the functional group of the molecules of the amino acid. The highly polar functional groups with oxygen atoms in the molecule tend to reduce the meanlife τ_2 more than the less polar part. The change of the values of λ_1 is found to follow with the change of the values of λ_2 . Probably, the same relationship also applies to λ_1 .

The intensity I_2 is found to be somewhat related to the isoionic point pI . However, the wide range of I_2 , 5 to 57%, for neutral amino acids with pI around 6 is a puzzle. Further study is required.

At present we are not sure whether the second component in the positron annihilation lifetime spectrum is due to the annihilation of *ortho*-positronium or free positrons. An experiment using the method of 2γ angular correlation is planned for the near future in order to clarify this point. However, it is interesting to find that positron annihilation in amino acids and possibly in proteins does follow a certain pattern. Further research should be undertaken in this area.

References and Notes

- (1) Work partially supported by USAEC.
- (2) G. DeBlonde, S. Y. Chuang, B. G. Hogg, D. P. Kerr, and D. M. Miller, *Can. J. Phys.*, **50**, 1619 (1972).
- (3) (a) V. I. Goldanskii, *At. Energy Rev.*, **6**, 3 (1968); (b) J. A. Merrigan, J. H. Green, and S. J. Tao, "Methods of Chemistry," Vol. 1, Part IIID, A. Weissberger and B. W. Rossiter, Ed., Wiley, New York, N. Y., 1972.
- (4) "Positron Annihilation" (Proceedings of the First International Positron Annihilation Conference, Detroit, Mich., 1965), A. T. Stewart and L. O. Roellig, Ed., Academic Press, New York, N. Y., 1967.
- (5) S. J. Tao, *J. Chem. Phys.*, **56**, 5499 (1972).
- (6) P. R. Gray, C. F. Cook, and G. P. Sturm, *J. Chem. Phys.*, **48**, 1145 (1968).
- (7) B. Levay, A. Vertes, and P. Hartojarvi, *J. Phys. Chem.*, in press; for the definition of "parachor," the reader is referred to J. R. Partington, "A Treatise on Physical Chemistry," Vol. II, Longmans, Green and Co., New York, N. Y., 1955.
- (8) J. R. Stevens and A. C. Mao, *J. Appl. Phys.*, **41**, 4273 (1970).
- (9) S. Y. Chuang, S. J. Tao, and J. M. Wilkenfeld, *J. Appl. Phys.*, **43**, 737 (1972).
- (10) S. Y. Chuang and S. J. Tao, *Material Res. Bull.*, in press.
- (11) D. R. Gustafson, *Biophys. J.*, **10**, 316 (1970).
- (12) S. J. Tao, *IEEE, NS-15*, **1**, 175 (1968).
- (13) R. J. Block, D. Bolling, and C. C. Thomas, "The Amino Acid Composition of Protein and Foods (Analytical Methods and Results)," Springfield, New York, N. Y., 1951; S. W. Fox and J. F. Foster, "Introduction to Protein Chemistry," Wiley, New York, N. Y., 1957.
- (14) S. J. Tao and J. H. Green, *Proc. Phys. Soc.*, **85**, 463 (1965).
- (15) S. Y. Chuang, S. J. Tao, and J. M. Wilkenfeld, *J. Appl. Phys.*, **43**, 737 (1972).

The Rate of the Photochemical Reaction of a Thin Powdered Layer

E. L. Simmons

Department of Chemistry, University of Natal, Durban, South Africa (Received November 19, 1973)

Publication costs assisted by the University of Natal

The rough-surfaced spherical-particle model for a powdered sample was used to derive an equation describing the rate of the photochemical reaction of a thin monoparticulate powdered layer. The equation obtained is in terms of the fundamental optical parameters. It was compared with a previously published result for the photochemical reaction of thin-layered powdered $K_3[Mn(C_2O_4)_3] \cdot 3H_2O$.

Introduction

A major problem encountered in the study of photochemical reactions of solid materials is the fact that diffusion of solid photoproducts is restricted and a concentration gradient is therefore created by the reaction. Hence, for solid samples, the variable of depth into the sample must be included in the equations describing the rate of the photochemical reaction. Equations describing the rate of the photochemical reaction of a solid with slab geometry have been derived.¹⁻³ These equations are, in general, applicable for determining the quantum yield of a solid photochemical reaction. However, many solids are most conveniently obtained in the form of a powder. Equations which involve empirical or functional absorption coefficients have been derived which describe the rate of the photochemical reaction of a powdered layer.^{4,5} In one of the treatments⁴ the powdered layer was considered thick enough that no light was transmitted by the layer. In the

other treatment,⁵ the problem of the creation of a concentration gradient was circumvented by considering the layer thin enough and hence absorption by the sample sufficiently low that the radiation intensity remained essentially constant throughout the layer. The equations obtained by both treatments were applied experimentally for the purpose of determining quantum yields.

In this investigation, a more rigorous derivation of the equation describing the photochemical reaction of a thin powdered sample was carried out. An equation was obtained in terms of the fundamental optical parameters, the absorption coefficient, and the index of refraction, by the use of a model representing a powdered sample as a collection of rough-surfaced spherical particles.⁶⁻⁸ The equation was compared with that obtained⁵ using empirical absorption coefficients and was compared with an experimental result for the photochemical reaction of thin layers of powdered $K_3[Mn(C_2O_4)_3] \cdot 3H_2O$.

Theoretical Considerations

Consider a single particle layer of a powdered sample made up of rough-surfaced spherical particles of uniform diameter, d . (The assumption of uniformly sized diameters is for convenience. It is shown in the Appendix that the assumption is unnecessary.) The layer is illuminated with perpendicularly incident monochromatic radiation of intensity, I . The sample is a substance, C, which reacts photochemically to give product, P



The rate of change of the number of moles, N , of C in a particle due to photochemical reaction is given by

$$dN/dt = -A\phi I\pi d^2/4 \quad (2)$$

where A is the fraction of incident light absorbed by the reactant, C, in the particle, ϕ the quantum yield, and $I\pi d^2/4$ the number of einsteins per second impinging on the particle.

The rate equation can be expressed in terms of the number of moles of C per unit area of the layer by the use of the following equation

$$[C] = mN/Z \quad (3)$$

where $[C]$ is the concentration of C in mole cm^{-2} , m the total number of particles in the layer, and Z the surface area of the layer. Combining eq 2 and 3 gives

$$d[C]/dt = -mA\phi I\pi d^2/4Z \quad (4)$$

The expression for A in terms of the fundamental optical parameters is obtained in a manner similar to that previously used^{6,7} the difference being that, in this case, there are two absorbing species, C and P, in the sample.

In this derivation the previously defined⁶ parameters, \bar{m}_e and \bar{m}_i , are used, \bar{m}_e being the fraction of the radiation impinging on the surface of a particle externally which is reflected and \bar{m}_i the fraction of the radiation impinging on the surface of a particle internally which is reflected. (It is assumed that for a monoparticulate layer, the fraction of light reflected onto a particle from other particles is small compared with I). The parameters, \bar{m}_e and \bar{m}_i , are related to the index of refraction of the particles.⁶ The fraction, $1 - \bar{m}_e$, of the radiation impinging externally on a particle enters the interior of the particle. It then travels an average distance of $2d/3$ before again encountering the particle surface.⁷ During the passage across the particle the fraction, $1 - a$, of the radiation is absorbed while the fraction, $1 - a_c$, is absorbed by the reactant, C. For small extents of reaction, the parameters, a and a_c , are given by the Lambert equation

$$a = \exp(-k_c N 2d/3N_0 - k_p N_p 2d/3N_0) \quad (5)$$

and

$$a_c = \exp(-k_c N 2d/3N_0) \quad (6)$$

where k_c is the absorption coefficient of C, k_p the absorption coefficient of P, N_0 the number of moles in a particle of pure C, and N_p the number of moles of product P in the particle

$$N_p = N_0 - N \quad (7)$$

On reaching the particle surface after the first passage across the particle, the fraction, \bar{m}_i , of the radiation is internally reflected back into the particle while the remainder passes from the interior of the particle. There are an infinite number of such internal reflections and passages

across the particle and therefore the fraction of the radiation absorbed by C is the sum of the fraction absorbed by C on each passage

$$A = (1 - \bar{m}_e)(1 - a_c) + \bar{m}_i a(1 - a_c) + \bar{m}_i^2 a^2(1 - a_c) + \dots \quad (8)$$

or

$$A = (1 - \bar{m}_e)(1 - a_c) \sum_{j=0}^{\infty} (\bar{m}_i a)^j \quad (9)$$

which converges to give

$$A = (1 - \bar{m}_e)(1 - a_c)/(1 - \bar{m}_i a) \quad (10)$$

combining eq 5, 6, and 10 gives

$$A = \frac{(1 - \bar{m}_e)[1 - \exp(-2k_c N d/3N_0)]}{[1 - \bar{m}_i \exp(-2k_c N d/3N_0 - 2k_p N_p d/3N_0)]} \quad (11)$$

Equations 4 and 11 relate this rate of the photochemical reaction of a thin powdered layer to the fundamental optical parameters.

The use of the rough-surfaced spherical particle model is only valid for weakly absorbing powdered samples. Also, the assumption that the radiation intensity remains constant throughout the layer is valid only if the layer is weakly absorbing. Equation 11 may be greatly simplified for weakly absorbing layers. For such layers, a and a_c are near unity so that

$$1 - \bar{m}_i a \cong 1 - \bar{m}_i \quad (12)$$

and

$$1 - a_0 = 1 - \exp(-2k_c N d/3N_0) \quad (13)$$

$$\cong 2k_c N d/3N_0 \quad (14)$$

Hence

$$A = (2k_0 N d/3N_0)(1 - \bar{m}_e)/(1 - \bar{m}_i) \quad (15)$$

It has previously been shown⁷ that

$$n^2 = (1 - \bar{m}_e)/(1 - \bar{m}_i) \quad (16)$$

where n is the relative index of refraction. Combining eq 4, 15, and 16 gives

$$d[C]/dt = -m\phi I\pi d^3 k_c N n^2/6N_0 Z \quad (17)$$

Combining eq 3 with eq 17 gives

$$d[C]/dt = -\phi I[C]\pi k_c d^3 n^2/6N_0 \quad (18)$$

The number of moles of C in a particle of pure C is given by

$$N_0 = \rho\pi d^3/6M \quad (19)$$

where ρ is the density of pure C and M the molecular mass of C. Hence, eq 18 becomes

$$d[C]/dt = -\phi I[C]k_c n^2 M/\rho \quad (20)$$

The rate equation is most conveniently expressed in terms of the molar absorption coefficient, ϵ (in cm^2/mol), given by

$$\epsilon = k_c M/\rho \quad (21)$$

Combining eq 20 and 21 gives

$$d[C]/dt = -\phi\epsilon n^2 I[C] \quad (22)$$

The rate expression for a thin weakly absorbing powdered sample is very simple in form and is independent of the particle diameter. The assumption has been included in the derivation of eq 22 that n is constant with time (that the index of refraction of the product does not differ greatly from that of the reactant).

Equation 22 can be integrated by making use of the condition that $[C] = [C_0]$ when $t = 0$ to give

$$[C] = [C_0]e^{-\phi I n^2 \epsilon t} \quad (23)$$

where $[C_0]$ is the concentration of C in pure C.

Comparison with Experiment

The equation previously derived for the photochemical reaction of a thin powdered layer is⁵

$$d[C]/dt = -\alpha \phi I [C] \quad (24)$$

where α is an empirical absorption coefficient. Comparing eq 22 and 24 shows that the empirical absorption coefficient is related to the fundamental optical parameters by

$$\alpha = \epsilon n^2 \quad (25)$$

Equation 24 was applied to the photochemical reaction of thin layers of $K_3[Mn(C_2O_4)_3] \cdot 3H_2O$ at 400 nm. The form of eq 24 was verified by the predicted linearity of experimental rate plots and by the determination of reasonable quantum yield values.⁵

The value of α for thin layers of $K_3[Mn(C_2O_4)_3] \cdot 3H_2O$ was found to be about $10^5 \text{ cm}^2 \text{ mol}^{-1}$ at 400 nm.⁵ In order to calculate theoretical values of α using eq 25, it is necessary to know values for ϵ and n and neither of these are known for solid $K_3[Mn(C_2O_4)_3] \cdot 3H_2O$ at 400 nm. However, an order of magnitude estimate can be made by making two assumptions. First, it is assumed that ϵ is independent of the state of the system and therefore the aqueous solution value of ϵ may be used. Second, it is assumed that n is within the range for index refraction values for most manganese compounds (1.3–2.3). The value of ϵ for $K_3[Mn(C_2O_4)_3] \cdot 3H_2O$ in aqueous solution at 400 nm has been found⁹ to be $5.1 \times 10^4 \text{ cm}^2 \text{ mol}^{-1}$. Hence, the theoretical value of α should lie between 8.7×10^4 and $2.7 \times 10^5 \text{ cm}^2 \text{ mol}^{-1}$. This is in very good order of magnitude agreement with the experimental value of $10^5 \text{ cm}^2 \text{ mol}^{-1}$.

Discussion

The form of eq 22 and the experimental applicability of the equation have previously been demonstrated.⁵ The main advantages of the application of the rough-surfaced spherical model to the photochemical problem are that the equations have been placed on a firmer theoretical basis and that the empirical absorption coefficient has been related to the fundamental optical parameters.

Equation 22 should prove useful for determining quantum yield values for solid-state photochemical reactions. Experimentally, the main problem is to ensure that the sample is thin enough that the radiation intensity remains approximately constant throughout the layer is valid. The sample particles need not be uniformly sized (see Appendix). Experimental determination of the sample reflectance and transmittance⁵ may be used to determine quan-

tum yield values or chemical analyses of the amount reacted as a function of time may be used.

The expression for the fraction of incident radiation absorbed by a particle, A, (eq 11) is valid only for rough-surfaced spherical particles and hence can only be applied to powdered samples which obey the Lambert cosine law. If a corresponding expression were derived for smooth-surfaced particles then the rate equations obtained in this investigation could perhaps be modified for single layers of biological cells or to layers of micells or vesicles.

Appendix

Effects of Nonuniform Particle Diameters. If the particles in the thin layer are not of uniform diameters, then the rate of reaction in the i th particle must be written as

$$dN_i/dt = A_i \phi I \pi d_i^2 / 4 \quad (A1)$$

The concentration of C (in mol/cm^2) in the layer is found by summing over all the particles

$$[C] = \sum_{i=1}^m N_i / Z \quad (A2)$$

The fraction of the radiation absorbed by the i th particle, A_i , is given by

$$A_i = 2k_c N_i d_i n^2 / 3N_{0i} \quad (A3)$$

Combining eq A1 and A3 gives

$$dN_i/dt = -\phi I \pi N_i d_i^2 n^2 / 6N_{0i} \quad (A4)$$

The total number of moles of C in pure C in the i th particle is given by

$$N_{0i} = \rho \pi d_i^3 / 6M \quad (A5)$$

Combining eq 21, A4, and A5 gives

$$dN_i/dt = -\phi I \epsilon n^2 N_i \quad (A6)$$

or, summing over all particles

$$\Sigma dN_i/dt = d \sum_{i=1}^m N_i/dt = -\phi I \epsilon n^2 \sum_{i=1}^m N_i \quad (A7)$$

Combining eq A2 and A7 gives

$$d[C]/dt = -\phi I \epsilon n^2 [C] \quad (A8)$$

which is identical with eq 22 obtained using the assumption that the particles are uniformly sized. Hence, eq 22 is valid for nonuniformly sized particles.

References and Notes

- (1) P. G. Barker, M. P. Halstead, and J. H. Purnell, *Trans. Faraday Soc.*, **65**, 2404 (1969).
- (2) H. Mauser, *Z. Naturforsch.*, **22b**, 569 (1967).
- (3) E. L. Simmons, *J. Phys. Chem.*, **75**, 588 (1971).
- (4) H. E. Spencer and M. W. Schmidt, *J. Phys. Chem.*, **74**, 3472 (1970).
- (5) E. L. Simmons and W. W. Wendlandt, *Anal. Chim. Acta.*, **53**, 81 (1971).
- (6) N. T. Melamed, *J. Appl. Phys.*, **34**, 560 (1963).
- (7) E. L. Simmons, *Opt. Acta.*, **18**, 59 (1971).
- (8) E. L. Simmons, *Opt. Acta.*, **19**, 845 (1972).
- (9) E. L. Simmons, Dissertation, Texas Tech. University, 1968.

Energetics of Formation of Some Structural Isomers of Gaseous $C_2H_5O^+$ and $C_2H_6N^+$ Ions

B. H. Solka and M. E. Russell*

Department of Chemistry, Northern Illinois University, DeKalb, Illinois 60115 (Received December 13, 1973)

Publication costs assisted by Northern Illinois University

Appearance potentials and heats of formation of a number of $C_2H_5O^+$ and $C_2H_6N^+$ ions have been determined. The 20 processes examined were chosen such that, based on the structure of the parent molecule, 4 isomers of $C_2H_5O^+$ and 5 isomers of $C_2H_6N^+$ would be formed. Thermochemical evidence was found which indicated that those processes expected to yield $CH_2CH_2OH^+$ and $CH_2CH_2NH_2^+$ involved rearrangements forming protonated ethylene oxide and protonated ethylenimine. The following heats of formation were obtained: $CH_3CH=OH^+$, 140 ± 1 kcal/mol; $CH_3O=CH_2^+$, 163 ± 1 kcal/mol; *c*- $C_2H_4OH^+$, 165 ± 2 kcal/mol; $CH_3CH_2O^+$, 198 ± 2 kcal/mol; $CH_3CH=NH_2^+$, 154 ± 4 kcal/mol; $CH_3NH=CH_2^+$, 154 ± 4 kcal/mol; *c*- $C_2H_4NH_2^+$, 173 ± 2 kcal/mol; $CH_3NCH_3^+$, 206 ± 4 kcal/mol. Data for $CH_3CH_2NH^+$ indicate a heat of formation on the order of 200 ± 10 kcal/mol but this is uncertain because of the possibility of rearrangement to $CH_3CH=NH_2^+$. Comments are made on the use of a double-focussing mass spectrometers electrostatic sector as a probe for excess ion kinetic energies and evidence found for the occurrence of a significant amount of excess energy in the formation of $CH_3NCH_3^+$ from *N,N*-dimethyl-*tert*-butylamine.

Introduction

The $C_2H_5O^+$ (m/e 45) ion is prominent in the mass spectra of many oxygen containing organic compounds. Consequently, a number of investigators have undertaken to demonstrate the occurrence of the various structural isomers of this ion. These studies have utilized the techniques of isotopic labeling,¹⁻³ metastable ion characteristics,⁴⁻⁶ ion-molecule reactions,⁷⁻⁹ and thermochemical properties.¹⁰⁻¹⁷ The isomers which have been considered, and previous determinations of their enthalpies of formation, are shown in Table I.

Evidence for the occurrence of isomers I, II, and III has been found in isotopic labeling and metastable ion experiments wherein I has been shown¹⁻⁴ to result from C-R (R = H, alkyl) bond cleavage in CH_3CHROH , II has been shown^{4,12} to be formed from C-R cleavage in CH_3OCH_2R , and III has been found²⁻⁴ to be formed *via* rearrangements in a number of compounds. Also, I and III have been generated in ion-molecule reaction studies *via* protonation of acetaldehyde and ethylene oxide, respectively.⁷⁻⁹ The energetic data for these isomers (Table I) seem to agree with the occurrence of three distinct species.

The enthalpy of formation of isomer I is well established, as Refaey and Chupka's¹⁰ photoionization appearance potential results for ethanol and 2-propanol are closely approached by electron impact studies.^{11,12}


Although electron impact appearance potential data¹¹⁻¹⁴ on the m/e 45 ion in dimethyl and methyl ethyl ethers agree fairly well as to the enthalpy of formation of isomer II, Haney and Franklin¹⁸ have observed excess translational energy in the m/e 45 ion from methyl ethyl ether and chloromethyl methyl ether which they feel could be the result of as much as 30 ± 10 kcal/mol excess energy in the threshold fragmentation. Subtracting this excess from the experimental enthalpies of formation would, within the combined uncertainties, give a value equal to that for isomer I. Haney and Franklin consider this to be evidence that threshold production of $C_2H_5O^+$ from

these molecules occurs *via* rearrangement instead of simple bond scission. However, Beauchamp and Dunbar⁷ and Blair and Harrison⁸ have found no evidence for any participation of I in the ion-molecule reactions of m/e 45 ions generated from methyl ethyl ether. Furthermore, in a recent study of kinetic energy release in metastable dissociations, Jones, *et al.*,¹⁵ have obtained evidence that the method of Haney and Franklin overestimates the excess energy term. In fact, for the metastable dissociation of chloromethyl methyl ether, Jones, *et al.*, find an excess energy δ term of only 5.5 kcal/mol. Using the appearance potential from ref 18, this yields $\Delta H_f(\text{isomer II}) = 155 \pm 10$ kcal/mol, a value equal to those of Table I within the combined uncertainties.

The problems of excess energy terms in appearance potential measurements, in the context of the quasiequilibrium theory of mass spectra,¹⁹ arise from two sources. First, instrumental factors such as sensitivity, sample temperature, ion source residence time, etc., will affect the accuracy with which the measured value approaches the true appearance potential. Second, chemical factors such as the extent of randomization of excess energy in the parent ion and the possibility of competing fragmentation pathways will also bear on the relationship between measured and true appearance potentials. Consequently, when agreement on a particular ion has been reached from several independent laboratories studying its formation *via* various processes, it is generally concluded that excess energy effects are probably small. Therefore, while the enthalpies of formation cited for isomer II in Table I must be considered upper bounds to the true value, the excess energy correction applied by Haney and Franklin appears to be too large.

Direct production of isomer III *via* fragmentation of some parent molecule is not possible so its enthalpy of formation cannot be measured by the appearance potential technique. However, Beauchamp and Dunbar⁷ have measured the proton affinity of ethylene oxide by brack-

TABLE I: C₂H₅O⁺ Structural Isomers and Their Heats of Formation

Isomer	Precursor	ΔH_f , kcal/mol (ref)
(I) CH ₃ CH=OH ⁺	CH ₃ CH ₂ OH (CH ₃) ₂ CHOH	141(10), 144(11,12) 142(10), 144(12)
(II) CH ₃ O=CH ₂ ⁺	CH ₃ OCH ₃ CH ₃ OCH ₂ Cl CH ₃ OCH ₂ CH ₃	158(11), 170(12), 167(13), 151(14) 155(15) 168(12)
(III) 	<i>a</i>	170(7)
(IV) ·CH ₂ CH ₂ OH ⁺	CH ₃ CH ₂ CH ₂ -OH	161(10), 164(16)
(V) CH ₃ CH ₂ O ⁺	(CH ₃ CH ₂) ₂ O ^b CH ₃ CH ₂ ONO	198(11), 187(12), 188(17) 192(17)

^a Value derived from proton affinity of ethylene oxide. ^b Assuming neutral to be C₂H₅ rather than H + C₂H₄.

eting its ICR proton transfer reactions with reagents of known proton affinity and calculating the enthalpy of formation of III. This approach is not subject to many of the uncertainties of threshold electron impact work and their value is probably reliable within their stated limits of ± 4 kcal/mol.

The occurrence of C₂H₅O⁺ isomers IV and V is much less certain than that of the other three isomers. Refaey and Chupka¹⁰ and Friedman, *et al.*,¹⁶ have measured the appearance potential of the C₂H₅O⁺ ion from 1-propanol, which, from the structure of the parent molecule, might be expected to be formed as IV. However the measured heat of formation seems to be quite low for the diradical structure which would be formed *via* ionization of one of the oxygen's lone-pair electrons and scission of the terminal carbon-carbon bond. From simple bonding considerations, ΔH_f for this isomer should be on the order of that for isomer V. Consequently, the energetic evidence does not necessarily lead to the conclusion that IV is formed in the fragmentation of normal alcohols.

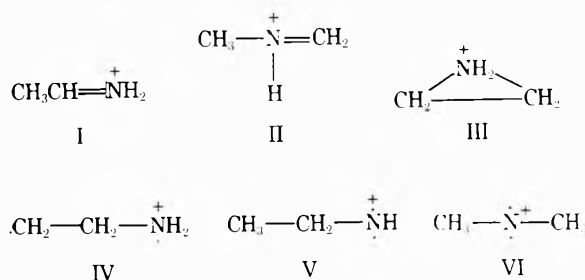
The energetic data for isomer V are in accord with the expectation that this structure should be less stable than I, II, or III. The ΔH_f cited for C₂H₅O⁺ from C₂H₅ONO is obtained from a reinterpretation of the ionization efficiency curve of Williams and Hamill¹⁷ in light of a recent determination of the electron affinity of NO.²⁰ Analysis of appearance potential data for *m/e* 45 ion production from (C₂H₅)₂O is clouded by the possibility of two fragmentation mechanisms. Formation of *m/e* 73 *via* loss of H α to the oxygen followed by elimination of ethylene through a four-centered transition state would result in the generation of C₂H₅O⁺ isomer I. Alternatively, simple C-O bond scission would generate isomer V with C₂H₅ as the neutral. The ΔH_f cited in Table I assumes the latter mechanism to be the threshold process, however, we have studied the formation of C₂H₅O⁺ from diethyl ether and have found the rearrangement (formation of isomer I) to be the favored pathway.²¹

Thus, it appears that at least four of the five possible structural isomers of C₂H₅O⁺ are formed in mass spectrometers and the thermochemical properties of these ions may be used as an indication of their structures.

However, this does not appear to be the case for the analogous sulfur containing ions. In appearance potential studies of a number of deuterium-labeled,²² and normal,²³ mercaptans and sulfides, it was found that the enthalpies

of formation of C₂H₅S⁺ isomers corresponding to I, II, and V in the oxygen system varied only slightly (from 3 to 8 kcal/mol) from one another. That is, given the precision of typical electron-impact work, it would not be possible to differentiate among the structural isomers of C₂H₅S⁺ by ion energetics alone.

The mass spectra of nitrogen-containing organic molecules often exhibit abundant C₂H₆N⁺ ions (*m/e* 44) which may exist as the structural isomers shown below.



Several studies²⁴⁻²⁸ have determined appearance potentials of *m/e* 44 ions from various parent molecules, but these results have been inconclusive regarding any relationship between the enthalpies of formation and the structures of the C₂H₆N⁺ isomers. As it is of some interest to determine whether the structures of these ions may, like those of the oxygen species, be elucidated by examination of their energetic properties, we have determined the appearance potentials of *m/e* 44 ions resulting from the fragmentation of a variety of amines which might be expected to yield five of the six possible structural isomers. Parent molecules were chosen so that each isomer might be formed by at least two different mechanisms. In addition, the kinetic energy of several fragment ions was measured relative to that of their respective parent ions in an attempt to detect the occurrence of an excess energy effect in those fragmentations.

We have also determined the appearance potentials of C₂H₅O⁺ ions from several parent molecules for comparison with previous work.

Experimental Section

A Hitachi Perkin-Elmer RMU-7 double-focussing mass spectrometer equipped with a Hitachi five electrode retarding potential difference (RPD) electron gun was used in this study.

The electron beam was generated by thermionic emission from a 0.15-mm rhenium filament and pulsed at 100 kHz. During a pulsing cycle, the electron beam and ion repeller electrode were each on for 4×10^{-6} sec with 1×10^{-6} sec dead time between pulses. The electron beam retarding potential was set to truncate the electron energy distribution at its maximum before each appearance potential determination and was usually -1.0 to -1.5 V with respect to the filament. A retarding potential difference of 0.05 or 0.10 V was used depending on the slope of the ionization efficiency curve near threshold. The electron target was maintained at zero potential with respect to the ionization chamber. Under these conditions, the total electron emission of 10.0×10^{-6} A, automatically regulated to $\pm 5 \times 10^{-9}$ A, resulted in a target current of about 10^{-7} A.

A heated sample inlet was used and maintained at 150°. The ion source temperature was maintained at 170°.

During appearance potential runs, the variable source, electrostatic sector, and collector slits were all maintained

at their maximum width of 1.00 mm. Ion currents were measured with a 10-stage Ag-Mg electron multiplier operated with a total potential drop across the dynodes of 2500 V. This was followed by a dc amplifier and the final signal was recorded on a strip-chart recorder.

The ion difference intensities were measured at 0.02- or 0.05-eV intervals up to 0.5 to 1.0 V above threshold. For those parent molecules whose ionization potentials have been determined by photoionization studies,^{10,29,30} the molecular ionization potential was used to calibrate the electron energy scale. In the remaining cases, the appearance potential of the ion of interest was determined, then ethanol was added, and its ionization potential measured for the calibration. This technique was checked with several molecules of known ionization potentials and found to give agreement within the deviation of replicate determinations. The onset potentials were evaluated by extrapolated voltage difference and semilog plots of the difference ion current as well as its vanishing point. Generally, from three to seven determinations were made of each appearance potential and each set of data evaluated by all three methods. The uncertainty cited for each appearance potential then represents the standard deviation of all values resulting from this treatment.

Instrumental performance was checked by periodically determining the appearance potential of $C_2H_5O^+$ from ethanol. Eight determinations made over a period of many months gave an appearance potential of 10.75 ± 0.03 eV, compared to the photoionization value¹⁰ of 10.78 ± 0.02 eV.

All samples used were commercially available and were purified by gas chromatography before use.

Results and Discussion

Energetics of $C_2H_5O^+$ Ion Formation. The threshold potentials for formation of $C_2H_5O^+$ obtained in this work are tabulated in Table II. In addition, Table II presents the presumed neutral fragments and the ionic enthalpy of formation calculated from the assigned process. Our values for ΔH_f° of isomers I, II, and V are in fair to excellent agreement with the values in Table I (as evaluated in the Introduction) and will not be discussed further. Isomers III and IV, however, do deserve further comment.

Generation of structure III by simple fragmentation from a stable parent molecule is not possible. However, the thermochemical evidence indicates that the threshold m/e 45 ions obtained from the RCH_2CH_2OH molecules studies here are formed as III. Simple bond scission from these parents would result in ions of the diradical structure IV, but the measured AP's appear to be much too low for this isomer. Using bond dissociation energies tabulated by Kerr,³¹ ΔH_f° of isomer IV may be estimated to be some 50 kcal/mol greater than isomer I, but the experimental values for m/e 45 from $CH_3CH_2CH_2OH$ and $BrCH_2CH_2OH$ are in agreement at 165 ± 1 kcal/mol, only 25 kcal/mol greater than isomer I. An alternative to the simple bond scission fragmentation is a rearrangement wherein, as the methyl group or bromine atom leaves, the oxygen, which bears an unpaired electron, binds to the β carbon in essentially a free-radical substitution reaction, generating isomer III. Thus, if this rearrangement described the threshold fragmentation of 1-propanol and 2-bromoethanol, our data yield a heat of formation of protonated ethylene oxide (III) of 165 ± 1 kcal/mol.

Beauchamp and Dunbar⁷ have found that the proton affinity of ethylene oxide is very nearly (± 4 kcal/mol)

TABLE II: Energetics of $C_2H_5O^+$ Ion Formation

Isomer	Parent	Neutral fragment	Appearance potential, eV	ΔH_f° (ion), ^a kcal/mol
I	CH_3CH_2OH	H	10.75 ± 0.03	140 ± 1
II	CH_3OCH_3	H	11.23 ± 0.04	163 ± 1
III	$CH_3CH_2CH_2OH$	CH_3	11.35 ± 0.04	165 ± 1
III	$BrCH_2CH_2OH$	Br	10.47 ± 0.05	166 ± 1
V	CH_3CH_2ONO	NO	10.62 ± 0.07	198 ± 2

^a ΔH_f° of neutrals taken from *Nat. Bur. Stand. Tech. Note, No. 270-3* (1968).

equal to that of acetaldehyde. Using a proton affinity of 183 kcal/mol for acetaldehyde they obtained ΔH_f° (III) of 170 ± 4 kcal/mol. We feel that the proton affinity of acetaldehyde is closer to 185 kcal/mol as indicated by ΔH_f° (I) (*vide supra*). Using this results in lowering the ICR value of ΔH_f° (III) to 168 ± 4 kcal/mol, a value in excellent agreement with those derived from the present appearance potentials.

The possibility remains that the heat of formation obtained here refers to isomers I or II with excess energy. Ion-molecule reaction studies^{7,8} have demonstrated clear differences between the chemical reactivity of isomers II and I or III and show that systems containing isomer III indicate no evidence of the participation of rearranged ions of structure II. Harrison and Blair⁶ have found that the apparent equilibrium constants for the proton transfer reactions of ions generated as I and III with dimethyl- d_6 ether differ by a factor of 6. This indicates that ions formed as isomer III probably do not rearrange to structure I. Recently Beauchamp and coworkers³² have found a clear difference in the reactivity of I and III with PH_3 furnishing further evidence that these are distinct isomers.

Thus, the energetics observed here strongly suggest that the threshold m/e 45 ions in 1-propanol and 2-bromoethanol are formed as isomer III and this interpretation is supported by the ion-molecule reaction characteristics of the $C_2H_5O^+$ isomers.

Energetics of $C_2H_6N^+$. The threshold potentials for formation of $C_2H_6N^+$ obtained in this work are tabulated in Table III and compared with previous results. The fragmentation processes chosen for the molecules listed are generally based on the presumption of simple fragmentation occurring at threshold. For several cases this presumption may be incorrect and these cases will be considered accordingly below.

Isomer I. The formation of isomer I from ethylamine by loss of an α hydrogen has been shown to occur in Collin's study of $CH_3CD_2NH_2$.³⁵ Our AP of 9.61 ± 0.09 eV leads to a ΔH_f° (I) equal to 158 ± 2 kcal/mol. The only literature value available for comparison to this is Collin's²⁴ early result of 210 kcal/mol.

By analogy with the oxygen compounds, it is expected that isomer I will also be formed by loss of CH_3 from isopropylamine. The present AP of 8.86 ± 0.05 eV leads to ΔH_f° (I) equal to 151 ± 1 kcal/mol in fair agreement with the result obtained from ethylamine. Again, the only literature result available for comparison is due to Collin:²⁴ 164 kcal/mol.

We note that Collin's result for isopropylamine is in much better agreement with the present work than that for ethylamine. This probably reflects differences in instrumental sensitivity because the ionization efficiency curve for m/e 44 from ethylamine approaches threshold with a much lower slope than for isopropylamine. Such behavior in ethylamine might be expected because thresh-

TABLE III: Energetics of C₂H₆N⁺ Formation

Isomer	Parent	Neutral fragment	Appearance potential, eV		$\Delta H_f(\text{ion})^a$ This work
			This work	Lit.	
I	CH ₃ CH ₂ NH ₂	H	9.61 ± 0.09	11.9 ± 0.2 ^c	158 ± 2
	(CH ₃) ₂ CHNH ₂	CH ₃	8.86 ± 0.05	9.4 ± 0.2 ^c	151 ± 1
II	(CH ₃) ₂ NH	H	9.41 ± 0.06	10.8 ± 0.2 ^c	160 ± 1
	CH ₃ CH ₂ NHCH ₃	CH ₃	8.49 ± 0.05		150 ± 1
III	CH ₃ (CH ₂) ₃ NHCH ₃	<i>i</i> -C ₃ H ₇	8.37 ± 0.06		152 ± 3
	CH ₃ (CH ₂) ₂ NH ₂	CH ₃	10.2 ± 0.3		184 ± 7
	CH ₃ (CH ₂) ₃ NH ₂	C ₂ H ₅	9.49 ± 0.09		172 ± 2
	CH ₃ (CH ₂) ₄ NH ₂	<i>i</i> -C ₃ H ₇	9.34 ± 0.10		171 ± 2
	(CH ₃) ₂ CH(CH ₂) ₂ NH ₂	<i>i</i> -C ₃ H ₇	9.59 ± 0.12		175 ± 2
V	(CH ₃ CH ₂) ₂ NH ^b	C ₂ H ₅	11.42 ± 0.05	13.65 ± 0.08 ^d	220 ± 1
	CH ₃ CH ₂ NHCHO ^b	HCO	9.7 ± 0.15		197 ± 3
VI	CH ₃ CH ₂ NH(CH ₂) ₃ CH ₃ ^b	<i>s</i> -C ₄ H ₉ (?)	8.61 ± 0.05		157 ± 1
	(CH ₃) ₃ N	CH ₃	10.68 ± 0.09	12.3, 11.7 ^e	206 ± 1
	(CH ₃) ₂ N(CH ₂) ₃ CH ₃ ^b	<i>s</i> -C ₄ H ₉	9.75 ± 0.10		190 ± 2
	(CH ₃) ₃ NC(CH ₃) ₃	<i>t</i> -C ₄ H ₉	10.96 ± 0.07		217 ± 1

^a ΔH_f of neutrals from ref 33 or estimated from ref 34. ^b May form isomer I or II; see text. ^c Reference 24. ^d Reference 28. ^e Reference 26.

old for the competing process forming CH₂NH₂⁺ is calculated (using Chupka's appearance potential for CH₂NH₂⁺ from propylamine¹⁹) to be about 0.3 eV lower than the threshold measured here for *m/e* 44 formation.

Averaging the present data, we conclude that ΔH_f for C₂H₆N isomer I is 154 ± 4 kcal/mol.

Isomer II. Three of the compounds studied here are expected to fragment to II, the simplest process being loss of H from dimethylamine. Our appearance potential of 9.41 ± 0.06 eV for *m/e* 44 from dimethylamine leads to $\Delta H_f(\text{II}) = 160 \pm 1$ kcal/mol, compared to Collin's value²⁴ of 210 kcal/mol.

Loss of CH₃ from methylethylamine could result in formation of either II or V. For the analogous case of methyl ethyl ether deuterium labeling¹² has shown that CH₃ loss forms C₂H₅O isomer II and we would expect a similar process here. Our appearance potential of 8.49 ± 0.05 leads to $\Delta H_f(m/e 44) = 150 \pm 1$ kcal/mol. This is in fair agreement with the result from dimethylamine and indicates that the presumably more stable isomer II is indeed formed.

Fragmentation of *N*-methyl-*n*-butylamine to form *m/e* 44 directly is confirmed in the 70-eV spectrum by observation of a metastable peak at *m/e* 22.3 (intensity 0.11% of base peak, calculated *m/e* 22.25 for *m/e* 87 → *m/e* 44). The measured threshold potential for *m/e* 44 of 8.37 ± 0.06 leads to a $\Delta H_f(m/e 44)$ of 151 ± 1 kcal/mol if *n*-C₃H₇ is assumed to be the neutral fragment, or to 154 ± 1 kcal/mol if *i*-C₃H₇ is the neutral fragment. This difference is on the order of the accuracy usually expected for electron impact and either value is within the range of values determined for isomer II from dimethylamine and methylethylamine. Hence, we shall take the $\Delta H_f(m/e 44)$ from *N*-methyl-*n*-butylamine to be 152 ± 3 kcal/mol, where the larger uncertainty represents the uncertainty in the identity of the neutral.

The average $\Delta H_f(m/e 44)$ for these three processes expected to yield isomer II is then 154 ± 4 kcal/mol.

Isomers III and IV. Results obtained for these C₂H₆N⁺ structures are directly analogous to those obtained for the C₂H₅O⁺ case. That is, the primary amines which might be expected to fragment to form IV have apparently cyclized to III.

For R-CH₂CH₂NH₂ (R = CH₃, CH₃CH₂, CH₃CH₂CH₂, and (CH₃)₂CH) β -carbon-carbon bond fission to form C₂H₆N⁺ should generate isomer IV, but the enthalpies of formation measured for *m/e* 44 from these compounds

(Table III) are too low for this diradical structure. With the exception of *n*-propylamine, the present results give a ΔH_f only some 20 kcal/mol less stable than isomer I, whereas bond energy³¹ considerations indicate that $\Delta H_f(\text{IV})$ should be about 40 kcal/mol less stable than I. The high result for propylamine probably reflects the interference of a lower energy competing fragmentation pathway. In the 70-eV mass spectra of each of these compounds *m/e* 30 (CH₂NH₂⁺) is the base peak and its calculated appearance potential (using $\Delta H_f(\text{CH}_2\text{NH}_2^+) = 169$ kcal/mol¹⁹) is less than that measured for *m/e* 44 in each case. While this difference is only 0.3 to 0.4 eV for butyl-, pentyl-, and isopentylamines, it is about 1.0 eV for propylamine. This implies that the measured appearance potential of *m/e* 44 from propylamine is probably unreliable. The average value for $\Delta H_f(m/e 44)$ from the other three compounds is 173 ± 2 kcal/mol. While no equivalent appearance potential data can be found in the literature for comparison to the present work, Bowers, *et al.*, have reported³⁶ a proton affinity of 220 ± 4 kcal/mol for ethylenimine, determined by ICR ion-molecule reaction studies. From this, ΔH_f of protonated ethylenimine can be calculated to be 176 ± 4 kcal/mol, a value in excellent agreement with the present appearance potential results and providing energetic evidence that the postulated rearrangement does occur.

Isomer V. The ion energetics observed for the three cases expected to generate V do not clearly establish its occurrence.

The formation of V from diethylamine would be analogous to production of C₂H₅O⁺ isomer V from diethyl ether. Simple bond scission at threshold to generate V plus C₂H₅ yields $\Delta H_f(\text{V}) = 220$ kcal/mol, but Collin and Franklin²⁸ have observed a metastable peak in the 70-eV spectrum diethylamine-*N-d* corresponding to formation of C₂H₅DN from (M - H)⁺. This indicates formation of *m/e* 44 via a two-step process, generating H and C₂H₄ as neutrals and C₂H₅DN as isomer I. If this describes threshold formation of *m/e* 44, its ΔH_f would be calculated to be 182 kcal/mol. This is rather high for I unless on the order of 1.5 eV excess energy was involved in the fragmentation.

The appearance potential of *m/e* 44 from *N*-ethylformamide yields $\Delta H_f(m/e 44) = 197 \pm 3$ kcal/mol if HCO is assumed to be the neutral. This mechanism of simple bond scission would generate *m/e* 44 as V. However, this system may be analogous to the production of C₂H₅O⁺ from ethylformate, in which deuterium labeling has

shown³⁷ that the formyl hydrogen is retained in some 65% of the m/e 45 ions. This indicates a two-step process involving successive loss of H and CO as neutrals, and generating $C_2H_5O^+$ isomer I. The same process is possible in the case of *N*-ethylformamide and, if it is assumed to be the process describing threshold formation of $C_2H_6N^+$, the appearance potential gives $\Delta H_f(I) = 158$ kcal/mol. This is in the range of values measured for this isomer, and the thermochemical evidence here does not permit us to distinguish between the two possible mechanisms.

N-Ethylbutylamine is a third compound which might be expected to form isomer V, but the energetics rather clearly indicate that rearrangement to either I or II occurs in the formation of m/e 44. The nature of this rearrangement is unclear. This molecule could undergo a two-step cyclic rearrangement to isomer I similar to that postulated for diethylamine²⁸ or diethyl ether but this is unlikely for two reasons; first, the 70-eV spectrum contains a metastable (m/e 19.2, $2 \times 10^{-3}\%$ base) corresponding to direct production of m/e 44 from the parent, and second, the two-step rearrangement would most likely generate H and a butene as neutrals. Assuming production of H and the most stable butene, the observed appearance potential leads to $\Delta H_f(m/e$ 44) equal to 122 kcal/mol. This is clearly too low to support the two-step rearrangement as the threshold mechanism.

Similarly, although weak metastables are found in the 70-eV spectrum indicating the sequence $M^+ \rightarrow m/e$ 58 $\rightarrow m/e$ 44, this would require generation of C_3H_7 and CH_2 as neutrals, leading to a $\Delta H_f(m/e$ 44) of 63 kcal/mol. Again, much too low to support such a threshold mechanism.

Thus, it appears that threshold formation of m/e 44 here occurs *via* a simple bond fission. The $\Delta H_f(m/e$ 44) will be 154, 157, or 164 kcal/mol depending on whether the neutral is formed as the *n*-, *sec*-, or *tert*-butyl radical. These values are too low to support formation as isomer V but are in the range of values measured for isomers I and II.

Isomer VI. Results obtained from three compounds expected to generate this isomer give fairly good evidence that it indeed is formed in at least two of the cases.

Trimethylamine rather unambiguously forms m/e 44 as VI by loss of CH_3 . Our appearance potential for this process is considerably lower than those of earlier work^{24,26} and leads to ΔH_f (isomer VI) equal to 206 ± 1 kcal/mol.

The appearance potential of m/e 44 in *N,N*-dimethylbutylamine gives $\Delta H_f(m/e$ 44) equal to 190 ± 2 kcal/mol if *sec*-butyl radical is assumed as the neutral. This may be in fair agreement with the value for VI from trimethylamine but this process is subject to the same rearrangement possibilities discussed for *N*-ethylbutylamine above. Here, loss of a methyl H, followed by loss of 1-butene through a four-membered transition state would form m/e 44 isomer II and the observed appearance potential, with these neutrals, leads to $\Delta H_f(m/e$ 44) equal to 153 kcal/mol. This is within the range of values obtained for isomer II and distinction between formation of II or VI cannot be made.

Finally, *N,N*-dimethyl-*tert*-butylamine will form VI by loss of *t*- C_4H_9 . The appearance potential here leads to $\Delta H_f(VI)$ equal to 217 ± 1 kcal/mol, a value about 10 kcal/mol higher than that obtained using trimethylamine. This is probably due to a requirement of excess energy for production of $C_2H_6N^+$ with *t*- C_4H_9 as the neutral. Lossing and Semeluk³⁸ have measured the ionization potential of the *t*- C_4H_9 radical to be 6.93 ± 0.05 eV and, although it

is not known, that of the CH_3NCH_3 radical is probably higher than this. Stevenson³⁹ has pointed out that in such a case formation of the $C_2H_6N^+$ ion will probably require excess energy.

Ion Kinetic Energies. We have measured the peaks of the kinetic energy distributions for several of the parent-daughter ion pairs studied by closing the β slit to less than 0.05 mm and changing the ion accelerating voltage in 0.010 V increments (measured with a Hewlett-Packard Model 3460B digital voltmeter across a 1:500 voltage divider). The peak in the parent ion distribution represents the energy for ions formed with no "excess" translational energy and if the daughter ion is formed without excess translational energy, its kinetic energy distribution should peak at the same accelerating voltage as the parent ions. On the other hand, if the daughter is formed with excess translational energy, it will require less accelerating voltage to be passed by the electrostatic sector and this difference, followed by conversion to center-of-mass coordinates, provides a measure of the excess internal energy in the dissociating parent ion. By making these measurements as a function of ionizing electron energy near threshold one might be able to detect any contribution of excess energy to the appearance potential.

These measurements were made on CH_3^+ from CH_4 and m/e 44 ions from isopropyl-, diethyl-, and *N,N*-dimethyl-*tert*-butylamines and *N*-ethylformamide. In all cases except *N,N*-dimethyl-*tert*-butylamine the maximum in the fragment ion kinetic energy distribution was at a lower energy (*i.e.*, higher accelerating voltage) than that of the respective parent ion. These "energy deficiencies" ranged from 0.03 ± 0.02 eV for CH_3^+ from CH_4 to 0.15 ± 0.03 eV for m/e 44 from *N*-ethylformamide.

This unexpected observation is probably due to the fact that near threshold a greater proportion of daughter ions are formed *via* slower reactions wherein the parent ion falls through a significant portion of the repeller field before fragmenting. In such a case the neutral product carries off its share of momentum and the daughter ion is left deficient in kinetic energy relative to the parent ion (which, of course, reflects the effect of the entire repeller field).

In the case of m/e 44 from *N,N*-dimethyl-*tert*-butylamine, from an extrapolation of data taken to within 1.0 eV of threshold, the fragment ion distribution peaked at 0.05 ± 0.03 eV greater than that of the parent, definitely indicating the release of excess translational energy in the dissociation. In center-of-mass coordinates this is an excess translational energy of 0.089 ± 0.036 eV. Because of the repeller effect described above this must certainly be a lower limit to the true value and because of uncertainty in the extent of internal energy equilibration for parent ions fragmenting in the ion source,¹⁵ it would be difficult to use this excess translational energy as a measure of total excess internal energy other than in a qualitative fashion. That is, we can only say that there is an excess energy effect in threshold production of m/e 44 ions here. This of course is in agreement with the AP evidence where $\Delta H_f(m/e$ 44) was found to be *ca.* 0.5 eV higher when formed from *N,N*-diethyl-*tert*-butylamine than when formed from trimethylamine.

Summary

On the basis of the present results, it appears that at least three different enthalpies of formation can be observed for $C_2H_6N^+$ ions, corresponding to structures I

and/or II, III, and V and/or VI. In contrast to earlier studies on aliphatic amines,²³⁻²⁷ this indicates that ion energetics can be a useful tool in characterizing the structural isomers of C₂H₆N⁺.

In the cases of C₂H₅O⁺ isomer II and isomer III in both sets, it is seen that gaseous ion properties obtained from ion-molecule reaction chemistry studies are most useful in the interpretation of ion energetics data.

Acknowledgment. We wish to thank the National Science Foundation for providing part of the funds necessary for the purchase of the mass spectrometer used in this study.

References and Notes

- (1) L. Friedman and J. Turkevich, *J. Amer. Chem. Soc.*, **74**, 1666 (1952).
- (2) D. Van Raalte and A. G. Harrison, *Can. J. Chem.*, **41**, 3118 (1963).
- (3) A. G. Harrison and B. G. Keyes, *J. Amer. Chem. Soc.*, **90**, 5046 (1968).
- (4) T. W. Shannon and F. W. McLafferty, *J. Amer. Chem. Soc.*, **88**, 5021 (1966).
- (5) F. W. McLafferty and W. T. Pike, *J. Amer. Chem. Soc.*, **89**, 5951 (1967).
- (6) F. W. McLafferty and H. D. R. Schuddemage, *J. Amer. Chem. Soc.*, **91**, 1866 (1969).
- (7) J. L. Beauchamp and R. C. Dunbar, *J. Amer. Chem. Soc.*, **92**, 1477 (1970).
- (8) A. S. Blair and A. G. Harrison, *Can. J. Chem.*, **51**, 703 (1973).
- (9) H. Pritchard and A. G. Harrison, *J. Chem. Phys.*, **48**, 5623 (1968).
- (10) K. M. A. Refaey and W. A. Chupka, *J. Chem. Phys.*, **48**, 5205 (1968).
- (11) M. S. B. Munson and J. L. Franklin, *J. Phys. Chem.*, **68**, 3191 (1964).
- (12) A. G. Harrison, A. Ivko, and D. Van Raalte, *Can. J. Chem.*, **44**, 1625 (1966).
- (13) R. H. Martin, F. W. Lampe, and R. W. Taft, *J. Amer. Chem. Soc.*, **88**, 1353 (1966).
- (14) C. D. Finney and A. G. Harrison, *Int. J. Mass Spectrom. Ion Phys.*, **9**, 221 (1972).
- (15) E. G. Jones, J. H. Beynon, and R. G. Cooks, *J. Chem. Phys.*, **57**, 2656 (1972).
- (16) L. Friedman, F. A. Long, and M. Wolfsberg, *J. Chem. Phys.*, **27**, 613 (1957).
- (17) J. M. Williams and W. H. Hamill, *J. Chem. Phys.*, **49**, 4467 (1968).
- (18) M. A. Haney and J. L. Franklin, *Trans. Faraday Soc.*, **65**, 1794 (1969).
- (19) W. A. Chupka, *J. Chem. Phys.*, **30**, 191 (1959).
- (20) M. W. Siegel, R. J. Celotta, J. L. Hall, J. Levine, R. A. Bennett, *Phys. Rev.*, **A6**, 607 (1972).
- (21) G. R. Phillips, B. H. Solka, and M. E. Russell, to be submitted for publication.
- (22) B. G. Keyes and A. G. Harrison, *J. Amer. Chem. Soc.*, **90**, 5671 (1968).
- (23) D. Amos, R. G. Gillis, J. L. Occolowitz, and J. F. Pisani, *Org. Mass Spectrom.*, **2**, 209 (1969).
- (24) J. Collin, *Bull. Soc. Chim. Belg.*, **62**, 411 (1953).
- (25) V. H. Dibeler, J. L. Franklin, and R. M. Reese, *J. Amer. Chem. Soc.*, **81**, 68 (1959).
- (26) B. G. Gowenlock, P. Pritchard-Jones, and R. J. Majer, *Trans. Faraday Soc.*, **57**, 23 (1961).
- (27) M. W. Akopyan and F. I. Vilesov, *Kinet. Katal.*, **4**, 39 (1963).
- (28) J. E. Collin and M. J. Franklin, *Bull. Soc. Roy. Sci. Liege*, 285 (1966).
- (29) K. Watanabe, *J. Chem. Phys.*, **26**, 1773 (1957).
- (30) K. Watanabe, T. Nakayama, and J. Mottl, *J. Quant. Spectrosc. Radiat. Transfer*, **2**, 369 (1962).
- (31) J. A. Kerr, *Chem. Rev.*, **66**, 465 (1966).
- (32) R. H. Staley, R. R. Corderman, M. S. Foster, and J. L. Beauchamp, *J. Amer. Chem. Soc.*, **96**, 1260 (1974).
- (33) J. L. Franklin, J. G. Dillard, H. M. Rosenstock, J. T. Herron, K. Draxl, and F. H. Field, *Nat. Stand. Ref. Data Ser., Nat. Bur. Stand., No. 26* (1969).
- (34) S. W. Benson, F. R. Cruickshank, D. M. Golden, G. R. Haugen, H. E. O'Neal, A. S. Rogers, R. Shan, and R. Walsh, *Chem. Rev.*, **69**, 279 (1969).
- (35) J. Collin, *Bull. Soc. Chim. Belg.*, **67**, 549 (1958).
- (36) D. H. Aue, H. M. Webb, and M. T. Bowers, presented at the Twentieth Annual Conference on Mass Spectrometry and Allied Topics, Dallas, Texas, June 4-9, 1972.
- (37) D. Van Raalte and A. G. Harrison, *Can. J. Chem.*, **41**, 2054 (1963).
- (38) F. P. Lossing and G. P. Semeluk, *Can. J. Chem.*, **48**, 955 (1970).
- (39) D. P. Stevenson, *Discuss. Faraday Soc.*, **10**, 35 (1951).

Mechanism of Hydroxyapatite Dissolution. The Synergistic Effects of Solution Fluoride, Strontium, and Phosphate

Mahendra G. Dedhiya, Fudah Young, and William I. Higuchi*

College of Pharmacy, University of Michigan, Ann Arbor, Michigan 48104 (Received June 4, 1973; Revised Manuscript Received February 7, 1974)

Publication costs assisted by the National Institute of Dental Research

The dissolution rates and apparent solubilities of synthetic hydroxyapatite in acetate buffers containing various concentrations of phosphate, strontium, and fluoride ions were determined. The synergistic effects of these ions in retarding the apatite dissolution were critically examined with a physical model in which a surface strontium-fluoride-apatitic complex was assumed to govern the driving force for the dissolution reaction. It is shown that a surface complex, Ca₆Sr₄(PO₄)₆F₂, with an activity product, $K_{ap} = a_{Ca^{2+}}^6 a_{Sr^{2+}}^4 a_{PO_4^{3-}}^6 a_{F^-}^2 = 1 \times 10^{-131 \pm 2}$ is consistent with the experimental data.

Introduction

It has been well established during recent years that dental caries is a disease involving the dissolution of dental

enamel in an ambient acid environment of bacterial origin. The enamel mineral is composed principally of hydroxyapatite, Ca₁₀(PO₄)₆(OH)₂. Consequently, numerous

research efforts have been directed toward understanding the dissolution behavior of dental enamel and synthetic hydroxyapatite.^{1,2}

During the last decade, in our laboratories, the dissolution kinetics of hydroxyapatite in acid buffer solutions has been studied using a physical model describing the solid-liquid interfacial conditions and diffusion in the stagnant liquid layer adjacent to the solid surface.^{3,4} The model has been critically examined for apatite dissolution under various conditions of solution pH, buffer type, buffer capacity, and common ions (calcium and phosphates). Self-consistent correlations between the model predictions and experimental results have been observed. The general physical model approach has also been used in studying the hydroxyapatite \rightarrow calcium fluoride conversions in situations where compressed pellets of synthetic hydroxyapatite and human enamel blocks were exposed to a buffer solution containing high fluoride concentrations.^{5,6}

More recent studies⁷ were aimed at understanding the mechanism of action of fluoride ions at low concentrations (around 1 ppm) upon the dissolution rate of hydroxyapatite in acidic buffers. The experimental data obtained over a wide range of conditions using powdered TVA hydroxyapatite led to the interpretation in which a fluoride-apatitic surface complex or a "surface phase" with a composition, $\text{Ca}_{10-n}\text{(PO}_4)_6\text{(F)}_2$, was assumed to govern the rate of dissolution. It was postulated⁷ that this surface complex constantly re-forms rapidly on the dissolving hydroxyapatite crystal surface through the rapid exchange of the surface hydroxyls by fluoride and thereby essentially maintains a steady-state surface "coating" that is able to govern interfacial conditions at the site of dissolution. Thus this surface complex was viewed not as a true bulk phase but as a surface "phase" probably not extending much beyond a single unit cell into the hydroxyapatite crystal at the site of dissolution.

Recent work in these laboratories has shown that the effects of solution strontium upon the dissolution rates of TVA hydroxyapatite might be explained by a similar mechanism. The investigators⁸ have shown that the dissolution process in this case is consistent with a mechanism involving an interfacial strontium-apatitic complex, $\text{Ca}_6\text{Sr}_4\text{(PO}_4)_6\text{(OH)}_2$, as the governing surface "phase" for dissolution.

In this report, the synergistic effects of solution strontium, fluoride, and phosphate in reducing the dissolution rates and apparent solubilities of TVA hydroxyapatite in acetate buffers has been systematically investigated on the basis of a physical model derived from the earlier studies.^{7,8} As will be seen, an interfacial strontium-fluoride-apatitic complex with a composition of $\text{Ca}_6\text{Sr}_4\text{(P-O}_4)_6\text{F}_2$ was found to be consistent with the experimental data.

Experimental Section

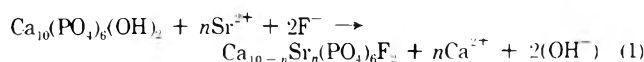
The TVA hydroxyapatite used in this study was prepared by the procedures previously described.^{4,9} The procedure for the preparation of this material involved the reaction of monocalcium phosphate monohydrate and calcium carbonate at high temperature (1200°) in an atmosphere of steam and nitrogen. These apatite crystals are characterized by the high degree of purity and well-annealed crystallinity. The acetate buffer solutions used in all the experiments contain 0.05 M total acetate. These solutions containing various concentrations of strontium, phosphate, and fluoride were adjusted to pH 4.5 with

ionic strength maintained at 0.5 M using sodium chloride. The procedures and materials for preparing these buffer solutions have been described previously.⁴ Phosphate was determined by a colorimetric procedure and calcium by atomic absorption spectrophotometry as have been described elsewhere.⁴

Procedures for Dissolution Studies. The hydroxyapatite powder (100 mg) was transferred to a 500-ml volumetric flask clamped to the arm of a Burrell wrist action shaker¹⁰ immersed in the water bath maintained at 30°. The dissolution experiments were started by adding to the flask 200 ml of the required buffer solution preequilibrated at 30°. The agitation of the flask was kept constant throughout the study. Samples of 5-ml buffer solutions were withdrawn from the flask at various time intervals by means of a hypodermic syringe and needle, and were filtered using Millipore¹¹ filters (0.22 μm pore size) with Swinny filter holders. These samples were then analyzed for calcium or phosphate in calculating the amount of hydroxyapatite dissolved.

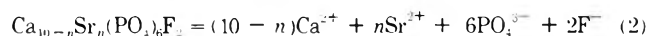
Theoretical Section

Strontium-Fluoride-Apatitic Surface Complex Model. The physical model (Figure 1) assumes that when hydroxyapatite crystals are exposed to acid buffers containing sufficiently high concentrations of strontium ions ($>10^{-4}$ M) in the presence of low fluoride (<100 ppm) the strontium-fluoride-apatitic complex, $\text{Ca}_{10-n}\text{Sr}_n\text{(PO}_4)_6\text{F}_2$, forms at the crystal surface by the rapid calcium-strontium and hydroxide-fluoride ion-exchange reaction

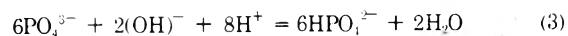


where n is the unknown number of strontium ions participating in the substitution reaction, which is in the range of $0 \leq n \leq 10$.

It is assumed that this surface complex, with a definite composition of $\text{Ca}_{10-n}\text{Sr}_n(\text{PO}_4)_6\text{F}_2$, governs the ionic equilibria at the crystal-liquid interface according to its activity product, $K_{\text{ap}} = a_{\text{Ca}^{2+}}^{10-n} a_{\text{Sr}^{2+}}^n a_{\text{PO}_4^{3-}}^6 a_{\text{F}^-}^2$, as shown in the following equilibrium expression



In the presence of acid species (acid buffer solution) the subsequent reaction should take place at the crystal-liquid interface



The model further assumes that the transport of the various molecular and ionic species to and from the crystal surface in the liquid diffusion layer follows the net of reactions 1-3, namely



The basic model for these processes is shown in Figure 1. This is shown for dissolution in acid buffer containing strontium and fluoride. The acid species (H^+ , HB) diffuse toward the crystal-liquid interface ($x = 0$), while calcium and phosphate ions diffuse outward into the bulk through the liquid diffusion layer of thickness h . Both solution strontium and fluoride are neither generated nor consumed during dissolution according to eq 4. Thus, the model assumes that the dissolution of hydroxyapatite crystals in an acid buffer containing a constant level of strontium and fluoride ions is controlled by the activity product of the surface strontium-fluoride-apatitic complex and the diffusion rates of various species involved.

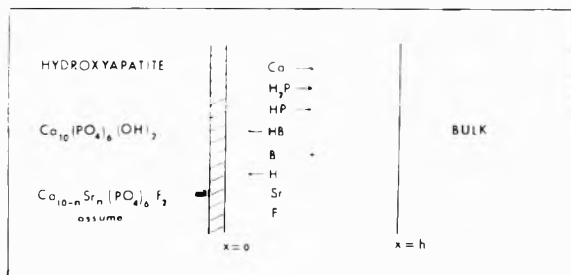


Figure 1. Model for the effect of fluoride and strontium on hydroxyapatite dissolution in acid buffer solutions. A calcium-strontium-fluoride apatite complex $\text{Ca}_{10-n}\text{Sr}_n(\text{PO}_4)_6\text{F}_2$ is assumed to form at the apatite surface.

The appropriate equations for this model are based on methods described in earlier studies^{3,7,8} on enamel dissolution in acid media. For a one-dimensional problem (Figure 1), the following quasi-steady-state equations can be written for the diffusional fluxes of total phosphates,¹² J_{TP} , total buffer species, J_{TB} , and total acid species, J_{TH} , in the diffusion layer per unit area

$$J_{\text{TP}} = D_{\text{H}_2\text{PO}_4^-} \frac{d[\text{H}_2\text{PO}_4^-]}{dx} + D_{\text{HPO}_4^{2-}} \frac{d[\text{HPO}_4^{2-}]}{dx} \quad (5)$$

$$J_{\text{TB}} = D_{\text{HB}} \frac{d[\text{HB}]}{dx} + D_{\text{B}^-} \frac{d[\text{B}^-]}{dx} \quad (6)$$

$$J_{\text{TH}} = D_{\text{H}^+} \frac{d[\text{H}^+]}{dx} + D_{\text{H}_2\text{PO}_4^-} \frac{d[\text{H}_2\text{PO}_4^-]}{dx} + D_{\text{HB}} \frac{d[\text{HB}]}{dx} \quad (7)$$

The D 's in the equations are the respective diffusion coefficients,¹³ where HB and B^- are the buffer acid molecule and its anion which in the present studies are acetic acid and acetate ions. Quantities in the brackets are terms expressing the concentrations of the respective species.

According to the congruency expressed by eq 4, the following equations can be written

$$J_{\text{TH}} = -(4/3)J_{\text{TP}} \quad (8)$$

$$J_{\text{Ca}} = (10/6)J_{\text{TP}} \quad (9)$$

Since strontium, fluoride, and total buffer are neither generated nor consumed, the following equations can also be written

$$J_{\text{Sr}^{2+}} = 0 \text{ or } [\text{Sr}^{2+}]_0 = [\text{Sr}^{2+}]_h \quad (10)$$

$$J_{\text{F}^-} = 0 \text{ or } [\text{F}^-]_0 = [\text{F}^-]_h \quad (11)$$

$$J_{\text{TB}} = 0 \text{ or } [\text{HB}]_0 + [\text{B}^-]_0 = [\text{HB}]_h + [\text{B}^-]_h \quad (12)$$

In addition to eq 5-12, the following equilibrium expressions apply at the crystal-liquid interface, at any position in the diffusion layer, and in the bulk solvent, i.e., at $x \geq 0$ $K_{2p}' = K_{2p}\gamma_{\text{H}_2\text{PO}_4^-}/\gamma_{\text{H}^+}\gamma_{\text{HPO}_4^{2-}}$, $K_{3p}' = K_{3p}\gamma_{\text{HPO}_4^{2-}}/\gamma_{\text{H}^+}\gamma_{\text{PO}_4^{3-}}$, and $K'_{\text{HB}} = K_{\text{HB}}\gamma_{\text{HB}}/\gamma_{\text{H}^+}\gamma_{\text{B}^-}$, where K_{2p} and K_{3p} are the respective second and third ionization constants of H_3PO_4 , and K_{HB} is the ionization constant of HB, the buffer acid (Table I). The γ 's are the activity coefficients of the respective species.

The model also assumes that at the crystal-solvent interface, $x = 0$, the ionic equilibrium conditions are governed by the activity product of the surface strontium-fluoride-apatitic complex

$$K_{\text{ap}} = K_{\text{ap}}' \gamma_{\text{Ca}^{2+}}^{10-n} \gamma_{\text{Sr}^{2+}}^n \gamma_{\text{PO}_4^{3-}}^6 \gamma_{\text{F}^-}^2 \quad (13)$$

and

TABLE I: Equilibrium Constants and Activity Coefficients for Theoretical Calculations

K_{2p}^a	$6.40 \times 10^{-8} M$
K_{3p}^a	4.73×10^{-13}
K_{HA} (acetic acid)	1.75×10^{-5}
$\gamma_{\text{F}^-} = 0.632$	$\gamma_{\text{H}^+} = 0.8$
$\gamma_{\text{H}_2\text{PO}_4^-} = 0.55$	$\gamma_{\text{HPO}_4^{2-}} = 0.23$
$\gamma_{\text{PO}_4^{3-}} = 0.095$	$\gamma_{\text{Ca}^{2+}} = 0.36$
$\gamma_{\text{Sr}^{2+}} = 0.36$	$\gamma_{\text{OH}^-} = 0.7$
$\gamma_{\text{acetate}} = 0.735$	

^a K_{2p} and K_{3p} are the second and third dissociation constants, respectively, of phosphoric acid.

$$K_{\text{ap}}' = [\text{Ca}^{2+}]_0^{10-n} [\text{Sr}^{2+}]_0^n [\text{PO}_4^{3-}]_0^6 (\text{F}^-)_0^2 \quad (14)$$

where

$$[\text{PO}_4^{3-}]_0 = \text{TP} / \left[1 + \frac{[\text{H}^+]_0}{K_{3p}'} + \frac{[\text{H}^+]_0^2}{K_{2p}'K_{3p}'} \right] \quad (15)$$

Substituting eq 7 into eq 8, and integrating over the limits $x = 0$ and $x = h$ using eq 12 and equilibrium expressions, the following equation can be derived

$$\frac{4}{3}J = \frac{D_{\text{H}_2\text{PO}_4^-}}{h} \times \left([\text{H}_2\text{PO}_4^-]_h - \left[J + \frac{D_{\text{HPO}_4^{2-}}}{h} [\text{HPO}_4^{2-}]_h + \frac{D_{\text{H}_2\text{PO}_4^-}}{h} \times [\text{H}_2\text{PO}_4^-]_h \right] / \left[\frac{K_{2p}'}{[\text{H}^+]_0} + \frac{D_{\text{H}_2\text{PO}_4^-}}{h} \right] \right) + \frac{D_{\text{HB}}}{h} \left\{ [\text{HB}]_h - \left[\frac{D_{\text{B}^-}}{h} [\text{B}^-]_h + \frac{D_{\text{HB}}}{h} [\text{HB}]_h \right] / \left[\frac{D_{\text{HB}}}{h} + \frac{D_{\text{B}^-}}{h} K_{\text{HB}}' \right] \right\} + \frac{D_{\text{H}^+}}{h} [[\text{H}^-]_h - [\text{H}^+]_h] \quad (16)$$

From eq 14, the following equation can be derived for K_{ap}' using eq 9-11 and 15

$$K_{\text{ap}}' = \frac{K_{3p}^6 K_{2p}^{10-n}}{[\text{H}^+]_0^{12}} \left[\frac{J}{0.6 \frac{D_{\text{Ca}^{2+}}}{h}} + [\text{Ca}^{2+}]_h \right]^{10-n} \times \left[\text{Sr}^{2+} \right]_h^n [\text{F}^-]_h^2 \left[\left(J + \frac{D_{\text{HPO}_4^{2-}}}{h} [\text{HPO}_4^{2-}]_h + \frac{D_{\text{H}_2\text{PO}_4^-}}{h} \times [\text{H}_2\text{PO}_4^-]_h \right) / \left(\frac{K_{2p}'}{[\text{H}^+]_0} + \frac{D_{\text{H}_2\text{PO}_4^-}}{h} \right) \right]^6 \quad (17)$$

where

$$J = -J_{\text{TP}} \quad (18)$$

Equations 16 and 17 are the integral expressions derived from the proposed physical model.

Dissolution Rate Calculations with the Model. The only unknown quantities in eq 16 and 17 are J , K_{ap}' , $[\text{H}^+]_0$, and n . The other quantities may be either estimated or determined from independent experiments. J is the disso-

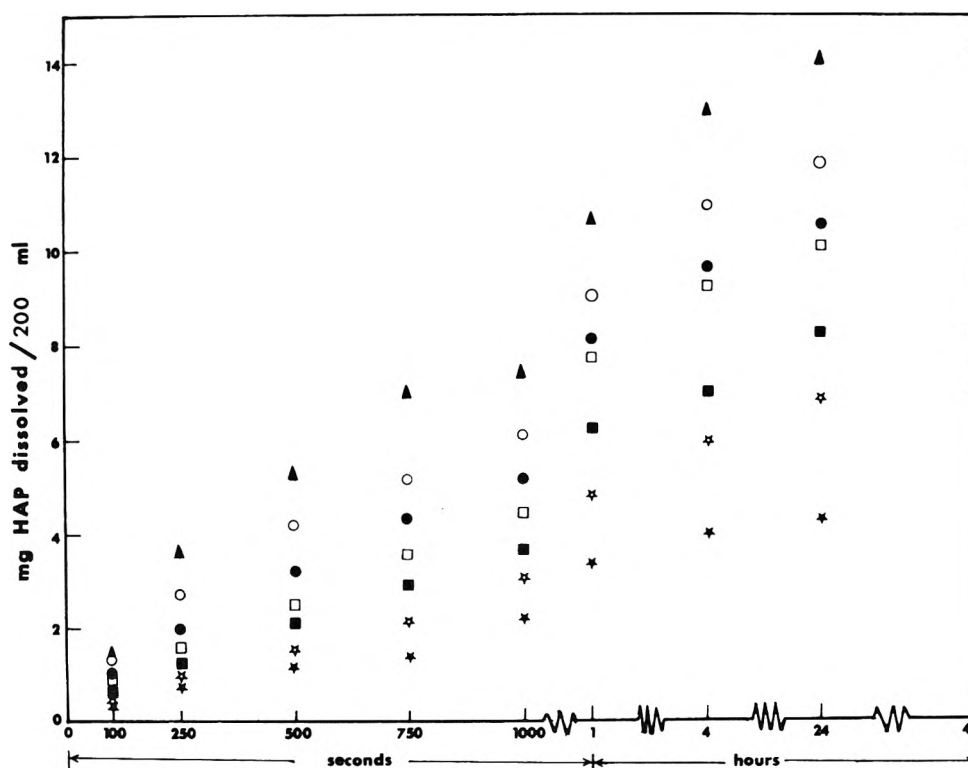


Figure 2. Dissolution rate of hydroxyapatite in 0.05 M acetate buffer at pH 4.5 with ionic strength of 0.5 M at 1 ppm fluoride and the following strontium and phosphate concentrations: ▲, 1 ppm F alone; ○, 1×10^{-4} M Sr; ●, 3×10^{-4} M Sr; □, 1×10^{-3} M Sr; ■, 1×10^{-4} M Sr and 1×10^{-4} M phosphate; ☆, 3×10^{-4} M Sr and 1×10^{-4} M phosphate; ★, 1×10^{-3} M Sr and 1×10^{-4} M phosphate

lution rate of hydroxyapatite expressed as moles of total phosphates transported per unit area, as defined by eq 5 and 18. K_{ap} is the activity product of the strontium-fluoride-apatitic complex, $\text{Ca}_{10-n}\text{Sr}_n(\text{PO}_4)_6(\text{F})_2$, as defined by eq 13, and can be calculated from K_{ap}' , which is defined by eq 14. $[\text{H}^+]_0$ is the concentration of hydrogen ions at the crystal-liquid interface ($x = 0$), and n is the number of strontium ions in the complex ranging from 0 to 10. Mathematically any two of these quantities can be calculated as a function of the other two by solving eq 16 and 17. When J is known eq 16 and 17 can be numerically solved for $[\text{H}^+]_0$ and K_{ap}' by proper digital computer programming for each preselected value of n . Values of the parameters entering into eq 16 and 17 are listed in Table I. J may be calculated from J_e , the experimental dissolution rate, using the relation $J = J_e/A$. The total surface area, A , of the hydroxyapatite crystals may be easily obtained from similar experiments conducted in the absence of strontium and fluoride and data evaluation employing the hydroxyapatite model and a K_{ap} value of $1 \times 10^{-132.4}$. A value of 1.0×10^{-5} cm²/sec was used for all the diffusion coefficients.

Apparent Solubility Calculations with the Model. When dissolution of hydroxyapatite in acid buffers containing known concentrations of strontium and fluoride ions reaches an apparent equilibrium, the apparent solubility product (or activity product), K_{ap} , can be determined by analyzing the calcium and the total phosphate concentrations in the bulk. Such data can be obtained for each dissolution rate experiment. Equation 14, which is applicable to the bulk equilibrium conditions, can then be written

$$K_{ap}' = [\text{Ca}^{2+}]_h^{10-n} [\text{Sr}^{2+}]_h^n [\text{PO}_4^{3-}]_h^6 [\text{F}^-]_h^2 \quad (20)$$

where the bracketed quantities are the apparent equilibri-

um concentrations in the bulk ($x \geq h$). The bulk concentrations of calcium and total phosphates (TP) can be easily analyzed. $[\text{PO}_4^{3-}]_h$ can be calculated by eq 15, when the bulk hydrogen ion concentration is known. The concentrations of strontium and fluoride are known quantities depending on the compositions of the buffer solutions. Thus, from the equilibrium data, the apparent solubility product, K_{ap} , can be calculated as a function of n values according to eq 13 and 20.

Results

The initial dissolution rates and apparent solubilities of TVA hydroxyapatite crystals were determined over a range of concentrations of strontium and phosphate ions in acetate buffers containing 1 ppm fluoride at pH 4.5. Figure 2 shows typical raw dissolution data in various buffer solutions with the amount of apatite dissolved plotted against time. The initial data points in these plots represent apatite dissolution under sink conditions. Slopes of these initial data points were taken in obtaining the experimental dissolution rates, J_e , expressed in terms of phosphates. The apparent solubilities of apatite, also expressed in terms of phosphates, were directly measured from the data points in the plateau regions of the dissolution curves as shown in Figure 2, which represents the apparent saturation of the solvent media with apatite. These experimental data obtained in acetate buffers containing various amounts of strontium, fluoride, and phosphate ions are presented in Table II.

Retarding Effects of Strontium, Fluoride, and Phosphate on TVA Hydroxyapatite Dissolution Rates. In Table II, the relative apatite dissolution rates (J_r) in the presence of strontium and/or fluoride and/or phosphate expressed as per cent of dissolution rate in the absence of all

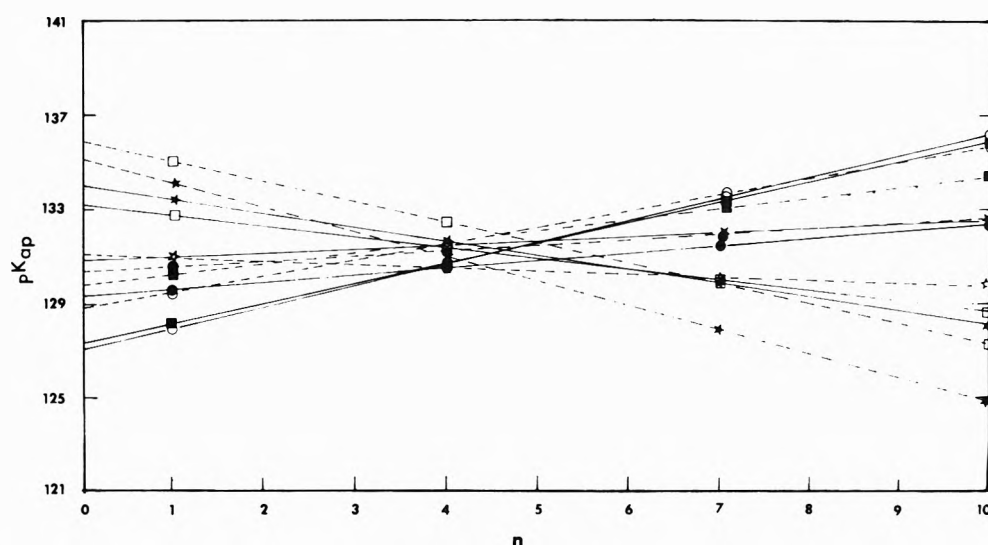


Figure 3. Calculations of pK_{ap} as a function of n from the initial dissolution rates of hydroxyapatite (TVA) in 0.05 M acetate buffer at pH 4.5 and ionic strength 0.5 M containing 1 ppm fluoride and the following concentrations of strontium and phosphate: O—O, 1×10^{-4} M Sr; ●—●, 3×10^{-4} M Sr; □—□, 1×10^{-3} M Sr; ■—■, 1×10^{-4} M Sr and 1×10^{-4} M phosphate; ☆—☆, 3×10^{-4} M Sr and 1×10^{-4} M phosphate; ★—★, 1×10^{-3} M Sr and 1×10^{-4} M phosphate; O---O, 1×10^{-4} M Sr and 3×10^{-4} M phosphate; ●---●, 3×10^{-4} M Sr and 3×10^{-4} M phosphate; □---□, 1×10^{-3} M Sr and 3×10^{-4} M phosphate; ■---■, 1×10^{-4} M Sr and 1×10^{-3} M phosphate; ☆---☆, 3×10^{-4} M Sr and 1×10^{-3} M phosphate; ★---★, 1×10^{-3} M Sr and 1×10^{-3} M phosphate.

TABLE II: Dissolution Rates (J_r), Relative Dissolution Rates (J_i), and Apparent Solubilities of TVA Hydroxyapatite (100 mg) in Acetate Buffers

Acetate buffers (pH 4.5)			$J_r \times 10^4$, mol/sec	J_i , %	Approximate solubilities $\times 10^5$, M
[F ⁻], ppm	[PO ₄ ³⁻], $\times 10^4$, M	[Sr ²⁺], $\times 10^4$, M			
0	0	0	16.49	100	12.34
0	0	30	11.87	71.98	9.13
0	0	100	8.84	53.64	6.97
0	10	10	6.32	38.32	6.98
0	10	30	4.69	28.45	3.53
0	10	100	1.09	11.57	1.52
1	0	0	9.04	54.84	7.02
1	0	1	7.73	46.87	5.92
1	0	3	5.70	34.57	5.04
1	0	10	3.32	20.16	3.24
1	1	0	7.50	45.48	6.34
1	1	1	7.12	43.19	5.28
1	1	3	4.15	25.18	3.99
1	1	10	2.47	15.00	2.27
1	3	0	5.85	35.48	5.17
1	3	1	4.79	29.04	2.72
1	3	3	3.60	21.83	2.36
1	3	10	1.28	7.75	0.84
1	10	0	4.13	25.07	3.64
1	10	1	2.5	15.13	1.58
1	10	3	2.08	12.59	1.05
1	10	10	0.83	5.06	0.09

these ions are presented. It can be seen from these data there is synergism among the fluoride, strontium, and phosphate ions. First, it was shown previously⁸ either strontium or phosphate alone of concentrations up to 10^{-3} M has little effect upon the dissolution rate. However, in combination, as can be seen, they are effective in reducing the rate to $J_i = 38.3\%$. Similarly, strontium at the level of 10^{-3} M is seen to enhance the effect of 1 ppm fluoride, from $J_i = 54.8\%$ (without strontium) to $J_i = 20.2\%$ (with strontium). These data clearly show that the influence of all the ions (fluoride, strontium, and phosphate) are synergistic. Each ion enhances the ability of the other ions to reduce the dissolution rate. In the following section, these

data are employed to assess the proposed model from a quantitative standpoint.

Calculations with the Model using Dissolution Rate Data. Figure 3 shows the results of model calculations based on 12 apatite dissolution rates, as shown in Table II, in buffers at pH 4.5 containing various concentrations of phosphate, strontium, and fluoride ions. The activity product, K_{ap} , of the strontium-fluoride-apatitic complex, $Ca_{10-n}Sr_n(PO_4)_6F_2$, was calculated from eq 17 and 18 as a function of n . The results are presented as plots of pK_{ap} vs. n ranging from 0 to 10. It can be seen that the calculated pK_{ap} values show relatively large spreads at the low ($n = 0$) and high ($n = 10$) n values. At around $n = 4$ there is a minimum spread of the pK_{ap} values. The minimum spread ranges from $10^{-130.5}$ to $10^{-132.5}$ in K_{ap} , with a mean value of $10^{-131.5 \pm 1}$.

Calculations with the Model using the Apparent Solubility Data. Figure 4 gives the results calculated using the apparent solubility data obtained with the 12 dissolution buffer conditions. As with the dissolution rate data, large spreads in pK_{ap} were found for high and low n values. A minimum spread is observed when $n \approx 4$ with a mean value of $10^{-132 \pm 2}$.

Discussion

The present approach, as was the case in an earlier study⁸ dealing with the strontium-phosphate synergism, has involved carrying out a sufficient number of independent experiments to demonstrate the self-consistency of the proposed model. The narrow spread in the pK_{ap} values at $n \approx 4$ in both Figures 3 and 4 supports the model in which a single complex, $Ca_6Sr_4(PO_4)_6(F)_2$, is involved in the rate-determining step for the dissolution of TVA hydroxyapatite in solutions containing strontium, fluoride, and phosphate ions. The spread in the pK_{ap} values at $n \approx 4$ in both Figures 3 and 4 are conservatively of the order of magnitude of the uncertainties in the experimental results. However, it is believed that the range of K_{ap} values at $n = 0$ and at $n = 10$ are much greater than what would be expected from the experimental uncertainties. It is known that calcium and strontium

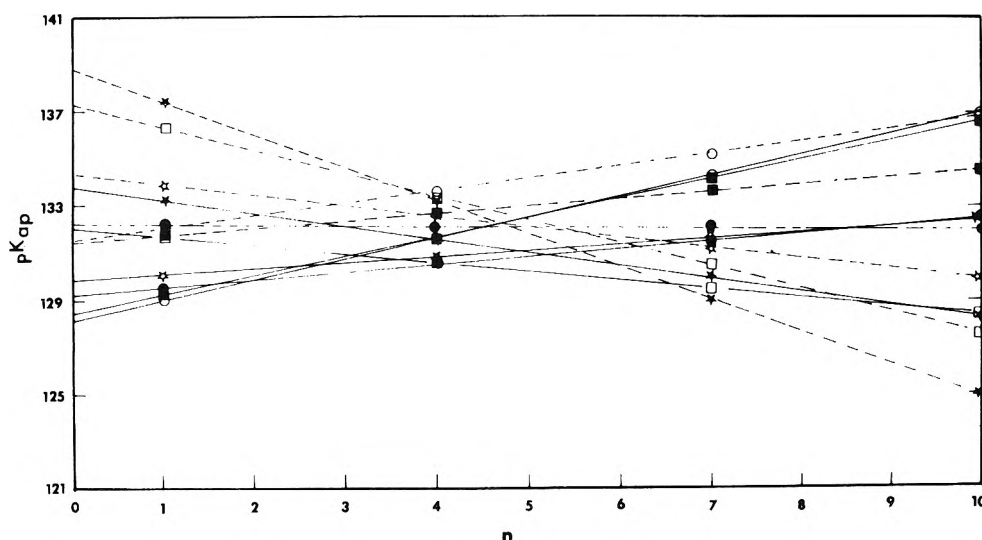


Figure 4. Calculations of pK_{ap} as a function of n from the apparent solubilities of hydroxyapatite (TVA) in 0.05 M acetate buffer at pH 4.5 and ionic strength of 0.5 M containing 1 ppm fluoride and the following concentrations of strontium and phosphate: O—O, 1×10^{-4} M Sr; ●—●, 3×10^{-4} M Sr; □—□, 1×10^{-3} M Sr; ■—■, 1×10^{-4} M Sr and 1×10^{-4} M phosphate; ☆—☆, 3×10^{-4} M Sr and 1×10^{-4} M phosphate; ★—★, 1×10^{-3} M Sr and 1×10^{-4} M phosphate; O---O, 1×10^{-4} M Sr and 3×10^{-4} M phosphate; ●---●, 3×10^{-4} M Sr and 3×10^{-4} M phosphate; □---□, 1×10^{-3} M Sr and 3×10^{-4} M phosphate; ■---■, 1×10^{-4} M Sr and 1×10^{-3} M phosphate; ☆---☆, 3×10^{-4} M Sr and 1×10^{-3} M phosphate; ★---★, 1×10^{-3} M Sr and 1×10^{-3} M phosphate.

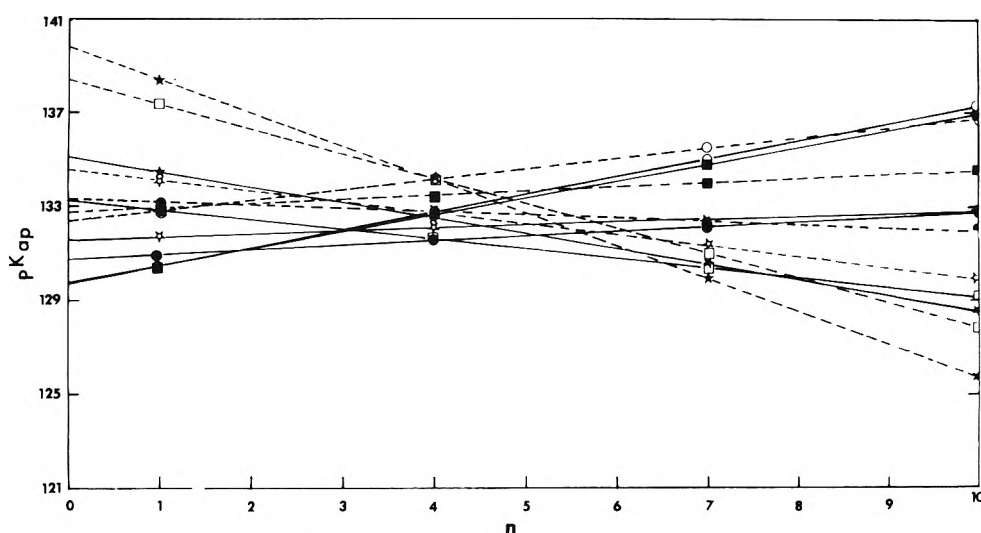


Figure 5. Calculations of pK_{ap} as a function of n after correction for the calcium and strontium complexes in the apparent solubilities of hydroxyapatite (TVA) in 0.5 M acetate buffer at pH 4.5 and ionic strength of 0.5 M containing 1 ppm fluoride and the following concentrations of strontium and phosphate: O—O, 1×10^{-4} M Sr; ●—●, 3×10^{-4} M Sr; □—□, 1×10^{-3} M Sr; ■—■, 1×10^{-4} M Sr and 1×10^{-4} M phosphate; ☆—☆, 3×10^{-4} M Sr and 1×10^{-4} M phosphate; ★—★, 1×10^{-3} M Sr and 1×10^{-4} M phosphate; O---O, 1×10^{-4} M Sr and 3×10^{-4} M phosphate; ●---●, 3×10^{-4} M Sr and 3×10^{-4} M phosphate; □---□, 1×10^{-3} M Sr and 3×10^{-4} M phosphate; ■---■, 1×10^{-4} M Sr and 1×10^{-3} M phosphate; ☆---☆, 3×10^{-4} M Sr and 1×10^{-3} M phosphate; ★---★, 1×10^{-3} M Sr and 1×10^{-3} M phosphate.

may form complexes such as $\text{CaH}_2\text{PO}_4^+$, CaHPO_4 , $\text{Ca}(\text{CH}_3\text{COO})^+$, $\text{SrH}_2\text{PO}_4^+$, and $\text{Sr}(\text{CH}_3\text{COO})^+$ under the experimental conditions of this study. The important question is then to what extent is the limitation of the physical model in calculating K_{ap} in which these complexes were not considered. Based on the same set of apparent solubility data used in Figure 4, pK_{ap} vs. n calculations, as shown in Figure 5, were carried out with the consideration of these complexes using appropriate stability constants.^{14,15} As can be seen, in comparison with Figure 4, the effect of complexes does not appear to be large enough to alter the main conclusions.

At this point it is instructive to consider the fundamental question regarding the constancy of $n(=4)$ and, therefore, of pK_{ap} in the interpretation of the results. It may

be argued that, in fact, both pK_{ap} and n are variable, that the minimal spread in n at $n \approx 4$ is accidental, and that the actual situation is much more complicated even though n may be a single-valued function of pK_{ap} (eq 13). The complete analysis of this general problem is complex and is not warranted in view of the rather large experimental uncertainties. However the present experimental data have been examined with the relationships suggested by Berndt and Stearns¹⁶ for the three-dimensional ideal solid solution case. Generally the data do not agree well with this situation but this is not conclusive in view of the experimental scatter. Clearly, more work is needed for a definitive resolution of this question.

Apatitic Complexes in Dissolution Rate Control. The role of solution fluoride in the dissolution kinetics of TVA

hydroxyapatite has been studied under various buffer conditions.⁷ Using a physical model featuring a fluoroapatite surface complex controlled dissolution, a value of $10^{-131 \pm 1}$ was deduced for the activity product of the complex ($K_{ap} = a_{Ca^{2+}}^{10} a_{PO_4^{3-}}^6 a_{F^-}^{-2}$) from a large number of experimental conditions. In a recent study⁸ on the influence of solution strontium upon the hydroxyapatite dissolution rate, it was concluded that a value of around 10^{-132} to 10^{-134} for the activity product of a crystal-solution interfacial complex of $(Ca)_6(Sr)_4(PO_4)_6(OH)_2$ gives the best consistent fit of all the experimental data with the proposed model. In the present study it has been shown that a dissolution governing complex, $Ca_6Sr_4(PO_4)_6F_2$, with an activity product of around $10^{-131 \pm 1}$ describes the synergism of strontium, fluoride, and phosphate in TVA hydroxyapatite dissolution.

All of the above observations are notably consistent with the original base line studies with TVA hydroxyapatite dissolution in the absence of strontium and fluoride.⁴ In these investigations overall good consistency among the various experimental results with the model predictions was achieved when a value of $10^{-131 \pm 1}$ for the activity product of hydroxyapatite was used. Thus all of the studies on the dissolution of TVA hydroxyapatite in our laboratories may be interpreted by postulating that the rate of dissolution is determined by an apatitic activity product having a K_{ap} value of around 10^{-131} . Furthermore, the analysis has suggested that the rate-determining apatitic complex should be one of the following depending upon whether or not strontium and/or fluoride is present in the

dissolution media: $(Ca)_{10}(PO_4)_6(OH)_2$, $(Ca)_{10}(PO_4)_6(F)_2$, $(Ca)_6(Sr)_4(PO_4)_6(OH)_2$, and $(Ca)_6(Sr)_4(PO_4)_6(F)_2$.

Acknowledgment. This investigation was supported by USPHS Research Grant No. DE-01830 from the National Institute of Dental Research, National Institute of Health, Bethesda, Md.

References and Notes

- (1) J. A. Gray, *J. Dent. Res.*, **41**, 633 (1962).
- (2) A. Stralfors, *Trans. Roy. Schools Stockholm Umea. Ser. 2*, **1**, 52 (1958).
- (3) W. I. Higuchi, J. A. Gray, J. J. Hefferren, and P. R. Patel, *J. Dent. Res.*, **44**, 330 (1965).
- (4) W. I. Higuchi, N. A. Mir, P. R. Patel, J. W. Becker, and J. J. Hefferren, *J. Dent. Res.*, **48**, 396 (1969).
- (5) Z. Liang and W. I. Higuchi, *J. Phys. Chem.*, **77**, 1704 (1973).
- (6) W. I. Higuchi, S. C. Valvani, and J. J. Hefferren, *Arch. Oral Biol.*, in press.
- (7) N. A. Mir, W. I. Higuchi, and J. J. Hefferren, *Arch. Oral Biol.*, **14**, 901 (1969).
- (8) M. G. Dedhiya, F. Young, and W. I. Higuchi, *J. Dent. Res.*, **52**, 1097 (1973).
- (9) Tennessee Valley Authority, Report No. 678 (1956), Wilson Dam, Ala.
- (10) Burrell Corp., Pittsburgh, Pa.
- (11) Millipore Filter Corp., Bedford, Mass.
- (12) The concentrations of H_3PO_4 and PO_4^{3-} in the acid buffers (pH 4.5) studied are negligible compared to those of $H_2PO_4^-$ and HPO_4^{2-} .
- (13) The influence of the electric diffusion potential are neglected here. This should be a good assumption especially as a swamping electrolyte was present in the experiments.
- (14) $K(Ca(CH_3COO)^+) = 18$, $K(Sr(CH_3COO)^+) = 15$ (A. N. Nancollas, *J. Phys. Chem.*, **60**, 744 (1956)).
- (15) $K(CaH_2PO_4^+) = 5.06$, $K(CaHPO_4) = 255.0$, $K(SrH_2PO_4^-) = 5.06$, $K(SrHPO_4) = 255.0$ (L. G. Sillen and A. E. Martell, *Stability Constants of Metal-Ion Complexes, Chem. Soc., Spec. Publ. Suppl. No. 7, No. 25* (1964)).
- (16) A. F. Berndt and R. I. Stearns, *J. Chem. Educ.*, **50**, 415 (1973).

Kinetics of Surface Reactions from Nuclear Magnetic Resonance Relaxation Times

H. A. Resing

Chemistry Division, Naval Research Laboratory, Washington, D. C. 20375 (Received December 17, 1973)

Publication costs assisted by the Naval Research Laboratory

The exchange between chemisorbed and physisorbed molecules is subject to the laws of chemical kinetics. It is shown how to use nmr measurements of such exchange rates along with adsorption isotherms to estimate reaction orders of these exchange reactions. The dissociation of the benzene-surface complex on a charcoal is unimolecular. The reactions of water with the surface hydroxyls of keratin and of zeolite X are estimated to be half order with respect to water.

I. Introduction

The power of nmr methods to measure the kinetics of exchange reactions between physisorbed (loosely bound) and chemisorbed (tightly bound) molecules on the surfaces of solids was partially revealed by the early work of Zimmerman¹ and Woessner² on the water-silica gel system. Interpretation of their experimental data according to the phase exchange theory of Zimmerman and Brittin³ (ZB) showed that at room temperature the transverse relaxation time T_2 is identically the mean lifetime of a pro-

ton in a physisorbed water molecule with respect to exchange with some proton species which is more tightly held. In this water-silica gel system this tightly held species is most likely⁴ the well-known silanol group. It soon appeared that many adsorption systems showed the characteristic behavior indicative of such exchange,⁵⁻⁸ namely, a decrease in T_2 as the temperature is raised, instead of the monotonic increase of T_2 with temperature which is characteristic of the dipolar relaxation mechanism in pure liquids (and solids).⁹ It is the purpose of this

paper to explore the chemistry of such exchanges and the implications of this chemistry in the definition of the various nmr parameters such as exchange times, correlation times, second moments, and relaxation times. It is necessary to define the exchange time in terms of the chemical activities of the species involved in the rate-limiting step of the exchange, and only the simplest possibilities are considered. These chemical activities must be deduced from adsorption isotherms.

Actually, there exist two relatively simple limiting conditions under which the nmr transverse relaxation may reflect chemical kinetics. One involves the transfer of the resonant nuclei between molecular environments of different chemical shift but approximately the same intrinsic transverse relaxation time, a condition typical of homogeneous liquids;¹⁰ therefore this condition has been heavily exploited for detailed studies of reaction kinetics in homogeneous liquids. The second simple condition involves the transfer of nuclei between environments of much different intrinsic relaxation time but approximately the same chemical shift;³ this condition, which approximates the situation in systems involving surfaces and macromolecules, has not been so heavily exploited, especially in regard to such details as reaction orders and mechanisms. It is this second condition which is the subject of this paper. The more complex cases in which exchange occurs between environments differing in both chemical shift and intrinsic relaxation time have been treated theoretically, and these treatments may be called upon should the need arise in the experimental situation.^{11,12}

Reactions between physisorbed and chemisorbed molecules are at the heart of industrial processes involving heterogeneous catalysis; it is hoped that the methods discussed here will be useful in basic studies of such catalytic reactions. Methods of studying the details of surface reactions are not common, especially methods for studying fast reactions; some of the reactions discussed herein reach turnover numbers for the chemisorbed species of 10^4 reactions per site per sec. But it is the possibility of deducing the reaction orders with respect to various species which should, hopefully, prove most important.

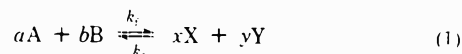
II. Surface Kinetics

A. The Exchange Probability. Under certain conditions it has been found, both theoretically and experimentally, that the observed nmr transverse relaxation time is equal to a mean time between "interphase" nuclear transfers;³ these conditions are summarized in Section IV. In this section we define this transfer or exchange time in terms of the kinetics of surface reactions.

The inverse exchange time is the *probability per unit time* that a nuclear spin forsakes one environment for another;³ as such it is the *ratio of the number of successful events per unit time to the total possible number of events*. A *successful event* is a chemical reaction (or other process) which transfers nuclei between environments; therefore the number of successful events per unit time is the *number density of reactions per unit time*. (i.e., it is the traditional forward chemical reaction rate, R_f) multiplied by the *number n_i of resonant nuclei transferred out of a molecule of species i per reaction*. The total possible number of events is the *total number density of nuclei (time independent) in the i th molecule, phase, or environment from which transfers occur*. This latter quantity is $m_i N_i$, where N_i is the number of molecules of species i

and m_i is the number of resonant nuclei per molecule. Let the resonant nuclei be protons in the remainder of this paper.

Let us formulate a general reaction as



If A has m_A protons per molecule (site) of which n_A leave the molecule per reaction and if there are a total N_A molecules (sites) of type A the probability per unit time C_A of a proton leaving the A environment is

$$C_A = k_f [A]^a [B]^b n_A (N_A m_A)^{-1} \quad (2)$$

Here the activities of the various components are indicated by [A], [B], etc. Similar equations can be written for C_B , C_X , and C_Y ; these quantities are related by stoichiometry and chemical equilibrium. It should be noted that the nmr methods discussed in this paper are limited to systems in dynamic equilibrium. Implicit in the above is the assumption that the stoichiometric reaction 1 is also the rate-limiting elementary reaction step, a condition which does not generally hold; within this assumption a and b are the reaction orders for the forward reaction with respect to species A and B, respectively. In the general case it will be necessary³ to specify also the probabilities p_{AX} , etc., that if a proton leaves molecule (phase, site) A it will go to molecule (phase, site) X; for a chemical reaction stoichiometry may suffice to define these p_{ij} , but if not, a detailed statement of the mechanism may be required. These quantities will be necessary to solve the family of coupled differential equations governing the nmr relaxation.³

B. The Kinetic Law. For reaction 1 the rate R_f of the forward reaction is, according to the activated state theory of chemical kinetics, proportional to the number N^* of activated complexes in equilibrium with the reactants¹³

$$R_f = \nu N^* = (kT/h) K_f^* [A]^a [B]^b / \gamma^* \quad (3)$$

$$= k_f [A]^a [B]^b \quad (4)$$

where $\nu = (kT/h)$ is the universal frequency (in which k is Boltzmann's constant, T the absolute temperature, and h Planck's constant). K_f^* is the equilibrium constant for formation of the activated complex from the reactants. γ^* is the activity coefficient of the activated complex, and $[A] = \gamma_A N_A$ is the activity of reactant A, etc.

In similar manner the reverse reaction rate may be written for (1) as

$$R_r = (kT/h) K_r^* [X]^x [Y]^y / \gamma_r^* \quad (5)$$

such that the equilibrium constant K_1 for (1) may be written as $K_1 = K_f^* / K_r^* = k_f / k_r$, i.e., at equilibrium $R_f = R_r$. Therefore, either the forward or reverse rate law may be used in expressing the exchange probability, whichever is more convenient (e.g., see section IV).

For low-pressure gas-phase reaction or for reactions involving neutral species in dilute solution it may be possible to set the activity coefficients γ^* , γ_A , etc., equal to unity, in which case (4) reduces to the law of mass action in the more conventional terms of concentration. For reactions between ions in solution the Debye-Hückel limiting law may be used to estimate the activity coefficients, including that for the activated complex; indeed such ionic reactions demonstrate the truth of eq 3.¹³ However, for surface systems it is with the assignment of γ^* that our rate formulation of necessity goes from the exact to the empirical, for there is no *a priori* information as to the de-

pendence of γ^* on the concentration variables of the system. Note that the rate constant k_f in (4) is constant only so long as γ^* is not a function of concentration.

A closely allied problem is the assignment of the activities of surface species themselves.¹⁴ Let all of the participating chemical species of reaction 1 be adsorbed on the surface. If each of these species is in equilibrium with the same species in the gas phase this problem is a simple one; it is not even necessary to choose standard states for the adsorbed species because those of the gas serve equally well for the adsorbed species.¹⁴ If the gas pressures are low the activities of the surface species are equal to the respective pressures (fugacities) of the gas-phase species. In fact the only difference between the system with catalytic surface present and without is that the catalytic surface allows a lower energy activated state (provided reaction 1 remains the elementary rate-limiting step under both conditions). On the other hand, a surface species may not have a gas-phase counterpart or be related to some gas-phase species in a simple way; in this case the author is unaware of any straightforward way of proceeding. An example of this latter case is a surface hydroxyl group. On a protein such as keratin the number of hydroxyl groups is clearly fixed, but their activity may vary with the amount of adsorbed water. Silica gel, however, is likely to be only in metastable equilibrium with respect to the slow hydrolysis of silica gel (at the same time the proton exchange between water and the surface hydroxyls is rapid); even though the activity of the hydroxyl groups and the ambient water pressure would be related at equilibrium, the metastable condition decouples these quantities from one another.

Because of the difficulty of specifying activities and activity coefficients it is not possible to proceed in a general fashion. Thus further theoretical consideration is limited herein to the system described as follows. Let the single physically adsorbed species be A and the chemisorbed species be B; let the activity of A, $[A]$ be equal to the pressure of A over the surface; assume that $[B]^p/\gamma^*$ is a constant (support for this will be given on a case by case basis); then the probability per unit time of proton exchange out of A, C_A , becomes (from (2) and (3))

$$C_A = k_f [A]^a / N_A \quad (6)$$

where

$$k_f' = (kT/h) K_f^* n_A [B]^p / (\gamma^* m_A) \quad (7)$$

Note that in eq 6 both the activity and the number density of the physisorbed species A appear; these are related by the adsorption isotherm.

III. Exchange Probability and Adsorption Isotherms

Let the standard state for the physisorbed species be the gas at 1 atm; then the activity of a physisorbed species is just the equilibrium pressure of its (assumed ideal) gas above the solid. Since the adsorption isotherm relates amount adsorbed to pressure, this isotherm determines the behavior of the exchange probability C_A as a function of amount adsorbed (for a given reaction order a) according to (6). Here we summarize the behavior of the exchange probability for the physisorbed species as it depends on the type of adsorption isotherm for various reaction orders. The isotherm types considered are (a) Henry's law, (b) Langmuir, and BET. The respective results are plotted in Figures 1-3. In constructing these figures it was arbitrarily decided to set the exchange time, C_A^{-1} , at 1 msec at a relative pressure (P/P_0) of 0.8.

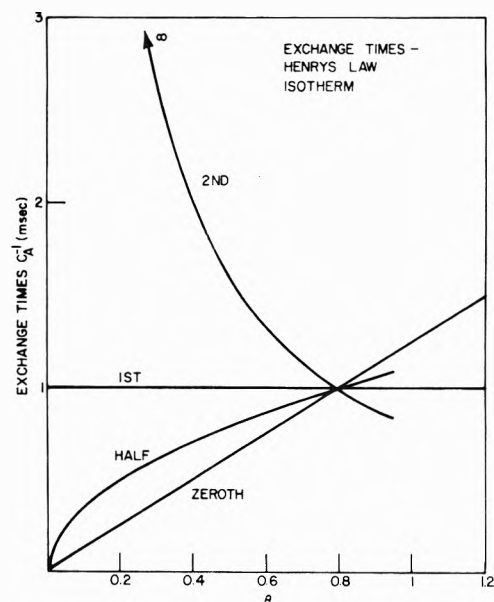


Figure 1. Exchange times C_A^{-1} vs. coverage θ for Henry's law adsorption isotherm. Each curve is labeled by the order of the reaction with respect to the physisorbed species in the hypothetical exchange reaction. All plots are normalized at $\theta = 0.8$.

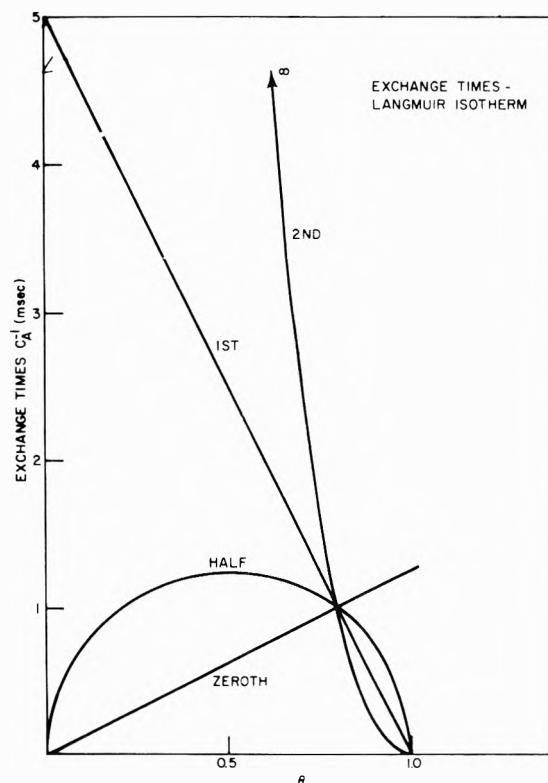


Figure 2. Exchange times C_A^{-1} vs. coverage θ for Langmuir adsorption isotherm. Each curve is labeled by the order of the reaction with respect to the physisorbed species in the hypothetical exchange reaction. All plots are normalized at $\theta = 0.8$.

According to Henry's law

$$N_A = \alpha [A] \quad (8)$$

where α is a proportionality constant, so that

$$C_A^{-1} = N_A^{1-a} (k_f' \alpha^a)^{-1} \quad (9)$$

as is shown in Figure 1.

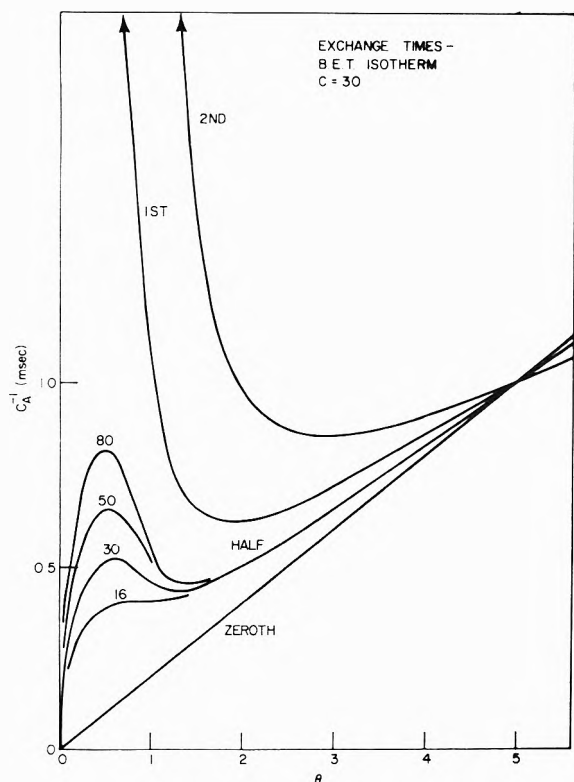


Figure 3. Exchange times C_A^{-1} vs. coverage θ for BET adsorption isotherm. Each curve is labeled by the order of the reaction with respect to the physisorbed species in the hypothetical exchange reaction; in addition the half-order plots are given for various values of C , the adsorption strength index of the first layer (see text). All plots are normalized at $P/P_0 = 0.8$.

The Langmuir isotherm yields¹⁵

$$N_A = N_{\max}[A](\beta + [A])^{-1} \quad (10)$$

in which β is $\gamma T^2 \exp(-Q/RT)$, T the absolute temperature, Q the heat of adsorption, R the gas constant, γ a proportionality constant, and N_{\max} is the number of surface sites for physisorption. It follows that

$$C_A^{-1} = (k_f' \beta^a)^{-1} N_A^{1-a} (N_{\max} - N_A)^a \quad (11)$$

These data are plotted in Figure 2; normalization makes this plot "independent" of temperature.

The BET isotherm is of the form¹⁶

$$N_A = \frac{N_{\text{mono}} \epsilon [A]}{1 + (\epsilon - 2)[A] + (\epsilon - 1)[A]^2} \quad (12)$$

where N_{mono} is the concentration at monolayer coverage and $\epsilon \sim \exp[(Q_1 - Q_l)/RT]$, where Q_1 is the heat of adsorption in the first layer and Q_l is the heat of liquifaction. See Figure 3 for the graphical display of C_A^{-1} . Note that in this case, for reaction order $1/2$, we show the marked dependence of the exchange time on the ϵ parameter; there is a pronounced maximum at coverages less than one monolayer for $\epsilon \geq 30$ ($Q_1 - Q_l \sim 2$ kcal/mol and $T = 300^\circ\text{K}$).

The three theoretical isotherms above do not exhaust the possible range of isotherms; they are at least representative. However the isotherm is really an experimental quantity which must be determined for the given system in which one might wish to inquire about kinetics. The effects cataloged above for various reaction orders show a great sensitivity to the reaction order, indicating a real

possibility for determining the order for those systems with reaction rates in the proper range for nmr study.

IV. Relaxation Times and Exchange Rates

As a hypothetical system for discussion let us take a high area surface with chemisorbed and physisorbed benzene molecules in equilibrium with each other and with the gas phase. (The gas phase can be neglected as far as relaxation of the system as a whole is concerned, because for proton containing molecules gas-phase relaxation is slow, and because there are relatively few molecules in the gas as compared to the adsorbed state.)⁹ Assume the chemical shifts are the same in all phases or environments. Assume that there are many more physisorbed than chemisorbed molecules. To calculate relaxation times for the exchanging system according to the ZB rules³ we must define intrinsic relaxation times for each molecule (phase) in addition to defining the probability for exchange as was done above. The results of such a calculation, done previously for a model of the benzene-charcoal system,⁴ are given in Figure 4 and this is our point of departure. This figure represents a section of constant concentration through the three dimensional surface which we are constructing on the axes (inverse temperature-relaxation time-concentration). To calculate a relaxation time according to the BPP theory¹⁷ a mean square local field (second moment) and a correlation time τ for molecular motion are required. A law for the variation of the correlation time with temperature must be assumed, and we use the Arrhenius law. We assume that the physisorbed and chemisorbed molecules differ only in that the chemisorbed species has a higher Arrhenius activation energy; they have the same Arrhenius preexponential factors and second moments. The second moment is chosen as that for a benzene molecule with rapid hexad axis rotation (*i.e.*, with partial motional narrowing). Finally, it is assumed that for the chemisorbed molecules the BPP correlation time τ_B is identical with the mean lifetime C_H^{-1} for a molecule in the chemisorbed state.

This assumption of equality between τ_B and C_H^{-1} for the chemisorbed species, though not necessary, is quite reasonable (and it has the virtue of reducing the number of free parameters by two). To support this assumption requires an inquiry into the nature of the correlation times and into the origins of the local field for adsorbed molecules. The local field for a nucleus in an adsorbed molecule may be intramolecular, intermolecular from other molecules, or intermolecular from some magnetic nuclei present in the surface. The correlation time is roughly the time between molecular or atomic jumps which move nuclear magnets with respect to one another, such as rotational and translational jumps. Now the transverse relaxation time (or inverse line width) is a measure of "spectral intensity" at zero frequency;¹⁷ *i.e.*, it is determined for a resonant nucleus by the *slowest* relative motions of its neighboring nuclear magnets. The essential distinction between the chemisorbed and physisorbed states is one of tightness of binding to the surface; because the chemisorbed species is more tightly bound it must overcome a higher barrier in order to jump, and *therefore jumps less often* with respect to its surroundings. The net result of the faster motion of the physisorbed molecules is that the contributions of their nuclear moments to the intermolecular local field of the chemisorbed species is much reduced by motional narrowing in comparison with intramolecular contributions of the

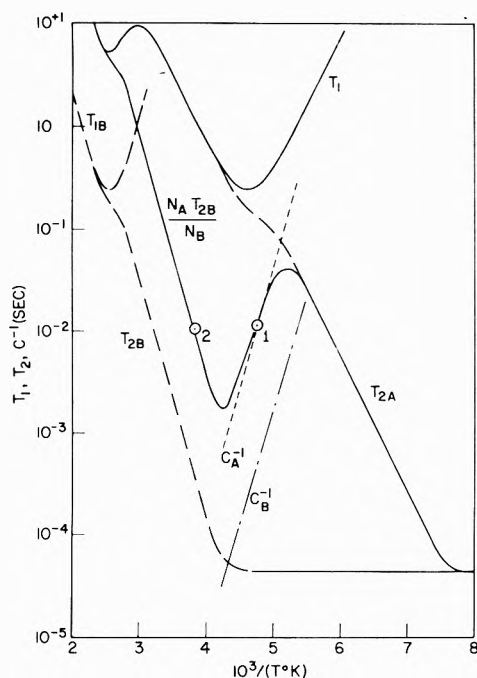


Figure 4. The relaxation times (T_1 , T_2 , T_{2B} , and T_{2A}) and the lifetimes in phase (C_A^{-1} , C_B^{-1}) as functions of reciprocal temperature calculated for benzene adsorbed on a hypothetical surface for which 4% of the sites have translational barriers of 10.8 kcal/mol and the remainder 6 kcal/mol. The subscript B refers to the high-energy sites and A to the normal sites (see ref 4). This is a "constant composition" diagram, which stands at the normalization points of Figures 1-3 and 5; the exchange time-composition isotherms of Figures 1-3 would intersect this diagram at point 1. The relaxation time-composition diagram of Figure 5 would intersect it at point 2.

chemisorbed molecule itself or contributions from magnetic ingredients of the surface. How does a nucleus in a chemisorbed molecule move with respect to the sources of its local field? It can move by translation directly to another chemisorption site; in this case the chemisorbed species have among themselves a translational correlation time. Included among such motions might be a pseudo rotation of hydroxyl groups bound to the same center. These motions are not affected by the chemistry of the exchange reaction and hence are not of direct interest in this paper; however, such motions have the same effect as zero-order reactions as far as the intrinsic relaxation time of the chemisorbed species is concerned. But the chemisorbed species can also move by the very act of transfer to the physisorbed state; the mean time between transfers is then identically the correlation time.¹⁸ Since this correlation time reflects the kinetic laws governing the exchange, so also must the intrinsic T_2 of the chemisorbed phase reflect these kinetic laws.

The intrinsic relaxation times for the model system defined above are indicated in Figure 4, along with the observable relaxation times; here again the physisorbed species is labeled A and the chemisorbed is labeled B. Note that except for low temperatures the intrinsic times for the chemisorbed phase are not directly measurable, but only reflect themselves in the observable weighted average. This observable T_2 is approximately given for $N_B/N_A \ll 1$ by

$$T_2^{-1} = (m_B N_B / m_A N_A) (T_{2B} + C_B^{-1})^{-1} + T_{2A}^{-1} \quad (13)$$

which follows²⁰ from the ZB theory.³ Since whole molecules are exchanging in the hypothetical system, m_B/m_A

= 1. There are three "terms" each of which dominates in a certain temperature range, as Figure 4 shows. At low temperatures the observed T_2 is T_{2A} ; at intermediate temperatures the observed T_2 is

$$T_2 = (N_A / N_B) C_B^{-1} = C_A^{-1} \quad (14)$$

and at high temperatures the observed T_2 is

$$T_2 = T_{2B} (N_A / N_B) \quad (15)$$

Sections II and III were devoted to the intermediate temperature region; isotherms were developed there which intersect Figure 4 at, e.g., point 1 as the point of normalization. Depending on the applicable kinetic law and isotherm some one of the isotherms of Figures 1-3 might emanate from this point. When only two species containing resonant nuclei are present, such as in the system under consideration, C_A and C_B are related by equilibrium and stoichiometry as

$$m_A N_A C_A = m_B N_B C_B \quad (16)$$

and this is the basis for the second equality of (14). Thus because the physisorbed phase is more mobile and because it is present in excess, the experimental quantity is C_A^{-1} . Note that the probability per unit time C_B of leaving the chemisorbed state is by definition the turnover number for the site to which the chemisorbed molecule is attached, i.e., it is the number of reactions per "active center" per unit time (within a factor m_B/n_B of order unity). An estimation of this turnover number *via* (16) requires both the experimental quantity C_A and a knowledge of the ratio N_A/N_B ; this ratio in favorable cases² may also be furnished by the nmr experiment.

In the high-temperature region, the BPP¹⁷ expression for T_2 can be used as

$$T_{2B}^{-1} = \sigma_B^2 \tau_B = \sigma_B^2 C_B^{-1} \quad (17)$$

where σ_B^2 is the Van Vleck second moment for the chemisorbed molecules. Therefore, at high temperatures the observed T_2 is, for the model of Figure 4

$$T_2 = (N_A / N_B) C_B / \sigma_B^2 \quad (17a)$$

and, using (6) and (16) this becomes

$$T_2 = (N_B^2 \sigma_B^2)^{-1} k_f' N_A [A]^0 \quad (17b)$$

If the number N_B of chemisorbed molecules remains constant, then again the adsorption isotherm can be called upon to relate N_A and $[A]$. Theoretical T_2 values can then be computed for various reaction orders. Such T_2 isotherm would intersect Figure 4 at point 2, for example. A sample isotherm, based on the BET adsorption isotherm, is given in Figure 5; it turns out that in this temperature region T_2 is not as markedly sensitive to the type of isotherm or reaction order. For example, the plot for a Henry's law isotherm would look much the same. The reason for this lies in the relative form of (6) in contrast to (17b); in the former the ratio $[A]^0/N_A$ appears in contrast to the product $[A]^0 N_A$ in the latter. Since the lowest order term in a power series expansion of $[A]$ in terms of N_A is the linear one (i.e., zero adsorption at zero pressure), the ratio allows C_A to go from zero to infinity at $N_A = 0$, depending on the reaction order, whereas the product must always go to zero at $N_A = 0$.

At low temperatures (e.g., $10^3/T > 4.5$ in Figure 4) the transverse nuclear magnetization actually decays as the sum of an exponential (with time constant given by (13)) and a "rigid lattice" decay function; if $N_B/N_A \ll 1$ obser-

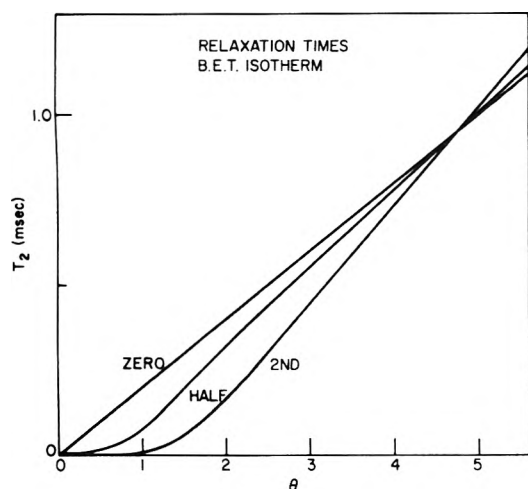


Figure 5. Relaxation times in the fast exchange region (see text) vs. coverage θ according to the BET adsorption isotherm. Each curve is labeled by the order of the reaction with respect to the physisorbed species in the hypothetical exchange reaction. All plots are normalized at $P/P_0 = 0.8$.

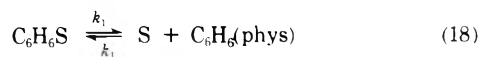
vation of this "rigid lattice" part of the decay will be difficult because of the low amplitude associated with it (if the relative concentration of the chemisorbed species is low) and because of its fast decay.

Although the nmr parameters chosen to construct Figure 4 are based on the molecule benzene, the results given there pertain in general to exchange equilibria between chemisorbed and physisorbed molecules, especially as regards the temperature dependence of the relaxation times.

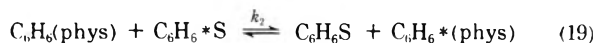
V. Comparison with Experiment

Many systems have been found in which the relaxation behavior is similar to that described in Figure 4,^{2,5-8,21,22} but in relatively few was the degree of surface coverage a variable; three of these latter are discussed briefly below.

A. *Benzene Adsorbed on Charcoal.*⁵ For the system described in III the exchange between chemisorbed and physisorbed benzene molecules might take place by a unimolecular dissociation of the chemisorption complex as



or it may be a cooperative process as



Here $\text{C}_6\text{H}_6(\text{phys})$ represents the physisorbed species (species A), $\text{C}_6\text{H}_6\text{S}$ the chemisorbed species (species B), and S the site for chemisorption. The asterisk in (19) is merely a bookkeeping device to indicate that exchange has taken place. For reaction 18 the forward rate R_f is

$$R_f = (kT/h)K_{1f}^*\gamma_B N_B/\gamma^* \quad (20)$$

One might suppose that for this unimolecular process the activated state is closely related in structure to the chemisorption complex, so that $\gamma_B = \gamma^*$; if this is true then the probability per unit time for dissociation of the surface complex, C_B , becomes (for $m_A = m_B = n_A = n_B$ in (2))

$$C_B = R_f N_B^{-1} = (kT/h)K_{1f}^* \quad (21)$$

which is independent of surface coverage. Likewise, *via* (16) the probability per unit time for a molecular departure from the physisorbed state becomes

$$C_A = N_B K_{1f}^* (kT/h) N_A^{-1} \quad (22)$$

Now both N_A and N_B are determined by adsorption isotherms. However the hypothesis is that the chemisorbed species (B) is much more strongly attached; this means that as benzene molecules are adsorbed N_B reaches its saturation value before N_A increases much from zero. Thus N_B is roughly constant in the pressure region where N_A is changing. Under these conditions C_A becomes

$$C_A = k'' N_A^{-1} \quad (22a)$$

which is essentially eq 6 for a reaction zero order with respect to the physisorbed species.

If the same assumptions, *i.e.*, $\gamma^* = \gamma_B$ and $N_B = N_{B\text{max}}$, are made in setting up C_A for the cooperative reaction 19, C_A becomes

$$C_A = (kT/h)K_{2f}^* N_B([A]/N_A) \quad (23)$$

The adsorption isotherm for the charcoal benzene system is Langmuir like;⁵ for this isotherm the exchange times are given in Figure 2, and the expected trends in C_A^{-1} are clearly different for first and zeroth order kinetics.

Experimentally, for benzene adsorbed on charcoal there was found a plateau in T_2 at high temperatures instead of the maximum and minimum in T_2 expected from the model leading to Figure 4. This plateau has been accounted for by allowing a distribution of barrier heights for the chemisorbed species,⁴ instead of the single barrier height for the chemisorbed species which was used in constructing Figure 4. (In constructing this model it was assumed that $N_B = N_{B\text{max}}$, the number of chemisorbed molecules is 8% of $N_{A\text{max}}$ the number of physisorbed molecules at full loading.) The values of T_2 on the plateau, according to the distribution model,⁴ represent a "convolution" of exchange and high-temperature relaxation effects. It is certainly possible to insert the kinetic ideas presented here in that distribution model, but such work has not yet been done. For the first-order kinetics though, as N_A is raised, the chemical exchange effects push the value of T_2 on the plateau toward lower values (Figure 2) in competition with the relaxation effects which tend to raise the value of T_2 on the plateau (Figure 5). In contrast, for the zeroth-order kinetics both relaxation and exchange effects tend to raise the T_2 value on the plateau in proportion to the coverage of benzene. Experimentally, the value of T_2 on the plateau is proportional to the coverage of benzene (Figure 8 of ref 5). Therefore the zeroth-order kinetics are indicated for the exchange process between chemisorbed and physisorbed benzene molecules.

B. *Water Adsorbed on Keratin.* Lynch and Marsden⁶ (LM) observed T_2 maxima in this system at various water contents, and pointed out that this process represented the exchange of water protons with the labile protons of the wool keratin, namely, those attached to oxygen, nitrogen, or sulfur atoms (which in this case we call the chemisorbed protons). LM were reluctant to extract the exchange rate for the water molecules from their data, because they had no way of deciding whether the observed effect was due to a single one of these, hydroxyl, amino, etc. groups or whether the effects from the various groups did in fact overlap. This possible source of heterogeneity is ignored here; it is assumed that all the observed "chemisorbed protons" have the same exchange rate. Equations 13 and 14 have been used to estimate C_A^{-1} at $\sim 110^\circ$ from the LM data, and these are shown in Figure 6; note the maximum in C_A^{-1} which is superimposed on a trend for

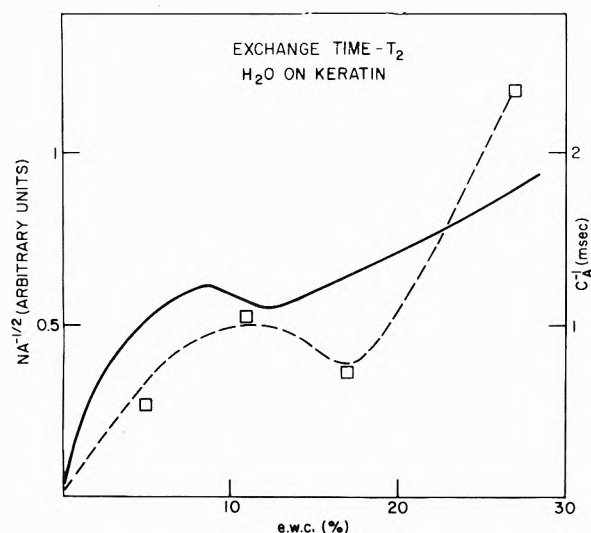
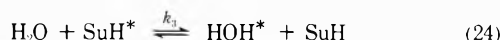


Figure 6. Exchange times at 110° for the system keratin-water; \square , from experiments of Lynch and Marsden (dashed curve for interpolation); and theoretical, based on adsorption isotherm C of Figure 7.

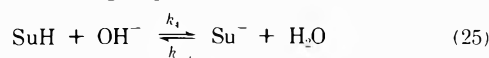
C_A^{-1} to rise with concentration of adsorbed water. Reference to Figure 1 of LM⁶ will show that this undulation is clearly not due to uncertainty in the data; the undulation appears similar to those shown in Figure 3 for the half-order reaction in a system governed by a BET isotherm. The isotherm, published earlier by these authors²³ is given in Figure 7, and shows a BET-like behavior. Reference to Figure 3, therefore, suggests that the order of the exchange reaction with respect to water is greater than zero but less than one. Let us assume that the order with respect to water is one-half, and use the isotherm to construct a theoretical plot of C_A^{-1} vs. loading. Unfortunately the isotherm lacks data at low water vapor pressures, and we must therefore interpolate in this region; three possible interpolations are given in Figure 7. Adsorption isotherm C of Figure 7 has been used with eq 6 to construct the theoretical C_A^{-1} curve of Figure 6, which does reproduce the trend of C_A^{-1} vs. equilibrium water concentration. First-order plots, based on the isotherms of Figure 7, resemble that of Figure 3, and hence do not reproduce the trend of the C_A^{-1} vs. equilibrium water concentration.

The stoichiometry of the exchange reaction must ultimately be

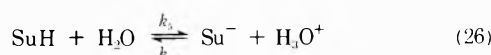


(where the asterisk is a bookkeeping device to indicate that exchange has occurred, and SuH indicates the proton "chemisorbed" to the surface) but it is not obvious that (24) has any "mechanistic" content. A six-membered hydrogen-bonded ring involving two water molecules and a surface hydroxyl might allow a concerted proton shift, but this reaction is second order in H_2O .

The rate-limiting steps may involve hydroxyl or hydronium ions (and thus the ionization equilibria of adsorbed water and of the surface groups themselves), as



and



even the surface diffusion coefficients of these mobile ions may be rate limiting. Consideration of such reactions re-

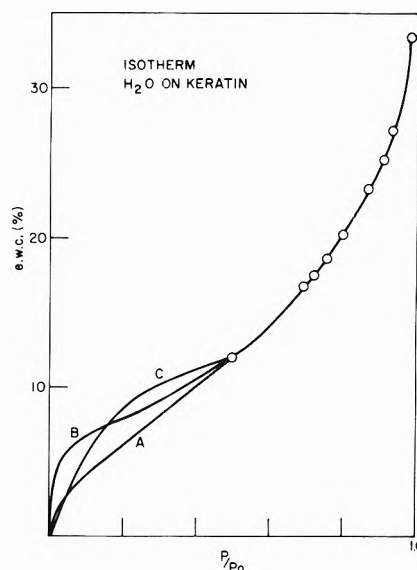


Figure 7. Adsorption isotherm for keratin-water system from data of Lynch and Marsden (ref 19). Possible extrapolations to zero pressure are given; that labeled C was chosen to construct the exchange time plot for Figure 6.

quires knowledge of the equilibrium constants involved in the surface situation, and also knowledge of the "surface" activity coefficients of the ions involved.

Thus, the mechanistic implications of an exchange reaction which is half order with respect to adsorbed water are not yet evident.

C. Water Adsorbed on Zeolite 13-X. Maxima in T_2 , as in Figure 4, have been found for the proton relaxation times for water adsorbed in zeolite 13-X in several studies.^{7,21,22} Pfeifer²⁴ has analyzed the data of Gutsze, *et al.*⁷ to yield $\tau_{\omega\omega}$ ($= C_B^{-1}$), the mean lifetime of a proton in the "chemisorbed" state, *i.e.*, presumably in a hydroxyl group. This analysis was based on ZB,³ *i.e.*, essentially on eq 14 and his²³ estimates of $N_{\text{H}_2\text{O}}$ ($= N_A$) and N_{OH} ($= N_B$). These data are presented in Table I for three degrees of filling of the zeolite pores. From the definition of C_B it follows (taking reaction 1 as a model) that

$$C_B = (kT/h)K_f^*[A]^a[B]^b/(\gamma^*N_B) \quad (27)$$

New evidence²⁵ suggests that the exchange reaction is first order in the surface hydroxyl concentration, *i.e.*, that $b = 1$. If it were known that the activated complex were structurally closely related to the hydroxyl group, then it would perhaps be reasonable to set $\gamma_B = \gamma^*$. The assumptions of first order with respect to hydroxyl and equality of γ_B and γ^* allow (27) to be simplified to

$$C_B = (kT/h)K_f^*[A]^a = k_f'''p_{\text{H}_2\text{O}}^a \quad (27a)$$

where $p_{\text{H}_2\text{O}}$ is the vapor pressure of water over the zeolite specimen, and a is the order of the exchange reaction with respect to water. The water adsorption isotherm for 13-X zeolite²⁵ has been used to calculate C_B for reaction orders $a = 1/2$ and $a = 1$; which are given in Table I; for $a = 0$ the value of C_B does not depend on $p_{\text{H}_2\text{O}}$. The best fit is clearly for $a = 1/2$; the order of the exchange reaction between surface hydroxyls and adsorbed water appears to be half order. In a subsequent paper²⁵ are presented data for higher relative pressures of water which also estimate the order of the reaction with respect to water of $1/2$.

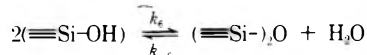
As for the system water on keratin, it is not clear what the mechanistic implications of the half-order reaction might be. In addition to the reactions written above for

TABLE I: Exchange Times for Zeolite Hydroxyls

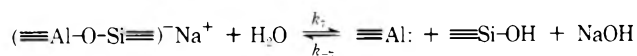
θ	$\tau_{\omega\omega}(\text{expt}),^a$ msec	P/P_0	$\tau_{\omega\omega}(\alpha=1)^a$	$\tau_{\omega\omega}(\alpha=1/2)^a$
0.66	0.2	0.0080	0.2 ^a	0.2 ^a
0.18	0.7	0.00035	4.6	0.96
0.1	<1.5	0.00014	11.4	1.52

^a $\tau_{\omega\omega} = C_B^{-1}$ of text.

that system, several lattice hydrolysis reactions might be of importance for the zeolite system²⁶



and



However, these reactions are likely to be slow and also likely to be not reversible.

VI. Summary and Conclusions

In this paper we have shown how nuclear magnetic resonance relaxation experiments can be used not only to measure rates of surface reactions but also to infer reaction orders with respect to the physisorbed and chemisorbed reactants. Knowledge of the details of the adsorption isotherm is important to satisfactorily extract such mechanistic information. For the benzene on charcoal system the exchange reaction between chemisorbed and physisorbed molecules is zero order in the physisorbed molecule activity. The rate of exchange of adsorbed water molecules with surface hydroxyls is best described as half order with respect to water activity, both in the water-zeolite and water-keratin systems.

Although reaction orders have been deduced for such surface reactions, the work of rationalizing these in terms of elementary reaction steps remains to be done. For instance the half-order reaction almost implies a preequilibrium in which a water molecule in conjunction with the surface breaks up into two equivalent parts each active in the exchange reaction. It is not clear in terms of surface structures just how this could be done. In fact the formulation of reaction rates at equilibrium in terms of such simple reactions as (18), (19), and (24) is most likely a gross oversimplification. Further theoretical development most likely must await more complete experimental data on carefully chosen systems. Ultimately, it may be possible to bring the state of reaction kinetics involving adsorbed water to the present state of understanding of aqueous solutions.²⁷

It should be reemphasized that the immobilization of the chemisorbed species gives it a much shorter relaxation time, which through the averaging brought about by chemical exchange, is able to cause a shortening of the overall relaxation time of the system, even though the chemisorbed species may contain only a few per cent of the resonant nuclei. Heretofore, this "kinetic microscope" has been used only when provided by nature; no conscious effort has been made to immobilize some species about which kinetic information may be desired by tying one end down (as onto some porous glass) and measuring the kinetics of the other. Methods for preparing such systems have been worked out.²⁸

Acknowledgments. Thanks are due to V. R. Deitz for helpful discussions leading to ref 14, to J. S. Murday and

N. H. Turner for critically reading the manuscript, and to B. L. Russell for preparing the manuscript for publication.

References and Notes

- (1) J. R. Zimmerman and J. A. Lasater, *J. Phys. Chem.*, **62**, 1157 (1958).
- (2) D. E. Woessner, *J. Chem. Phys.*, **39**, 2783 (1963).
- (3) J. R. Zimmerman and W. E. Brittin, *J. Phys. Chem.*, **61**, 1328 (1957).
- (4) H. A. Resing, *Advan. Mol. Relaxation Proc.*, **1**, 109 (1958).
- (5) J. K. Thompson, J. J. Krebs, and H. A. Resing, *J. Chem. Phys.*, **43**, 3853 (1965).
- (6) L. J. Lynch and K. H. Marsden, *J. Colloid Interface Sci.*, **42**, 209 (1973).
- (7) A. Gutsze, D. Deininger, H. Pfeifer, G. Finger, W. Schirmer, and H. Stach, *Z. Phys. Chem. (Leipzig)*, **249**, 383 (1972).
- (8) See also H. A. Resing, J. K. Thompson, and J. J. Krebs, *J. Phys. Chem.*, **68**, 1621 (1964); T. F. Child, *Polymer*, **259** (1972); V. V. Morariu and R. Mills, *Z. Phys. Chem. (Frankfurt am Main)*, **83**, 41 (1973); G. J. Kruger and G. Helcke in "Proceedings of the 14th Colloque Ampere," R. Blinc, Ed., North Holland Publishing Co., Amsterdam, 1967; H. A. Resing and R. A. Neihof, *J. Colloid Interface Sci.*, **34**, 480 (1970); D. E. Woessner and B. S. Snowden, *ibid.*, **34**, 290 (1970).
- (9) The interaction of the nuclear magnetic moment with the molecular rotational magnetic moment may also give rise to T_2 (and T_1) maxima. See H. A. Resing, *Advan. Mol. Relaxation Proc.*, **3**, 199 (1972), for an example. Such effects are likely in the surface chemical context for spherical nonpolar molecules which would not be likely to chemisorb or react at the low temperatures thus far investigated. For spin-rotation interaction review see M. Bloom, *MTP Int. Rev. Sci., Phys. Chem. Ser. 1*, **4**, 1 (1971).
- (10) J. Kaplan, *J. Chem. Phys.*, **28**, 278 (1958); H. S. Gutowsky, D. W. McCall, and C. P. Slichter, *ibid.*, **21**, 279 (1953).
- (11) J. S. Leigh, Jr., *J. Magn. Resonance*, **4**, 308 (1971); L. W. Reeves and K. N. Shaw, *Can. J. Chem.*, **48**, 3641 (1970); J. P. Carver and R. E. Richards, *J. Magn. Resonance*, **6**, 89 (1972); C. Deverell, R. E. Morgan, and J. H. Strange, *Mol. Phys.*, **18**, 553 (1970).
- (12) D. E. Woessner and J. R. Zimmerman, *J. Phys. Chem.*, **67**, 1590 (1963).
- (13) M. Boudart, "Kinetics of Chemical Processes," Prentice-Hall, Englewood Cliffs, N. J., 1968.
- (14) Although it is clear from thermodynamic considerations that activities rather than concentrations must appear in the rate formulation, it is difficult to find works in which serious attempts are made to do this for surface systems. A review article by Wagner, however, gives detailed recipes for obtaining activities of surface species (C. Wagner in "Heterogeneous Kinetics at Elevated Temperatures," G. R. Belton and W. L. Worrell, Ed., **21**, 323 (1970)).
- (15) S. Brunauer, "The Adsorption of Gases and Vapors," Princeton University Press, Princeton, N. J., 1943, p 60.
- (16) Reference 15, p 151.
- (17) N. Bloembergen, E. M. Purcell, and R. V. Found, *Phys. Rev.*, **73**, 679 (1948).
- (18) Limit consideration to the intramolecular dipolar interactions between the nuclei of the chemisorbed molecule; since these nuclei are at fixed distances, we are then concerned only with the orientation (specified by the angles θ and φ) of the internuclear vectors with respect to the magnetic field direction. This orientation remains constant until the molecule jumps from its chemisorption site. Then, because the motion of the physisorbed molecule is much faster (by hypothesis), this vector is immediately free to assume any orientation with equal probability. The correlation function of interest for T_2 calculations is¹⁷

$$k(t) = \langle (1 - 3 \cos^2 \theta_0)(1 - 3 \cos^2 \theta(t)) \rangle_t,$$

which has the equivalent ensemble average¹⁹

$$k(t) = \int \int P(\theta, \theta_0, t)(1 - 3 \cos^2 \theta)(1 - 3 \cos^2 \theta_0)P(\theta_0) d\theta d\theta_0,$$

where $P(\theta_0) = \frac{1}{2} \sin \theta_0$ is the probability of original orientation within $d\theta_0$, $P(\theta, \theta_0, t)$ is the conditional probability of orientation θ in $d\theta$ at time t , given θ_0 , and θ is the angle between the magnetic field direction and the internuclear vector. $P(\theta, \theta_0, t)$ can be written as $\sum_n P(\theta, \theta_0; n) P_n(t)$ in which $P(\theta, \theta_0; n)$ is the conditional probability of θ in $d\theta$ after n jumps, given θ_0 . Thus $P(\theta, \theta_0; 0) = \delta_{\theta, \theta_0}$ and $P(\theta, \theta_0; n) = \frac{1}{2} \sin \theta$ for $n > 0$, by hypothesis. If the Poisson distribution is used to estimate $P_n(t)$, we have that the probability of no jump in time t , $P_0(t) = \exp(-t/\tau)$ and that the probability of one or more jumps

$$P_1'(t) = \sum_{n=1}^{\infty} P_n(t)$$

is given by $1 - \exp(-t/\tau)$; here $\tau \equiv C_B^{-1}$ is the mean residence time of a molecule in a chemisorption site. Integration yields directly

$$k(t) = (4/5) \exp(-t/\tau)$$

which is, incidentally, the BPP¹⁷ result. For intermolecular dipolar interactions of the nuclei of the chemisorbed molecule with those of other chemisorbed molecules or with those of the surface, the essential problem in the calculation of T_2 is one of the diffusion of the fleeing entity about its former dipolar partners, but the result should be essentially the same.

(19) H. C. Torrey, *Phys. Rev.*, **92**, 962 (1953).

(20) D. E. Woessner, *J. Chem. Phys.*, **35**, 41 (1961).

(21) H. A. Resing and J. K. Thompson, *Advan. Chem. Ser.*, **No. 101**, 473 (1971).

(22) H. A. Resing and J. S. Murday, *Advan. Chem. Ser.*, **No. 121**, 414 (1973).

(23) L. J. Lynch and K. H. Marsden, *J. Chem. Phys.*, **51**, 5681 (1969).

(24) H. Pfeifer, in *Proceedings of the Third International Conference on Molecular Series*, J. B. Uytterhoeven, Ed., Leuven University Press, Leuven, p 53; see also comment there by H. A. Resing, p 54.

(25) J. S. Murday, R. A. Patterson, H. A. Resing, J. K. Thompson, and N. H. Turner, manuscript in preparation.

(26) G. T. Kerr, *Advan. Chem. Ser.*, **No. 121**, 219 (1973).

(27) M. Eigen in "Nobel Symposium 5," S. Claesson, Ed., Interscience, New York, N. Y., 1967, p 245.

(28) T. Mitchell, Thesis, Northwestern University, 1971.

Volume Change for the Formation of Magnesium Sulfate Ion Pairs at Various Temperatures

Frank J. Millero* and William L. Masterton

The University of Miami, Rosenstiel School of Marine and Atmospheric Science, Miami, Florida 33149 (Received May 7, 1973; Revised Manuscript Received February 4, 1974)

Publication costs assisted by the Office of Naval Research and the National Science Foundation

The apparent molal volumes of aqueous MgSO₄ solutions from 0 to 1 *m* at 0, 25, and 50° have been used to estimate the apparent molal volume of the ion pair MgSO₄[°], $\phi_V(\text{MgSO}_4^\circ)$ using the relation $\phi_V(\text{obsd}) = (1 - \alpha)\phi_V(\text{MgSO}_4^\circ) + \alpha\phi_V(\text{Mg}^{2+}, \text{SO}_4^{2-})$ where $\phi_V(\text{obsd})$ is the observed apparent molal volume for MgSO₄ solutions at molality m_T , α is the fraction of free ions, and $\phi_V(\text{Mg}^{2+}, \text{SO}_4^{2-})$ is the apparent molal volume of the free ions Mg²⁺ and SO₄²⁻ at the ionic strength $I_m = 4\alpha m_T$. Using known association constants for the formation of MgSO₄[°] and various estimates for $\phi_V(\text{Mg}^{2+}, \text{SO}_4^{2-})$, we have determined the ϕ_V of MgSO₄[°] and $\Delta\phi_V$ for its formation as a function of temperature and concentration. The infinite dilution values for the ϕ_V° of the ion pair MgSO₄[°] appear to be independent of the various estimates of the ϕ_V of the free ions Mg²⁺ + SO₄²⁻. The $\Delta V^\circ = \Delta\phi_V^\circ$ for the formation of MgSO₄[°] at 25° is in reasonable agreement with the results calculated from the high-pressure conductance data of Fisher and theoretical estimates. The ΔV° calculated from the density data appears to go through a minimum when plotted *vs.* temperature similar to the volume change for the ionization of weak acids and bases. The ϕ_V° and $\Delta\phi_V^\circ$ results for MgSO₄[°] are briefly discussed in terms of the structure of the ion pair.

Introduction

Although the volume changes for the ionization of weak acids and bases have been studied by a number of workers,¹ the volume changes associated with ion pair formation



have received little attention. Most of our knowledge on the volume changes of ion pair formation at infinite dilution

$$\Delta \bar{V}^\circ(\text{MA}^\circ) = \bar{V}^\circ(\text{MA}^\circ) - \bar{V}^\circ(\text{M}^+) - \bar{V}^\circ(\text{A}^-) \quad (2)$$

comes from measurements on the effect of pressure on ion pair formation constants

$$(\partial \ln K_A / \partial P)_T = -\Delta \bar{V}^\circ / RT \quad (3)$$

For example, Fisher and coworkers^{2,3} have measured the effect of pressure on the formation of MgSO₄[°], MnSO₄[°], and LaSO₄⁺ ion pairs in water; Hale and Spedding⁴ have measured the effect of pressure on the formation of EuSO₄⁺, and Hamann and coworkers⁵ have measured the effect of pressure on the formation of LaFe(CN)₆[°] ion pairs in water.

Direct measurements of the volume change of ion pair formation have been made by Spiro, *et al.*⁶ They found that the volume changes for the formation of both inner- and outersphere complexes were similar and also of the same order of magnitude as for weak acids. Their comparison of the volume changes for related systems under closely similar conditions have proved very useful although the establishment of a general criterion for distinguishing between the two structural types was not possible (see, also, recent work of Hemmes⁷).

In recent years, general methods of examining the apparent molal volume (ϕ_V) and partial molal volume (\bar{V}_2) of electrolyte solutions in terms of ion pair formation have been developed.^{1,8-14} The methods applied to the apparent volume change ($\Delta\phi_V$) for the formation of the MA[°] ion pair (eq 1) are outlined briefly below.

If we apply Young's rule¹⁵ to the volume components of the solution (M⁺, A⁻, and MA[°]), we obtain

$$\phi_V(\text{obsd}) = \alpha\phi_V(\text{M}^+, \text{A}^-) + (1 - \alpha)\phi_V(\text{MA}^\circ) \quad (4)$$

where α is the fraction of free ions, $\phi_V(\text{obsd})$ is the observed apparent molal volume at total molality m_T , $\phi_V(\text{M}^+, \text{A}^-)$ is the apparent molal volume of the free ions

at $I = \alpha m_T$ (for a 1-1 electrolyte), and $\phi_V(\text{MA}^\circ)$ is the apparent molal volume of the ion pair. By rearranging eq 4, we have

$$\phi_V(\text{MA}^\circ) = [\phi_V(\text{obsd}) - \alpha\phi_V(\text{M}^+, \text{A}^-)]/(1 - \alpha) \quad (5)$$

$$\Delta\phi_V(\text{MA}^\circ) = [\phi_V(\text{obsd}) - \phi_V(\text{M}^+, \text{A}^-)]/(1 - \alpha) \quad (6)$$

where $\Delta\phi_V(\text{MA}^\circ)$ is the apparent volume change that takes place when the ion pair is formed (at infinite dilution $\Delta\phi_V^\circ = \Delta\bar{V}^\circ$, the partial molal volume change for the formation of the ion pair).

Equations 5 and 6 can be used to determine $\phi_V(\text{MA}^\circ)$ or $\Delta\phi_V(\text{MA}^\circ)$ from $\phi_V(\text{obsd})$ provided $\phi_V(\text{M}^+, \text{A}^-)$ and $(1 - \alpha)$ can be estimated. By rearranging eq 6 and solving for $(1 - \alpha)$, we have

$$(1 - \alpha) = \frac{\phi_V(\text{obsd}) - \phi_V(\text{M}^+, \text{A}^-)}{\Delta\phi_V(\text{MA}^\circ)} \quad (7)$$

Equation 7 can be used to determine the fraction of ions paired $(1 - \alpha)$ from $\phi_V(\text{obsd})$ provided $\phi_V(\text{M}^+, \text{A}^-)$ and the volume change for formation of the ion pair can be estimated from solution theory. Millero has used an equation similar to eq 7 to estimate α 's in NaCl solutions⁸ and in seawater,⁹ while Wirth and coworkers^{10,11} have used eq 7 to estimate the α 's in R_4NBr solutions¹⁰ and HSO_4^- in H_2SO_4 and NaHSO_4 solutions.¹¹ Since one must estimate both ϕ_V for the ion pair and free ions to calculate $(1 - \alpha)$ or α , the results are not very reliable.

The calculation of the ϕ_V of the MA° ion pair from eq 5 [or $\Delta\phi_V$ from eq 6] is simpler since $(1 - \alpha)$ can be determined from known association constants (K_A) given by

$$K_A = (1 - \alpha)/\alpha^2 f_+ f_- m_T \quad (8)$$

where f_+ and f_- are the activity coefficients of the free ions [$f_+ f_- = (f_\pm)^2$ for the free ions] and the activity coefficient of the ion pair is taken to be 1.0. The activity coefficients of the free ions are related to the stoichiometric mean activity coefficient (γ_\pm) by

$$(f_+ f_-)^{1/2} = (f_\pm) = (\gamma_\pm)/\alpha \quad (9)$$

Combining eq 8 and 9 and solving for α , we obtain

$$\alpha = 1 - K_A(\gamma_\pm)^2 m_T \quad (10)$$

Lee¹² has used eq 5 and 10 to estimate the ϕ_V of the MgSO_4° ion pair as a function of ionic strength in aqueous solutions; Millero¹³ has used these equations to estimate the partial molal volumes of the ion pairs MgSO_4° , NaSO_4^- , and CaSO_4° in seawater; and recently Masterton, *et al.*,¹⁴ have determined the $\Delta\phi_V$ for the formation of RbNO_3° and TlNO_3° ion pairs. Many other workers¹ have used eq 5 and 10 to determine the ϕ_V (or V) of weak acids and bases.

The estimation of the ϕ_V of free ions needed in the calculation of $\phi_V(\text{MA}^\circ)$ can be made by using the following.

(1) The Debye-Hückel equation¹³

$$\phi_V(\text{M}^+, \text{A}^-) = \phi_V^\circ(\text{M}^+, \text{A}^-) + S_V \sqrt{c} \quad (11)$$

where $\phi_V^\circ(\text{M}^+, \text{A}^-)$ is the infinite dilution apparent molal volume for the free ions, S_V is the limiting law slope,¹ and c is the molarity [$c = md^\circ/(1 + 10^{-3}md^\circ\phi_V)$]. Millero¹³ has used this method to estimate the \bar{V} of the free ions Mg^{2+} and SO_4^{2-} .

(2) An extended form of the Debye-Hückel

$$\phi_V(\text{M}^+, \text{A}^-) = \phi_V^\circ(\text{M}^+, \text{A}^-) + \frac{S_V \sqrt{c}}{1 + \bar{a}B\sqrt{c}} + Kc \quad (12)$$

where \bar{a} is the ion size parameter, B is an extended Debye-Hückel term,⁸ and K is an empirical constant; Millero⁸ has used this method to estimate the \bar{V} of free Na^+ and Cl^- ions, while Masterton, *et al.*,¹⁴ have used this method to estimate the ϕ_V of Rb^+ , NO_3^- and Tl^+ , NO_3^- free ions. The \bar{a} for Mg^{2+} , SO_4^{2-} could be assigned values between 2.7 (the crystal radii) and 15 Å (the Bjerrum distance). A value of $\bar{a} = 0$ gives the simple limiting law.

(3) By using the additivity principle

$$\phi_V(\text{M}^+, \text{A}^-) = \phi_V(\text{M}^+, \text{X}^-) + \phi_V(\text{N}^+, \text{A}^-) - \phi_V(\text{N}^+, \text{X}^-) \quad (13)$$

Lee,¹² for example, estimated that ϕ_V of the free ions Mg^{2+} and SO_4^{2-} using the additivity principle

$$\phi_V(\text{Mg}^{2+}, \text{SO}_4^{2-}) = \phi_V(\text{MgCl}_2) + \phi_V(\text{Na}_2\text{SO}_4) - 2\phi_V(\text{NaCl}) \quad (14)$$

where $\phi_V(\text{MgCl}_2)$, $\phi_V(\text{Na}_2\text{SO}_4)$, and $\phi_V(\text{NaCl})$ are the observed apparent molal volumes of MgCl_2 , Na_2SO_4 , and NaCl at the same ionic strength $I = 4cm_T$ (where m_T is the total molality of MgSO_4). Since ion pair formation may be important in Na_2SO_4 solutions,¹⁶ $\phi_V(\text{Na}_2\text{SO}_4)$ is likely to be greater than $\phi_V(2\text{Na}^+, \text{SO}_4^{2-})$ and hence one might expect the $\phi_V(\text{Mg}^{2+}, \text{SO}_4^{2-})$ calculated in this manner to be too high.

(4) Various semiempirical equations to estimate the ϕ_V of free ions, for example, Millero⁹ has used the following equation to estimate the partial molal volumes of Mg^{2+} , SO_4^{2-} , Ca^{2+} , CO_3^{2-} , and Na^+ "free" ions in seawater

$$\bar{V} = \bar{V}^\circ + A(Z^2/r) + B \quad (15)$$

where Z is the charge on the ion, A and B are concentration dependent parameters,⁹ and r is the crystal radius of the ion (in Å units).

In an attempt to extend the work of Lee¹² and Millero¹³ to other temperatures and low ionic strengths, and to test the general concepts of using molal volume studies to study ion pairing, we have made this study on the ϕ_V of MgSO_4 , Na_2SO_4 , MgCl_2 , and K_2SO_4 solutions from 0 to 1 m and 0 to 50°.

The results of these studies should prove useful to other workers studying ion pairing systems.

Calculation of $\phi_V(\text{obsd})$ and $\phi_V(\text{Mg}^{2+}, \text{SO}_4^{2-})$

The apparent molal volume of the magnesium sulfate ion pair MgSO_4° can be calculated from

$$\phi_V(\text{MgSO}_4^\circ) = [\phi_V(\text{obsd}) - \alpha\phi_V(\text{Mg}^{2+}, \text{SO}_4^{2-})]/(1 - \alpha) \quad (16)$$

while the apparent molal volume change for the formation of the ion pair can be calculated from

$$\Delta\phi_V(\text{MgSO}_4^\circ) = [\phi_V(\text{obsd}) - \phi_V(\text{Mg}^{2+}, \text{SO}_4^{2-})]/(1 - \alpha) \quad (17)$$

To obtain the necessary data for the calculation of ϕ_V and $\Delta\phi_V$ for MgSO_4° the apparent molal volumes at 0, 25, and 50° for NaCl , KCl , MgCl_2 , Na_2SO_4 , K_2SO_4 , and MgSO_4 obtained by various workers^{8,12,17-23} have been fit to equations of the form (from 0 to 1 m)

$$\phi_V = \phi_V^\circ + Am^{1/2} + Bm + Cm^{3/2} + Dm^2 + Em^{5/2} \quad (18)$$

The constants A , B , etc., are given in Table I, along with the average deviations. The observed ϕ_V 's for MgSO_4 solutions [calculated from eq 18] are shown in Figures 1-3.²⁴ As is quite apparent from Figures 1-3,²⁴ the observed ϕ_V

TABLE I: Constants for Eq 18 for Aqueous NaCl, Na₂SO₄, KCl, K₂SO₄, MgCl₂, and MgSO₄ Solutions at 0, 25, and 50°

	ϕ_V°	A	B	C	D	E	Av deviation
0°							
NaCl ^h	12.90	-0.053	6.153	-3.610			0.06
Na ₂ SO ₄ ^a	2.33	0.964	57.195	-76.722	34.822		0.054
KCl ⁱ	23.63	1.407	1.235				0.005
K ₂ SO ₄ ^a	23.79	3.467	83.526	-204.836	164.316		0.011
MgCl ₂ ^a	10.42	8.132	-0.820				0.019
MgSO ₄ ^a	-13.06	33.528	-43.528	41.845	-15.203		0.025
25°							
NaCl ^f	16.62	1.871	-0.041				0.011
Na ₂ SO ₄ ^d	11.62	11.461	0.450				0.020
KCl ^g	26.85	1.802	0.135				0.005
K ₂ SO ₄ ^e	31.99	16.493	-20.205	35.520	-21.403		0.022
MgCl ₂ ^c	14.49	8.633	-13.305	18.592	-8.156		0.053
MgSO ₄ ^b	-7.18	35.44	-73.72	98.400	-48.800		0.052
50°							
NaCl ^a	17.83	2.417	-0.701				0.047
Na ₂ SO ₄ ^a	14.09	12.396	-0.956				0.024
KCl ^a	27.57	2.428	-0.308				0.020
K ₂ SO ₄ ^a	33.63	27.735	-57.202	77.171	-36.414		0.055
MgCl ₂ ^a	13.40	9.087	-5.422	3.136			0.041
MgSO ₄ ^a	-8.14	55.564	-162.896	284.123	-235.799	74.657	0.015

^a From the work of Millero and Knox.¹⁷ ^b From the work of Lee¹² and Franks and Smith.¹⁸ ^c From the work of Lee¹² and Dunn.¹⁹ ^d From the work of Lee¹² and Geffcken and Price.²⁰ ^e From the work of Wirth,²¹ Dunn,¹⁹ and Jones and Ray.²² ^f From the work of Vaslow,²³ Dunn,¹⁹ and Millero.⁸ ^g From the work of Vaslow,²³ Dunn,¹⁹ and Franks and Smith.¹⁸ ^h From the work of Dunn¹⁹ and Millero.⁸ ⁱ From the work of Dunn.¹⁹

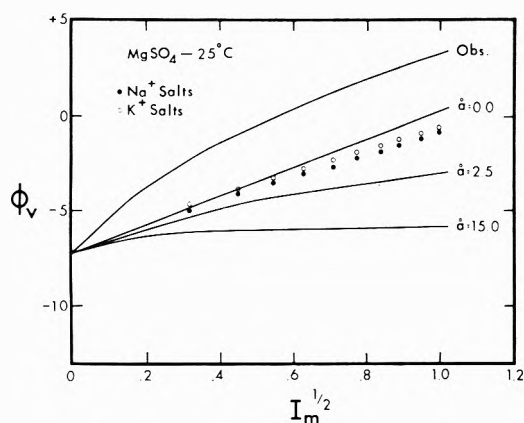


Figure 2. Observed ϕ_V for MgSO₄ solutions at 25° compared to the values calculated from the extended Debye-Hückel equation (solid curves) and the additivity of Na⁺ and K⁺ salts [i.e., $\phi_V(\text{MgCl}_2) + \phi_V(\text{Na}_2\text{SO}_4) - 2\phi_V(\text{NaCl})$ and $\phi_V(\text{MgCl}_2) + \phi_V(\text{K}_2\text{SO}_4) - 2\phi_V(\text{KCl})$].

for MgSO₄ solutions at 0, 25, and 50° show very large positive deviations from the Debye-Hückel limiting law¹

$$\phi_V = \phi_V^\circ + S_V \sqrt{c} \quad (19)$$

where c is the molarity and S_V is the limiting law slope.¹ If one uses a simplified form of the extended limiting law (eq 12) of the form ($K \approx 0$, if one assumes $\partial \hat{a} / \partial P \approx 0$)⁸

$$\phi_V = \phi_V^\circ + \frac{S_V \sqrt{c}}{1 + A \hat{a} \sqrt{c}} \quad (20)$$

(where $A = 0.3241$, 0.3286 , and 0.3342 , respectively, at 0, 25, and 50° and $c = I_V / 4\alpha$) to represent the ϕ_V of the free ions, the deviations are larger (Figures 1-3).²⁴ To fit the $\phi_V(\text{obsd})$ for the MgSO₄ solutions using the extended Debye-Hückel equation a negative \hat{a} would have to be used or one would have to add additional terms (Kc , etc.). This is similar to most electrolytes (since the ϕ_V of most electrolytes, especially at low temperatures, deviate positively from the simple Debye-Hückel equations).^{1,8} The

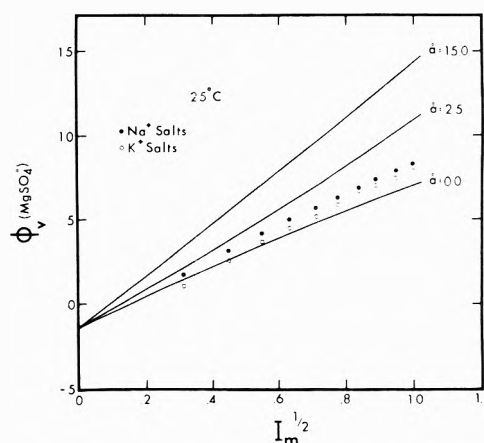


Figure 5. Apparent molal volume of MgSO₄ at 25° obtained by using the extended Debye-Hückel equation (solid curves) and the additivity of Na⁺ and K⁺ salts for the apparent molal volume of the free ions, Mg²⁺ + SO₄²⁻.

failure of the extended Debye-Hückel to fit the observed ϕ_V data is due to ion pairing (as well as other types of ion-ion interactions not accounted for in the Debye-Hückel theory).^{1,8}

The ϕ_V 's of MgSO₄ solutions calculated from additivity from eq 14 or

$$\phi_V(\text{Mg}^{2+}, \text{SO}_4^{2-}) = \phi_V(\text{MgCl}_2) + \phi_V(\text{K}_2\text{SO}_4) - 2\phi_V(\text{KCl}) \quad (21)$$

at 25 and 50° fall between the ϕ_V 's calculated from eq 19 and 20 with $\hat{a} = 15$ Å. The ϕ_V 's at 0° obtained by additivity are larger than the ϕ_V 's with the simple Debye-Hückel equation.

There is little difference between the additivity ϕ_V 's obtained from the K⁺ and Na⁺ salts. The K⁺ salt additivity ϕ_V 's are slightly higher than the Na⁺ salt. These results can be interpreted in terms of ion pairing in the Na₂SO₄ and K₂SO₄ solutions.^{16,25-29} At low temperatures the ion pairing is more predominant, KSO₄⁻ ion pair formation is slightly greater than NaSO₄⁻.^{27,29}

Calculation of α the Fraction of Free Ions

In order to estimate the fraction of free ions in MgSO_4 solutions from eq 10, both K_A and γ_{\pm} data are needed. From the work of Nair and Nancollas,³⁰ who determined K_A from 0 to 40°, we obtain $K_A = 92, 179, \text{ and } 340$, respectively, at 0, 25, and 50°. The K_A at 50° has been estimated by extrapolation of a plot of $\log K_A$ vs. $1/T$. The general procedure used to calculate γ_{\pm} for MgSO_4 solutions at 0, 25, and 50° is outlined below.

A standard value of γ_{\pm} is taken to be 0.170 at 0.1 m and 0°. This value seems to be on more solid ground³¹ than the value of $\gamma_{\pm} = 0.150$ at 0.1 m and 25°, which was selected more or less arbitrarily by Harned and Owen³² and Robinson and Stokes.³³ The γ_{\pm} 's for MgSO_4 solutions at concentrations below 0.1 m at 0° were determined from the osmotic coefficient (ϕ) data derived from the freezing point measurements of Brown and Prue³⁴ from the equation

$$\log [\gamma_{\pm}(m)/\gamma_{\pm}(0.1 m)] = \phi(m) - \phi(0.1 m) + \int_{0.1}^m (\phi - 1) d \ln m \quad (22)$$

For the integration of ϕ of MgSO_4 solutions below 0.1 m were fit to the equation

$$1 - \phi = 4.468m^{1/2} - 25.416m + 74.338m^{3/2} - 82.207m^2 \quad (23)$$

with an average deviation of ± 0.008 . The values of γ_{\pm} below 0.1 m at 0° calculated from eq 22 are given in Table II.²⁴ The values of γ_{\pm} below 0.1 m at 25° were calculated from the 0° data using the equation

$$\log \gamma_{\pm}(25^\circ) = \log \gamma_{\pm}(0^\circ) - (y/2)\bar{L}_2(25^\circ) + (z/2)\bar{J}_2(25^\circ) \quad (24)$$

where $10^8(y/2) = 3350, 0, \text{ and } -2835$ and $10^8(z/2) = 43, 0, \text{ and } 34.5$, respectively, at 0, 25, and 50°; \bar{L}_2 is the relative partial molal enthalpy (cal/mol) and \bar{J}_2 is the relative partial molal heat capacity (cal deg⁻¹ mol⁻¹). The \bar{L}_2 data used in these calculations were obtained from the heats of dilution for MgSO_4 solutions given in Harned and Owen³² and our recent results.³⁵ The \bar{J}_2 data used in these calculations were obtained from the heat capacities given in the Critical Tables.³⁶ The values of γ_{\pm} below 0.1 m at 50° were calculated from the 25° data using

$$\log \gamma_{\pm}(t^\circ) = \log \gamma_{\pm}(25^\circ) + (y/2)\bar{L}_2(25^\circ) - (z/2)\bar{J}_2(25^\circ) \quad (25)$$

The values of γ_{\pm} calculated from eq 25 below 0.1 m at 25 and 50° are given in Table II.²⁴ The values of γ_{\pm} from 0.1 to 1.0 m at 25° were calculated from the data tabulated by Robinson and Stokes³³ after a revision was made for $\gamma_{\pm}(0.1 m) = 0.159$ instead of 0.150 [$\gamma_{\pm}(\text{revised}) = \gamma_{\pm}(\text{RS})(159/150)$]. The values of γ_{\pm} at 0 and 50° above 0.1 m were calculated from the 25° data using eq 25. The resulting γ_{\pm} (given in Table II)²⁴ have been fit (to within ± 0.002)

$$\log \gamma_{\pm} = a + bm^{1/2} + cm + dm^{3/2} \quad (26)$$

where $a = -0.195, -0.217, -0.236$; $b = -2.409, -2.421, -2.491$; $c = 2.138, 2.099, 2.127$; and $d = -0.796, -0.753, -0.759$, respectively, at 0, 25, and 50°.

The fractions of free ions in MgSO_4 solutions at various molalities at 0, 25, and 50° were calculated from eq 10 (using $K_A = 92, 179, \text{ and } 340$, respectively) and γ_{\pm} given in Table II²⁴ and calculated from eq 26. The α 's over the

range of 0.03 to 1.0 m have been fit to an equation of the form (± 0.004)

$$\alpha = a_1 + b_1m^{-1} + c_1m + d_1m^2 \quad (27)$$

where $a_1 = 0.716, 0.526, 0.198$; $b_1 = 1.87 \times 10^{-3}, 2.57 \times 10^{-3}, 4.65 \times 10^{-3}$; $c = 6.5 \times 10^{-3}, 8.6 \times 10^{-3}, 0.350$; and $d_1 = 0, 0, 0.220$, respectively, at 0, 25, and 50°.

Calculation of $\phi_V(\text{MgSO}_4^\circ)$ and $\Delta\phi_V(\text{MgSO}_4^\circ)$

The apparent molal volume of MgSO_4° and the apparent molal volume change for the formation of MgSO_4° can be calculated from eq 16 and 17. The values for ϕ_V and $\Delta\phi_V$ calculated by using eq 20 to estimate the ϕ_V of the free ions $\text{Mg}^{2+}, \text{SO}_4^{2-}$ are shown plotted vs. $I_m^{1/2}$ (the molal ionic strength) in Figures 4-9.²⁴ As is quite apparent from these figures, the infinite dilution values of ϕ_V° and $\Delta\phi_V^\circ$ for MgSO_4° (given in Table III) appear to be independent of the value selected for the ion size parameter.

Since all the ϕ_V 's for the free ion calculated from eq 20 approach the simple Debye-Hückel (eq 19) in dilute solutions, it is not surprising that the ϕ_V° and $\Delta\phi_V^\circ$ appear to be independent of the ion size parameter. One must keep in mind, however, that the magnitude of ϕ_V° and $\Delta\phi_V^\circ$ varies according to the method used for the extrapolation to infinite dilution (unlike the ϕ_V of electrolytes, the ϕ_V of MgSO_4° does not follow any limiting law behavior). These findings, if true for other systems, can prove to be very important since it means that any reasonable values for \bar{a} (i.e., between the crystal radii and the Bjerrum distance) can be used to determine ϕ_V° and $\Delta\phi_V^\circ$ for ion pairing processes from volume data.

The ϕ_V° and $\Delta\phi_V^\circ$ for MgSO_4° calculated by using the additivity estimates for the ϕ_V of $\text{Mg}^{2+}, \text{SO}_4^{2-}$ are also given in Figures 4-9.²⁴ The infinite dilution values given in Table III obtained from the additivity estimates of $\text{Mg}^{2+}, \text{SO}_4^{2-}$ are in reasonable agreement with those obtained using the extended Debye-Hückel equation. The spread of ϕ_V° and $\Delta\phi_V^\circ$ values obtained by the additivity method are due to the uncertainty of extrapolation to infinite dilution.

All of the values of $\Delta\phi_V^\circ = \Delta\bar{V}^\circ$ obtained for MgSO_4° at 25° (like the results of Lee¹² and Millero¹³) are in reasonable agreement with the value of 7.3 cm³/mol obtained by Fisher² from direct conductance measurements. No direct measurements have been made on the effect of temperature on the $\Delta\bar{V}^\circ$ or \bar{V}° for MgSO_4° .

Discussion of Errors in the Calculation of ϕ_V and $\Delta\phi_V$ for MgSO_4°

A number of assumptions were made in the calculations of ϕ_V and $\Delta\phi_V$ and in this section we will discuss the effect of errors due to the assumptions made or the data used in the calculations.

(1) *Assumption that $\gamma(\text{MgSO}_4) = 1.0$.* Since MgSO_4° is a polar species, one might expect $\gamma(\text{MgSO}_4^\circ)$ to be less than 1.0. If $\gamma(\text{MgSO}_4^\circ)$ is less than one, ϕ_V of MgSO_4° would be smaller and $\Delta\phi_V$ would be larger. If the concentration behavior of $\gamma(\text{MgSO}_4)$ follows the normal behavior (i.e., becomes closer to 1.0 in dilute solutions), the effect would be greater at higher concentrations. Thus, the infinite dilution values for ϕ_V° and $\Delta\phi_V^\circ$ would not be greatly affected.

(2) *Errors in K_A .* The 25° values of K_A for MgSO_4° obtained by various workers^{30,37-41} are in reasonable agreement (values range from $K_A = 159$ to 229). The values for K_A at 0 and 50° used in this study could be in error.

TABLE III: Partial Molal Volume of the Magnesium Sulfate Ion Pair (\bar{V}°) and the Volume Change for Ion Pair Formation ($\Delta\bar{V}^\circ$) at Infinite Dilution

Method ^a	0°		25°		50°	
	\bar{V}°	$\Delta\bar{V}^\circ$	\bar{V}°	$\Delta\bar{V}^\circ$	\bar{V}°	$\Delta\bar{V}^\circ$
Debye-Hückel	-3.5	9.6	-1.4	5.8	-2.4	5.7
Additivity (Na ⁺ salts)	-3.1	10.0	-0.2 to -1.6	7.0 to 5.6	-1.0 to -2.4	7.1 to 5.7
Additivity (K ⁺ salts)	-3.8	9.3	-1.3 to -2.5	5.9 to 4.7	-1.8 to -3.3	6.3 to 4.8
Combined Na ⁺ and K ⁺ salts			0.0 to 1.1	7.2 to 8.3		

^a Method used to estimate the ϕ_V of the free ions.

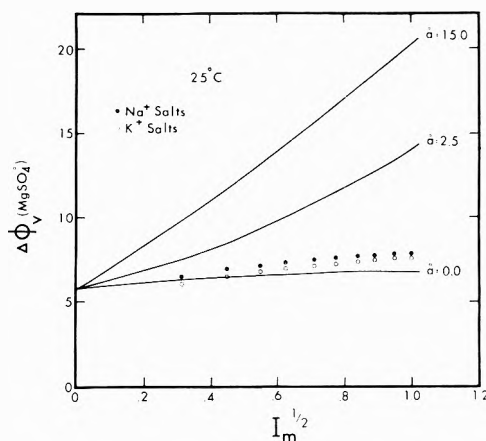


Figure 8. Apparent molal volume change for the formation of MgSO₄[°] at 25° obtained by using the extended Debye-Hückel equation (solid curves) and the additivity of Na⁺ and K⁺ salts for the apparent molal volume of the free ions, Mg²⁺ + SO₄²⁻.

Values quoted for the enthalpy change, ΔH_A , for the formation of MgSO₄[°] at 25° vary from 0.51 to 5.7 kcal/mol.^{26,42} The use of the smaller ΔH_A value for calculating K_A at temperatures other than 25° would yield larger values at 0° and smaller values at 50° than those used here. This would yield a smaller ϕ_V at 0° and a larger ϕ_V at 50° for MgSO₄[°] (the reverse would be true for the $\Delta\phi_V$ values).

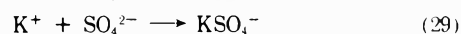
(3) *Errors in γ_{\pm} .* The only important source of error in γ_{\pm} is in the value assigned to the standard value at 0.1 *m* and 0°; the uncertainty here is very small and would be nearly independent of concentration and temperature.

(4) *Errors in ϕ_V Data.* Since the errors in the observed ϕ_V data are within ± 0.1 cm³/mol, the major error here is in the estimation of the ϕ_V for the free ions. If the extended Debye-Hückel equation is used, the infinite dilution ϕ_V° and $\Delta\phi_V^\circ$ for MgSO₄ do not appear to be greatly affected by the choice of \tilde{a} . However, the concentration dependence of ϕ_V and $\Delta\phi_V$ vary considerably and there is no *a priori* method of selecting the "best" ion size parameter. For this reason, we feel that the additivity method is a more reliable approach for calculating the concentration dependence of $\phi_V(\text{Mg}^{2+}, \text{SO}_4^{2-})$. The additivity ϕ_V 's calculated for free ions do not appear to be greatly different for the Na⁺ and K⁺ salts. A better value might possibly be obtained by using Li⁺ salts; however, at present no reliable ϕ_V data are available. The major source of error in the additivity method is in neglecting the effect of ion pairing of Na⁺ and K⁺ salts with the SO₄²⁻ ion. Possible methods of correcting for this effect are discussed in the next section.

Corrections for Ion Pairing in Na₂SO₄ and K₂SO₄ Solutions

Since the Na⁺ and K⁺ ions may also form ion pairs

with SO₄²⁻



the additivity estimates for the ϕ_V of the free ions Mg²⁺ and SO₄²⁻ [using eq 14 and 21] may be in error. By examining the observed ϕ_V 's of Na₂SO₄ and K₂SO₄ solution in terms of ion pairing, we have, respectively

$$\phi_V(\text{Na}_2\text{SO}_4) = \phi_V(2\text{Na}^+, \text{SO}_4^{2-}) + (1 - \alpha_1)\Delta\phi_V(\text{NaSO}_4^-) \quad (30)$$

$$\phi_V(\text{K}_2\text{SO}_4) = \phi_V(2\text{K}^+, \text{SO}_4^{2-}) + (1 - \alpha_2)\Delta\phi_V(\text{KSO}_4^-) \quad (31)$$

where α_1 and α_2 are, respectively, the fraction of free SO₄²⁻ ions in Na₂SO₄ and K₂SO₄ solutions. For Na₂SO₄ and K₂SO₄ solutions the α 's can be calculated from the association constant K_A and activity coefficients by

$$\alpha^2 = 1 - \frac{4\gamma_{\pm}^3(\text{Na}_2\text{SO}_4)m_T K_A}{\gamma(\text{Na})\gamma(\text{NaSO}_4^-)} \quad (32)$$

where $\gamma_{\pm}(\text{Na}_2\text{SO}_4)$ is the mean stoichiometric activity coefficient of Na₂SO₄ (or K₂SO₄) solutions, $\gamma(\text{Na})$ and $\gamma(\text{NaSO}_4^-)$ are the activity coefficients of the ions Na⁺ and NaSO₄⁻. If one assumes $\gamma(\text{NaSO}_4^-) \approx \gamma(\text{Cl}^-)$, one can replace $\gamma(\text{Na}^+)\gamma(\text{NaSO}_4^-)$ with $\gamma_{\pm}^2(\text{NaCl})$.

To correct the additivity estimate of $\phi_V(\text{Mg}^{2+}, \text{SO}_4^{2-})$ for ion pairing in the Na₂SO₄ and K₂SO₄ systems, one must subtract $(1 - \alpha_1)\Delta\phi_V(\text{NaSO}_4^-)$ and $(1 - \alpha_2)\Delta\phi_V(\text{KSO}_4^-)$, respectively, from eq 14 and 21. Combining eq 14, 17, 21, 30, and 31, we obtain

$$\phi_V(\text{obsd}) - \phi_V(\text{MgCl}_2) - \phi_V(\text{Na}_2\text{SO}_4) + 2\phi_V(\text{NaCl}) = (1 - \alpha)\Delta\phi_V(\text{MgSO}_4^\circ) - (1 - \alpha_1)\Delta\phi_V(\text{NaSO}_4^-) \quad (33)$$

$$\phi_V(\text{obsd}) - \phi_V(\text{MgCl}_2) - \phi_V(\text{K}_2\text{SO}_4) + 2\phi_V(\text{KCl}) = (1 - \alpha)\Delta\phi_V(\text{MgSO}_4^\circ) - (1 - \alpha_2)\Delta\phi_V(\text{KSO}_4^-) \quad (34)$$

The first terms on the right of eq 33 and 34 are equal to the values obtained for $(1 - \alpha)\Delta\phi_V(\text{MgSO}_4^\circ)$ without correcting for ion pairing in Na₂SO₄ and K₂SO₄. To solve these equations one must make some assumptions, since we have two equations and three unknowns: $\Delta\phi_V(\text{MgSO}_4^\circ)$, $\Delta\phi_V(\text{NaSO}_4^-)$, and $\Delta\phi_V(\text{KSO}_4^-)$. The simplest assumption one could make is to take $\Delta\phi_V(\text{NaSO}_4^-) = \Delta\phi_V(\text{KSO}_4^-)$. Using γ_{\pm} data for Na₂SO₄, K₂SO₄, NaCl, and KCl solutions³³ and $K_A = 5.0^{29,30}$ and $7.0^{7,0,28,29}$ respectively, for NaSO₄⁻ and KSO₄⁻ formation, we have calculated the α 's for Na₂SO₄ solutions at 25° from 0.1 to 1.0 ionic strength [from eq 32]. The results are given in Table IV. These α 's have been used to calculate $\phi_V(\text{MgSO}_4^\circ)$ and $\Delta\phi_V(\text{MgSO}_4^\circ)$ from eq 33 and 34 assuming $\Delta\phi_V(\text{NaSO}_4^-) = \Delta\phi_V(\text{KSO}_4^-)$. The $\Delta\phi_V$ and ϕ_V calculated from eq 33 and 34 are given in Table IV. The infinite dilution $\Delta\phi_V^\circ = \Delta\bar{V}^\circ$ and $\phi_V^\circ = \bar{V}^\circ$ for MgSO₄[°] are given in Table III. Similar calculations at 0 and 50° are not possible at present due to lack of reliable K_A 's (or ΔH_A 's) for the NaSO₄⁻ and KSO₄⁻ systems.

TABLE IV: Calculation of $\Delta\phi_V(\text{MgSO}_4^\circ)$ and $\phi_V(\text{MgSO}_4^\circ)$ by Correcting for Ion Pairing in Na_2SO_4 and K_2SO_4 Solutions at 25°

I_m	α		$\phi_V(\text{MgSO}_4^\circ)$	$\Delta\phi_V(\text{MgSO}_4^\circ)$
	NaSO_4^-	KSO_4^-		
0.1	0.881	0.837	3.42	9.59
0.2	0.820	0.755	4.62	10.03
0.3	0.785	0.723	5.83	10.85
0.4	0.762	0.690	6.46	10.85
0.5	0.747	0.670	7.08	10.95
0.6	0.738	0.657	7.58	10.96
0.7	0.733	0.653	8.07	11.01
0.8	0.731	0.650	8.55	11.08
0.9	0.731	0.650	9.01	11.16
1.0	0.733	0.651	9.27	10.97

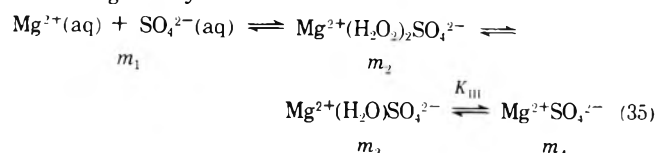
The $\Delta\phi_V^\circ = 7.2$ to 8.5 cm^3/mol obtained by correcting for ion pairing in the Na_2SO_4 and K_2SO_4 solutions are in excellent agreement with the value (7.3) obtained by Fisher.²

Discussion of Results

Besides the fact that reliable $\Delta\bar{V}^\circ$'s can be estimated from density data for ion pair formation, three significant findings are indicated in our calculations: (1) both $\Delta\phi_V$ and ϕ_V for MgSO_4° appear to increase with increasing concentration or ionic strength; (2) the temperature behavior of the V° of MgSO_4° is similar to most electrolytes in that it appears to go through a maximum; (3) the ΔV° for the formation of MgSO_4° goes through a minimum when plotted *vs.* temperature similar to the behavior of acid and base ionization. These findings will be briefly discussed in the next section.

Although one can question the reliability of the concentration dependence of $\phi_V(\text{MgSO}_4^\circ)$ and $\Delta\phi_V(\text{MgSO}_4^\circ)$ found in this study (due to the problems in estimating a reliable ϕ_V for the free ions), all of our results indicate that both ϕ_V and $\Delta\phi_V$ for MgSO_4° increase with increasing concentration or ionic strength. Since one cannot be certain that the extended Debye-Hückel equation correctly represents the concentration dependence of ϕ_V for free ions and what is the correct ion size parameter, we prefer the additivity estimates for the ϕ_V of the free ions. Using these estimates, a change in I_m of 1.0 changes ϕ_V by 9–11 cm^3/mol between 0 and 50° (the larger changes being at 0 and 50°). For a similar change in I_m , the $\Delta\phi_V$ changes by 2 to 8 cm^3/mol (the larger values being at 0°). This increase in both ϕ_V and $\Delta\phi_V$ can be attributed to the loss of electrostricted water molecules by the ion pair at higher concentrations. At higher ionic strengths the $\Delta\phi_V$ is larger because more innersphere or contact ion pairs are formed. These findings are in agreement with recent high-pressure Raman spectra measurements of Davis.⁴²

It should be pointed out that the ϕ_V (and $\Delta\phi_V$) of MgSO_4° determined in this study is the ϕ_V (and $\Delta\phi_V$) of the total ion paired species (*i.e.*, both inner- and outer-sphere types). Eigen and Tamm⁴³ have proposed a four state (three step) model for the formation of MgSO_4° . The model is given by



The conventional association constant (K_A) is given by

$$K_A = \frac{m_2 + m_3 + m_4}{m_1^2(f_{\pm})^2} = K_I K_{II} K_{III} + K_I K_{II} + K_I \quad (36)$$

where m_i is the molality of the respective i states. The stepwise association constants (related to the rates of formation of the two states, $K_I = k_{12}/k_{21}$) are given by $K_I = m_2/m_1^2(f_{\pm})$, $K_{II} = m_3/m_2$, and $K_{III} = m_4/m_3$. Eigen and Tamm⁴³ proposed two sets of values for the parameters needed to describe the four state model ($K_I = 41.7$, 25.0, $K_{II} = 2.0$, 1.0, and $K_{III} = 0.13$, 0.11, respectively, at 20°). Atkinson and Petrucci³⁷ have determined more complete ultrasonic estimates for the stepwise K 's that yield an overall K_A [from eq 36] in excellent agreement with the conductance value. They obtained $K_I = 50$, $K_{II} = 1.96$, and $K_{III} = 0.17$ at 25° (compared to $K_I = 58.8$, $K_{II} = 2.0$, and $K_{III} = 0.13$ obtained by Eigen and Tamm⁴³).

Using this model, the total $\phi_V(\text{MgSO}_4^\circ)$ is given by

$$\phi_V(\text{MgSO}_4^\circ) = (m_2/m_p)\phi_V[\text{Mg}^{2+}(\text{H}_2\text{O})_2\text{SO}_4^{2-}] + (m_3/m_p)\phi_V[\text{Mg}^{2+}(\text{H}_2\text{O})\text{SO}_4^{2-}] + (\bar{m}_4/m_p)\phi_V[\text{Mg}^{2+}\text{SO}_4^{2-}] \quad (37)$$

where the total paired species $m_2 + m_3 + m_4 = m_p = (1 - \alpha)m_T$. By differentiating eq 36 with respect to pressure, the total $\Delta\bar{V}_A^\circ$ is given by

$$\Delta\bar{V}_A^\circ = \Delta\bar{V}_I^\circ + (m_4/m_p)[\Delta\bar{V}_{III}^\circ + \Delta\bar{V}_{II}^\circ + \Delta\bar{V}_{II}^\circ/K_{III}] \quad (38)$$

Using the K_{II} and K_{III} constants obtained by Atkinson and Petrucci,³⁷ we obtain $m_2/m_p = 0.30$, $m_3/m_p = 0.60$, and $m_4/m_p = 0.10$. Recently, Davis and Oliver⁴⁴ have determined from Raman spectroscopy that $m_4/m_p = 0.10$ to 0.13 from 0.1 to 2.5 m ; which is in good agreement with the ultrasonic estimates. If one could make a reliable estimate for the ϕ_V of the contact ion pair $\text{Mg}^{2+}\text{SO}_4^{2-}$ as a function of concentration, it would be possible to separate our total $\phi_V(\text{MgSO}_4^\circ)$ into inner- and outer-sphere types. Unfortunately, as will be discussed later, the contact ion pair $\text{Mg}^{2+}\text{SO}_4^{2-}$ is hydrated and one cannot make the simple assumption that its ϕ_V does not change with increasing concentration. Since m_4/m_p and m_p are constant over a wide concentration range (0.1 to 2.0 m),^{12,44} the increase in $\phi_V(\text{MgSO}_4^\circ)$ with increasing concentration could be attributed to changes in the relative amounts of $\text{Mg}^{2+}(\text{H}_2\text{O})_2\text{SO}_4^{2-}$ and $\text{Mg}^{2+}(\text{H}_2\text{O})\text{SO}_4^{2-}$ (*i.e.*, if $\phi_V(\text{Mg}^{2+}\text{SO}_4^{2-})$ is not a function of concentration).

Eigen and Tamm⁴³ have estimated the volume changes ($\pm 20\%$) for the individual steps as being $\Delta\bar{V}_I^\circ = 0$, $\Delta\bar{V}_{II}^\circ = 14$ and 18, and $\Delta\bar{V}_{III}^\circ = 3$ cm^3/mol . Fisher^{45,46} has shown that these individual $\Delta\bar{V}^\circ$'s yield a plot of $RT \log K_A$ [where K_A is calculated from eq 36] that is in excellent agreement with the experimental value (the slope gives 7.7 cm^3/mol). From eq 38, we obtain

$$\Delta\bar{V}_A^\circ = 0 + 0.05_2[3 + 14 \text{ to } 18 + (14 \text{ to } 18)/0.11] = 6.5 \text{ to } 3.3 \text{ cm}^3/\text{mol} \quad (39)$$

using $K_{II} = 1.0$ and $K_{III} = 0.11$. If the $K_{II} = 1.97$ and $K_{III} = 0.17$ of Atkinson and Petrucci³⁷ are used, we obtain $\Delta\bar{V}_A^\circ = 9.9$ to 12.7 cm^3/mol , which is 2.7 to 5.5 cm^3/mol larger than the experimental value. It, thus appears that if the stepwise K 's estimated by Atkinson and Petrucci³⁷ are reliable the $\Delta\bar{V}_{II}^\circ$ and $\Delta\bar{V}_{III}^\circ$ estimated by Eigen and Tamm⁴³ are in error. By adjusting $\Delta\bar{V}_{II}^\circ$ to 10 cm^3/mol one obtains a value for $\Delta\bar{V}_A^\circ$ (7.2) that is in excellent agreement with the directly determined value.

From these $\Delta\bar{V}^\circ$'s we can estimate the V° values of the three paired species at infinite dilution. Using $V^\circ = -7.2$

cm³/mol for the free ions, we obtain $\bar{V}^\circ[\text{Mg}^{2+}(\text{H}_2\text{O})_2\text{SO}_4^{2-}] = -7.2$ cm³/mol, $\bar{V}^\circ[\text{Mg}^{2+}(\text{H}_2\text{O})\text{SO}_4^{2-}] = 2.8$ cm³/mol, and $\bar{V}^\circ[\text{Mg}^{2+}\text{SO}_4^{2-}] = 5.8$ cm³/mol. From eq 37 we obtain $\bar{V}^\circ(\text{MgSO}_4^\circ) = (0.30)(-7.2) + (0.60)(2.8) + (0.10)(5.8) = 0.1$ cm³/mol, which is also in excellent agreement with the measured value.

By comparing the \bar{V}° 's for the various ion paired species with the $\bar{V}^\circ(\text{int})$ for the intrinsic partial molal volume of Mg²⁺ and SO₄²⁻, we can obtain an understanding of the structure of the ion pairs. As discussed elsewhere,^{1,47} the $\bar{V}^\circ(\text{int})$ for an ion is made up of two components; the crystal partial molal volume, $\bar{V}^\circ(\text{cryst}) = 2.52r^3$ (when r is in Å units), and the void space or disordered partial molal volume, $\bar{V}^\circ(\text{disord})$.

By using various semiempirical methods,⁴⁷ $\bar{V}^\circ(\text{int})$ can be estimated to be 39.8 to 42.7 cm³/mol for Mg²⁺ + SO₄²⁻ (using $r(\text{Mg}^{2+}) = 0.65$ and $r(\text{SO}_4^{2-}) = 2.05$ Å). These values of $\bar{V}^\circ(\text{int})$ can be compared to $\bar{V}^\circ(\text{cryst}) = 22.4$ cm³/mol, which would be the $\bar{V}^\circ(\text{int})$ if void space packing effects do not occur (which may be the case for a nonhydrated contact ion pair). Using $\bar{V}^\circ(\text{int}) = 41.0$ cm³/mol, we obtain $\bar{V}^\circ(\text{elect}) = \bar{V}^\circ(\text{ion pair}) - \bar{V}^\circ(\text{int}) = -48.2, -38.2,$ and -25.2 cm³/mol, respectively, for Mg²⁺(H₂O)₂SO₄²⁻, Mg²⁺(H₂O)SO₄²⁻, and Mg²⁺SO₄²⁻. Even if $\bar{V}^\circ(\text{int})$ is assumed to be equal to $\bar{V}^\circ(\text{cryst})$, the electrostriction of the contact ion pair Mg²⁺SO₄²⁻ is quite large in magnitude (-16.6 cm³/mol). By using a hydration model,^{1,48} the number of water molecules (n) associated with the various ion pairs can be estimated

$$n = \frac{\bar{V}^\circ(\text{ion pair}) - \bar{V}^\circ(\text{int})}{\Delta v} = \frac{\bar{V}^\circ(\text{elect})}{\Delta v} \quad (40)$$

where Δv is the change in volume that occurs when a water molecule is taken from the bulk phase to the electrostricted region around the ion pair. This Δv can be estimated from

$$\Delta v = V_E - V_B \quad (41)$$

where V_E is the molar volume of water in the electrostricted region and V_B is the molar volume of water in the bulk (18.0). Padova⁴⁸ has estimated that $\Delta v = -2.1$ cm³/mol; while the maximum estimate of -11.4 cm³/mol is obtained if we assume the $V_E = \bar{V}^\circ(\text{cryst})$ for the water molecule ($r = 1.38$ Å). Using Padova's⁴⁸ Δv and the minimum $\bar{V}^\circ(\text{elect})$ calculated for the contact ion pair, we obtain $n = 8$ for the hydration number. Due to the difficulties of estimating $\bar{V}^\circ(\text{int})$ for the ion pair, it is not possible at present to know how reliable this value may be.

Theoretically, the volume change for ion pair formation can be examined by using the electrostatic theory. Hemmes⁷ has recently reviewed the theory. He calculated the theoretical $\Delta\bar{V}_A^\circ$ by differentiating the association constant by using the Bjerrum⁴⁹ and Fuoss⁵⁰ methods. For the Fuoss⁵⁰ method, Hemmes⁷ found

$$\Delta\bar{V}_A^\circ = \frac{Z_+Z_-Ne^2}{\bar{a}D} \left(\frac{\partial \ln D}{\partial P} \right)_T - \beta RT \quad (42)$$

where Z_i is the charge, D is the dielectric constant, β is the compressibility, and the other symbols have their normal meaning. The last term, $\beta RT = 1.1$ cm³/mol at 25°, results from expressing K_A in molar units. This equation can only be used for outersphere pairs. The ion size parameter (\bar{a}) needed in the calculation can be determined from the Fuoss expression of K_A by using the measured K_A . For MgSO₄[°], Hemmes⁷ obtained $\Delta\bar{V}^\circ = 7.42$ cm³/mol, which is in excellent agreement with the earlier esti-

mates of Hamann, *et al.*^{51,52} and the experimental value. This agreement indicates that the "sphere in continuum" or Born model gives a reasonable representation of the MgSO₄[°] ion pairing process. A similar calculation at 0 and 50°, respectively, gives $\Delta\bar{V}^\circ = 6.13$ and 8.92 cm³/mol.

The theoretical $\Delta\bar{V}^\circ$'s increase in a linear manner with increasing temperature, while the experimental $\Delta\bar{V}^\circ$'s appear to go through a minimum. This behavior is similar to that found for the dissociation of weak acids.^{53,54} It is interesting to note that the correlation between the volume change, $\Delta\bar{V}^\circ$, and compressibility change, $\Delta\bar{K}^\circ$, that occurs for the ionization of weak acids,⁵⁵ also appears to hold for the formation of ion pairs.⁵⁶ Since the $\Delta\bar{V}^\circ$ and \bar{V}° do not have the same temperature dependence, this effect cannot be attributed entirely to the free ions (whose \bar{V}° 's are known to go through a maximum when plotted *vs.* temperature). The failure of the Born model to predict the temperature behavior of the $\Delta\bar{V}^\circ$ and \bar{V}° of ion pairs (as well as ions), has been discussed in detail elsewhere.^{1,47} The similarity in the temperature behavior of the \bar{V}° of MgSO₄[°] and free ions is not surprising since MgSO₄[°] (in all its forms) appears to be a highly hydrated species and most of the temperature dependence of ions appears to be related to $\bar{V}^\circ(\text{elect})$. It is interesting to note that the \bar{V}° 's of highly hydrated nonelectrolytes such as B(OH)₃ also appear to go through a maximum when plotted *vs.* temperature.⁵⁴ If $\bar{V}^\circ(\text{elect})$ is assumed^{1,57} to be proportional to the compressibility of the solvent (β) instead of $1/D(\partial \ln D/\partial P)$, the theoretical temperature variation of ions as well as other hydrated solutes like ion pairs will be similar to the experimental measurements. Marshall,⁵⁸ for example, has shown that the volume change for ion pair formation is proportional to the compressibility of the solvent. At present it is not possible to theoretically predict the temperature dependence of $\Delta\bar{V}^\circ$ for ion pair formation or acid and base dissociation. The truth is probably somewhere between the simple Born model and the compressibility model for electrostriction. Temperature dependent, high-pressure conductance, or Raman work would be very helpful in determining if the density calculated temperature dependence is correct.

In summary, the apparent molal volume change for ion pair formation and the apparent molal volume of an ion pair can be calculated from volume and activity coefficient data provided a reliable association constant is available. This makes it possible to study the structure of ion pairs using volume data at 1 atm (*i.e.*, without making high-pressure measurements). We presently are studying the ϕ_v and $\Delta\phi_v$ of other ion pairing systems by similar techniques and, hopefully, we can obtain new information concerning the structure of ion pairs in aqueous solutions.

Acknowledgments. The authors would like to acknowledge the support of the Office of Naval Research (N00014-67-A-0201-0013) and the Oceanographic Section of the National Science Foundation (GA-17386) for this study.

Supplementary Material Available. Figures 1, 3 (at 0 and 50°), 4, 6, 7, and 9 and Table II will appear following these pages in the microfilm edition of this volume of the journal. Photocopies of the supplementary material from this paper only or microfiche (105 × 148 mm, 24× reduction, negatives) containing all of the supplementary material for the papers in this issue may be obtained from the Journals Department, American Chemical Society, 1155

16th St., N.W., Washington, D. C. 20036. Remit check or money order for \$3.00 for photocopy or \$2.00 for microfiche, referring to code number JPC-74-1287.

References and Notes

- (1) F. J. Millero, *Chem. Rev.*, **71**, 147 (1971).
- (2) F. H. Fisher, *J. Phys. Chem.*, **66**, 1607 (1962).
- (3) F. H. Fisher and D. F. Davis, *J. Phys. Chem.*, **69**, 2595 (1965); **71**, 819 (1967).
- (4) C. F. Hale and F. H. Spedding, *J. Phys. Chem.*, **76**, 2925 (1972).
- (5) S. D. Hamann, P. J. Pearce, and W. Strauss, *J. Phys. Chem.*, **68**, 375 (1964).
- (6) T. G. Spiro, A. Revesz, and J. Lee, *J. Amer. Chem. Soc.*, **90**, 4000 (1968).
- (7) P. Hemmes, *J. Phys. Chem.*, **76**, 895 (1972).
- (8) F. J. Millero, *J. Phys. Chem.*, **74**, 356 (1970).
- (9) F. J. Millero, *Limnol. Oceanogr.*, **14**, 376 (1969).
- (10) H. E. Wirth, *J. Phys. Chem.*, **71**, 2922 (1967).
- (11) R. E. Lindstrom and H. E. Wirth, *J. Phys. Chem.*, **73**, 218 (1969).
- (12) S. Lee, Ph.D. Thesis, Yale University, New Haven, Conn.; University Microfilm, Ann Arbor, Mich. Ord. No. 66-4906; *Diss. Abstr.*, **B27**, 131 (1966).
- (13) F. J. Millero, *Geochem. Cosmochim. Acta*, **34**, 1261 (1970).
- (14) W. L. Masterton, H. Welles, J. H. Knox, and F. J. Millero, *J. Solution Chem.*, **3**, 91 (1974).
- (15) T. F. Young, *Recl. Chem. Progr.*, **12**, 81 (1951); T. F. Young and M. B. Smith, *J. Phys. Chem.*, **58**, 716 (1954).
- (16) R. M. Pytkowicz and D. R. Kester, *Amer. J. Sci.*, **267**, 217 (1969).
- (17) F. J. Millero and J. H. Knox, *J. Chem. Eng. Data*, **18**, 407 (1973).
- (18) F. Franks and H. T. Smith, *Trans. Faraday Soc.*, **63**, 2586 (1967).
- (19) L. A. Dunn, *Trans. Faraday Soc.*, **64**, 1898, 2951 (1968); **62**, 2348 (1966).
- (20) W. Geffcken and D. Frice, *Z. Phys. Chem.*, **B26**, 81 (1934).
- (21) H. E. Wirth, *J. Amer. Chem. Soc.*, **59**, 2549 (1937).
- (22) G. Jones and W. A. Ray, *J. Amer. Chem. Soc.*, **59**, 187 (1937).
- (23) F. Vaslow, *J. Phys. Chem.*, **70**, 2286 (1966).
- (24) See paragraph at end of text regarding supplementary material.
- (25) I. L. Jenkins and C. B. Monk, *J. Amer. Chem. Soc.*, **72**, 2695 (1950).
- (26) R. M. Izatt, D. E. Eatough, J. J. Christensen, and C. H. Bartholomew, *J. Chem. Soc. A*, **45**, 47 (1969).
- (27) C. W. Davies, "Ion Association," Butterworths, London, 1962.
- (28) A. H. Truesdell and P. B. Hostetler, *Geochim. Cosmochim. Acta*, **32**, 1019 (1968).
- (29) E. C. Righellato and C. W. Davies, *Trans. Faraday Soc.*, **26**, 592 (1930).
- (30) V. S. K. Nair and G. N. Nancollas, *J. Chem. Soc.*, 3706 (1958).
- (31) E. Glueckauf, *Proc. Roy. Soc., Ser. A*, **313**, 131 (1969).
- (32) H. S. Harned and B. B. Owen, "The Physical Chemistry of Electrolytic Solutions," American Chemical Society Monograph, Series No. 137, Reinhold, New York, N. Y., 1958.
- (33) R. A. Robinson and R. H. Stokes, "Electrolyte Solutions," Butterworths, London, 1959.
- (34) P. G. Brown and J. E. Prue, *Proc. Roy. Soc., Ser. A*, **232**, 320 (1955).
- (35) W. Leung and F. J. Millero, *J. Chem. Thermodynam.*, to be submitted for publication.
- (36) B. L. Vanzetti in "International Critical Tables," Vol. V, E. W. Washburn, Ed., McGraw-Hill, New York, N. Y., 1929.
- (37) G. Atkinson and S. Petrucci, *J. Phys. Chem.*, **70**, 3122 (1966).
- (38) H. S. Dunsmore and J. C. James, *J. Chem. Soc.*, 2925 (1951).
- (39) A. Paterson, Jr., and H. Freitag, *J. Electrochem. Soc.*, **108**, 529 (1961).
- (40) F. E. Baily, Jr., and A. Paterson, Jr., *J. Amer. Chem. Soc.*, **74**, 4426 (1952).
- (41) H. W. Jones and C. B. Monk, *Trans. Faraday Soc.*, **48**, 929 (1952).
- (42) A. R. Davis, personal communication, 1973.
- (43) M. Eigen and K. Tamm, *Z. Elektrochem.*, **66**, 93 (1962).
- (44) A. R. Davis and B. G. Oliver, *J. Phys. Chem.*, **77**, 1315 (1973).
- (45) F. H. Fisher, *J. Phys. Chem.*, **69**, 695 (1965).
- (46) F. H. Fisher, *J. Acoust. Soc.*, **38**, 805 (1965).
- (47) F. J. Millero in "Water and Aqueous Solutions," R. A. Horne, Ed., Wiley-Interscience, New York, N. Y., 1972, Chapter 13.
- (48) J. Padova, *J. Chem. Phys.*, **39**, 1552 (1963); **40**, 691 (1964).
- (49) N. Bjerrum, *Kgl. Dan. Vidensk. Selsk. Mat. Fys. Medd.*, **7**, 1 (1926).
- (50) R. M. Fuoss, *J. Amer. Chem. Soc.*, **80**, 5059 (1958).
- (51) S. D. Hamann, *J. Acoust. Soc. Amer.*, **68**, 375 (1964).
- (52) S. D. Hamann, P. J. Pearce, and W. Strauss, *J. Phys. Chem.*, **68**, 375 (1964).
- (53) F. J. Millero, E. V. Hoff, and L. Kahn, *J. Solution Chem.*, **1**, 309 (1972).
- (54) G. K. Ward and F. J. Millero, *J. Solution Chem.*, in press.
- (55) D. A. Lown, H. R. Thirsk, and Lord Wynne-Jones, *Trans. Faraday Soc.*, **64**, 2073 (1968).
- (56) R. T. Emmet and F. J. Millero, Paper presented at American Chemical Society Meeting-in-Minature, May, 1971, Abstract No. 53, F. L. A. C. S., Vol. XXIV, Gainesville, Fla.
- (57) T. J. Webb, *J. Amer. Chem. Soc.*, **48**, 2589 (1926).
- (58) W. L. Marshall, *J. Phys. Chem.*, **74**, 346 (1970).

Electron Paramagnetic Resonance Identification of Molten Salt Produced Superoxide Ions

Pier Giorgio Zambonin

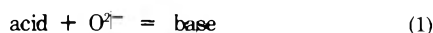
Instituto di Chimica Analitica, Università degli Studi, Bari, Italy, 70126 (Received June 18, 1973; Revised Manuscript Received March 11, 1974)

Superoxide ions produced in molten alkali nitrates were detected by esr spectroscopy in the corresponding quenched matrixes. Perfectly similar esr signals were recorded with solutions of superoxide prepared by chemical or electrochemical methods. This paper, while indicating a further analytical tool for fused salt studies, represents a confirmation of the molten salt "superoxide model" previously suggested on the basis of electroanalytical information. In particular, the present results eliminate the doubt recently expressed by some authors that the model proposed for oxides reactions could be, in some way, influenced by "interfacial artifacts" connected with the voltammetric detection of per-superoxide ions in molten salts.

Introduction

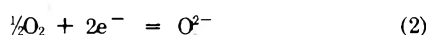
Three decades ago Lux and Flood proposed a general acid-base model^{1,2} for molten electrolytes. An acid was

considered an oxide acceptor, while a base was an oxide donor, so that a typical acid-base reaction could be expressed by the general scheme



For many years this was the principle model invoked to interpret most molten salt chemical reactions, thus assuming that oxide was a particularly nonreactive species (for reviews see ref 3-6).

Similarly the basis of interpretation⁷⁻¹⁰ of the electrochemistry of oxides and oxygen was the model of an oxygen electrode working reversibly according to the overall electrodic process



In effect this simple Lux-Flood (LF) formalism, which was quite successful in molten silicates and other nonoxidizing high temperature solvents, proved insufficient to explain several phenomena observed in medium-temperature melts, particularly molten nitrates. Thus "solvation effects" on oxide ions which result in the formation of orthonitrate¹¹ or pyronitrate¹² ions has been hypothesized to explain the experimental findings. However, even these schemes (substantially equivalent, indeed, to the LF formalism) proved insufficient. More sophisticated models were necessary to interpret the experimental data collected by various authors and often presented without satisfactory explanations.

A reasonable solution of the problem transpired from recent systematic¹³⁻¹⁹ studies. Contrary to previous assumptions, oxide (O^{2-}) was characterized as a very reactive species usually capable of existence only at very low concentration levels. Consequently its oxidation products, superoxide ($\text{O}_2^{\cdot-}$) and peroxide (O_2^{2-}); emerged as stable and important entities. These conclusions from molten nitrates appeared to be indicative of the behavior of other^{16,19} fused systems.

While several authors have accepted the new point of view, others still consider the problem partially open (for recent reviews see ref 19-22). The main perplexity about the per-superoxide model concerns the fact that it was formulated on the basis of "indirect evidence" derived from electrochemical data. The extreme hypothesis²³ has been made that some of the electroanalytical findings supporting the existence of superoxide ions in melts could be due to interfacial phenomena not indicative of the actual situation in solution.

Only a specific "bulk" analytical method could eliminate residual doubts. Electron spin resonance (esr) spectroscopy is a specific analytical tool for chemical species having unpaired electrons, such as superoxide ions.

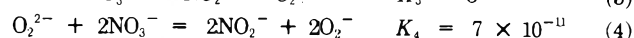
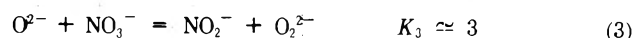
The most significant ways previously used to produced superoxide in molten alkali nitrates have been duplicated in the course of the present study. The esr technique in place of electroanalytical methods was used to detect the actual presence of $\text{O}_2^{\cdot-}$ ions.

Experimental Section

The solvent was an equimolar mixture of reagent-grade sodium and potassium nitrate (melting point $\sim 500^\circ\text{K}$) maintained, in the course of the samples' preparation, under inert gas atmosphere or vacuum at a temperature of about 510°K . The following methods, described in the literature, were used to produce molten salt solutions of superoxide.

(a) *Addition of Oxide (O^{2-})*. According to our conclusions,¹³ in the given nitrate melt equilibrated with an alkali metal oxide, for example, Na_2O , a mixture of peroxide and superoxide can be obtained by the following reac-

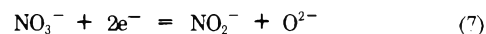
tions



where the numerical (molal) values are relevant to a temperature of 502°K . By passing dry oxygen at the pressure of 1 atm over this mixture, the conversion^{13,17} of any oxide to superoxide is practically complete



Similar results can be obtained when oxide ions are added to the melt by controlled-potential cathodic electrolysis^{14,24} of the melt anions



(b) *Addition of Peroxide (O_2^{2-})*. By equilibrating the melt with a compound such as Na_2O_2 , electrochemical results, qualitatively similar to the addition of oxide, were obtained.¹³ This is due to reactions 4 and/or 6.

(c) *Addition of Superoxide ($\text{O}_2^{\cdot-}$)*. Compounds such as KO_2 and NaO_2 rapidly dissolve¹⁵ (under gas stirring) in nitrate melts.

In general, to minimize oxides-silica interactions,¹⁹ the superoxide solutions were prepared, *via* the described methods, in cells lined with inert material (platinum or Teflon). They were then injected, *via* a thin Teflon pipe, into silica or Pyrex containers suitable for esr studies (tubing of internal diameter ~ 3 mm) and rapidly quenched. In every case these small containers were flame sealed immediately after the introduction of the samples.

The high dissolution rate of potassium or sodium superoxides also made the preparation of the samples directly possible in the testtubes without appreciable attack of the silica walls (operation time before quenching, 1-2 min). In contradistinction this procedure was not possible when methods a and b were employed since alkali oxides and peroxides are only slightly soluble and their dissolution (followed by reactions 3-6) is quite slow.

The samples were stored at room temperature and usually analyzed by esr spectroscopy within 1 week of their preparation. Specimens of the solutions, prepared as described and diluted if necessary, were analyzed by the electroanalytical techniques (potentiometry and voltammetry) previously^{13,14,19} tested. The presence of moisture and other acidic impurities in the melt and in the working atmosphere proved, as expected,^{13,18} very critical.

The esr spectra were recorded by using Varian Model E-3 and E-9 spectrometers equipped with variable temperature accessories.

Results and Discussion

Sodium peroxide prepared²⁵ by action of molecular oxygen on sodium metal (which contains esr-detectable²⁶ traces of the higher oxide NaO_2) was employed to test our apparatus with samples consisting of superoxide magnetic centers diluted in an ionic matrix. The relevant derivative esr spectra, recorded at various temperatures, are given in Figure 1. Their shape is characteristic of a doublet species, with an axial symmetric g factor, contained in a powder.²⁷ On increasing the temperature signals more and more like a single-line spectrum were recorded (see Figure 1). At temperature values around 160°K the spectrum shows a marked shoulder at low fields which becomes a net peak as the temperature is decreased further. On the

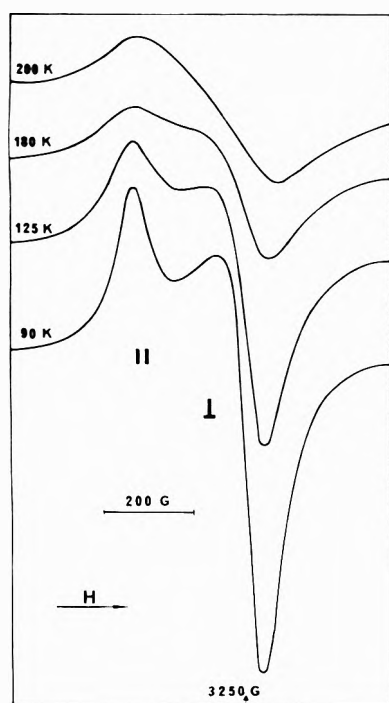


Figure 1. Temperature effect on first-derivative esr signals of superoxide contained in a matrix of Na₂O₂: microwave frequency 9.148 GHz.

curve recorded at 90°K the following values of g were calculated: $g_{\perp} = 2.013$ and $g_{\parallel} = 2.164$.

Typical first-derivative esr spectra relevant to a quenched (Na,K)NO₃ melt containing 0.15 m KO₂ are reported in Figure 2. In this case, temperature had no significant effect on the shape of the spectra; it had, however, a marked influence on the intensity of the signal which increased on cooling the system. This was probably because of a slight broadening in the spectra, occurring when the temperature rises. The influence of temperature on this kind of signal is well known. For all the superoxide systems described in the literature (*vide infra*) the best-defined esr spectra were obtained at low temperatures (below 90°K).

The spectra reported in Figure 2 present a marked asymmetry and no hyperfine structure. This is in agreement with the actual presence of superoxide which is characterized by an axial symmetry while the nuclear spin for ¹⁶O is zero. At 90°K a value of $g = 2.0068$ was measured. This finding is in agreement with the requirement²⁸ that diatomic radicals having three electrons in a π level (such as O₂⁻) usually present a g factor greater than the free-spin value 2.0023.

The different shape of the derivative esr profiles reported in Figures 1 and 2 is merely attributed to a lower "rigidity" of the nitrate solvent with respect to the peroxide matrix. A higher freedom of motion possible in nitrates can in fact lead to a partial averaging of the g_{\perp} and g_{\parallel} factors. This hypothesis is in agreement with the marked temperature dependence (see Figure 1) of the shape of the superoxide spectra obtained in sodium peroxide; a signal close to a single-line curve was obtained in this last case only by increasing the temperature, *viz.*, on increasing the freedom of motion of the superoxide ions.

As shown in Figure 3, similar spectra were obtained by using different methods of preparing the superoxide solution. In first approximation the intensity of the signal

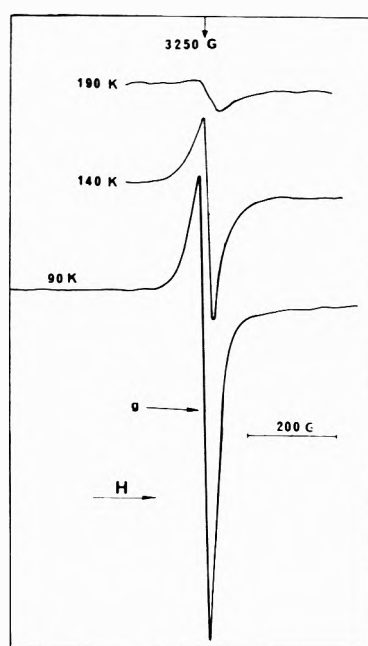


Figure 2. Temperature effect on first-derivative esr signals of superoxide (2%) trapped in a matrix of (Na_{0.5}K_{0.5})NO₃: microwave frequency 9.152 GHz.

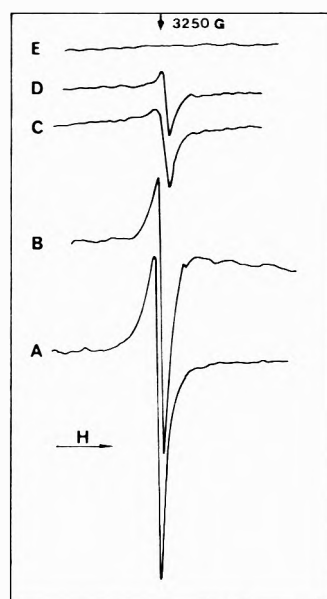
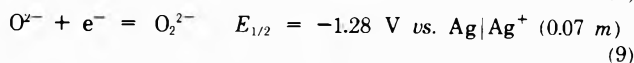
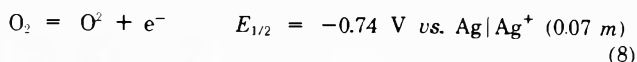


Figure 3. Examples of first-derivative esr spectra recorded at the temperature of 90°K in the presence of variable concentrations of O₂⁻ in (Na,K)NO₃ eutectic. Superoxide was produced in the molten matrix according to the specified manner (see Experimental Section): microwave frequency 9.152 GHz: (curve A) O₂⁻ = 4 × 10⁻² m , solution prepared by direct introduction of solid KO₂ in the melt under flux of nitrogen; (curve B) O₂⁻ = 3 × 10⁻² m , solution prepared by adding Na₂O₂ to the melt stirred with dry oxygen; (curve C) O₂⁻ = 1 × 10⁻² m , solution prepared by adding Na₂O to the melt stirred with dry oxygen; (curve D) O₂⁻ = 8 × 10⁻³ m , solution prepared by adding electrochemically produced oxide ions (eq 7) to the melt stirred with dry oxygen; (curve E) pure (Na,K)NO₃ eutectic.

(*i.e.*, the total peak height²⁹ between the two halves of the derivative presentation) was proportional (at a given temperature) to the concentration of superoxide.

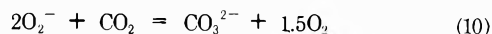
When an esr spectrum could be obtained for a certain quenched sample, the electrochemical test for O₂⁻ in the corresponding molten solution was also positive, *i.e.*, both

oxidation and reduction voltammetric waves^{13,14} for superoxide



were present. The contrary was only not verified for concentrations close to the applicability limits of the voltammetric technique. Apparently, under the present experimental conditions, the electroanalytical detection of superoxide in molten phase is a little more sensitive than the equivalent esr detection in the solid matrix.

Complete disappearance of the esr signal was noted after contamination of the samples with water or carbon dioxide. This is in agreement with the known^{18,25} "destructive" reactions



and it can be considered further proof for the actual presence of superoxide.

Spectra slightly different from those reported in Figures 2 and 3 (appearance of a small peak at low field) have been obtained in some cases by analyzing samples of O_2^- in alkali nitrate matrixes several months after their preparation and storage at room temperature. An example of such signals is reported in Figure 4 (curve a) where it is compared with the spectrum obtained on a freshly prepared sample (curve b) and the one characteristic of superoxide in a peroxide matrix (curve c). In general, one-line spectra (such as curve b) could be reobtained after melting and rapidly quenching "old" samples. This seems to indicate that the variation of the signal (from curve b to curve a) is to be ascribed to a very slow matrix modification occurring in the quenched sample stored at room temperature rather than to the formation of new esr active species. Curve a is reminiscent of the shape of both curves b and c and the phenomena perhaps can be explained on the basis of progressive slow formation of crystalline, "rigid" nuclei in the bulk of the original "soft" matrix obtained by quenching the molten nitrate mixture. In conclusion all the spectra reported in Figure 4 can be assigned to superoxide, the differences likely being due to matrix effects.

Literature indicates that often the superoxide species dissolved in various solid matrixes or present on the surface of solids give origin to esr signals presenting nonaxial tensors. This is certainly in disagreement with the geometry³⁰ of the "free" superoxide ions. By analyzing most recent data, Symons drew the conclusion³¹ that, in general, the experimental findings better describe the existence of nonlinear entities such as X-OO rather than true superoxide ions. According to the author, the formation of nonlinear species can be due to the presence of strong interaction with the matrix: this is, for example, the case³²⁻³⁴ of the formation of HO_2 molecules by proton extraction from solvents such as DMF, H_2O_2 , etc. No valid indication for the formations of nonlinear species or for the existence of donor-acceptor phenomena in the present system can be derived from the results obtained in the course of this study. The mean value of g calculated on the basis of the relation

$$g = (2g_{\perp} + g_{\parallel})/3$$

by using the values of g_{\perp} and g_{\parallel} obtained from the curves

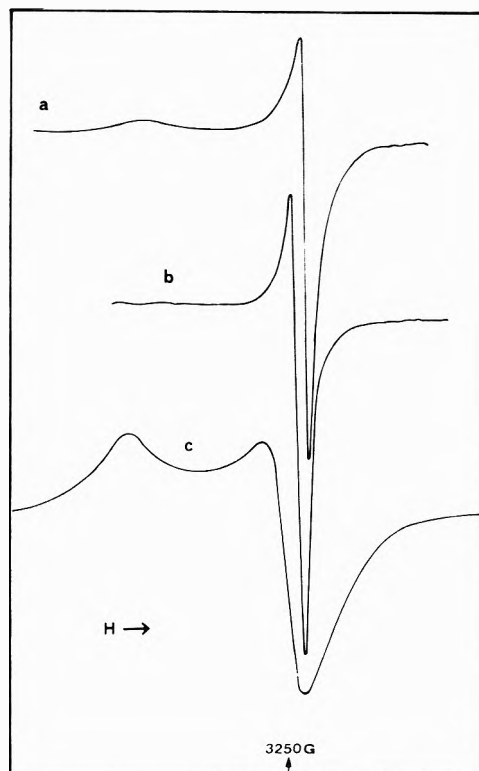


Figure 4. Comparison of esr signals for superoxide contained in various ionic matrixes: (a) quenched (Na,K) NO_3 eutectic maintained for several months at room temperature under perfectly inert atmosphere; (b) quenched (Na,K) NO_3 freshly prepared; (c) sodium peroxide containing traces of NaO_2 : microwave frequency 9.152 (curve a and b) and 9.148 GHz (curve c).

reported in Figure 1 is equal to 2.063. It is quite different from the value calculated for the curves in Figure 2. This discrepancy, however, cannot question, *per se*, the conclusions of the present study since the numerical value of g for superoxide trapped in solids can be largely dependent on the surrounding medium. A systematic investigation in the field of the ionic matrixes has been performed by Zeller and Kanzig³⁰ who have studied the esr behavior of superoxide in various alkali metal halides. Wide variations of g have always been observed by substituting both cations (Na^+ , K^+ , Rb^+) and anions (Cl^- , Br^- , I^-). So it is not surprising that different g tensors were obtained on substituting the matrix Na_2O_2 with (Na,K) NO_3 .

Acknowledgment. Work sponsored in part by the Italian National Research Council (C.N.R., Rome). The author thanks Drs. C. Corvaja, G. Farmia (University of Padua), and C. Hartzell (The Pennsylvania State University) for useful discussions and help in recording the esr spectra.

References and Notes

- (1) H. Lux, *Z. Electrochem.*, **45**, 303 (1939).
- (2) H. Flood and T. Forland, *Acta Chem. Scand.*, **1**, 592 (1947).
- (3) B. R. Sundheim, Ed., "Fused Salts," McGraw-Hill, New York, N. Y., 1964.
- (4) H. Blander, Ed., "Molten Salt Chemistry," Interscience, New York, N. Y., 1964.
- (5) F. R. Duke, *Advan. Chem. Ser.*, **No. 49**, 220 (1965).
- (6) G. Mamantov, Ed., "Molten Salts," Marcel Dekker, New York, N. Y., 1969.
- (7) R. W. Laity in "Reference Electrodes," D. J. G. Ives and G. J. Janz, Ed., Academic Press, New York, N. Y., 1961, Chapter 9.
- (8) Y. K. Delimarskii and B. F. Markov, "Electrochemistry of Fused Salts," Sigma Press, Washington, D. C., 1961.

- (9) A. F. Alabyshev, M. F. Lantratov, and A. G. Morachevskii, "Reference Electrodes for Fused Salts," Sigma Press, Washington, D. C., 1965.
- (10) A. D. Graves, G. J. Hills, and D. Inman in "Advances in Electrochemistry and Electrochemical Engineering," Vol. 4, P. Delahay and C. W. Tobias, Ed., Interscience, New York, N. Y., 1966.
- (11) R. N. Kust, *Inorg. Chem.*, **3**, 1035 (1964).
- (12) A. A. El Hosary and A. M. Shams El Din, *J. Electroanal. Chem.*, **35**, 35 (1969).
- (13) P. G. Zambonin and J. Jordan, *J. Amer. Chem. Soc.*, **91**, 2225 (1969).
- (14) P. G. Zambonin, *J. Electroanal. Chem.*, **24**, 368 (1970).
- (15) P. G. Zambonin and A. Cavaggoni, *J. Amer. Chem. Soc.*, **93**, 2854 (1971).
- (16) P. G. Zambonin, *J. Electroanal. Chem.*, **24**, 25 (1970).
- (17) P. G. Zambonin, *J. Electroanal. Chem.*, **33**, 243 (1971).
- (18) P. G. Zambonin, F. Paniccia, and A. Bulo, *J. Phys. Chem.*, **76**, 422 (1972).
- (19) P. G. Zambonin, *J. Electroanal. Chem.*, **45**, 451 (1973).
- (20) D. Bauer and J. P. Beck, *J. Electroanal. Chem.*, **40**, 233 (1972).
- (21) J. H. R. Clarke and G. I. Hills, *Chem. Brit.*, **9**, 12 (1973).
- (22) K. W. Fung and G. Mamantov, "Electroanalytical Chemistry in Molten Salts" in "Advances in Molten Salt Chemistry," Braunstein, Mamantov, and Smith, Ed., Vol. II, Plenum Press, New York, N. Y., 1973, Chapter 4.
- (23) M. Fredericks, R. B. Temple, and G. W. Thickett, *J. Electroanal. Chem.*, **38**, 5 (1972).
- (24) H. S. Swofford and H. A. Laitinen, *J. Electrochem. Soc.*, **110**, 814 (1963).
- (25) I. I. Volnov in "Peroxides, Superoxides Ozonides of Alkali and Alkaline Earth Metals," A. W. Petrocelli, Ed., Plenum Press, New York, N. Y., 1966.
- (26) J. E. Bennett, D. J. E. Ingram, M. C. R. Symons, P. George, and J. S. Griffith, *Phil. Mag.*, **46**, 443 (1955).
- (27) H. G. Hecht, "Magnetic Resonance Spectroscopy," Wiley, New York, N. Y., 1967, p 130.
- (28) M. C. R. Symons, *Advan. Chem. Ser.*, **No. 36** 80 (1962).
- (29) I. M. Kolthoff and P. J. Elving, "Treatise on Analytical Chemistry," Part I, Vol. 4, Wiley, New York, N. Y., 1963.
- (30) H. R. Zeller and W. Kanzig, *Helv. Phys. Acta*, **40**, 845 (1967).
- (31) M. C. R. Symons, *J. Phys. Chem.*, **76**, 3095 (1972).
- (32) D. L. Maricle and W. G. Hodgson, *Anal. Chem.*, **37**, 1562 (1965).
- (33) S. J. Wyard, R. C. Smith, and F. J. Adrian, *J. Chem. Phys.*, **49**, 2780 (1968).
- (34) R. C. Catton and M. C. R. Symons, *J. Chem. Soc. A*, 1393 (1969).

Transition State Theory for Vaporization and Condensation

Alan W. Searcy* and Dario Beruto

Inorganic Materials Research Division, Lawrence Berkeley Laboratory and Department of Materials Science and Engineering, College of Engineering, University of California, Berkeley, California 94720 (Received December 6, 1973)

Publication costs assisted by Lawrence Berkeley Laboratory

A theory of Langmuir exactly predicts the rates of many vaporization reactions as functions of temperature. For these reactions his theory is shown to be superior to absolute reaction rate theory, which can be made to yield the same rate equation, in requiring fewer and more general hypotheses and in utilizing a kinetic factor that has been directly verified by experiment. Langmuir's theory is extended to provide an exact description of the kinetics of some dissociative vaporization reactions. It is pointed out that Langmuir's gas-like kinetic factor has been experimentally verified for the desorption step of two substances that undergo retarded vaporization. It is argued that the transition state particles for desorption are free gas molecules and for surface diffusion in the self-adsorption layer are particles with gas-like velocities parallel to the surface. Rate equations which utilize gas-translation kinetic factors are derived for substances that vaporized with nonequilibrium distributions of electronic states and for substances with vaporization rates limited by separation of self-adsorbed particles from catalytic surface sites or particles. The equations for dissociative vaporization reactions require that transition state particles consist sometimes of a coupled flux of particles of two or more different kinds.

Introduction

Vaporization reactions are exceptional among chemical processes in that they are characterized by maximum possible rates that can be precisely predicted for any substance from thermodynamic data and from the kinetic theory of gases.¹⁻³ Furthermore, many substances have been found to vaporize into vacuum at their maximum possible rates, a result predicted by Langmuir¹ by means of a theoretical analysis that included the first explicit formulation of what is now usually called the principle of microscopic reversibility.⁴ Vaporization at this maximum possible rate can be called unretarded vaporization, as distinct from retarded vaporization, a term which can be applied to describe vaporization at any lower rate.⁵

The rate of unretarded vaporization J in *vacuo* in moles per unit time per unit area is given for a substance which has only one major vapor species by the Hertz-Knudsen-

Langmuir (HKL) equation

$$J = (2\pi MRT)^{-1/2}P \quad (1a)$$

where M is the molecular weight of the vapor, R the gas constant, T the temperature, and P is the equilibrium vapor pressure. Elimination of P by means of the Clausius-Clayron relation yields the HKL equation in terms of the standard pressure P° of the vapor, the standard enthalpy of vaporization, ΔH_v° , and the standard entropy of vaporization, ΔS_v°

$$J = (2\pi MRT)^{-1/2}P^\circ \exp(S_v^\circ/R) \exp(-\Delta H_v^\circ/RT) \quad (1b)$$

This equation is readily generalized for dissociative congruent vaporization reactions (e.g., $A_m B_n = mA(g) + nB(g)$) in which the individual vapor molecules do not have the same composition as the condensed phase.^{3,6}

It has been claimed³ for substances that obey eq 1 that

(a) the activated complex is identical with the vapor molecule produced in the reaction and that (b) the product of the frequency factor ν and transmission coefficient κ , as ordinarily defined in transition state theory,^{7,8} is identified with the numerical value of $(kT/2\pi m_g)^{1/2} Q^l$ where Q^l is the standard translational partition function of the vapor molecules. A substantiation of these claims is of considerable importance because in most types of chemical reactions the activated complex cannot be directly studied; its composition and properties must be inferred from the dependence of the reaction rate on system variables, and its inferred thermodynamic properties depend upon an estimated value of the frequency of decomposition of the presumed activated complex. In this paper the assumptions made by Langmuir in deducing eq 1a are compared to the assumptions that lead through the theory of absolute reaction rates⁹ to an equivalent relation, and it is then shown that experimental data for several substances that undergo unretarded vaporization confirm the kinetic factor and thermodynamic factor assumed by Langmuir rather than those of the absolute reaction rate theory.

The analysis of unretarded vaporization provides insights into the nature of diffusion in the self-adsorbed layer. It will be argued that the product of the frequency factor and transmission coefficient for movement in the self-adsorption layer can be evaluated by means of the assumption that the activated complex is a two-dimensional gas, whether the vaporization process is retarded or not. This conclusion is used in simplifying a rate equation which is derived for vaporization when the rate is retarded by the availability of catalytic reaction sites or of catalytic adsorbed particles.

The paper concludes with a discussion of experiments that might test whether the rate-limiting step in vaporization reactions is the desorption of excited molecules, whether it is the catalyzed dissociation of molecules from active sites or particles, or whether it is some other surface step of the vaporization process.

Unretarded Vaporization and Condensation without Dissociation

Langmuir's prediction¹ that vaporization rates would obey eq 1a was derived from three postulates. (1) Molecules of the equilibrium vapor come to complete equilibrium with the condensed phase upon every collision. (2) Vaporization equilibrium is maintained by detailed balancing of independent fluxes of vaporizing and condensing molecules. (3) The flux of molecules that escape from the condensed phase to the vapor is unchanged during vaporization into vacuum from its value under equilibrium conditions. This kind of postulate is commonly made in transition state theory.⁸ Such postulates are expected sometimes to fail because any changes in the reaction environment can influence the reaction paths.¹⁰

The first of Langmuir's postulates asserts that there is no thermodynamic barrier to condensation at equilibrium, so that the rate of condensation is a function of the equilibrium properties of the vapor molecules and of their dynamics of movement under equilibrium conditions. The second and third postulates then lead to the prediction that vaporization *in vacuo* occurs by exactly the reverse of the path(s) defined for condensation under equilibrium conditions.

Langmuir's theory, which he developed primarily to describe the vaporization of metals, predated transition

state theory. However, it can be viewed as equivalent to the special case in transition state theory in which the activated complex is identical with the reaction product.

For consideration of Langmuir's theory as a form of transition state theory, it is convenient to substitute different thermodynamic variables into the temperature-dependent form of Langmuir's rate equation. No new assumptions or approximations are required for the substitutions, which yield

$$j = \left(\frac{kT}{2\pi m_g} \right)^{1/2} [X_g^{\circ}] \left[\frac{(2\pi m_g kT)^{1/2}}{h} \right] \frac{\pi Q_g^l}{\pi Q_c} \exp(-\Delta E_0^{\circ}/kT) \quad (2)$$

Here j is the number of molecules that vaporize per unit area per second, m_g is their mass, k is the Boltzmann constant, h is Planck's constant, $[X_g^{\circ}]$ is the standard concentration of vapor, and ΔE_0° is the energy difference per molecule at absolute zero between the vapor and the condensed phase. The term $(kT/2\pi m_g)^{1/2}$ is the velocity of a thermally equilibrated gas, while the quantity $(2\pi m_g kT)^{1/2} h^{-1}$ is the standard translational partition function of the vapor in dimension l normal to the surface. This quantity has been separated from the remainder of the total partition function of the vapor, which is symbolized by πQ_g^l , for subsequent comparison with the equation of absolute reaction rate theory. The quantity πQ_c is the total partition function of the condensed phase.

The general rate equation for vaporization in terms of absolute reaction rate theory is⁹

$$j = \kappa \frac{kT}{h} [Z^{*o}] \frac{\pi Q^*}{\pi Q_c} \exp(-\Delta E_0^*/kT) \quad (3a)$$

For comparison of eq 3a with the Langmuir equation (2), the term kT/h , which is viewed as a universal frequency term, can be interpreted as the product of the average velocity of the activated complex particles moving in one direction over the potential energy barrier of length δ times the translational partition function corresponding to the motion of a particle of mass m^* in one-dimensional box of length δ .⁹ When this procedure, which is equivalent to other derivations accepted for the general rate eq 3a,⁷ is followed eq 3a becomes

$$j = \kappa \left(\frac{kT}{2\pi m^*} \right)^{1/2} \frac{1}{\delta} \frac{(2\pi m^* kT)^{1/2}}{h} \delta [Z^{*o}] \frac{\pi Q^*}{\pi Q_c} \times \exp(-\Delta E_0^*/kT) \quad (3b)$$

The transmission coefficient, κ , is introduced in transition state theory to account for possible reflection of molecules that have crossed the potential energy barrier to reaction. The term πQ^* is the partition function for the activated complex, as defined by Glasstone and coworkers;⁹ πQ_c is the total partition function for the condensed phase and ΔE_0^* is the energy of formation of the activated complex from the condensed phase at absolute zero.

To derive the Langmuir eq 2 from the rate eq 3b^{11,12} requires some further assumptions beside the basic ones made in transition state theory. It is assumed that πQ^* is the same as the partition function for the gas, aside from the omitted translational motion away from surface.¹¹ The energy of activation ΔE_0^* is assumed to be identical with the energy of the equilibrium vaporization reaction, the transmission coefficient κ is assumed to have unit value, and the mass of the activated complex is assumed to be equal to the mass of the vapor molecules. Equation 3b then becomes identical with eq 2, the Langmuir rate equation, because $l = 1$, and the quantity $[Z^{*o}]$ and $[X_g^{\circ}]$,

which are the standard concentrations of the assumed activated complex and of the vapor molecules which impinge on the surface, are chosen, as is usual, to be one particle per cm^2 and per cm^3 , and therefore can be omitted from both equations.

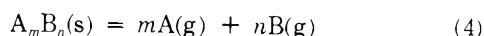
While the expression for the molecular flux thus derived from absolute reaction rate theory is identical with that in Langmuir's theory, the identification of the activated complex in absolute reaction rate theory as a particle with the same partition function as the gas, aside from the omitted translational motion away from the surface,¹¹ might induce the mistaken impression that the activated complex is a kind of two-dimensional adsorbed gas. Since the next section of this paper deals with retarded condensation and vaporization reactions for which the activated particles are assumed to be in a two-dimensional gas state, it is important to draw attention to the difference between the nature of the activated complexes described in that section of this paper and the nature of those that might be considered to be involved in unretarded vaporization.

It is well established that molecules of an equilibrium vapor impinge on surfaces at the rate given by kinetic theory, which is the rate assumed by Langmuir in considering the condensation of vapors. Since by the definition of unretarded condensation, each collision of a vapor molecule with the surface must result in condensation, Langmuir's postulated kinetic factor $(kT/2\pi M_g)^{1/2}$ is experimentally confirmed for unretarded condensation. The frequency factor kT/h , on the other hand, does not directly describe the physically measurable parameter.

Direct measurements by the torsion-Langmuir method¹³ of the forces produced in free surface vaporization confirm for several solids³ the Langmuir hypothesis that molecules which leave a surface in free surface vaporization have a kinetic energy distribution identical with a flux of the equilibrium vapor. The Langmuir frequency factor $(kT/2\pi M_g)^{1/2}$ is, therefore, also experimentally confirmed for unretarded vaporization.

Unretarded Congruent Dissociative Vaporization and Condensation

Just as a maximum possible rate can be calculated for simple vaporization processes such as those of interest to Langmuir, a maximum possible rate can be calculated for vaporization of substances that undergo dissociative congruent vaporization, that is, vaporization according to the general equation



where A or B may represent either atoms or molecules such as O_2 or S_2 . The maximum possible rate for congruent vaporization is given by^{3,6}

$$(J_A)^m (J_B)^n = (2\pi RT)^{-(m+n)/2} (M_A)^{-m/2} (M_B)^{-n/2} (P_A^\circ)^m \times (P_B^\circ)^n \exp(\Delta S_v^\circ/R) \exp(-\Delta H_v^\circ/RT) \quad (5)$$

where J_A and J_B are the molar fluxes of the two vapor species, M_A and M_B are their molecular weights, and ΔH_v° and ΔS_v° are the standard enthalpy and entropy of the equilibrium reaction 4.

Equation 5 can be readily transformed into a more conventional rate equation which gives the flux of $A_m B_n$ that vaporizes or condenses, but the form given in (5) has the advantage of emphasizing the essential connection between the rate equation for unretarded vaporization and the equation for flux through the orifice of an effusion cell

inside which the equilibrium pressures of the vapor species have been established. The kinetic expression that describes free surface vaporization for any particular vaporization reaction and the expression for the rate of effusion from a cell of the equilibrium vapors from that reaction are identical functions of heat and entropy of the equilibrium reaction and of the kinetics of vapor movement.

It is an important experimental fact that the rates of at least two substances that vaporize dissociatively, cadmium telluride¹⁴ and cadmium selenide,¹⁵ have been demonstrated to be unretarded or nearly unretarded (vaporization coefficients 0.8 ± 0.2 and 0.7). Furthermore, since both demonstrations were made by means of the torsion-Langmuir method, they also showed that the vapor species leave the surface with a distribution of kinetic energies that must be close to Maxwellian normal to the surface.

To extend Langmuir's theory to unretarded dissociative reactions, it is only necessary to generalize the first of Langmuir's postulates while retaining the postulates of microscopic reversibility and independence of fluxes. We assume that molecules of A and B at equilibrium in the vapor of near stoichiometric composition always come to complete equilibrium with their solid upon striking the surface. Then by the postulates of microscopic reversibility and independence of fluxes, free surface vaporization *in vacuo* must yield a flux of molecules directed away from the surface which is indistinguishable in energy distribution and angular distribution from the flux of molecules that would pass through a plane in the equilibrium vapor.

To derive eq 5 from transition state theory and at the same time to predict correctly the experimentally observed pressure exerted against the surface by the vaporizing molecules, the transition state particles must be assumed to be identical in thermodynamic properties and in kinetic energy and energy distribution with the A and B molecules which pass through a plane in the equilibrium vapor. In such a transition state, the A and B molecules which together constitute the transition state particles are not even loosely bonded to each other because the highest potential energy along the reaction path in unretarded vaporization or condensation is coincident with the potential energy of the separated gas molecules.

To summarize the conclusions that can be drawn from what we have discussed up to this point for unretarded vaporization processes, Langmuir's theory has advantages over absolute reaction rate theory in that it requires fewer and more general postulates with no subsequent approximations. Dissociative unretarded vaporization can be understood by extending Langmuir's original assumptions to both (or all) vapor species that leave the surface. Langmuir's theory is inadequate to describe retarded vaporization reactions, but, in the next section, modifications of transition state theory that adopt two of Langmuir's three hypotheses are developed. The resultant equations should provide an improved basis for analyses for some retarded vaporization processes.

Transition States for Some Retarded Vaporization Processes

Several substances that undergo retarded vaporization have apparent enthalpies of activation which are greater than the enthalpy of the equilibrium reaction and apparent entropies of activation, when Langmuir's frequency factor is assumed, which are close to the entropy of the

equilibrium reaction. It has been suggested that for such substances the rate-limiting vaporization process may probably be either (1) desorption of the reaction products in excited states or (2) desorption of equilibrium products to leave excited particles on the surface.³

The second of these suggested processes requires more detailed analysis because direct desorption of vapor molecules, such as direct vaporization from ledge or kink sites, must be a higher energy and therefore probably a less important process than is dissociation of particles from catalytic sites, which might, for example, be kinks in ledges, to noncatalytic adsorption sites of the surface, followed later by desorption.^{16,17} A model for vaporization by this more probable sequence of steps can be developed by considering first the condensation process.

It will be assumed that the vapor molecules can be brought to complete equilibrium with the bulk condensed phase only if (a) they encounter thermally activated surface sites or molecules of the self-adsorbed layer whose equilibrium mole fraction of total surface sites X_s is given by $X_s = \exp(-\Delta G_s^*/RT)$, and (b) a fraction of the encounters of vapor molecules with these sites or molecules given by $\exp(-\Delta G_e^*/RT)$ results in complete equilibration. If ΔG_e^* is small relative to RT , $\exp(\Delta G_e^*/RT) \cong 1$, and essentially all encounters with the catalyst sites or molecules will cause equilibration. However, in general, the fraction of the collisions of the vapor that result in immediate equilibration is given by $\exp(\Delta G_e^*/RT) \exp(-\Delta G_s^*/RT) = \exp(-\Delta G_r^*/RT)$.

The equation for the net molar flux J_n of the vapor which not only strikes the surface, but comes to equilibrium with the bulk condensed phase at a catalytic site or molecule, can be written

$$J_n = (2\pi MRT)^{-1/2} P \left[\exp(-\Delta G_r^*/RT) + \frac{\{1 - \exp(-\Delta G_r^*/RT)\} \gamma_m \exp(-\Delta G_m^*/RT) \times \exp(-\Delta G_s^*/RT)}{\gamma_m \exp(-\Delta G_m^*/RT) \exp(-\Delta G_r^*/RT) + \gamma_d \exp(-\Delta G_d^0/RT)} \right] \quad (6a)$$

The terms outside the bracket constitute the Langmuir expression for the total number of moles that strike the surface. The first term inside the bracket expresses the probability for direct reactive collisions of vapor molecules with the thermally activated catalytic sites. The quantity $[1 - \exp(-\Delta G_r^*/RT)]$ expresses the probability that molecules of the vapor will make nonreactive collisions with the surface. These molecules that make nonreactive collisions can be assumed, in agreement with Langmuir's original hypothesis, to come to equilibrium with the surface with respect to their kinetic energies, and rotational and vibrational states. But some process necessary for complete equilibration such as a change in electronic state or bond breaking and molecular rearrangement is assumed not to be possible except at the catalytic sites.

The adsorbed vapor molecules will still come to complete equilibrium if they make a reactive collision with an active site before desorbing. The remainder of the second term inside the brackets is an expression for the fraction of those molecules that initially adsorb without reaction,

but that, rather than desorbing, undergo reactive collisions as a result of surface diffusion. The fraction is formed of a numerator that describes the frequency of reactive collisions by molecules that were initially adsorbed without reaction and a denominator that consists of the sum of the frequencies with which molecules either desorb or react. Here ΔG_d^0 is the standard molar free energy for desorption of self-adsorbed vapor molecules, ΔG_m^* is the standard molar free energy of activation for surface diffusion, and the term $\exp(-\Delta G_r^*/RT)$, as before, gives the probability that those molecules which move to a new surface site will there undergo a reactive collision. The constants γ_d and γ_m are the molar frequencies with which molecules pass through the transition states for desorption and surface diffusion.

de Boer has concluded that the frequency terms for surface jumps and for desorption are of the same magnitude.¹⁸ There appears good reason for concluding they are often essentially equal. As noted above, the demonstration of unretarded vaporization by direct measurements of the force exerted by the vapor which leaves the surface proves a Maxwellian distribution of kinetic energies for molecules which acquire sufficient energy to escape. Furthermore, by comparing the mass flux and pressure for the vaporization of gallium nitride by the reaction $2\text{GaN}(s) = 2\text{Ga}(g) + \text{N}_2$, Mar and Searcy¹⁹ demonstrated the kinetic energy of the products of this retarded reaction to also be Maxwellian, and Balooch, *et al.*,²⁰ proved the kinetic energy and angular distribution of As_4 produced in retarded vaporization of arsenic both to be Maxwellian.

Surface diffusion is often interpreted in terms of random walk models for movement of vacancies in near-surface crystal layers and of atoms in the self-adsorption layer. Observations such as those which have just been mentioned suggest that both desorption and diffusion in the self-adsorption layer can be viewed as manifestations of what might be called a random rocket launch model for movement of molecules of the adsorbed layer.

If a large number of rockets were randomly loaded with a relatively small amount of fuel and randomly pointed for launching without any limit to the minimum amount of fuel assigned to any rocket, relatively few rockets would have sufficient energy to escape from a gravitational field. Many rockets would fall back to the surface at various distances from their launching sites. Still more of the rockets would have insufficient energy to lift clear of the launching sites at all and would fall back on those sites. If the launches were from a stationary source into a frictionless atmosphere, components of movement parallel to the launching surface could be viewed as unrestrained translation, even though gravity acted on the rocket in a direction normal to the surface of the launching site.

Similarly, those molecules which vaporize are known to escape from the field of attraction of the condensed phase with kinetic energy distributions in all three coordinates that are random, that is, with equilibrium or near equilibrium kinetic energy distributions for free gas molecules. More molecules must leave adsorption sites with insufficient kinetic energy normal to the surface for escape, but with energies and directions which can carry them out of the potential energy well formed by the surface particles that lie immediately adjacent to their adsorption sites. Those molecules which have left their potential energy wells would experience negligible forces in the plane parallel to the surface, and could in that plane achieve essentially gas-like velocity distributions. If motions in the two

dimensions parallel to the surface are gas-like, the kinetic factor for surface diffusion in the self-adsorption layer γ_m should approach that for desorption.

A quantitative evaluation of the contribution to surface diffusion of particles moving by the random rocket launch mechanism requires complex summations,²¹ which we hope to complete in our laboratory. Fortunately, the model for catalyzed vaporization does not require solution of this problem; the probability of a reactive collision by surface diffusion should depend mainly on the number of jumps before desorption and should be insensitive to the distance of movement in a single jump. This conclusion follows because molecules, viewed as projectiles launched from the surface, will encounter catalytic sites of the surface layer only at their points of impact and will seldom encounter other adsorbed particles in midjump.

When we accept the argument that $\gamma_d \cong \gamma_m$, use Langmuir's conclusion that vaporization *in vacuo* will occur by just the reverse of the steps followed for condensation in the equilibrium vapor, and make the substitution $P_{eq} = P^\circ \exp(-\Delta G_v^\circ/RT)$ we obtain from eq 6a

$$J_v = \frac{P^\circ \exp(-\Delta G_v^\circ/RT)}{(2\pi MRT)^{1/2}} \left[\exp(-\Delta G_r^*/RT) + \frac{\{1 - \exp(-\Delta G_r^*/RT)\} \exp\{-(\Delta G_m^* + \Delta G_r^*)/RT\}}{\exp\{-(\Delta G_m^* + \Delta G_r^*)/RT\} + \exp(-\Delta G_d^\circ/RT)} \right] \quad (6b)$$

where ΔG_v° is the standard free energy of vaporization.

If ΔG_r^* is small relative to RT or is small relative to $\Delta G_d^\circ - \Delta G_m^*$, the expression inside the square brackets of eq 6b reduces to unity, and eq 1b, the temperature-dependent form of Langmuir's equation for vaporization *in vacuo*, is recovered. This result is consistent with the arguments that led to eq 6b because at temperatures high enough so that ΔG_r^* is small compared to RT , all surface sites should be active in causing complete equilibration of vapor particles.

If ΔG_r^* is greater than RT so that $0 < \exp(-\Delta G_r^*/RT) \ll 1$, eq 6b can be approximated

$$J_v = \frac{P^\circ \exp(-\Delta G_v^\circ/RT)}{(2\pi MRT)^{1/2}} \times \left[\frac{\exp\{-(\Delta G_m^* + \Delta G_r^*)/RT\}}{\exp\{-(\Delta G_m^* + \Delta G_r^*)/RT\} + \exp(-\Delta G_d^\circ/RT)} \right] \quad (7)$$

The physical meaning of this equation is that the vapor molecules commonly reach complete equilibrium with the condensed phase only after undergoing surface diffusion. For ΔG_r^* much greater than $\Delta G_d^\circ - \Delta G_m^*$, the first term of the denominator inside the square brackets of eq 7 is negligible in comparison to the second, and eq 7 becomes

$$J_v = \frac{P^\circ \exp(-\Delta G_v^\circ/RT)}{(2\pi MRT)^{1/2}} \{ \exp[-(\Delta G_m^* + \Delta G_r^* - \Delta G_d^\circ)/RT] \} \quad (8)$$

However $(\Delta G_v^\circ - \Delta G_d^\circ + \Delta G_m^*)$ is the standard molar free-energy difference ΔG_a^* between molecules in the two-dimensional gas transition state for surface diffusion and in the bulk condensed phase. Accordingly, eq 8 becomes

$$J_v = \frac{P^\circ \exp[-(\Delta G_a^* + \Delta G_r^*)/RT]}{(2\pi MRT)^{1/2}} \quad (9)$$

Equation 9 differs from the result for a model which assumes that direct desorption occurs from active sites³ in

that eq 9 has ΔG_a^* where the direct desorption model would place ΔG_v° .

Equation 9 can be generalized to describe the steady-state coupled fluxes of molecules in catalyzed dissociative vaporization. As an example, suppose for reaction 4, $A_m B_n(s) = mA(g) + nB(g)$, vaporization of A atoms or molecules is unretarded, but B atoms or molecules vaporize at a rate limited by their dissociation from thermally activated surface sites. Then

$$J_A = \frac{P_A^\circ \exp(-\overline{\Delta G}_A^\circ/RT)}{(2\pi M_A RT)^{1/2}} \quad (10)$$

and

$$J_B = \frac{P_B^\circ \exp(-\overline{\Delta G}_B^*/RT)}{(2\pi M_B RT)^{1/2}} \quad (11)$$

where $\overline{\Delta G}_A^\circ$ is the partial molar standard free energy of vaporization of A in the equilibrium reaction and also the partial molar free energy of activation of A to the transition state for vaporization; $\overline{\Delta G}_B^*$ is the partial molar free energy of activation for the retarded process that involves dissociation of B molecules from catalytic sites or particles. With the standard pressures chosen as 1 atm

$$J_A^m J_B^n = (2\pi RT)^{-(m+n)/2} (M_A)^{-m/2} (M_B)^{-n/2} \times \exp(-\Delta G^*/RT) \quad (12)$$

where $\Delta G^* = m\overline{\Delta G}_A^\circ + n\overline{\Delta G}_B^*$. Note that eq 12 is identical with eq 5 which describes unretarded dissociative vaporization except that $\Delta G^* > \Delta G_v^\circ = \Delta H_v^\circ - T\Delta S_v^\circ$.

Discussion

As pointed out in earlier papers, plots of the logarithm of pressures in free surface vaporization against the reciprocal of the temperature provide useful tests of the nature of the probable rate-limiting step.^{3,6} Three of the conclusions of the earlier papers are the following. (1) When the apparent enthalpy of activation for the reaction, which can be calculated from the slope of the plot, is smaller than the enthalpy of the equilibrium reaction, the rate-limiting step must be a surface step rather than desorption. (2) The apparent activation enthalpy should be the same to within expected experimental error as the enthalpy of the equilibrium reaction, if the free angle ratio theory, which has been used to explain retarded vaporization for polar molecular substances,^{12,22} is applicable. (3) Non-linearity in the plot is evidence that two successive steps of different activation enthalpies have comparable rates in the range of study.¹⁷

It was argued in previous papers that when the Langmuir equation or its generalization for dissociative vaporization is used for a substance with retarded vaporization to calculate the apparent entropy of activation and that entropy is found to be nearly identical with the entropy of the corresponding equilibrium vaporization reaction, the near identity constitutes strong, but not conclusive, evidence that the rate-limiting process is either desorption of vapor in excited states or desorption of vapor molecules in a process that leaves excited surface sites or surface particles behind.^{3,6} We wish to discuss here in more detail and on the grounds of the analysis made in the previous section, the vaporization of such substances.

We can conveniently discuss in terms of eq 9 the range of possible apparent enthalpies and entropies of activation for vaporization when its rate is limited by dissociation from catalytic sites or particles, since the generalization for congruent dissociative vaporization follows directly.

The entropy contributions to $\Delta G_a^* + \Delta G_r^*$ of eq 5 or 9 are ΔS_a^* , the entropy of formation of a two dimensional gas transition state, ΔS_s the entropy of formation of the activated site or surface particle, and ΔS_e , which would represent an extra thermal entropy of excitation if not all collisions between the two dimensional gas molecules and catalytic sites or particles are reactive.

The entropy of formation of a two-dimensional gas from a bulk condensed phase should be less than for formation of the corresponding three-dimensional gas by the difference between the entropy contribution of one translational degree of freedom and the low-frequency vibrational entropy that acts on the two-dimensional gas normal to the surface. For a gas molecule of molecular weight 100 at 1000°K, the difference between ΔS_d^* and ΔS_v° the entropy of vaporization lies between -16 and 0 cal mol⁻¹ deg⁻¹. The molar entropy of formation of surfaces for metals can be calculated from the temperature dependence of their surface tensions to range from 1 to 6 cal (mol of surface atoms)⁻¹ deg⁻¹. Entropies of formation of special surface sites such as kinks in ledges must be more positive than the average for surface formation, and the entropies associated with extrathermal excitations for reactive collisions are also positive.

A range of apparent activation entropies from perhaps 15 cal mol⁻¹ deg⁻¹ less than the entropy of the equilibrium reaction to perhaps 6 cal mol⁻¹ deg⁻¹ more could be consistent with a catalyzed vaporization process of the kind considered in this paper.

But the apparent activation free energy for any retarded process must exceed the standard free energy of the equilibrium reaction. Consequently, when apparent activation entropies for vaporization are equal to or greater than the entropies of the equilibrium reaction, the apparent activation enthalpies for retarded vaporization must be greater than the enthalpies of the equilibrium reactions. This means that measurement of vaporization fluxes and of their temperature dependence do not yield sufficient evidence to distinguish vaporization reaction which yield vapor species in activated states from reactions which are retarded by catalyzed reactions in the self-adsorption layer.

Fortunately, the properties of the vapor molecules that leave the surface can be studied to further delineate the probable rate-limiting step. The saddle point potential energy for the desorption step must coincide with the energy of the molecules that escape from the surface so that those molecules must be the transition state particles for the desorption step of the vaporization process whether or not the overall reaction rate is limited by desorption.

Unless high energy encounters with catalytic sites or particles is rate limiting for condensation, the assumed reversibility of paths makes it unlikely that molecules would vaporize with significant excess kinetic energy. Consequently, an experimental observation of excess kinetic energy or of a nonequilibrium angular distribution of spacial trajectories of molecules that leave the surface would constitute evidence for a catalyzed surface step.

However, the observation of an equilibrium distribution of energies does not prove that a catalyzed surface step can be ruled out as rate limiting. Excess kinetic energy may be lost to the surface after a molecule separates from a catalytic site. Brumbach and Rosenblatt²³ have used a Lennard-Jones 9-3 potential to calculate for As₄ the extent to which gaseous and evaporating molecules should equilibrate with the surface for various assumed potential

energy wells. Our eq 9, when only a fraction of gas molecule encounters with catalytic sites given by $\exp(-\Delta G_e^*/RT) < 1$ results in equilibration, corresponds with their assumed conditions. They conclude that some detectable fraction of evaporating As₄ molecules may leave the surface thermally excited, but that a significant fraction would attain equilibrium.

Some vaporization processes may be retarded because the formation of vapor molecules in their ground electronic states from atoms adsorbed on the condensed phase surface requires forbidden spectroscopic transitions, such as many singlet to triplet transitions.²⁴ The products of free surface vaporization may then include a lower than equilibrium concentration of molecules in ground electronic states. Whether or not a nonequilibrium concentration of ground-state molecules is formed in free surface vaporization should be determinable by spectroscopic means.

Conclusions

It has been shown that the prediction of Langmuir that molecules should leave a surface in free surface vaporization with an equilibrium distribution of kinetic and internal energy states has been confirmed experimentally for a number of substances, including two that undergo congruent dissociative vaporization. To reconcile transition state theory to the experimental observations for these unretarded vaporization reactions requires that the kinetic term of the rate expression be derived from the average velocity of the equilibrium gas molecule normal to the surface. And to predict rates of unretarded dissociative vaporization from transition state theory requires that the transition state particle be identified, not as clusters of a single kind of particle, but as the separated molecular products of the equilibrium vaporization reaction.

Those substances that experience a potential energy barrier to complete equilibration when their vapor molecules strike their surfaces need not vaporize to molecules that are equilibrated with respect to translational and internal excitations. Experimental data for two such substances, however, show that their translational states are equilibrated.

These observations make it appear probable that particles of the self-adsorption layer of substances which undergo retarded vaporization often almost fully equilibrate with respect to vibrational, rotational, and translational degrees of freedom, though they may not be at equilibrium with the bulk condensed phase with respect to forbidden electronic transitions or with respect to bond-breaking and rearrangement processes. An expression for catalyzed vaporization that assumes the rate of arrival at catalytic sites to depend upon gas-like translation in the self-adsorption layer parallel to the surface was derived to accord with these inferences. The model is generally consistent with the extensive experimental observations and the theoretical conclusions formed by Rosenblatt and coworkers as to the critical rate of sites associated with ledges in arsenic vaporization.^{25,26}

It should be emphasized that we do not consider that the postulates that we have described need be appropriate to all retarded vaporization reactions. In particular, for vaporization that occurs with an activation energy much lower than the energy of the equilibrium reaction, such as ammonium chloride dissociative vaporization,²⁷⁻²⁹ rate equations that employ a frequency factor such as that used in absolute reaction rate theory may well be superi-

or. But the kinetic factor for the desorption step, whether or not that step is maintained at equilibrium with the bulk condensed phase, is better derived from the average translational velocities of the equilibrium products of the desorption process. Fortunately, as pointed out above, this assumption is subject to direct experimental test.

Acknowledgments. The authors are indebted to Alfred Büchler and David J. Meschi for their helpful advice and comments throughout the course of this work.

This work was supported by the Metallurgy and Materials Branch of the Division of Research of the United States Atomic Energy Commission. Part of the work was completed while Alan W. Searcy was supported by a Miller Research Professorship. Dario Beruto was supported by a Nato fellowship and by a Fulbright-Hays travel fellowship.

References and Notes

- (1) I. Langmuir, *Phys. Rev.*, **8**, 149 (1916).
- (2) R. C. Paule and J. L. Margrave in "The Characterization of High Temperature Vapors," J. L. Margrave, Ed., Wiley, New York, N. Y., 1967, Chapter 6.
- (3) A. W. Searcy in "Chemical and Mechanical Behavior of Inorganic Materials," A. W. Searcy, D. V. Ragone, and U. Colombo, Ed., Wiley, New York, N. Y., 1970, Chapter 6.
- (4) R. C. Tolman, "The Principles of Statistical Mechanics," Oxford University Press, Oxford, 1938.
- (5) G. M. Rosenblatt, P. K. Lee, and M. B. Dowell, *J. Chem. Phys.*, **45**, 3454 (1966).
- (6) R. J. Galluzzo and A. W. Searcy, *High Temp. Sci.*, **3**, 491 (1971).
- (7) K. J. Laidler, "Chemical Kinetics," 2nd ed, McGraw-Hill, New York, N. Y., 1965, p 79.
- (8) S. W. Benson, "The Foundation of Chemical Kinetics," McGraw-Hill, New York, N. Y., 1960, p 247.
- (9) S. Glasstone, K. J. Laidler, and H. Eyring, "The Theory of Rate Processes," McGraw-Hill, New York, N. Y., 1941.
- (10) A. W. Searcy, A. Buchler, and D. Beruto, *High Temp. Sci.*, **6**, 64 (1974).
- (11) E. M. Mortensen and H. Eyring, *J. Phys. Chem.*, **64**, 846 (1960).
- (12) H. Eyring, F. M. Wanlass, and E. M. Eyring in Condensation and Evaporation of Solids," E. Rutner, P. Goldfinger, and J. P. Hirth, Ed., Gordon and Breach, New York, N. Y., 1964, pp 4-28.
- (13) J. L. Margrave, ref 2, p 139.
- (14) B. A. H. Blank and A. W. Searcy, Inorganic Materials Research Division Annual Report, 1967, No. 18043, 159 (1968).
- (15) L. Seacrist and Z. A. Munir, *High Temp. Sci.*, **3**, 340 (1971).
- (16) O. Knacke and I. N. Stranski, *Progr. Metal Phys.*, **6**, 181 (1956).
- (17) D. J. Meschi and A. W. Searcy, *High Temp. Sci.*, in press.
- (18) J. H. de Boer, "The Dynamical Character of Adsorption," Oxford University Press, London, 1958, p 30.
- (19) R. W. Mar and A. W. Searcy, *J. Chem. Phys.*, **49**, 182 (1968).
- (20) M. Balooch, A. E. Dabiri, and R. E. Stickney, *Surface Sci.*, **30**, 483 (1972).
- (21) D. J. Meschi and A. W. Searcy, work in progress.
- (22) G. Wyllie, *Proc. Roy. Soc., Ser. A*, **197**, 383 (1949).
- (23) S. B. Brumbach and G. Rosenblatt, *Surface Sci.*, **29**, 555 (1972).
- (24) S. P. McGlynn, T. Azumi, and M. Kinoshita, "Molecular Spectroscopy of the Triplet State," Prentice-Hall, Englewood Cliffs, N. J., 1969.
- (25) G. M. Rosenblatt, M. B. Dowell, P. K. Lee, and H. R. O'Neal in "The Structure and Chemistry of Solid Surfaces," G. A. Somorjai, Ed., Wiley, New York, N. Y., 1969, p 38.
- (26) G. M. Rosenblatt in "Heterogeneous Kinetics at Elevated Temperatures," G. R. Belton and W. R. Worrell, Ed., Plenum Press, New York, N. Y., 1970, p 209.
- (27) H. Spingler, *Z. Phys. Chem. (Frankfurt am Main)*, **B52**, 90 (1942).
- (28) R. D. Schultz and A. O. Bekker, *J. Phys. Chem.*, **60**, 1095 (1956).
- (29) R. F. Chaiken, D. J. Sibett, J. E. Sutherland, D. K. Van de Mark, and A. Wheeler, *J. Chem. Phys.*, **37**, 2311 (1962).

Raman Spectra and Structure of Water from -10 to 90°

James R. Scherer,* Man K. Go, and Saima Kint

Western Regional Research Laboratory, Agricultural Research Service, U. S. Department of Agriculture, Berkeley, California 94710 (Received December 29, 1973)

Publication costs assisted by the U. S. Department of Agriculture

Raman spectra were obtained for liquid H_2O and D_2O from -10 to 90° and for HOD from 10 to 90° . Quantitative intensities were measured for H_2O and D_2O and the intensity sum rule is found to hold to within 10%. The difference between the depolarization ratios of the OH and OD stretches of HOD is explained on the basis of approximate normal coordinates and bond polarizability theory. The occurrence of apparent isosbestic points in observed Raman data that has not been decomposed into its isotropic and anisotropic parts is shown to be fortuitous. The isotropic and anisotropic spectra of the OH and OD stretching regions of H_2O and D_2O are interpreted in terms of four bands. These bands are attributed to the symmetric and antisymmetric OH and OD stretching vibrations of a symmetrically hydrogen-bonded complex and the stretching vibrations of an asymmetrically hydrogen-bonded complex. Fermi resonance is shown to be responsible for the dip in the spectrum at the position of the first overtone of the HOH and DOD bending vibrations. The band-fitting procedure is constrained by assumptions involving half-widths, band centers, and intensity arguments. The resulting analysis associates the intensity increase with decreasing temperature at 3430 cm^{-1} (2530 cm^{-1} for D_2O) in the anisotropic spectrum with the antisymmetric OH stretching vibrations of the symmetric hydrogen-bonded complex.

I. Introduction

We may sort previous models for the structure of liquid water^{1,2} into two categories: one invokes a mixture of dis-

crete species and the other a continuum of geometric (and energetic) states. In an extreme mixture model,³ water structures are assumed to have nine configurations that

differ in the number and position of their hydrogen bonds. Previous workers have generally assumed that it is possible to distinguish whether a water molecule is or is not "hydrogen bonded." In fact, many authors^{4,5} have assigned to the equilibrium $\text{O-H}\cdots\text{O} \rightleftharpoons \text{O-H} + \text{O}$ an enthalpy of about 3 kcal/mol. In a continuum model, we assume that all water molecules are hydrogen bonded, but strengths of the bonds vary greatly and depend on the degree of distortion or bending of the $\text{O-H}\cdots\text{O}$ unit. In principle, the mixture model is simpler. However, there is no convincing experimental evidence for a clear distinction between "hydrogen bonded" and "non-hydrogen-bonded" species. Falk and Ford⁶ call attention to this confusion in a table of "per cent broken hydrogen bonds" in water, according to various authors and methods of detection. The values in this table range from 0.1 to 71.5%. Clearly, the concept of a broken hydrogen bond in liquid water is easier to postulate than evaluate.

In a previous paper,⁷ we developed a simple model that accounts for the OH stretching region of the Raman spectrum of water in dimethyl sulfoxide (DMSO) over a wide concentration range. We showed that the infrared band attributed to the antisymmetric OH stretching vibration of the $2\text{DMSO}:\text{H}_2\text{O}$ complex does not appear in the isotropic Raman spectrum. Therefore, we concluded that the two hydrogen bonds in the 2:1 complex must be of equal or very nearly equal strength. Further, we attributed the presence of a weak broad band near 3650 cm^{-1} to a "nearly free" OH stretching vibration of an asymmetrically hydrogen-bonded complex which closely resembles a 1:1 complex. From these observations for the water-DMSO system we postulated the existence of two states for a water molecule in liquid H_2O : one state involves two strong symmetric hydrogen bonds, and the other state one strong and one very weak hydrogen bond. We assumed that the strongly hydrogen bonded OH's of both states have distributions of hydrogen-bond strengths arising principally from hydrogen-bond bending.

We also showed that Fermi resonance of the OH... stretching fundamental of the asymmetric complex and the symmetric OH... stretch of the symmetric complex with the first overtone of the bending vibration gives rise to a significant perturbation in the observed Raman spectrum. Also, gas-phase values of the resonance constant can quantitatively account for the observed band shapes of the water-DMSO spectra. In this paper, we wish to extend our model to account for variations of the observed intensities of the OH and OD stretching regions of pure H_2O , D_2O , and HOD as a function of temperature. We will also discuss some of the physical implications of this model and call attention to limitations that prevent a more exact analysis.

II. Experimental Section

We prepared degassed water samples from triply distilled water and sealed them in Raman capillary cells⁸ of 0.25–0.35-mm i.d. D_2O (99.84%) was obtained from Bio Rad⁹ and used without further purification. The details of the spectrometer system, data acquisition system, and heater/cooler have been given previously.⁷ The spectral resolution used in this work was 5 cm^{-1} in the OH stretching region and 6 cm^{-1} in the OD stretching region. The exciting wavelength was 4880 \AA .

We collected Raman scattering 90° (X) to the incident beam (polarized (Z)). The horizontal (Z) and vertical (Y) components were measured with a polaroid analyzer. The

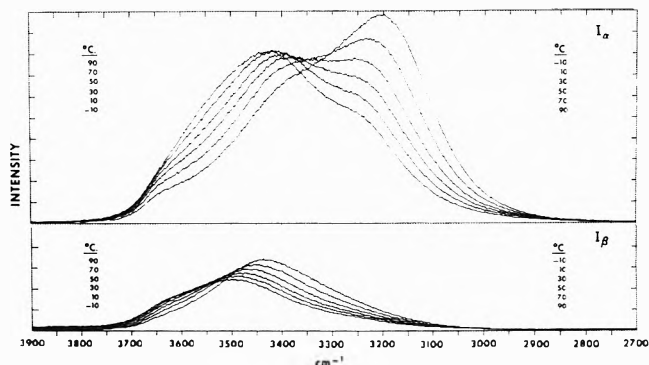


Figure 1. I_α and I_β spectra of H_2O at -10 , 10 , 30 , 50 , 70 , and 90° . Intensities must be multiplied by 0.630 to be compared with the intensities of D_2O in Figure 2.

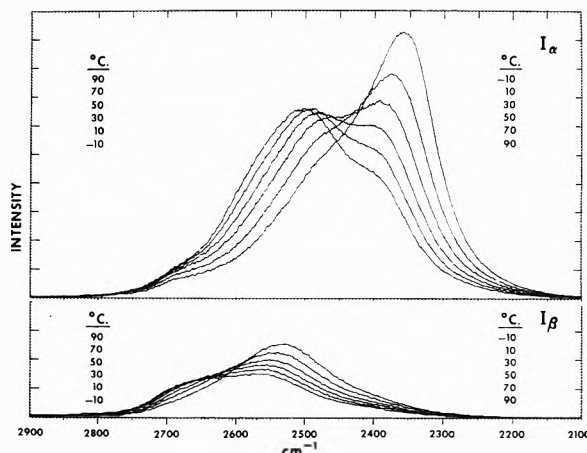


Figure 2. I_α and I_β spectra of D_2O at -10 , 10 , 30 , 50 , 70 , and 90° .

spectra were intensity corrected^{10a} and transformed into isotropic (I_α) and anisotropic (I_β) spectra.^{10b}

$$I_{\text{obsd}}(Y(ZZ)X) = I_\alpha + I_\beta$$

$$I_{\text{obsd}}(Y(ZY)X) = 3I_\beta/4$$

where $I_\alpha \propto 45\bar{\alpha}^2\kappa(\nu)$, $I_\beta \propto 4\bar{\beta}^2\kappa(\nu)$, and $\kappa(\nu) = (\nu_L - \nu)^4/\nu(1 - e^{-h\nu/kT})$. ν_L is the laser frequency, ν is the vibrational frequency, and $\bar{\alpha}$ and $\bar{\beta}$ are the mean polarizability derivative and mean anisotropy derivative, respectively. In Figures 1 and 2, we show I_α and I_β spectra of H_2O and D_2O at -10 , 10 , 30 , 50 , 70 , and 90° , and in Figures 3 and 4, similar data for HOD (5 mol % H_2O in D_2O and 5 mol % D_2O in H_2O) at 10 , 50 , and 90° .

We removed H_2O and D_2O backgrounds in the observed HOD spectra by digital subtraction of I_α and I_β water spectra at corresponding temperatures. All baselines are zero with respect to photomultiplier dark count. No arbitrary baselines have been drawn to make the intensity in the wings of the observed spectra go to zero. To facilitate use of this data, we have prepared digital listings of the intensities in supplementary Tables ST-1 through ST-36. These will appear immediately following this article in the microfilm edition of this volume of the Journal.¹¹

In our first paper,⁷ we pointed out that in considering resonances between transitions within distributions of vibrational modes, we must use the terms $45\bar{\alpha}^2$ and $4\bar{\beta}^2$. Since we consider the breadth of the bands in the water spectrum to arise from different normal coordinate oscillators, we transform the I_α and I_β spectra to $\bar{\alpha}$ and $\bar{\beta}$ spectra by multiplying by the factor $\nu_i(1 - e^{h\nu_i/kT})/(\nu_L - \nu_i)^4$

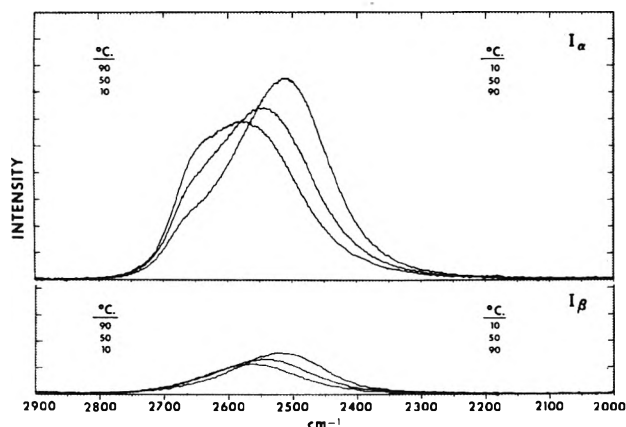


Figure 3. I_α and I_β spectra of the OD stretching region of HOD at 10, 50, and 90°.

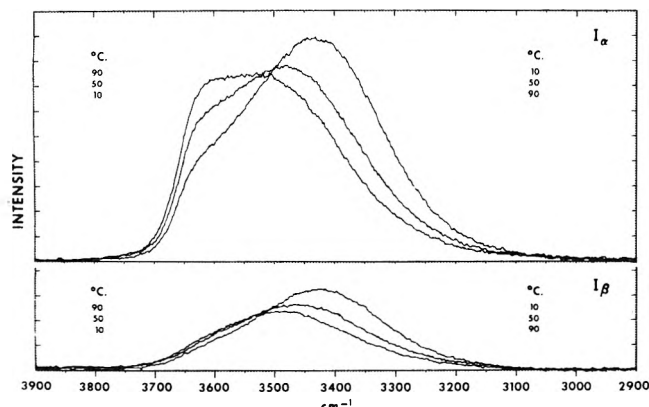


Figure 4. I_α and I_β spectra of the OH stretching region of HOD at 10, 50, and 90°.

at each ν_i of the spectrum. Note that the term ν_i in the numerator arises from the assumption of harmonic oscillator wave functions in evaluating the polarizability derivative expansion in normal coordinates to first order. Consequently, the $\bar{\alpha}$ and $\bar{\beta}$ spectra are in a form suitable for subsequent first-order interpretation.

Isosbestic Points.¹² Walrafen¹³ has interpreted the presence of isosbestic points in his observed mercury-excited Raman data as evidence for discrete molecular species in liquid water. Clearly, the isotropic and anisotropic spectra of H₂O in Figure 1 and D₂O in Figure 2 do not show isosbestic points. The HOD spectra in Figures 3 and 4 show an isosbestic region near 2565 (OD) and 3510 cm⁻¹ (OH) in the isotropic spectrum. But, the corresponding anisotropic spectra show isosbestic regions about 10 cm⁻¹ higher for both the OH and OD data. Walrafen's¹⁴ "quantitative" mercury-excited HOD data, obtained over the temperature range of 32 to 93°, shows an isosbestic point at 2570 cm⁻¹. Lindner's¹⁵ laser-Raman data, obtained over the range 20 to 400°, shows no isosbestic point. However, his OD spectra for 20 and 100° show an intersection near 2560 cm⁻¹. Walrafen¹⁴ compared his data with Lindner's and suggested that intensity errors in the laser-Raman data were responsible for the discrepancy. However, we feel that the differences between the two types of intensity measurement are responsible for the apparent discrepancy. In the case of Walrafen's unpolarized mercury-excited spectra, the intensity should be the same as the total scattered Raman intensity at 90° using unpolarized laser excitation, viz. $45\bar{\alpha}^2 + 13\bar{\beta}^2$. The intensity for analyzed 90° Raman scattering from a polarized source (as defined

earlier) is $45\bar{\alpha}^2 + 4\bar{\beta}^2$. Since the anisotropic spectra have isosbestic regions that fall at slightly different positions than the isotropic spectra, we should not expect the mercury-excited data to agree with the laser-excited data. In Figure SF-1 of the supplementary material we show that $45\bar{\alpha}^2 + 13\bar{\beta}^2$ spectra of H₂O synthesized from the data of Figure 1 (having no isosbestic points) are extremely close to Hg-excited data reported by Walrafen¹³ (showing an isosbestic point). In order to conclude the presence of species, both the I_α and I_β spectra should have exhibited isosbestic points (although not necessarily at the same point). We conclude that the presence of an isosbestic point in Walrafen's H₂O data is due to an unfortunate combination of accidental factors. We shall give an alternative explanation of the observed temperature dependence of the HOD spectra in a later section.

III. The Two Species Model

In this model, we classify hydrogen-bonded water molecules into two categories. We place all those molecules that have strong hydrogen bonding on both their hydrogens, ...HOH..., in one category. The two O-H bonds are assumed to have equal or very nearly equal strengths. In the second category we place all those molecules that have one strong hydrogen bond and one very weak hydrogen bond,^{16,17} ...HOH.... We call a molecule in the first category a "symmetric complex," and, a molecule in the second category an "asymmetric complex." We assume that there is a distribution of hydrogen-bond strengths for the strongly hydrogen-bonded OH... groups of both the symmetric and asymmetric complex. A second narrower distribution is assumed for the very weak hydrogen-bonded OH.... of the asymmetric complex. We expect that bonding of the lone pair electrons in H-O-H affects the strength of the O-H bond and that this contributes to the frequency shift and broadening of the associated OH stretching bands. However, we assume that hydrogen-bond bending,¹⁸ O-H...O is primarily responsible for the breadth of the distribution of strong hydrogen bonds and their associated OH stretching bands.

The symmetric complex has two OH stretching bands. ν_d^s is a symmetric OH... stretch which appears in both the isotropic and anisotropic spectrum. ν_d^a is an antisymmetric OH... stretch appearing only in the anisotropic spectrum. The asymmetric complex has a bonded OH... stretch, ν_b , and a weakly bonded OH.... stretch, ν_w . Both vibrations appear in their isotropic and anisotropic spectra.

As in our previous work,⁷ we assume that the spectral bands are symmetric and that they can be approximated with a four parameter product function. Our assumption of symmetrical band shapes is an approximation that seriously undercuts arguments regarding the physical significance of weak bands. For this reason, we have abandoned our earlier position in which we suggested that the presence of a weak band in the high-frequency region might indicate a third type of hydrogen-bonded species. However, we do not rule out the presence of such a species in concentrated salt solutions. Possible band skewing mechanisms will be discussed in the next section.

Fermi resonance between overtones of a distribution of HOH bending vibrations and the levels of a distribution of OH stretching vibrations was described previously.⁷ Values of the Fermi resonance constant, W , of 36 cm⁻¹ for H₂O and 25 cm⁻¹ for D₂O were calculated from the cubic force constant, k_{122} , in normal coordinate space, deter-

TABLE I: Approximate Normal Coordinates for Hydrogen Bonded Water^a

Molecule	Label	ω , cm^{-1}	r_1	r_2	α
.....HOD.....	$\nu_w(\text{OH})$	3845	1.0252	-0.0501	-0.0155
.....HOD...	$\nu_w(\text{OH})$	3845	1.0255	-0.0452	-0.0159
.....HOD.....	$\nu_w(\text{OD})$	2791	0.0464	0.7452	-0.0280
...HOD.....	$\nu_w(\text{OD})$	2791	0.0583	0.7445	-0.0275
...HOD...	$\nu_b(\text{OH})$	3654	1.0250	-0.0518	-0.0100
...HOD.....	$\nu_b(\text{OH})$	3655	1.0245	-0.0589	-0.0095
...HOD...	$\nu_b(\text{OD})$	2652	0.0484	0.7448	-0.0186
.....HOD...	$\nu_b(\text{OD})$	2653	0.0395	0.7453	-0.0191
.....HOH.....	$\nu^a(\text{OH})$	3897	0.7315	-0.7315	
.....HOH.....	$\nu^s(\text{OH})$	3787	0.7195	0.7195	0
...HOH...	$\nu_{i^b}(\text{OH})$	3706	0.7315	-0.7315	
...HOH...	$\nu_{i^s}(\text{OH})$	3597	0.7191	0.7191	0.0122
...HOH.....	$\nu_w(\text{OH})$	3857	-0.2727	0.9935	-0.0019
...HOH.....	$\nu_b(\text{OH})$	3637	0.9889	0.2561	0.0082
.....DOD.....	$\nu^a(\text{OD})$	2855	0.5360	-0.5360	
.....DOD.....	$\nu^s(\text{OD})$	2732	0.5206	0.5206	-0.0700
...DOD...	$\nu_{i^b}(\text{OD})$	2716	0.5360	-0.5360	
...DOD...	$\nu_{i^s}(\text{OD})$	2593	0.5204	0.5204	-0.0628
...DOD.....	$\nu_w(\text{OD})$	2817	-0.2752	0.7024	-0.0303
...DOD.....	$\nu_b(\text{OD})$	2631	0.6945	0.2548	-0.0592

^a $k_r(\text{OH}\cdots) = 8.26 \text{ m dyn}/\text{\AA}$; $k_r(\text{OH}\cdots) = 7.46 \text{ m dyn}/\text{\AA}$; $k_{r\alpha} = 0.221 \text{ m dyn}/\text{rad}$; $k_{rr} = -0.1 \text{ m dyn}/\text{\AA}$; $k_\alpha = 0.695 \text{ m dyn } \text{\AA}/\text{rad}^2$.

mined by Smith and Overend.¹⁹ The normal coordinate for a symmetrically dibonded water molecule is not appreciably different from unbonded (gaseous) water. However, asymmetric hydrogen bonding uncouples the OH oscillators and our previous assumption that the W for this complex should be the same as that for dibonded water is not entirely justified. Although the resonance constant for asymmetrically bonded water should be directly correlated with the degree of uncoupling, we have used a constant value of 25 and 18 cm^{-1} for W of asymmetric H_2O and D_2O in computing the interaction of $2\nu_2$ with the levels of the ν_b distribution. These values were determined by calculating²⁰ the change in k_{122} of the Smith-Overend force field produced by a 12% decrease in the quadratic stretching constant of one OH bond of the H_2O molecule.

In our attempt to unravel the water spectrum, we ran headlong into this question: how much unique information can we obtain from band decompositions? The Raman spectrum of dilute water in DMSO⁷ exhibits three "lumps" (one major and two minor). We were successful with an analysis assuming two bands (one for the weak high-frequency band) and one resonance perturbation. The resonance perturbation introduces two half-width parameters, one overtone distribution band center, and one resonance constant, W , and is similar in information content to the parameters of a band, *viz.* two half-width parameters, one band center, and one peak height. The perturbation parameters essentially determine the "band shape" of the Evans hole.⁷ The pure water spectrum at low temperatures also has three "lumps" (two major and one minor). However, it is impossible to achieve even a fair fit to the observed spectrum with two bands and one resonance. See Figure SF-2 of the supplementary material.

On the basis of our model, the weak band at 3650 cm^{-1} in the H_2O spectrum should be associated with a stronger band, ν_b , somewhere near the bonded decoupled oscillator frequency. However, inclusion of this third band along with the resonance perturbation places us in the awkward position of trying to obtain band parameters for four bands (three bands plus one hole) from a spectrum with only three "lumps." In this case the uniqueness of the re-

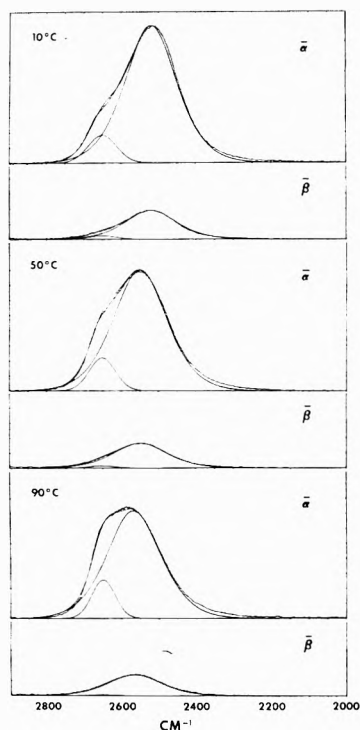
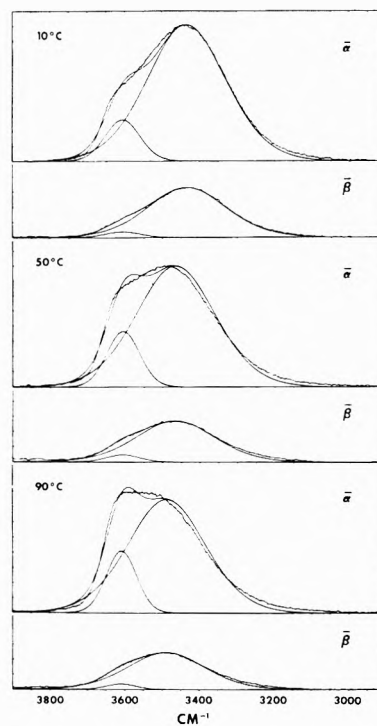
sults may be questioned. In order to alleviate this problem, we have resorted to constraining the fitting procedure. These constraints will be discussed in the following sections.

IV. Application of Model to HOD

Species. According to the foregoing discussion, HOD should have three types of hydrogen bonded structures, *i.e.*, ...HOD..., ...HOD....., andHOD... To gain some insight about the coordinate coupling in these molecules, we obtained approximate normal coordinates using the harmonic force field of Nibler and Pimentel²¹ with modified OH stretching force constants to account for hydrogen bonding. We estimate the O-H stretching constants for OH..... and OH... to be 8.26 and 7.46 $\text{m dyn}/\text{\AA}$, respectively. These estimates are in approximate agreement with more extensive calculations made by Burneau and Corset²² for the symmetric and asymmetric complexes. Table I shows the calculated (harmonic) frequencies for various configurations of hydrogen bonding and the changes in internal coordinates with respect to a unit change in normal coordinate. Note that the normal coordinates and frequencies for ν_b and ν_w for the OH oscillator are independent of the state of bonding of its adjacent OD bond. We conclude that the degree of decoupling produced by isotopic substitution overshadows the differences produced by hydrogen bonding. Therefore, the OH stretching region of the HOD spectrum should contain two bands, *viz.* $\nu_w(\text{OH})$ fromHOD... and a superposition of $\nu_b(\text{OH})$ from ...HOD..... and ...HOD... A similar argument holds for the OD stretching region. Figure 5 and 6 show the results of interactively fitting²³ two bands to the $\bar{\alpha}$ and $\bar{\beta}$ spectra of liquid HOD in the OD and OH stretching regions. The band parameters are given in Table II. We first note that the band associated with ν_b does not have a pure Gaussian shape as suggested by Walfrafen.¹⁷ This difference is most likely derived from the different methods of background subtraction. Our assumption that half-width parameters for corresponding bands in the $\bar{\alpha}$ and $\bar{\beta}$ spectra are the same is fairly good. A major difference between these decompositions and Walfrafen's is that our ν_b band does not markedly increase in

TABLE II: Band Parameters for $\bar{\alpha}$ and $\bar{\beta}$ Spectra of HOD at 10, 50, and 90°

Temp, °C	$\bar{\alpha}$						$\bar{\beta}$		
	ν_0	I_0	L	C	$\Delta\nu_{1/2}$	Area	I_0	Area	Total area
OD Region									
10	2520	999	220	260	161	18.09	210	3.80	21.89
	2650	200	240	100	90	1.92	25	0.24	2.16
50	2549	880	240	260	168	16.58	180	3.39	19.97
	2650	240	240	90	82	2.11	17	0.15	2.26
90	2568	790	240	260	168	14.89	152	2.86	17.75
	2650	280	240	80	74	2.22	8	0.06	2.28
OH Region									
10	3435	999	440	316	246	26.76	360	9.64	36.4
	3606	300	240	128	109	3.52	40	0.47	3.99
50	3466	880	440	316	246	23.57	299	8.00	31.57
	3606	400	240	118	103	4.41	50	0.55	4.96
90	3489	820	440	316	246	21.96	270	7.23	29.19
	3610	450	240	108	96	4.62	40	0.41	5.03

Figure 5. Two-band decompositions of the OD $\bar{\alpha}$ and $\bar{\beta}$ spectra of HOD at 10, 50, and 90°.Figure 6. Two-band decompositions of the OH $\bar{\alpha}$ and $\bar{\beta}$ spectra of HOD at 10, 50, and 90°.

intensity with increasing temperature. Instead, the intensity increase in this region results from a shift of the ν_b band to higher frequencies. The temperature dependence of the ν_b bands is shown in Figure SF-3.¹¹

Band Shapes. Note in Figures 5 and 6 that the observed band shapes are not fit well with two symmetric bands. In general, we could improve our fitting by raising the intensity below the band center and decreasing the intensity above the band center. Eisenberg and Kauzmann¹ have reasoned that the distribution of hydrogen bond strengths cannot be symmetric because intermolecular repulsion would reduce the number of hydrogen bonded species at short O...O distances. We expect the stretching frequencies for OH bonds involved in weak hydrogen bonding to be crowded together in the high-frequency region with their values approaching gas-phase limits. The stretching frequencies for bonds involved in strong hydrogen bonding extend over wider frequency intervals at lower frequen-

cies. This effect can lead to a sharp band edge at the high-frequency limit.

Lindner¹⁵ has obtained Raman spectra of the OD stretch of HOD (10 mol % D₂O in H₂O) from 25 to 400° at constant density. His data show a threefold decrease in the overall intensity of the OD stretching band when the temperature is increased from 25 to 400°. The corresponding shift in the band maximum is from 2520 to 2640 cm⁻¹. Frank²⁴ suggests that the high-frequency band increases its intensity in these spectra. However, as we have seen, it is possible to interpret the increasing intensity in terms of a shift of ν_b to higher frequencies. We suggest that the distinction between ...HOD... and ...HOD... at high temperatures is meaningless because of the severe distortion and weakening of hydrogen bonds. Consequently, the bands from ν_w and ν_b should merge. The sharpening of ν_b and overall intensity reduction suggests that $\delta\alpha/\delta Q$ decreases with decreasing hydrogen bond strength.

In Figure SF-4 of the supplementary material we show that the position of ν_{\max} can be shifted to lower frequencies by such a dependence of intensity with frequency (hydrogen bonding). Further, we show that skew band shapes are to be expected from this effect. We conclude that it is likely that the bands produced by a symmetric distribution of oscillators are slightly skewed because of a dependence of $\delta\alpha/\delta Q$ on hydrogen bond strength. However, the nature of this dependence has not yet been explored sufficiently to include a skewing parameter in our analysis. Further, the possibility that the original distribution itself may not be symmetric is an additional unknown factor that complicates any attempt of a quantitative band decomposition analysis. For these reasons, we decided to carry out our analysis using symmetric band shapes, making allowance for the imperfect fits to the observed data.

Depolarization Ratios. Weston²⁵ has reported depolarization ratios for the OD and OH stretching bands of HOD as being 0.13 and 0.20, respectively. Cunningham²⁶ has shown the variation of the depolarization ratio of the OD stretching band with frequency. Figure SF-5¹¹ shows depolarization ratios calculated from the data of Figures 3 and 4. The curves for the OD stretch agree well with those obtained by Cunningham. The small variation of the depolarization ratio through the major portion of the OH and OD stretching bands agrees with the expectations of our model. The difference between the depolarization ratios in the ν_b part of the spectrum is easily understood in terms of the zeroth order normal coordinates of Table I. ν_b for an OH oscillator appears to be more antisymmetric than for an OD oscillator, and the depolarization ratio is correspondingly higher. From simple bond polarizability theory,²⁷ the depolarization ratio, ρ_k , for the k th normal coordinate is

$$\rho_k = \frac{(3/4)[(1 + 3 \cos^2 \theta) + 3R_k^2 \sin^2 \theta]S}{45 + [(1 + 3 \cos^2 \theta) + 3R_k^2 \sin^2 \theta]S}$$

$$R_k = (L_{1k} - L_{2k}) / (L_{1k} + L_{2k})$$

$$S = \bar{\beta}_b'^2 / \bar{\alpha}_b'^2$$

where θ is the HOH angle, R_k is the ratio of the antisymmetric to symmetric terms in the k th eigenvector in symmetry coordinates, L_{ik} is the variation of bond stretch i with a unit change in normal coordinate, Q_k . $\bar{\beta}_b'$ and $\bar{\alpha}_b'$ are the anisotropy and mean polarizability derivatives for a single OH bond. In Figure 7, we show a plot of ρ_k as a function of R_k^2 with $S = 3.17$ ($\bar{\beta}_b' / \bar{\alpha}_b' = 1.78$), and we see that the observed depolarization ratios are in fair agreement with this simple theory. Further, the ratio of $\bar{\beta}_b' / \bar{\alpha}_b'$ is of the correct general magnitude when compared with the same ratio for the CH bond (2.2) or the CC single bond (1.93) of ethane.²⁸ The simple theory predicts a ρ_k of 0.06 for a symmetrical dibonded ...HOH... molecule. However, our present results and those obtained previously⁷ indicate a lower value of 0.03 to 0.04. We may derive an expression for ρ_k without recourse to bond polarizabilities. Again consider a symmetrically dibonded molecule and let $\bar{\beta}_s'$ and $\bar{\alpha}_s'$ be the anisotropy and mean polarizability of the symmetric stretch. Let $\bar{\beta}_a'$ be the anisotropy of the antisymmetric stretch ($\bar{\alpha}_a' = 0$). It is easily derived that

$$\rho_k = \frac{3(A + BR_k^2)}{45 + 4(A + BR_k^2)}$$

where $A = \bar{\beta}_s'^2 / \bar{\alpha}_s'^2$ and $B = \bar{\beta}_a'^2 / \bar{\alpha}_s'^2$. We find A to be 0.55

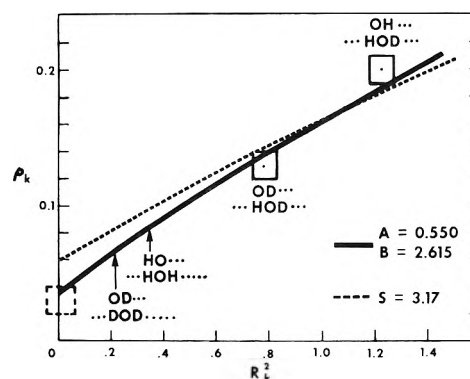


Figure 7. Dependence of depolarization ratios of water on normal coordinate. R_k is defined in the text. Broken line represents one parameter bond polarizability model; solid line, two parameter symmetry polarizability model.

when ρ_k is estimated to be 0.035 (ν_a^s). An average value for B of 2.615 was chosen to minimize the differences between observed and calculated ρ_k for OH... and OD... ν_b stretching bands of HOD. The solid line in Figure 7 shows the dependence of ρ_k on R_k for this two parameter model.

In the high-frequency region of the HOD spectrum, the depolarization ratio has been observed to dip lower²⁷ than in the ν_b region, *viz.* Figure SF-5.¹¹ The zeroth order normal coordinates for ν_w lead us to predict that $\nu_w(\text{OH})$ should have a depolarization ratio that is 0.003 lower than $\nu_b(\text{OH})$. Similarly, ρ for $\nu_w(\text{OD})$ is predicted to be 0.005 lower than $\nu_b(\text{OD})$. While these shifts are in the correct direction, the observed lowerings of 0.08 for OH and 0.04 for OD are too large to be explained by our approximate normal coordinates.

Intensities. Crawford²⁹ has shown that the sum $\Sigma \bar{\alpha}(\nu_i) / \nu_i^2$ or $\Sigma I \alpha(\nu_i - \nu_i^s) / \nu_i$ is invariant on isotopic substitution. Since the intensities of the bands in Figures 1-4 are relative within each figure, the ratios of the intensity sum invariants (ISI) between two isotopic species should be a constant factor at all temperatures. The bending mode, neglected in these sums, has negligible intensity. In Table ST-37,¹¹ we list the ISI's at various temperatures for H₂O, D₂O, and HOD. In Table ST-38, we list the ratios of the invariants at the same temperatures. We find that the ratios involving $\bar{\alpha}$ are constant at all temperatures. The ratios involving $\bar{\beta}$ appear to be temperature dependent. A test of the application of the intensity sum rule will be discussed in the next section.

V. Application of Model to H₂O and D₂O

Intensities. Weston²⁵ reported that the intensity sum invariant ($\Sigma I_i / \nu_i$) for D₂O is 35% greater than for H₂O. In order to check this result, we constructed a special capillary cell that can be filled with different liquids while the cell is in position in the spectrometer. The details of this cell will be reported elsewhere. Figure 8 shows the isotropic and anisotropic spectra of H₂O and D₂O from 40 to 4000 cm^{-1} obtained with this cell under the same conditions of laser power (20 mW at 5682 Å), spectral slit width (5-7 cm^{-1}), and excitation geometry. In Table III, we list the ISI's obtained from these spectra. Note that, contrary to Weston's results, the ISI for H₂O is 10% greater than the ISI for D₂O. These results were found to be consistent to within 0.5% for two separate measurements involving resetting the cell geometry and refilling the cell. We repeated the experiment with 4880-Å excitation and found agreement with the results in Table V to within 1%. We

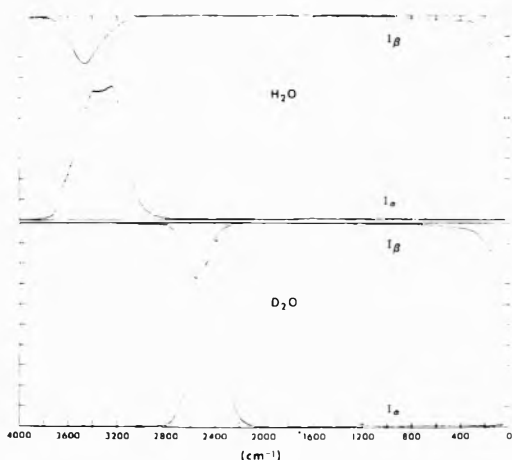


Figure 8. I_α and I_β (reversed) spectra of H_2O and D_2O at 23° under the same experimental conditions of excitation and light collection. The intensities are directly comparable.

TABLE III: Relative Intensity Sum Invariants for H_2O and D_2O (from Figure 8)

		Stretching	Bending	Complete spectrum
H_2O		2600–4000 cm^{-1}	1500–1800 cm^{-1}	40–4000 cm^{-1}
	ISI_α	0.5086	0.0036	0.5374
	ISI_β	0.1329	0.0050	1.247
D_2O		2000–3300 cm^{-1}	1100–1400 cm^{-1}	40–4000 cm^{-1}
	ISI_α	0.4530	0.0058	0.4836
	ISI_β	0.1297	0.0046	1.146

conclude that the intensity sum rule is approximately obeyed by liquid water and that the observed 10% deviation is not an experimental artifact. The ISI's in Table III allow us to calculate the intensity scale factor between the spectra in Figures 1 and 2. We find that the H_2O intensities in Figure 1 must be multiplied by 0.630 to be compared with the D_2O intensities in Figure 2. On the same intensity scale (Figure 8), we find that $I_\alpha(\text{H}_2\text{O at } 3240 \text{ cm}^{-1}) = 0.710 I_\alpha(\text{D}_2\text{O at } 2390 \text{ cm}^{-1})$ at 23° .

Species. According to our model, liquid water should have two types of species: symmetrically hydrogen-bonded water and asymmetrically hydrogen-bonded water. In the spirit as previously done for HOD, approximate normal coordinates for $\cdots\text{HOH}\cdots$, $\cdots\text{DOD}\cdots$, $\cdots\text{HOH}\cdots$, $\cdots\text{DOD}\cdots$, $\cdots\text{HOH}\cdots$, and $\cdots\text{DOD}\cdots$ are given⁹ in Table I. Note that the normal coordinates for $\cdots\text{HOH}\cdots$ and $\cdots\text{DOD}\cdots$ are nearly identical with those for $\cdots\text{HOH}\cdots$ and $\cdots\text{DOD}\cdots$. We feel that this agreement and our previous experience with water bound to DMSO justifies fixing the Fermi resonance constant for symmetrically hydrogen-bonded H_2O and D_2O at the Smith–Overend values of 36 and 25 cm^{-1} , respectively.

The normal coordinate for ν_b of asymmetrically hydrogen-bonded water depends on the degree of asymmetry. For the hypothetical case assumed in Table I, we see that the ν_b normal coordinate is more symmetric than ν_b of the symmetric or asymmetric hydrogen-bonded HOD molecule. The frequency for ν_b of $\cdots\text{HOH}\cdots$ is correspondingly lower than ν_b of HOD and ν_w of $\cdots\text{HOH}\cdots$ is higher than ν_w of HOD. As the strength of hydrogen-bonding increases (lower temperatures), we expect ν_b of $\cdots\text{HOH}\cdots$ to move closer to ν_b of HOD. Conversely, as the strength of hydrogen-bonding decreases (higher temperatures), we expect ν_b to move lower than ν_b of HOD and gradually approach ν^8 of $\cdots\text{HOH}\cdots$. These arguments are nicely il-

lustrated in Figure 2 of ref 22. On the basis of these normal coordinates and the graph of depolarization ratio ν_s . R_k in Figure 7, we estimate the dp for ν_b of asymmetric $\cdots\text{HOH}\cdots$ and $\cdots\text{DOD}\cdots$ to be 0.085 and 0.066, respectively.

The Fermi resonance constant, W , for $\cdots\text{HOH}\cdots$ should increase to a limiting value of 36 cm^{-1} for very high values of ν_b and decrease to 13 cm^{-1} (HOD value) for very low values of ν_b . We feel that the correlation between hydrogen bonding and the value of W is not well enough established to approximate the actual frequency dependence. Accordingly, we have fixed the value of W at 25 cm^{-1} for $\cdots\text{HOH}\cdots$ and 18 cm^{-1} for $\cdots\text{DOD}\cdots$ on the basis of Overend's calculations.²⁰

From the normal coordinates in Table I, we may easily calculate that the ratio of the isotropic intensity of ν_w to the isotropic intensity of ν_b for $\cdots\text{HOH}\cdots$ should be about 1:3. One might argue that the ν_w band is too weak to be attributed to the asymmetric complex. However, in view of the possible dependence of intensity on hydrogen-bonding discussed previously, the observed intensity ratio of 1:7.8 may be acceptable.

Constraints. In the following, we indicate the constraints used in fitting the $\bar{\alpha}$ and $\bar{\beta}$ spectra of H_2O and D_2O . As we previously mentioned, constraints are necessary because of the ambiguity of fitting a spectrum ($\bar{\alpha}$) that has three "lumps" with four bands (three fundamental distributions and one hole distribution) whose symmetrical shape is open to serious question. Four of the seven constraints are minor and are listed in the supplementary material.

(1) We assume that the half-width parameters for the ν_b distribution of the asymmetric complex are the same as for those for ν_b of HOD. We allow the height of the ν_b band to vary freely but require that its position be lower or the same as the position of ν_b of HOD at corresponding temperatures.

(2) We assume that the depolarization ratio of the ν_b band is determined by the expected dependence on the normal coordinates shown in Figure 7. After adjusting the height of ν_b in the $\bar{\alpha}$ spectrum, the intensity of ν_b in the $\bar{\beta}$ spectrum is fixed at the value given by the calculated depolarization ratio.

(3) We assume that the species concentration in H_2O are equivalent to those in D_2O at equivalent temperatures. From this we conclude that the ratios of ISI's $(\text{ISI}_\alpha(\nu_b) + \text{ISI}_\alpha(\nu_w))/\text{ISI}_\alpha(\nu_d)^8$ for H_2O should be the same as those for D_2O . Since our assumption of symmetrical band shapes seems to work better for the OD stretching region than for the OH region, we first fit the $\bar{\alpha}$ spectra of D_2O . We then use the above ratios to constrain the H_2O fitting process.

These three conditions impose quite severe constraints in fitting the $\bar{\alpha}$ and $\bar{\beta}$ spectra of H_2O and D_2O .

Results and Discussion

Our band decompositions for the $\bar{\alpha}$ and $\bar{\beta}$ spectra of D_2O and H_2O are presented in Figures 9 and 10. Graphs showing the dependence of the band centers, half-widths, and areas on temperature are shown in Figures SF-6 and SF-7.¹¹ Band parameters are listed for the -10° spectra in Table IV. The intensities and areas for H_2O in Figures 10 and SF7 and Table IV must be multiplied by 0.91 to be compared with the corresponding data for D_2O .

Note that at high temperatures the fits to the $\bar{\alpha}$ spectra of D_2O and H_2O are poorer than at low temperatures.

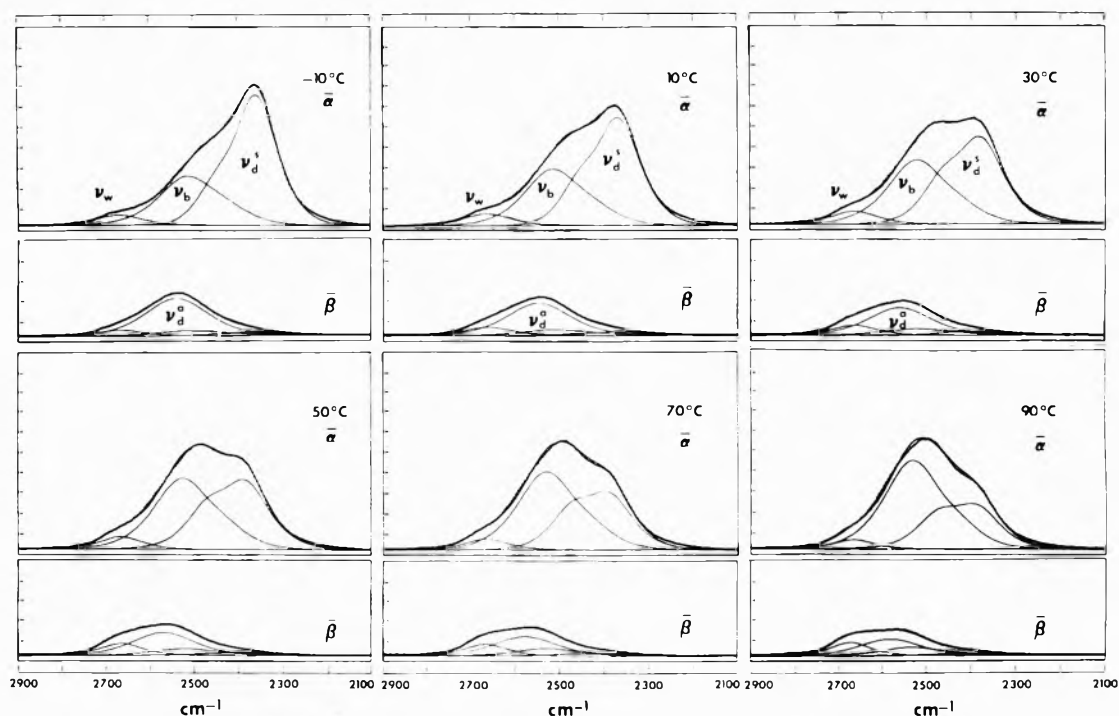


Figure 9. Band decompositions of the $\bar{\alpha}$ and $\bar{\beta}$ spectra of D_2O at -10 , 10 , 30 , 50 , 70 , and 90° .

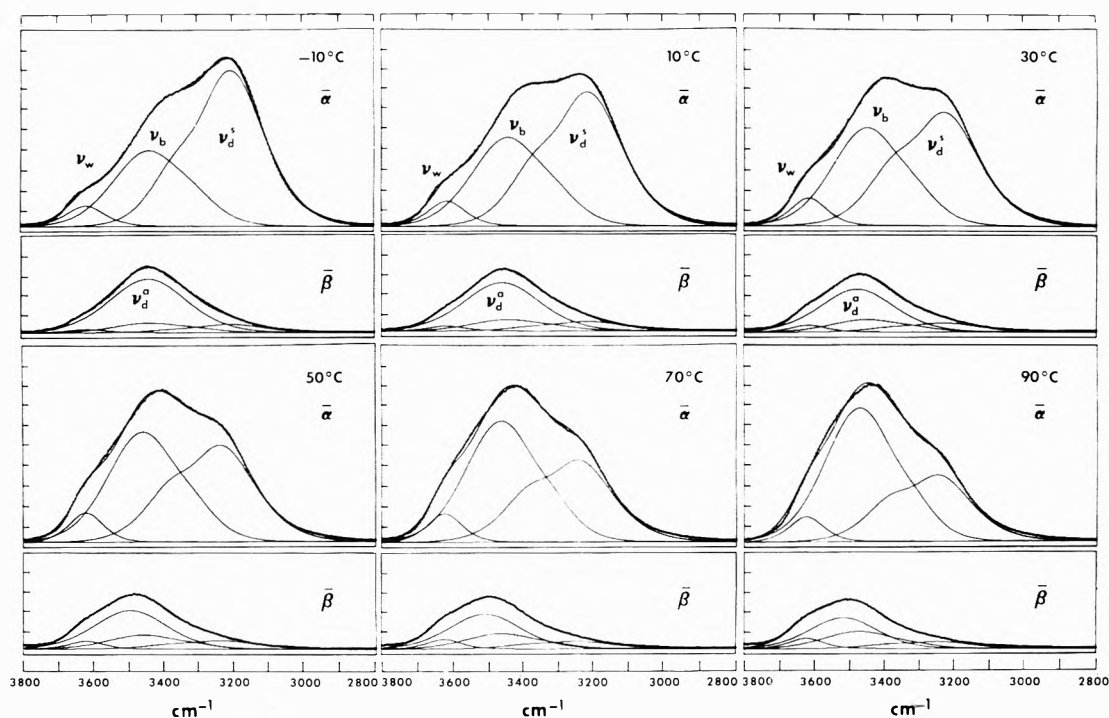


Figure 10. Band decompositions of the $\bar{\alpha}$ and $\bar{\beta}$ spectra of H_2O at -10 , 10 , 30 , 50 , 70 , and 90° .

However, the band profile at high temperatures is determined principally by the ν_b band whose half-width parameters were transferred from the observed HOD spectra. In view of this assumption, we consider the observed fits remarkably good.

We should like to point out an interesting feature about the dependence of the intensities of the I_α and I_β spectra on temperature. In Figures 1 and 2, we see that a decrease in the temperature produces an increase in intensity of I_α at 3200 cm^{-1} (2350 cm^{-1} OD) and a corresponding increase in the intensity of I_β at 3450 cm^{-1} (2530 cm^{-1} OD). Our model correlates these regions with the ν_d^s and ν_d^a

distributions. We should find that the per cent change in the intensities of these distributions are the same. Indeed, we see in Figure SF-7 that the band areas for ν_d^s and ν_d^a are approximately halved over the temperature range of -10 to 90° . We consider this correlation a good test of our interpretation of these two distributions.

It is interesting to make a comparison of the spectra of water and ice at low temperatures. In Figure 11, we show Raman spectra of a single crystal of D_2O ice at -4° . The crystal was oriented with its c axis parallel to the electric vector of the incident beam. The (cc) and (ca') intensities were measured. a' refers to a direction perpendicular to c

TABLE IV: Band Parameters for $\bar{\alpha}$ and $\bar{\beta}$ Spectra of D₂O and H₂O at -10°C

Band	cm ⁻¹	$\bar{\alpha}$						$\bar{\beta}$			ρ	
		I_0	I	G	$\Delta\nu_{1/2}$	Area	ISI $_{\alpha}$	I_0	Area	ISI $_{\beta}$		
D ₂ O	2 ν_2	2440		300	130	116						
	ν_1	2501	284	220	260	161	1.03	1.65	28	0.10	0.16	0.066
	ν_d^a	2373	777	175	195	124	2.17	3.86	22	0.06	0.11	0.020
	ν_w	2668	56	160	220	124	0.16	0.22	31	0.09	0.12	0.27
	ν_d^s	2539		235	260	167			210	0.78	1.22	0.750
H ₂ O	2 ν_2	3340		600	170	161						
	ν_1	3422	440	440	316	246	2.36	2.02	56	0.30	0.26	0.085
	ν_d^s	3225	896	400	340	247	4.88	4.71	46	0.25	0.24	0.036
	ν_w	3615	114	170	236	132	0.34	0.26	19	0.06	0.04	0.11
	ν_d^a	3440		420	350	257			300	1.69	1.43	0.75

^a Intensities areas and ISI's for H₂O must be multiplied by 0.91 to be compared with D₂O.

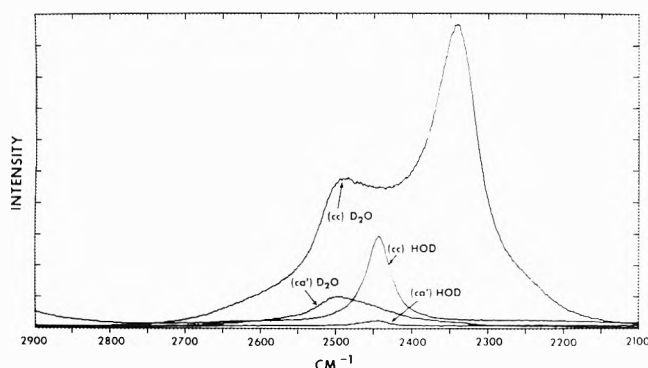


Figure 11. Intensity corrected Raman spectra of single crystal D₂O ice and HOD (5 mol % D₂O in H₂O) ice at -4° . c refers to the c axis and a' refers to a direction perpendicular to c and in the a axis plane.

and in the a plane. We readily see that the positions of the ν_d^a and ν_d^s distributions of D₂O at -10° are near the "antisymmetric stretching" and "symmetric stretching" distributions of ice.

The depolarization ratios for ν_d^s in Table VI appear to be reasonable. Not much significance should be placed in the depolarization ratios of bands as weak as ν_w . However, it seems that the trend is for ρ of ν_w of D₂O to be greater than ρ of ν_w of H₂O. Again, the normal coordinates in Table I show that ν_w for $\cdots\text{DOD}\cdots$ has more antisymmetric character than ν_w of $\cdots\text{HOH}\cdots$. $\nu_w(\text{OD})$ of D₂O is predicted to be 26 cm⁻¹ above $\nu_w(\text{OD})$ of HOD and $\nu_w(\text{OH})$ for H₂O is predicted to be 12 cm⁻¹ above $\nu_w(\text{OH})$ of HOD. The band center for ν_w of D₂O is 18 cm⁻¹ above $\nu_w(\text{OD})$ for HOD, whereas the band center of ν_w of H₂O is only 9 cm⁻¹ above the $\nu_w(\text{OH})$ of HOD. We feel that the results of our band decompositions qualitatively bear out our expectations based on simple normal coordinates.

The reader will have undoubtedly noticed that the frequency for the OH stretch of HOD is not midway between the symmetric ν_d^s and ν_d^a distributions. In the gas phase, the OD stretch of HOD occurs at ~ 2719 cm⁻¹,^{30,31} whereas the antisymmetric and symmetric stretches of D₂O are at 2789 and 2661 cm⁻¹, respectively. It is interesting to draw comparisons with the ice spectrum. Figure 11 shows that the "uncoupled oscillator OD stretch" of HOD ice at -4° is distinctly closer to the "antisymmetric stretching" distribution of D₂O ice than to the "symmetric stretching" distribution. Undoubtedly, intermolecular coupling plays some role in determining the positions of these distributions in ice. Similarly, intermolecular coupling in the liquid state may contribute to moving ν_{OH} of HOD closer to the ν_d^a distribution. Also, one must re-

member that our assumption of symmetric bands may lead to band centers which may be shifted from distribution centers. If we ignore the bands from the asymmetric hydrogen-bonded species, the similarity of water at -10° to ice at -4° is striking.

We feel the weakest point of our analysis is the assumption of symmetrical bands. However, before we can legitimately proceed with an analysis based on skew band shapes, it will be necessary to discover more about the dependence of intensity on hydrogen bonding. In general, our analysis provides an explanation for the behavior of the Raman spectra of water with variations in temperature.

We also conclude that an appreciable number of molecules of room temperature water (or water at -10°) have one hydrogen strongly bonded and the other comparatively free. This conclusion is in agreement with a recently expressed view³² that a significant fraction of the OH functions in the liquid be unbonded. An estimate of this fraction is made in the supplementary material.

Acknowledgment. We wish to thank Dr. R. G. Snyder for the approximate normal coordinates in Table I and for many helpful, stimulating discussions. We are also indebted to Professor John Overend for his anharmonic calculations and the Lawrence Berkeley Laboratory for making available their computer facilities. One of us (M. K. G.) wishes to thank the National Science Foundation for financial assistance through the Presidential Intern Program.

Supplementary Material Available. Additional tables and figures will appear following these pages in the microfilm edition of this volume of the journal. Photocopies of the supplementary material from this paper only or microfiche (105 × 148 mm, 24× reduction, negatives) containing all of the supplementary material for the papers in this issue may be obtained from the Journals Department, American Chemical Society, 1155 16th St., N.W., Washington, D. C. 20036. Remit check or money order for \$11.00 for photocopy or \$2.00 for microfiche, referring to code number JPC-74-1304.

References and Notes

- (1) D. Eisenberg and W. Kauzmann, "The Structure and Properties of Water," Oxford University Press, London, 1969.
- (2) F. Franks, "Water, A Comprehensive Treatise," Vol. 1, Plenum Press, New York, N. Y., 1972.
- (3) E. C. W. Clarke and D. N. Glew, *Can. J. Chem.*, **50**, 1655 (1972).
- (4) G. Salchard, G. M. Kavanaugh, and L. B. Ticknor, *J. Amer. Chem. Soc.*, **74**, 3715 (1952).
- (5) G. E. Walrafen, *J. Chem. Phys.*, **48**, 244 (1968).

- (6) M. Falk and T. A. Ford, *Can. J. Chem.*, **44**, 1699 (1966).
 (7) J. R. Scherer, M. K. Go, and S. Kint, *J. Phys. Chem.*, **77**, 2108 (1973).
 (8) G. F. Bailey, S. Kint, and J. R. Scherer, *Anal. Chem.*, **39**, 1040 (1967).
 (9) Reference to a company and/or product name by the Department is only for purposes of information and does not imply approval or recommendation of the product to the exclusion of others which may also be suitable.
 (10) (a) J. R. Scherer and S. Kint, *Appl. Opt.*, **9**, 1615 (1970); (b) J. R. Scherer, S. Kint, and G. F. Bailey, *J. Mol. Spectrosc.*, **39**, 146 (1971).
 (11) See paragraph at end of text regarding supplementary material.
 (12) These points in Raman spectra should be labeled "isoskedastic points." (G. F. Bailey and R. J. Horvat, *J. Amer. Oil Chem. Soc.*, **49**, 494 (1972).) However, in view of current usage, we will continue to use the prevalent terminology to avoid confusion.
 (13) G. E. Walrafen, *J. Chem. Phys.*, **47**, 114 (1967).
 (14) G. E. Walrafen, Chapter 5 of ref 2.
 (15) H. Lindner, Ph.D. Dissertation, University of Karlsruhe, 1970.
 (16) H. S. Frank, Chapter 14 of ref 2. There is a question whether this is a hydrogen bond or an interstitial OH bond perturbed by its surroundings.
 (17) G. E. Walrafen, *J. Chem. Phys.*, **50**, 567 (1969).
 (18) J. A. Pople, *Proc. Roy. Soc., Ser. A*, **205**, 163 (1951).
 (19) D. F. Smith and J. Overend, *Spectrochim. Acta, Part A*, **28**, 471 (1972).
 (20) J. Overend, private communication.
 (21) J. W. Nibler and G. C. Pimentel, *J. Mol. Spectrosc.*, **26**, 294 (1968).
 (22) A. Burneau and J. Corset, *J. Chim. Phys.*, **1**, 153 (1972).
 (23) A computer program was written for the IBM 1800 that allows calculation of band shapes from input parameters of a product function and graphic comparison on a CRT of the calculated and input bands. Parameters are changed until a best visual fit is obtained. This is not a least-squares fit however it is sufficiently good to make an analysis of the component band shapes.
 (24) E. U. Frank, *Pure Appl. Chem.*, **24**, 13 (1970).
 (25) R. E. Weston, Jr., *Spectrochim. Acta*, **18**, 1257 (1962).
 (26) K. M. Cunningham, Thesis, Yale University, 1972.
 (27) D. A. Long, *Proc. Roy. Soc., Ser. A*, **217**, 203 (1953).
 (28) R. G. Snyder, *Vijnana Parishad Anusandhan Patrika*, **14**, No. 3-4, 139 (1971).
 (29) B. L. Crawford, Jr., *J. Chem. Phys.*, **20**, 977 (1952).
 (30) D. H. Rank, K. D. Larsen, and E. R. Bordner, *J. Chem. Phys.*, **2**, 464 (1934).
 (31) E. F. Barker and W. W. Sleator, *J. Chem. Phys.*, **3**, 660 (1935).
 (32) H. S. Frank, Chapter 14 of ref 2, p 523.
 (33) G. E. Walrafen and L. A. Blatz, *J. Chem. Phys.*, **59**, 2646 (1973).

Nitrogen-14 and Oxygen-17 Hyperfine Interactions in Perturbed Nitroxides

Allan H. Cohen¹ and Brian M. Hoffman*²

Department of Chemistry and the Materials Research Center, Northwestern University, Evanston, Illinois 60201
 (Received February 20, 1974)

Publication costs assisted by the Petroleum Research Fund

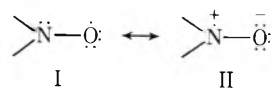
We have measured the isotropic and anisotropic hyperfine splittings for di-*tert*-butyl nitroxide (DTBN) and 2,2,6,6-tetramethylpiperidine *N*-oxyl (TMPN) perturbed by molecular complex formation, by hydrogen bonding, and by solvent effects in aprotic solvents. We use these measurements to obtain the σ - π interaction parameters for a Karplus-Fraenkel equation ($a_i = Q_{ii}^1 \rho_i^\pi + Q_{jj}^1 \rho_j^\pi$) which relates the ¹⁴N and ¹⁷O isotropic hyperfine splittings to the spin density in the nitroxide N-O π -electron system; $Q_{NN}^N = 23.9 \pm 1.0$ G, $Q_{OO}^N = 3.6 \pm 0.4$ G, $Q_{OO}^O = 31.7 \pm 0.7$ G, and $Q_{NN}^O = 4.7 \pm 0.5$ G. In addition for protonated nitroxides $Q_{OO}^N = 13.2 \pm 0.3$ G. The values of Q_{NN}^N for TMPN and DTBN are identical and discussion of the angle dependence of the parameter suggests that the radicals in solution do not differ with respect to planarity at nitrogen.

Introduction

The stability of aliphatic nitroxides, the simplicity of their epr spectra, and, in particular, the sensitivity of their epr spectra to environmental perturbations have made them objects of considerable interest and wide application.³ In this work we have measured the spin-Hamiltonian parameters for di-*tert*-butyl nitroxide (DTBN) and 2,2,6,6-tetramethylpiperidine *N*-oxyl (TMPN) perturbed by molecular complex formation, by hydrogen bonding, and by solvent effects in aprotic solvents. We use these measurements to obtain the σ - π interaction parameters which relate the ¹⁴N and ¹⁷O isotropic hyperfine splittings (hfs), a_N and a_O , to π -electron spin densities, ρ_N^π and ρ_O^π . This approach is possible because linear relations between ¹⁴N and ¹⁷O hfs indicate that environmentally induced changes in the epr spectra result from a redistribution of π -electron spin density within the N-O moiety without significant changes in structure⁴ and be-

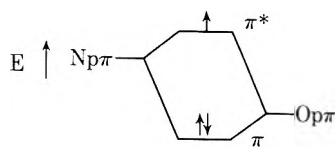
cause the perturbations do not affect the σ - π parameters themselves.

As has been previously discussed,⁵⁻⁷ the various perturbations can be viewed as favoring resonance structure II over structure I



causing a shift of charge density toward oxygen but of spin density toward nitrogen.

A similar result is obtained by consideration of a simple MO scheme in which the three electrons of the nitroxide bond are in orbitals derived from linear combinations of the nitrogen and oxygen $2p\pi$ orbitals. Two of the electrons occupy the bonding π orbital and the unpaired electron is in the antibonding π^* orbital. The effective electronegativity of oxygen is enhanced by σ interaction⁸ with an electron-withdrawing agent, increasing the oxygen character of the π



orbital. Consequently, the nitrogen character of the π^* orbital and thus ρ_N^π is increased.

The redistribution of spin density within the N-O π system changes the nuclear hfs. We obtain σ - π interaction parameters for ^{14}N and ^{17}O from correlations between isotropic hfs and the electron-nuclear dipolar splittings (T_i ; $i = ^{14}\text{N}, ^{17}\text{O}$) as determined from combined measurements of isotropic and anisotropic hfs. This is equivalent to correlating isotropic hfs with π -electron spin densities, since

$$\rho_i^\pi = T_i / (T_i)_0 \quad (1)$$

where for a second row element, $(T_i)_0$ is the electron-nuclear dipolar hfs constant for a single electron in a $2p\pi$ orbital on atom i .⁹ The availability of T_N and T_O for perturbed nitroxides further permits an experimental verification of *ab initio* calculations of $(T_O)_0$ and $(T_N)_0$.

For both ^{17}O and ^{14}N a Karplus-Fraenkel equation¹⁰ of the form

$$a_i = Q_{ii} \rho_i^\pi + Q_{ij} \rho_j^\pi \quad (2)$$

gives a satisfactory representation of the experimental data. Because results from the molecular complexes¹¹ are included, this relationship covers a much wider range of splitting constants than is ordinarily accessible. However, as we discuss, this fit does not necessarily rule out a contribution to a_i proportional to the overlap spin density, ρ_{ON}^π .

These empirical ^{17}O and ^{14}N σ - π polarization parameters are compared to previously reported values, in particular, those recently calculated by Hayat and Silver¹² for the C_2NO nitroxyl fragment. The discussion of Q_{NN}^N leads to the suggestion that, in solution, DTBN and TMPN do not differ in their degree of nonplanarity at nitrogen. We also report the σ - π parameter relating ρ_O^π to the isotropic hfs of a proton bonded to oxygen for a protonated nitroxide (R_2NOH^+).

Experimental Section

DTBN was synthesized by the method of Hoffmann¹³ or purchased from Eastman-Kodak Co. and purified by vacuum distillation. TMPN was synthesized by the method of Briere¹⁴ and purified by vacuum sublimation. TMPN enriched in ^{17}O (TMPN(^{17}O)) was prepared by oxidation of the parent amine with gaseous oxygen of 11 atom % ^{17}O in the presence of α, α' -azobisisobutylnitrile. The resulting reaction mixture was *ca.* $5 \times 10^{-3} M$ in total TMPN(^{17}O) (~11%) and was used without purification. The procedure is similar to that used by Baird for synthesizing di-*sec*-butyl nitroxide enriched in ^{17}O .¹⁵

Samples were prepared in a preparative high vacuum system. In a typical two component sample containing nitroxide plus organic solvent, a measured volume of the nitroxide vapor, in equilibrium with condensed nitroxide at a known temperature, was transferred into a quartz epr sample tube and then the solvent was distilled in, under vacuum, to give a *ca.* $5 \times 10^{-4} M$ solution. Preparation of the nitroxide Lewis acid molecular complexes and protonated nitroxide is described elsewhere.^{6, 11, 16}

Samples with TMPN enriched in ^{17}O were prepared as

above, but with the TMPN(^{17}O) reaction mixture replacing the pure TMPN. The two component samples of TMPN(^{17}O) contained 5% by volume of the reaction mixture.

A gas-phase DTBN sample was prepared by filling an evacuated 11-mm quartz sample tube with DTBN vapor in equilibrium with the liquid at 14° (vapor pressure = 0.17 mm^{17}).

Epr spectra were recorded at X-band on a Varian Associates Model E-4 spectrometer equipped with a Hewlett-Packard Model X532-B wave meter or a Model V-4502 spectrometer equipped with the same wave meter and a V-4532 dual cavity. Magnetic field calibration employed an aqueous solution of peroxyamine disulfonate saturated with potassium carbonate ($a_N = 13.091 \text{ G}$).¹⁸ When hyperfine splittings were obtained on the V-4502 spectrometer, the incremental field control was used as described by Libertini and Griffith.¹⁹ These values were completely consistent with those measured on the E-4. Differential determination of g values on the V-4502 was accomplished using the incremental field control and peroxyamine disulfonate as the reference ($g = 2.00550$).²⁰ The mechanical wave meter is not sufficiently accurate to allow direct g value measurements on the E-4 spectrometer. It was nevertheless possible to perform differential g value measurements by overlapping spectra of sample and peroxyamine reference obtained at the same microwave frequency. This is accomplished by replacing the sample with the reference without changing the Klystron frequency, and retuning the cavity to its original frequency (AFC error voltage = 0) by appropriate placement of the reference. The procedure is equivalent to using a tunable cavity and gives g values reproducible to ± 0.00003 .

All values reported are the average of two or more measurements and are corrected for second-order effects. Unless explicitly indicated in the figures errors are $\pm 0.04 \text{ G}$ for the isotropic coupling constants, $\pm 0.1 \text{ G}$ for the anisotropic coupling constants, and ± 0.00003 for the g values.

Isotropic epr spectra were recorded at room temperature for the stable two component samples. Due to instability at room temperature the TMPN(^{17}O); SnCl_4 and TMPN(^{17}O) H^+ isotropic spectra were recorded at -20° . At higher temperatures these samples decomposed rapidly and at a much lower temperature the ^{17}O lines were too broad to be measured. Spectra recorded at -20° used a conventional variable temperature apparatus employing cold nitrogen gas. Frozen solution spectra were taken with the sample immersed in liquid nitrogen.

Optical spectra were recorded on a Beckman Acta III spectrophotometer.

Results

Epr Spectra. The fluid solution epr spectra of both TMPN and DTBN consist of three main lines due to hfs from ^{14}N . In addition, splitting can usually be observed from ^{13}C , ^{15}N , and, for DTBN under ideal conditions, from ^{17}O ,²¹ all in natural abundance. ^{17}O hfs are easily observed in solution spectra of TMPN(^{17}O), Figure 1. Free radical molecular complexes between nitroxides and Lewis acids (MX_n) may exhibit additional splitting from the metal (M) nucleus.^{6, 11}

In frozen nitroxide solutions the breadth of the epr spectrum is usually dominated by the anisotropic ^{14}N hfs; however, coupling with M of MX_n and with ^{17}O in TMPN(O^{17}) may be important (Figure 2A). To a good ap-

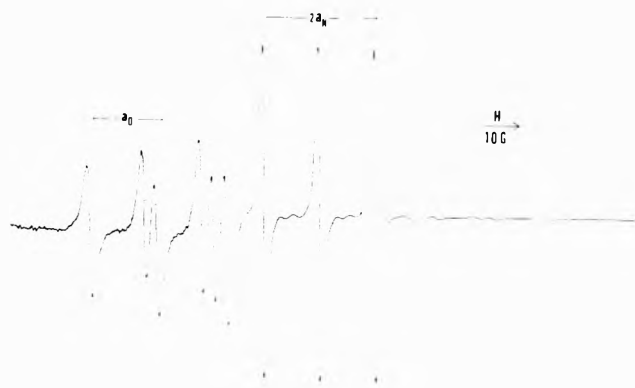


Figure 1. Solution spectrum of TMPN(¹⁷O) in 2,2,6,6-tetramethylpiperidine. The signal amplitude of the low-field portion of the spectrum is 50 times that of the remainder.

proximation, nitroxides have axial hfs and the powder spectra can be interpreted on the basis of the spin Hamiltonian¹⁹

$$\mathcal{H} = \beta S \cdot g \cdot H + \sum_i [A_i S_z I_{iz} + B_i (S_x I_{ix} + S_y I_{iy})] \quad (3)$$

using appropriate spectral features and computer simulations (Figure 2B). The A_i for $i = ^{14}\text{N}$, and ^{17}O when observed (Figure 2A), gives rise to well-resolved splittings and are obtained with good accuracy, but the splittings due to B_i are not resolved. For the molecular complexes where $M = \text{Al}$ or Sn , both A_i and B_i are observed.^{11,22} For the weaker perturbing agents accidental degeneracy of the parallel anisotropic ¹⁷O lines give stronger signals than could be expected from the extent of labeling (Figure 2A). Larger uncertainties in A_0 for some of the more strongly perturbed nitroxides arise where there is no longer such degeneracy. Anisotropic ¹⁷O hfs could not be observed for the SnCl_4 complex because of the presence of the anisotropic ¹¹⁷⁻¹¹⁹Sn splittings in the region where the ¹⁷O lines are expected to appear. The anisotropic ¹⁷O hfs for TMPN(¹⁷O)H⁺ were unobservable in dilute frozen solution, in part because the expected value of A_0 gives no increased sensitivity from degenerate lines; increasing the concentration produces spin exchange and poor spectral resolution.

Signs of Isotropic Hfs. The signs of a_i can be obtained from combined measurements of a_i and A_i . To an excellent first approximation, nonlocal dipolar interactions can be neglected so that the anisotropic hfs determined from powder spectra may be written²³ (however see Appendix A)

$$A_i = a_i + T_i \quad (4)$$

$$B_i = a_i - T_i/2 \quad (5)$$

Since, for both ¹⁷O and ¹⁴N, $|A_i| > |a_i|$, (Figure 2), then T_i and a_i are of the same sign. Since $(T_i)_0$ has the sign of γ_i , the gyromagnetic ratio for nucleus i ,²³ than a_0 and a_N have the signs of γ_0 and γ_N , respectively.

The sign of a_0 as directly determined here for TMPN(¹⁷O) is the same as that determined for a_0 in Fremy's salt by an analysis of line width variations.²⁴ Indeed, although measurement of line width variations for the perturbed nitroxides is unfavorable because of line overlap, the observation that for the pair of lines with $m_N = 0$, $m_O = \pm 5/2$ the low field line is narrower than that at high field can also be shown to require that a_0 and γ_0 have the same sign.

We have followed Broze and Luz²⁵ and for convenience use $|\gamma_0|$ in the definition of $(T_0)_0$, thus changing the sign of T_0 , a_0 , and of the σ - π interaction parameters reported.

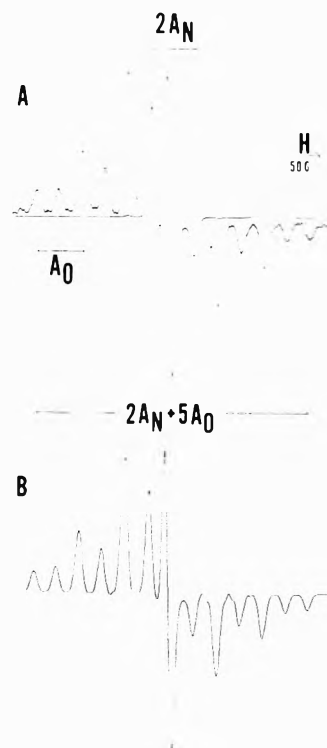


Figure 2. (A) Powder spectrum of TMPN(¹⁷O) in 2,2,6,6-tetramethylpiperidine. The signal amplitude of the ¹⁷O parallel region is 1.6×10^2 times that of the central ¹⁴N portion of the spectrum: $T = 77^\circ\text{K}$. (B) Computer simulation, with $A_N = 34.45$ G, $B_N = 6.26$ G, $A_0 = 72.0$ G, $B_0 = 7.2$ G, $g_\perp - g_\parallel = 0.0054$ and line width = 10 G.

A line width analysis for R_2NOH^+ shows that, as expected, $a_{H^+} < 0$.²⁶

Empirical Correlations between Hfs. We wish to correlate experimental values of isotropic hfs constants, a_i , with experimentally determined electron-nuclear dipolar interaction parameters, T_i , as well as to correlate the T_i among themselves. From eq 4 and 5, T_i can be calculated from the parameters (A_i , B_i) or from (a_i , A_i). Since neither B_N nor B_O are resolved in frozen solution, the latter procedure was used and then verified by simulating the powder spectra using the measured values for A_N and A_0 and the calculated values of B_N and B_O (Figure 2B). As described in Appendix A, minor corrections to A_i due to nonlocal dipolar interactions have been included in the calculations of T_i .

Figures 3 and 4 are, respectively, plots of a_N vs. T_N and a_0 vs. T_N for DTBN and TMPN perturbed by a variety of interactions. Results for newly prepared free-radical molecular complexes are included (A-G).^{6,11} Excluding the points for protonated nitroxides (H-J), the figures show that both a_0 and a_N are linearly related to T_N . These linear variations include perturbation by the "simple" solvent effects of non-hydrogen-bonding solvents (points a-c, f), perturbation by hydrogen-bond formation (points 1-7), and also perturbation by actual molecular complex formation (points A-G). These results are similar to observations in which variations of isotropic hfs constants for different sites on a radical are linearly related when the spin density distribution is perturbed by intermolecular interactions without structural changes in the radical or change in total spin density.⁴

The straight lines in Figures 3 and 4 are determined by the method of linear least squares with exclusion of

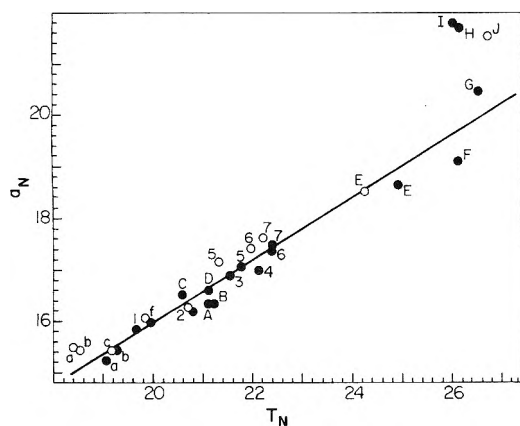


Figure 3. Plot of a_N vs. T_N for DTBN (●) and TMPN (○) in the aprotic solvents (a) *n*-hexane, (b) toluene, (c) 2,2,6,6-tetramethylpiperidine, and (f) nitromethane; in the hydrogen bonding solvents (1) decyl alcohol, (2) methanol, (3) phenol, (4) 4-fluorophenol, (5) 3-fluorophenol, (6) 1,1,1,3,3,3-hexafluoro-2-propanol (HFIP), and (7) pentafluorophenol; complexed with (A) $Ti(OPh)_4$, (B) $GeCl_4$, (C) $SiCl_4$, (D) pentacarbonylchromium di-*tert*-butyl stannylene, (E) $SnCl_4$, (F) $TiCl_4$, and (G) $AlCl_3$ (error in T_N is ± 0.7 G);²² protonated by (H) $H_2O:TiCl_4$, (I) $H_2O:TiBr_4$, and (J) $H_2O:BF_3$.

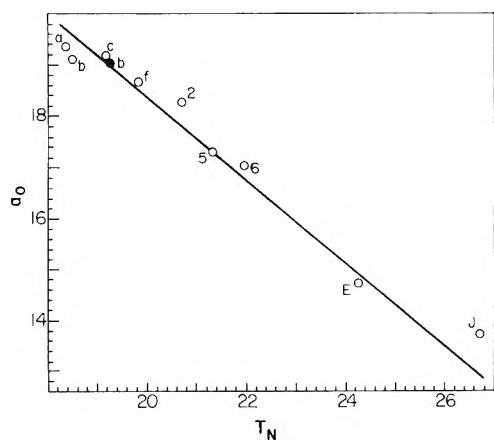


Figure 4. Plot of a_O vs. T_N for DTBN (○) and TMPN (^{17}O) (○) in the aprotic solvents (a) *n*-hexane, (b) toluene, (c) 2,2,6,6-tetramethylpiperidine and (f) nitromethane; in the hydrogen bonding solvents (2) methanol, (5) 3-fluorophenol, and (6) HFIP; complexed with (E) $SnCl_4$; protonated by (J) $H_2O:BF_3$.

points H, I, and J and the errors given are the probable

$$a_N(G) = (0.61 \pm 0.02)T_N + (3.8 \pm 0.4) \text{ G} \quad (6)$$

$$a_O(G) = (-0.81 \pm 0.04)T_N + (34.5 \mp 0.8) \text{ G} \quad (7)$$

errors in the slope and intercept.²⁷ Because of the inclusion of results from the molecular complexes, these relationships cover a much wider range of splitting constants than is ordinarily accessible. Results for a series of nitroxides oriented in host single crystals are in agreement with eq 6.²⁸

Isotropic hfs can also be fit to a linear relationship with T_O (Figures 5 and 6) although the fewer available values for T_O have a substantially greater experimental error than for T_N

$$a_N = (-0.26 \pm 0.02)T_O + (29.4 \mp 1.2) \text{ G} \quad (8)$$

$$a_O = (0.30 \pm 0.02)T_O + (3.3 \pm 1.2) \text{ G} \quad (9)$$

The ^{14}N hfs for $DTBNH^+$ do not fit eq 6 (Figure 5), al-

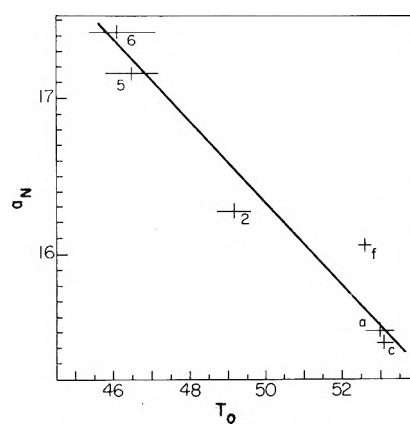


Figure 5. Plot of a_N vs. T_O for TMPN (^{17}O) in the aprotic solvents (a) *n*-hexane, (c) 2,2,6,6-tetramethylpiperidine, and (f) nitromethane; in the hydrogen bonding solvents (2) methanol, (5) 3-fluorophenol, and (6) HFIP.

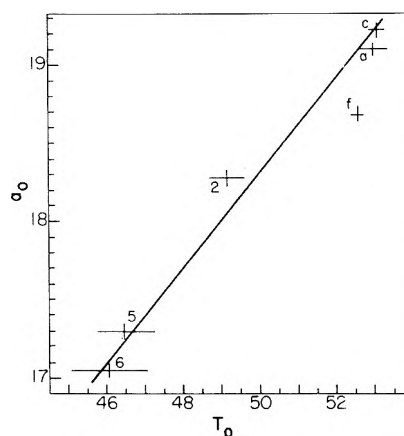


Figure 6. Plot of a_O vs. T_O for TMPN (^{17}O) in the aprotic solvents (a) *n*-hexane, (c) 2,2,6,6-tetramethylpiperidine, and (f) nitromethane; in the hydrogen bonding solvents (2) methanol, (5) 3-fluorophenol, and (6) HFIP.

though the ^{17}O hfs of $TMPN(^{17}O)H^+$ obey eq 7 reasonably well (Figure 4). A possible explanation for these observations is that for the protonated species, R_2NOH^+ , there is in addition to a redistribution of charge and spin density, also a change in the geometry and, therefore, hybridization of the nitrogen atom with only a minimal effect at oxygen. (See Discussion for the effect of hybridization changes.)

Figure 7 plots T_O vs. T_N . The result of a linear least-squares fit of the experimental data is

$$T_O = (-3.07 \pm 0.49)T_N + (111.8 \mp 9.8) \text{ G} \quad (10)$$

Dipolar Interaction Constants. The matrix elements of the spin density in the nitroxide N-O π -electron system may be calculated from measurements of T_i (eq 1). These matrix elements, ρ_O^π , ρ_N^π , and ρ_{ON}^π , and thus the T_i are related through the normalization condition

$$\rho_N^\pi + \rho_O^\pi + \rho_{ON}^\pi \simeq 1 - \epsilon \quad (11)$$

where $\rho_{ON}^\pi = -2S(\rho_O^\pi \rho_N^\pi)^{1/2}$;²⁹ $S = \langle 2p\pi N | 2p\pi O \rangle \simeq 0.15$ ³⁰ for an N-O bond distance of 1.29 Å. A nonzero value of ϵ would represent loss of spin density from the nitroxide N-O π system to the nitroxide alkyl groups or to the perturbing agent.

TABLE I: Electron–Nuclear Dipolar Interaction Constants (G)^a

	(T _O) ₀ /(T _N) ₀	(T _O) ₀	(T _N) ₀	Ref
Experimental	3.07 ± 0.49	96.4 ± 8.5 ^b	29.6 ± 4.7 ^b	This work
		102.2 ± 9.0 ^c	31.4 ± 3.2 ^c	
Theoretical				
Hartree–Fock orbitals	3.05	102	33.5	31
Slater orbitals	2.87	80.5	28.0	d

^a (T_i)₀ = 1/4gβg_Nβ_N(1/r³)_{av}.³³ ^b Using ρ_{ON}^π = -0.16 and assuming ε = 0.0. ^c Using ρ_{ON}^π = -0.16 and assuming ε = 0.07. ^d Calculated using effective nuclear charges; Z_N = 3.90 and Z_O = 4.55. (See F. L. Pilar, "Elementary Quantum Chemistry," McGraw-Hill, New York, N. Y., 1968, p 194.)

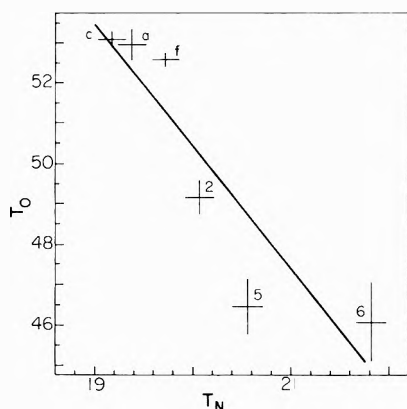


Figure 7. Plot of T_O vs. T_N for TMPN(¹⁷O) in the aprotic solvents (a) *n*-hexane, (c) 2,2,6,6-tetramethylpiperidine, and (f) nitromethane; in the hydrogen bonding solvents (2) methanol, (5) 3-fluorophenol, and (6) HFIP.

Using the experimental range of 18.46 ≤ T_N ≤ 26.56 G and (T_N)₀ 33.5 G³¹ (see below), eq 1 gives 0.55 ≤ ρ_N^π ≤ 0.79. Then from the normalization equation and considering 0 < ε ≤ 0.1, ρ_{ON}^π is found to be a constant (ρ_{ON}^π = -0.16 ± 0.01) for the entire range of spin densities, independent of both ε and of any reasonable choice of (T_N)₀. Thus, in this work the term ρ_{ON}^π may be replaced everywhere by -0.16.

Equation 11 can be rewritten as a linear relationship between T_O and T_N. The definition of spin densities in terms of dipolar hfs (eq 1) including the overlap term as a constant gives

$$T_O = \left[-\frac{(T_O)_0}{(T_N)_0} \right] T_N + (1.16 - \epsilon)(T_O)_0 \quad (12)$$

Equating terms of eq 10 and 12 gives an experimental value for the ratio (T_O)₀/(T_N)₀ without assumption about ε. Table I shows that this ratio is in remarkably good agreement with that calculated using Hartree–Fock orbitals, with Slater orbitals giving a smaller value.

Given that the experimental and Hartree–Fock ratios are the same, then using Hartree–Fock values for the individual (T_i)₀,³¹ eq 10 and 12 give the quite reasonable value of ε = 0.07 ± 0.01. On the other hand, taking ε = 0.0 eq 10 and 12 give values for (T_i)₀ slightly smaller than the Hartree–Fock values. These results are consistent with the idea that we can treat a perturbed nitroxide as a two atom π-electron system with the sum of the spin density on the N–O moiety, a constant.

σ–π Interaction Parameters. As we have previously shown,⁵ the empirical linear relationships between isotropic and anisotropic hfs can be used to evaluate the Karplus–Fraenkel σ–π interaction parameters, Q_{NN}^N and

Q_{OO}^N, which relate, respectively, the nitroxide ¹⁴N isotropic hfs to ρ_N^π and ρ_O^π

$$a_N = Q_{NN}^N \rho_N^\pi + Q_{OO}^N \rho_O^\pi \quad (13)$$

A similar equation can be written for isotropic ¹⁷O hfs, with N and O interchanged. Using the definition of spin densities in terms of the dipolar hfs, eq 1, and the spin density normalization, eq 11, eq 13 can be written as

$$a_N = \left[\frac{Q_{NN}^N - Q_{OO}^N}{(T_N)_0} \right] T_N + (1 - \epsilon - \rho_{ON}^\pi) Q_{OO}^N \quad (14)$$

for ¹⁴N and similarly for ¹⁷O

$$a_O = \left[\frac{Q_{NN}^O - Q_{OO}^O}{(T_N)_0} \right] T_N + (1 - \epsilon - \rho_{ON}^\pi) Q_{OO}^O \quad (15)$$

Since the overlap spin density is effectively constant for the perturbed nitroxides and the σ–π parameters are invariant to perturbation (see Discussion), these equations have the same form as eq 6 and 7. Equating terms in eq 6 and 14 and in eq 7 and 15 with (T_N)₀ = 33.5 G³¹ and then using [ρ_{ON}^π = -0.16; ε = 0.07] or [ε = ρ_{ON}^π = 0.0], we obtain the ¹⁴N and ¹⁷O Karplus–Fraenkel σ–π interaction parameters listed in Table II.

It is equally possible to rewrite eq 13 and its ¹⁷O equivalent in terms of T_O rather than T_N. Comparing such equations with the empirical relationships, eq 8 and 9, using (T_O)₀ = 102³¹ gives values for the ¹⁴N and ¹⁷O σ–π parameters (Table II) in good agreement with values obtained using eq 14 and 15.

The polarization parameters for the proton bonded to oxygen in R₂NOH⁺ and for the hydrogen bonding proton in R₂NO–methanol can also be determined. The proton hfs of R₂NOH⁺ is expected to obey a McConnell³² equation

$$a_{H^+} = Q_{OO}^H \rho_O^\pi \quad (16)$$

For TMPNH⁺ and DTBNH⁺, a_{H⁺} = -3.8 ± 0.1 and -4.1 ± 0.1 G, respectively. From the observed T_N (Figure 3) and eq 1 with (T_N)₀ = 33.5 G,³¹ choosing [ρ_{ON}^π = -0.16; ε = 0.07], eq 11 gives ρ_O^π = 0.29 (TMPNH⁺), 0.31 (DTBNH⁺), and thus Q_{OO}^H = -13.2 ± 0.3 G for these protonated nitroxides.

From the nmr contact shift, a_{H⁺} for the hydroxyl proton of methanol hydrogen bonded to DTBN is -0.49 G.³³ Assuming that this coupling also obeys eq 16 and using ρ_O^π = 0.47 for DTBN–methanol, determined as above, the effective value of Q_{OO}^H is -1.06 G, more than a factor of 10 smaller than for full proton transfer to oxygen and in order of magnitude agreement with a theoretically calculated value, Q_{OO}^H = -3.26 G.³⁴

g Values. Figure 8 plots g_{iso} vs. a_N for nitroxides perturbed by aprotic (points a–f) and protic (points 1–7) solvents. All of the data in Figure 8 can be included in a single least-squares relationship

TABLE II: Nitroxide σ - π Interaction Parameters for Eq 2 (G)

Source	Q_{NN}^N	Q_{OO}^N	Q_{OO}^O	Q_{NN}^O	
DTBN, TMPN Figures 3 and 4, eq 6 and 7 Figures 5 and 6, eq 8 and 9	24.2 ± 1.0	3.8 ± 0.4	34.5 ± 0.8	7.5 ± 0.6	$\epsilon = \rho_{ON}^\pi = 0.0$
	23.9 ± 1.0	3.6 ± 0.4	31.7 ± 0.7	4.7 ± 0.5	$\epsilon = 0.07; \rho_{ON}^\pi = -0.16$
	27.0 ± 1.0	0.3 ± 1.3	33.7 ± 3.0	3.0 ± 1.0	$\epsilon = 0.07; \rho_{ON}^\pi = -0.16$
C_2NO fragment a	41.2	-4.8	45.0	-16.5	$\epsilon = 0.07; \rho_{ON}^\pi = -0.16$

^a Calculated, as described in the text, from parameters¹² for a three term-equation (eq 19).

$$g_{iso} = -(2.67 \pm 0.16) \times 10^{-4} a_N + 2.01014 \pm 0.00026 \quad (17)$$

A previous suggestion based on fewer data points, that different linear relationships are required for protic and aprotic solvents,³⁵ appears to be unnecessary. The arrow in Figure 8 indicates g_{iso} for gaseous DTBN. Even at low pressure (0.71 mm) hfs were not resolved. From the measured gas-phase g_{iso} , eq 17 predicts $a_N = 15.0$ G and, using eq 6 and 1 with $(T_N)_0 = 33.5$,³¹ $\rho_N^\pi = 0.57$.

For nitroxide molecular complexes g_{iso} is greater than the value that would be calculated from a_N and eq 17, and these results are not included in Figure 8. This positive deviation has been attributed to spin-orbit coupling with atoms of the Lewis acid and can be used to estimate spin densities on MX_n .^{6,11} The results for R_2NOH^+ are in reasonable agreement with eq 17. However when $DTBNH^+$ is prepared by protonation with $H_2O:MX_n$, $a_N = 21.7 \pm 0.1$ G independent of MX_n , but g_{iso} differs significantly according to the identity of MX_n with $TiBr_4$ having the largest value (2.00466) and $SbCl_5$ the smallest (2.00405), and BF_3 (2.00437) and $TiCl_4$ (2.00422) intermediate. This influence of the protonating species suggests that the R_2NOH^+ in methylene chloride exists as a tight ion pair with a small but finite spin-orbit interaction with atoms of the counter ion. Small, partially resolved hfs, observed when TMPN is protonated by $H_2O:AlCl_3$, are also evidence for ion pairing.²⁶

Discussion

We have shown that for aliphatic nitroxides the dependence of both ^{14}N and ^{17}O on π -electron spin densities can be successfully described by equations of the Karplus-Fraenkel type (eq 2). From the linear relations between a_i and T_N , eq 6 and 7, Q_{OO}^N and Q_{OO}^O are obtained without assumption as to the magnitude of any σ - π parameter and without using valence-theory calculations of π -electron wave functions; values of Q_{NN}^O and Q_{NN}^N obtained from these equations do depend on the value of $(T_N)_0$. The value of Q_{OO}^H for R_2NOH^+ is also dependent only on $(T_N)_0$.

The linear relationships between a_i and T_O , eq 8 and 9, give values of Q_{NN}^O and Q_{NN}^N directly and values of Q_{OO}^N and Q_{OO}^O dependent only on $(T_O)_0$. Although based on fewer and less accurate data, the agreement of these parameters with those derived from eq 6 and 7 is reasonable.

From Table II, $Q_{jj}^i/Q_{ii}^i \approx 0.15$ for both ^{14}N and ^{14}O . Since for the systems studied here, $0.55 \leq \rho_N^\pi \leq 0.79$ and $0.53 \leq \rho_O \leq 0.30$, then a_i for both nuclei depend primarily, but not exclusively, on the local spin density. This result corrects earlier suggestions that a_N for aliphatic nitroxides follows a simple McConnell relationship with $Q_{NN}^N = 18$ G^{7,36}, as well as earlier estimates of ρ_N^π .³⁷ Furthermore, theoretically calculated spin densities for DTBN should probably be compared with the estimated gas-phase value, $\rho_N^\pi = 0.57$.

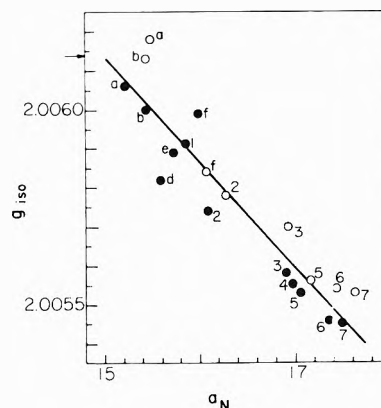


Figure 8. Plot of g vs a_N for DTBN (●) and TMPN (○) in the aprotic solvents (a) *n*-hexane, (b) toluene, (d) dimethyl sulfoxide, (e) methylene chloride, and (f) nitromethane; in the hydrogen bonding solvents (1) decyl alcohol, (2) methanol, (3) phenol, (4) 4-fluorophenol, (5) 3-fluorophenol, (6) HFIP, and (7) pentafluorophenol. The arrow indicates the g value of gas-phase DTBN.

In evaluating the nitroxide σ - π parameters we have assumed they are not significantly altered by environmental perturbations, although these perturbations do cause a redistribution of the σ -electron spin density.³⁸ To examine this assumption we consider the general equation for elements of the π - π polarization matrix as given by Henning^{39d}

$$q_{rs}^i = \frac{16}{3} \pi g_i \beta_n \sum_j \sum_p \frac{\langle \sigma_j(p_z) | e^2/r_{12} | (p_z)_{s,p} \sigma_p^* \rangle}{\Delta E(j \rightarrow p)} \sigma_j(r_i) \sigma_p^*(r_i) \quad (18)$$

where g_i is the nuclear g value for nucleus i , β_n the nuclear Bohr magneton, σ_j and σ_p^* occupied and unoccupied σ MO's, $\sigma_j(r_i)$ is the value of the orbital σ_j at nucleus i , $(p_z)_{r(s)}$ is the $2p\pi$ orbital on atom $r(s)$, and $\Delta E(j - p)$ is the singlet-triplet transition energy for an excitation from the σ_j to the σ_p^* orbital (As seen below, q_{rs}^i and the Karplus-Fraenkel parameter, Q_{rs}^i , are not necessarily identical.)

An environmental effect on q_{rs}^i would come through changes in $\Delta E(j - p)$. For a dialkyl nitroxide the excitations which need to be considered are the $O(n)$ - $NO(\sigma^*)$, $CN(\sigma)$ - $CN(\sigma^*)$, $CN(\sigma)$ - $NC(\sigma^*)$, $CN(\sigma)$ - $NO(\sigma^*)$, $NC(\sigma)$ - $NC(\sigma^*)$. However, strong hydrogen bonding or molecular complexation primarily involves interaction with the n orbitals on oxygen.^{6,8} Therefore, it is expected that the $O(n)$ - $NO(\sigma^*)$ excitation energy ($\Delta E(n-\sigma^*)$) will exhibit the largest change upon environmental perturbation, with other excitation energies exhibiting smaller changes.

A rough estimate of the variation in the σ - π parameters caused by changes in $\Delta E(n-\sigma^*)$ is available from consideration of the optical spectrum of DTBN. The $n-\pi^*$ transition⁴⁰ shifts 2900 cm^{-1} going from *n*-hexane (λ_{max} 21,500 cm^{-1} ,⁴¹ $a_N = 15.20$ G) to HFIP (λ_{max} 24,400, $a_N = 17.35$

G), while Hayat and Silver¹² estimate $\Delta E(n-\sigma^*) \approx 1.15$ au (252,500 cm⁻¹). If in first approximation all variation in the $n-\pi^*$ and in the $n-\sigma^*$ transition is attributed to effects on the nonbonding orbital, then both transitions would undergo similar shifts in wavelength and $\Delta E(n-\sigma^*)$ would thus change by only $\approx 1\%$. Since the other excitation energies were also estimated to be 1.15 au or greater¹² their variation would be even less. Thus, these order of magnitude estimates show that any variations in the $\sigma-\pi$ parameters will be substantially smaller than the reported probable errors (Table II).

Comparison with Other Karplus-Fraenkel Parameters. Previous, mostly semiempirical, correlations of a_N with π -electron spin densities using an equation of the form of eq 2 have been made for ¹⁴N in N-heterocyclic ion radicals. The reported values for Q_{NN^N} (19–31 G)³⁹ range around the present result for DTBN and TMPN while a semiempirical estimate of $Q_{NN^N} \approx 36$ G for diphenyl nitroxide⁴² is considerably larger than our result. Only one of these previous determinations of the Q_{NN^N} was independent of assumptions about $\sigma-\pi$ parameters, usually Q_{CC^H} , or of semiempirical spin density calculations: $Q_{NN^N} = 27.3$ G for heterocyclic radical anions.³⁹

The value of Q_{OO^N} is small but it is positive outside of experimental error. This is contrary to simple considerations of spin polarization which take into account only L-shell orbitals on N and O. Values of the comparable parameter for heterocyclic anions, Q_{CC^N} , have ranged from -4 to +9 G.³⁹ Of these determinations, only three were independent of assumptions about $\sigma-\pi$ parameters or of semiempirical spin density calculations; $Q_{CC^N} = 2.6$ G³⁹ for protonated diazines, -1.7 G for nitrogen heterocyclic anions,³⁹ and -1.56 G for the pyrazine and 3,5-lutidine anions.³⁹

Previous semiempirical determinations of ¹⁷O Karplus-Fraenkel parameters have been made for ¹⁷O enriched semiquinone and hydroquinone radicals and for nitroaromatic anions. For the former $Q_{OO^O} \sim 40-45$ G^{25,43} and for the latter $Q_{OO^O} = 49.7$ G⁴⁴ have been reported, noticeably larger ($\sim 30\%$) than for R₂NO (Table II).

The nitroxide Q_{NN^O} is positive (Table II), again contrary to simple considerations of spin polarization. In contrast $Q_{NN^O} = -2.92$ G is reported for nitroaromatics. The comparable parameter in the quinone radicals is given the range $Q_{CC^O} \approx 0-16.9$ G,^{25,43} of the same sign as Q_{NN^O} for nitroxides.

In general, when fitting hfs and spin density data to a Karplus-Fraenkel relationship, overlap terms in the spin density normalization (eq 11), proportional to overlap integrals, have been omitted, but as shown above, it is relatively easy to include the overlap spin density as a constant in the normalization equation. Values of $\sigma-\pi$ parameters depend in a systematic way on the treatment of both overlap spin density and of ϵ (eq 14 and 15). For example, Table II includes values of $\sigma-\pi$ parameters calculated with $\rho_{ON^\pi} = -0.16$, $\epsilon = 0.07$, and also with $\rho_{ON^\pi} = \epsilon = 0$.

Inclusion of q_{cross} . Examination of eq 18 shows that completeness would require an additional term in the $\sigma-\pi$ polarization equation, one directly involving the overlap spin density. The resulting three-term equation for nitroxides can be written¹² (i, j = ¹⁴N, ¹⁷O)

$$a_i = q_{ii}^i \rho_i^\pi + q_{jj}^j \rho_j^\pi + q_{\text{cross}}^i (\rho_O^\pi \rho_N^\pi)^{1/2} \quad (19)$$

Although eq 2 gives a satisfactory description of the ¹⁴N and ¹⁷O isotropic hfs for DTBN and TMPN, the product,

$(\rho_O^\pi \rho_N^\pi)^{1/2}$ is essentially a constant over the range of our experiments. Under this condition a_i will still be linearly dependent on T_N or T_O even if $q_{\text{cross}}^i \neq 0$. This fact underlies previous observations^{25,45} that semiempirical correlations between hfs and spin density are often insufficiently accurate to determine the parameters in an equation of the form of eq 19.

It is possible to equate the empirical correlations between isotropic and anisotropic hfs (eq 6–9) to the complete $\sigma-\pi$ polarization equation (eq 19) with a reinterpretation of terms. (The intercept in eq 6, becomes $[(1 + \rho_{ON^\pi} - \epsilon)q_{OO^O} + (\rho_O^\pi \rho_N^\pi)^{1/2} q_{\text{cross}}^N]$ and the intercept of eq 7 becomes $[(1 + \rho_{ON^\pi} - \epsilon)q_{OO^O} + (\rho_O^\pi \rho_N^\pi)^{1/2} q_{\text{cross}}^N]$. Thus, Q_{ii}^i and Q_{jj}^j as determined here are directly comparable to $\{q_{ii}^i + [(\rho_O^\pi \rho_N^\pi)^{1/2} q_{\text{cross}}^i / (1 + \rho_{ON^\pi} - \epsilon)]\}$ and $\{q_{jj}^j + [(\rho_O^\pi \rho_N^\pi)^{1/2} q_{\text{cross}}^j / (1 - \rho_{ON^\pi} - \pi)]\}$, respectively.)

Recently Hayat and Silver¹² have calculated the $\sigma-\pi$ polarization parameters of eq 19 for the nitroxide C₂NO fragment using a theoretical treatment due to Melchoir⁴⁶ which employs localized σ bonds. Their results, recalculated as indicated above for comparison purposes, are summarized in Table II. The calculated value of Q_{OO^O} is of the same sign, but larger ($\sim 30\%$) than our directly determined value. However, the theoretically calculated Q_{jj}^j 's for both ¹⁴N and ¹⁷O are opposite in sign to our experimental values.

Direct comparison between an empirical Q_{NN^N} and a theoretical q_{NN^N} from eq 18 is not possible because of the consequences of the possibility of nonplanarity at nitrogen. However, Hayat and Silver¹² arrive at (but do not explicitly write) a semiempirical value $q_{NN^N} = 40.5$ G by combining calculated q_{OO^N} , q_{OO^O} , and q_{NN^O} with observed a_N , a_O for 2,2,6,6-tetramethyl-4-piperidone *N*-oxyl. The value for Q_{NN^N} calculated from their result (Table II) differs considerably from that reported here.

Geometry at Nitrogen. Consideration of Q_{NN^N} can also give information about the degree of nonplanarity for a nitroxide. Theoretical expressions based on eq 18 assume C₂NO to be planar, but the elements of the polarization matrix will not be significantly affected by bending.¹² Bending does introduce an additional contribution to a_N by introducing some s character in the nitrogen orbital containing the odd electron. An empirically measured Q_{NN^N} or q_{NN^N} is then the sum of two terms: $Q_{NN^N} = Q_{NN^N}(\phi = 0) + f(\phi)$, where ϕ is the angle between the N-O bond and the (C-N-C) plane. Hayat and Silver write $f(\phi)$ as the product of the hfs for one electron in a ¹⁴N 2s orbital and the fraction of s character of the orbital containing the odd electron.⁴⁷

$$f(\phi) = 550(2 \tan^2 [\theta(\phi)]) \quad (20)$$

Symmetry about nitrogen is approximated to be C_{3v}, θ is the angle between the N-O bond and the plane defined by oxygen and the two carbons bonded to nitrogen, and θ and ϕ are related by the identity⁴⁸

$$\phi = \theta + \sin^{-1}[2 \sin \theta / (3 \sin^2 \theta + 1)^{1/2}] \quad (21)$$

For six-membered ring nitroxides X-ray structure determinations show $\phi \sim 16-21^\circ$,⁴⁹ which gives $f(\phi) = 10.1-16.7$ G. However, DTBN was considered to be planar in an electron diffraction study.⁵⁰ Thus $\phi = \theta = 0$, and $f(\phi) = 0$.

If the hfs data for TMPN and DTBN are separately fit to linear relationships of the form of eq 6, the derived

Q_{NN}^N are essentially identical: $Q_{NN}^N(\text{TMPN}) = 23.8 \pm 1.6$ G and $Q_{NN}^N(\text{DTBN}) = 24.1 \pm 1.2$ G. This result suggests that the out of plane angle, ϕ , is similar for the two radicals in solution.

Conclusion

Through the measurement of isotropic and anisotropic hfs we have directly determined the ^{14}N and ^{17}O σ - π polarization parameters for DTBN and TMPN as well as Q_{OO}^H for protonated nitroxide. The ^{14}N and ^{17}O neighboring atom σ - π parameter are positive, contrary to simple considerations. We have also shown that at least in solution DTBN and TMPN do not differ in their degree of non-planarity.

Melchior's theory for elements of the σ - π polarization matrix predicts that Q_{ii}^i elements should be relatively insensitive to the σ bonding at i whereas Q_{jj}^i elements should be much more dependent on bonding at i .^{46,51} Thus our Q_{OO}^O and possibly Q_{NN}^N should be transferable to aromatic nitroxides and possibly other N or O π system such as N heterocyclics, semiquinones, the C-CHNH₂ π fragment, and nitroaromatic ions.

Appendix

A complete description of the magnetic dipolar interaction in the nitroxide π -electron system must include dipolar interactions between nucleus i and spin density on its neighbor j , T_{jj}^i , and with the overlap spin density, T_{ij}^i , giving for ^{14}N

$$A_N = a_N + T_N + T_{OO}^N + T_{ON}^N$$

and a similar equation for ^{17}O with the N and the O interchanged. The last two terms are opposite in sign and, because of the r^{-3} dependence of the dipolar interaction, are small, but for completeness have been included. These terms are obtained using $T_{jj}^i = (T_{jj}^i)_0 \rho_{ij}$ with the $(T_{jj}^i)_0$ and $(T_{ij}^i)_0$ referring to the appropriate dipolar hfs due to one electron.

The calculation of $(T_{ii}^i)_0$ is straightforward, using the equations of McConnell and Strathdee⁵² as modified by Barfield.⁵³ To calculate $(T_{ij}^i)_0$, we assumed that the overlap spin density could be represented as a p orbital located midway between N and O and experiencing a nuclear forcefield with Slater Z , the average of Z_N and Z_O (arithmetic and geometric means give indistinguishable results); these calculations gave $(T_{OO}^N)_0 = -0.66$ G, $(T_{ON}^N)_0 = -1.30$ G, $(T_{NN}^O)_0 = +1.12$ G, and $(T_{NO}^O)_0 = +2.47$ G. Because the nonlocal terms are small the spin densities can be iteratively calculated by neglecting non-local contributions, in the initial value for T_i , and then adjusting T_i by reintroducing these terms. These minor corrections to T_i are insensitive to the choice of $(T_i)_0$ from among reported values as well as to the $(T_{ij})_0$. Thus the T_N may still be considered experimental quantities, derived from (a_i, A_i) , and effectively independent of any theoretically calculated $(T_i)_0$.

Acknowledgment. We thank Dr. George P. Lozos for assistance with epr spectral simulations, Dr. James C. Baird for a detailed description of the preparation of ^{17}O enriched di-*sec*-butyl nitroxide, and Dr. Tobin J. Marks for a gift of the pentacarbonylchromium di-*tert*-butyl stannylene. We acknowledge the donors of the Petroleum Research Fund, administered by the American Chemical Society.

References and Notes

- (1) NDEA Predoctoral Fellow, 1969-1972.
- (2) Alfred P. Sloan Fellow.
- (3) (a) E. G. Rozantsev, "Free Nitroxyl Radicals," Plenum Press, New York, N. Y., 1970; (b) P. Jost and O. H. Griffith in "Methods in Pharmacology," Vol. 11, C. Chignell, Ed., Appleton-Century-Crofts, New York, N. Y., 1972.
- (4) A. H. Reddoch, *J. Chem. Phys.*, **43**, 225 (1965).
- (5) A. H. Cohen and B. M. Hoffman, *J. Amer. Chem. Soc.*, **95**, 2061 (1973).
- (6) T. B. Eames and B. M. Hoffman, *J. Amer. Chem. Soc.*, **93**, 3141 (1971).
- (7) (a) H. Lemaire and A. Rassat, *J. Chim. Phys. Physicochim. Biol.*, **61**, 1580 (1964); (b) G. B. Berthier, H. Lemaire, A. Rassat, and A. Veillard, *Theor. Chim. Acta*, **3**, 213 (1965).
- (8) A. S. Kabankin, G. M. Zhidomirov, and A. L. Buchachenko, *J. Magn. Resonance*, **9**, 199 (1973).
- (9) P. W. Atkins and M. C. R. Symons, "The Structure of Inorganic Radicals," American Elsevier, New York, N. Y., 1967, p. 22.
- (10) M. Karplus and G. K. Fraenkel, *J. Chem. Phys.*, **35**, 1312 (1961).
- (11) A. H. Cohen and B. M. Hoffman, *Inorg. Chem.*, in press.
- (12) H. Hayat and B. Silver, *J. Phys. Chem.*, **77**, 72 (1973).
- (13) A. K. Hoffmann, A. M. Feldman, E. Geldblurr, and W. G. Hodgson, *J. Amer. Chem. Soc.*, **86**, 639 (1964).
- (14) R. Briere, H. Lemaire, and A. Rassat, *Bull. Soc. Chim. Fr.*, 3273 (1965).
- (15) J. C. Baird, *J. Chem. Phys.*, **37**, 1879 (1962).
- (16) B. M. Hoffman and T. B. Eames, *J. Amer. Chem. Soc.*, **91**, 2169 (1969).
- (17) A. H. Cohen and B. M. Hoffman, to be submitted for publication.
- (18) R. J. Faber and G. K. Fraenkel, *J. Chem. Phys.*, **47**, 2462 (1967).
- (19) L. J. Libertini and D. H. Griffith, *J. Chem. Phys.*, **55**, 1359 (1970).
- (20) "EPR at Work," Instrument Division of Varian Associates, No. 29.
- (21) R. J. Faber, F. W. Markley, and J. A. Weil, *J. Chem. Phys.*, **46**, 1652 (1967).
- (22) G. P. Lozos and B. M. Hoffman, *J. Phys. Chem.*, **78**, 200 (1974).
- (23) A. Carrington and A. D. McLachlan, "Introduction to Magnetic Resonance," Harper and Row, New York, N. Y., 1967, p. 99 ff.
- (24) Z. Luz and B. L. Silver, *J. Chem. Phys.*, **44**, 4421 (1966).
- (25) M. Broze and Z. Luz, *J. Chem. Phys.*, **51**, 738 (1969).
- (26) T. B. Eames, Ph.D. Thesis, Northwestern University, Evanston, Ill., 1972.
- (27) A. G. Worthing and J. Geffner, "Treatment of Experimental Data," Wiley, New York, N. Y., 1943, p. 158.
- (28) P. C. Jost, L. J. Libertini, V. Herbert, and O. H. Griffith, *J. Mol. Biol.*, **59**, 77 (1971), and references therein.
- (29) J. D. Memory, "Quantum Theory of Magnetic Resonance Parameters," McGraw-Hill, New York, N. Y., 1968, p. 183.
- (30) R. S. Mulliken, C. A. Rieke, D. Orloff, and H. Orloff, *J. Chem. Phys.*, **17**, 1248 (1949).
- (31) B. A. Goodman and J. B. Raynor, *Advan. Inorg. Chem. Radiochem.*, **13**, 135 (1970).
- (32) H. M. McConnell, *J. Chem. Phys.*, **24**, 764 (1956).
- (33) N. A. Sysoeva and A. L. Buchachenko, *J. Struct. Chem. (USSR)*, **13**, 42 (1972).
- (34) A. S. Kabankin, G. M. Zhidomira, and A. L. Buchachenko, *J. Struct. Chem. (USSR)*, **13**, 423 (1972).
- (35) T. Kawamura, S. Matsunami, and T. Yonezawa, *Bull. Chem. Soc. Jap.*, **40**, 1111 (1967).
- (36) A. M. Vasserman and A. L. Buchachenko, *J. Struct. Chem. (USSR)*, **7**, 633 (1966).
- (37) E. G. Rozantsev and V. D. Sholle, *Russ. Chem. Rev.*, **40**, 233 (1971).
- (38) B. L. Silver, private communication.
- (39) (a) A. Carrington and J. dos Santos-Veiga, *Mol. Phys.*, **5**, 21 (1962); (b) R. L. Ward, *J. Amer. Chem. Soc.*, **83**, 3623 (1961); (c) N. M. Atherton, F. Gerson, and J. N. Murrell, *Mol. Phys.*, **5**, 509 (1962); (d) J. C. M. Henning, *J. Chem. Phys.*, **44**, 2139 (1966); (e) E. W. Stone and A. H. Maki, *ibid.*, **39**, 1635 (1963); (f) D. H. Geske and G. R. Padmanabhan, *J. Amer. Chem. Soc.*, **87**, 1651 (1965); (g) C. L. Talcott and R. J. Myers, *Mol. Phys.*, **12**, 549 (1967); (h) P. T. Cottrell and P. H. Reiger, *ibid.*, **12**, 149 (1967); (i) P. J. Black and C. A. McDowell, *ibid.*, **12**, 233 (1967); (j) B. L. Barton and G. K. Fraenkel, *J. Chem. Phys.*, **41**, 1455 (1964).
- (40) R. Briere, H. Lemaire, and A. Rassat, *Bull. Soc. Chim. Fr.*, 3273 (1965).
- (41) A. K. Hoffmann and A. T. Henderson, *J. Amer. Chem. Soc.*, **83**, 4671 (1961).
- (42) P. B. Ayscough and F. P. Sargent, *J. Chem. Soc. B*, 907 (1966).
- (43) (a) W. M. Gulick, Jr., and D. H. Geske, *J. Amer. Chem. Soc.*, **4119** (1966); (b) M. Broze, Z. Luz, and B. L. Silver, *J. Chem. Phys.*, **46**, 4891 (1967); (c) V. K. Dimroth, A. Berndt, F. Bar, R. Volland, and A. Schweig, *Angew. Chem.*, **79**, 69 (1967); (d) P. D. Sullivan, J. R. Bolton, and W. E. Geiger, Jr., *J. Amer. Chem. Soc.*, **92**, 4176 (1970).
- (44) W. M. Gulick, Jr., W. E. Geiger, Jr., and D. H. Geske, *J. Amer. Chem. Soc.*, **90**, 4218 (1968).
- (45) T. Yonezawa, T. Kawamura, and H. Kato, *J. Chem. Phys.*, **50**, 3482 (1969).
- (46) M. T. Melchior, *J. Chem. Phys.*, **50**, 511 (1969).
- (47) R. W. Fessenden, *J. Phys. Chem.*, **71**, 74 (1967).

- (48) Although Hayat and Silver (ref 12) calculate $\theta = 17^\circ$, using their procedure and data we obtain $\theta = 12^\circ$ which corresponds to $\phi = 36^\circ$ and $q_{\text{NN}}^{\text{N}}(36^\circ) = 24.4$ G.
- (49) (a) L. J. Berliner, *Acta Crystallogr., Sect. B*, **26**, 1198 (1970); (b) A. Capiomon, *ibid.*, **28**, 2298 (1972); (c) P. J. Lajzerowicz-Bonne-teau, *ibid.*, **24**, 196 (1968).
- (50) B. Anderson and P. Anderson, *Acta Chem Scand.*, **20**, 2728 (1966).
- (51) R. Poupko, B. L. Silver, and M. Rubenstein, *J. Amer. Chem. Soc.*, **92**, 4512 (1970).
- (52) H. M. McConnell and J. Strathdee, *Mol. Phys.*, **2**, 129 (1959).
- (53) M. Barfield, *J. Chem. Phys.*, **53**, 3836 (1970).

Estimating Microsecond Rotational Correlation Times from Lifetime Broadening of Nitroxide Electron Spin Resonance Spectra Near the Rigid Limit^{1a}

Ronald Paul Mason^{1b} and Jack H. Freed*

Department of Chemistry, Cornell University, Ithaca, New York 14850 (Received October 3, 1974)

A simple method of estimating rotational correlation times (τ_R) of the order of microseconds using the widths of the outer esr hyperfine extrema is discussed. An earlier method allowed determination of τ_R from the ratio of the outer hyperfine extrema separation at a given τ_R to the rigid limit separation. The present method, however, permits the determination of τ_R even when the separation of the outer hyperfine extrema is experimentally indistinguishable from the rigid limit value. It should be useful for many macromolecules with a rigidly bound nitroxide spin label, since they typically exhibit values of τ_R on the order of microseconds in solution.

There have been recent efforts in developing simplified methods for estimating rotational correlation times from the slow-motional esr spectra of nitroxide free radicals.² They are based on measuring the shifts, arising from the motion of the hyperfine extrema from their rigid limit values. In particular one need only measure $S \equiv A_z'/A_z$ where A_z' is one-half the separation of the outer hyperfine extrema and A_z is the rigid limit value for the same quantity.² Such methods become very insensitive for motions with rotational correlation times $\tau_R > 1 \times 10^{-7}$ sec where $(1 - S) < 3\%$ and, furthermore, in the region $\tau_R > 10^{-8}$ sec the predicted results are very sensitive to a choice of residual width δ .^{2a} There has also been interest in extending the range in which τ_R can be measured to longer times by means of more sophisticated techniques such as saturation studies³ and modulation-frequency-dependent adiabatic-rapid-passage methods.⁴

We have been able to develop a simple technique, based on measuring the line width variations of the outer extrema of the spectra,⁵ that may, in many cases, be useful in extending the range of measurable τ_R 's to $\tau_R < 5 \times 10^{-6}$ sec. The basic idea is a very simple one. The residual motional broadening in the near rigid limit may simply be regarded as arising from "uncertainty-in-lifetime broadening" due to the rotational motion carrying the nitroxide radical between different orientations corresponding to substantially different esr frequencies (some corrections must, of course, also be made for broadening due to nuclear spin flips). Then one would expect this width contribution to be given, to a rough approximation, by τ_R^{-1} , the reorientational rate. This is indeed found to be the case, to within a factor of 2 (or $1/2$), over most of the range of interest! Furthermore, the greater sensitivity of the widths (*vs.* the shifts in position) of the extrema is analogous to the well-

known case of exchange in magnetic resonance where lines first broaden before they shift.⁶ We develop a more accurate method and analysis below.

In the rigid limit the outer hyperfine extrema (for an isotropic distribution of nitroxide spin labels) arise from those nitroxide radicals for which the 2p π orbital of the nitrogen atom is nearly parallel to the applied field direction. One may use standard methods to compute such spectra,⁷ but we note from a simple analysis of McConnell, *et al.*,^{8,9} that the derivative patterns of the outer hyperfine extrema are reasonably approximated as absorption curves with a shape function characteristic of the inhomogeneous broadening. Experimentally, one finds that the outer hyperfine extrema have line shapes ranging from almost perfect Lorentzian to intermediate between Lorentzian and Gaussian.^{7,9} (The low-field side of the high-field line and the high-field side of the low-field line are somewhat distorted by overlap with the central region of the spectrum.) We have found that the average of the half-widths at half-heights (Δ) for the two outer extrema of a rigid limit spectrum is, to a very good approximation, equal to $(\sqrt{3}/2)\delta$, where δ is the peak-to-peak derivative Lorentzian line width used in our simulations of computed rigid limit spectra.⁷ (The heights of the hyperfine extrema are measured from the true base line (*cf.* Figure 1).) More precisely we have found that

$$2\Delta_l^r = 1.59 \delta \quad (1a)$$

and

$$2\Delta_h^r = 1.81 \delta \quad (1b)$$

(where subscripts l and h refer to the low- and high-field lines, respectively, and the superscript r refers to the rigid limit value). This result is found to be independent of δ

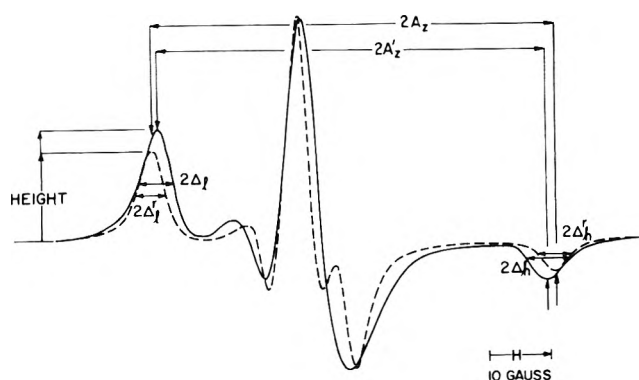


Figure 1. Superposition of computed rigid limit nitroxide spectrum with a computed slow-tumbling spectrum at $\tau_R = 5.0 \times 10^{-8}$ sec demonstrating the measurements required for the parameters $S = A_z'/A_z$, $W_l = \Delta_l/\Delta_l^r$, and $W_h = \Delta_h/\Delta_h^r$. In an actual experiment it is often necessary to estimate the Δ_i^e in place of the Δ_i^r as described in the text. The magnetic parameters utilized for this figure are $\delta = 3.0$ G, $g_x = g_y = 2.0075$, $g_z = 2.0027$, $A_x = A_y = 6.0$ G, $A_z = 32.0$ G, $B_0 = 3300$ G.

over the range $1.0 \leq \delta \leq 4.0$ G and virtually independent of A_z over the range $27 \leq A_z \leq 40$ G. It is, of course, essentially independent of variations in the other nitroxide rigid limit parameters. It is a result obtained for the assumption of Lorentzian inhomogeneous broadening.

In the slow-motional region, near the rigid limit, the line width Δ_i , for Lorentzian line shapes, can be decomposed into two contributions.¹⁰ (1) the Lorentzian inhomogeneous component given by eq 1a and 1b and (2) the excess motional width (of order of magnitude τ_R^{-1}). (It is convenient to think in terms of this decomposition even though it is not necessary for the method below.) A useful dimensionless parameter for describing these spectra is then

$$W_i \equiv \Delta_i/\Delta_i^r \quad (2)$$

or

$$W - 1 = (\Delta_i - \Delta_i^r)/\Delta_i^r$$

where $i = l, h$. We have found that, in general $(W - 1)$ is about an order of magnitude larger than $(1 - S)$ for a particular value of τ_R (cf. Figure 2), and furthermore it could be measured to at least comparable accuracy ($\sim 1\%$ cf. Figure 1), but note that the $(W - 1)$ parameter would be quite sensitive to distortion of the true line width by over modulation and/or power saturation. Our results in Figure 2 have been calculated from the rigorous theory of Freed, Bruno, and Polnaszek, as was done in I. We have studied how W_i is affected by changes in (1) the spin parameters, (2) line width, and (3) rotational diffusion model. We have found that W_i , like S , is insensitive to deviations from axial A and g tensors used in I, as well as to variations in A_\perp , g_\parallel , and g_\perp , typical of a nitroxide. However, in contrast to S , which is dependent on the product of $\tau_R A_z$, W_i is virtually independent of A_z over the range $27 \leq A_z \leq 40$ G (we have used $A_z = 32$ G in obtaining the results in Figure 2). However, $W_i - 1$ is found to depend upon δ . Generally, a smaller δ implies a larger $(\Delta_i - \Delta_i^r)$ for a given τ_R . In particular, a $\delta = 1$ G yields values of $(\Delta_i - \Delta_i^r)$ ranging from 1.3–2.5 times greater than those for $\delta = 3$ G. A qualitative explanation of this observation is as follows. The rigid limit extrema of finite width Δ_i^r arise from those nitroxide radicals whose $2p \pi$, N atom orbitals lie within a cone of angle Ω about the applied field direction, and the size of the cone increases rapidly with an in-

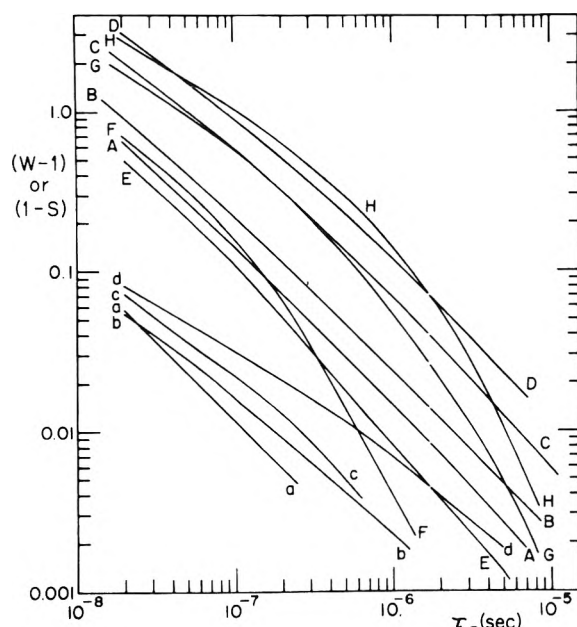


Figure 2. Graph of $(W - 1)$: curves A–H; and $(1 - S)$: curves a–d vs τ_R for nitroxide isotropic rotational reorientation from computer simulations of Brownian diffusion and approximate free diffusion. Curves a and b are for approximate free diffusion and derivative widths $\delta = 3.0$ and 1.0 G, respectively, and curves c and d are for Brownian diffusion where $\delta = 3.0$ and 1.0 , respectively. Curves a through d may be approximated by $\tau_R = a(1 - S)^b$ to a high degree of accuracy with (b) $a = 5.90 \times 10^{-10}$ sec, $b = -1.24$; (d) $a = 2.95 \times 10^{-10}$, $b = -1.68$. The equations for a and c are given in I. Curves A and B are for approximate free diffusion, $\delta = 3.0$ G, and the low- and high-field extrema, respectively, and curves C and D are the same as A and B, respectively, except δ equals 1.0 G. Curves E and F are for Brownian diffusion, $\delta = 3.0$ G, and the low- and high-field extrema, respectively, and curves G and H are the same as E and F, respectively, except $\delta = 1.0$ G. See also Table I.

TABLE I: Parameters for Relating τ_R to $(W - 1)^a$

Curve	$a \times 10^7$, sec	b	Max deviation, %
A	1.31	1.033	3
B	1.94	1.062	6
C	5.16	1.076	18
D	8.33	1.125	18
E	1.16	0.943	5
F	2.07	0.778	18
G	5.28	0.999	30
H	10.11	1.014	55

^a Table is based on approximate fit of Figure 2 data to eq 3 for $(W - 1) > 0.01$. ^b Based on comparing values in Figure 2 with eq 3.

crease in the rigid limit δ .⁸ If we roughly identify the excess width $(\Delta_i - \Delta_i^r)$ with the rate that radicals reorient out of the cone, then extrema from the larger cones (which result from greater values of δ) will be less broadened, since it takes longer for the radicals to leave the cone.¹¹ Another observation, *viz.* $(\Delta_h - \Delta_h^r)$ is always significantly larger than $(\Delta_l - \Delta_l^r)$, at a given τ_R is explained in a similar manner. It is known that the high-field resonance for a single-crystal spectrum changes with angle more rapidly than the low-field resonance: thus the range of Ω contained in the observed cone (from a polycrystalline sample) must be smaller for the high-field line.⁸ Reorientations out of the high-field cone thus occur at a more rapid rate, and, in general, W_h is a more sensitive function of τ_R than W_l as may be seen from Figure 2.

The choice of a proper δ must now be considered. Near the rigid limit the appropriate range of δ for these calculations and those of I can be deduced from the Δ_i^r . The narrowest rigid limit δ found in our laboratory is 1.5 G which corresponds to $2\Delta_i^r = 2.4$ G. Hubbell and McConnell⁹ report values of 4.6 and 5.5 G for $2\Delta_i^r$ for pseudoaxial "rigid limit" spectra, corresponding to δ of 2.9 and 3.5 G, respectively. The rigid limit spectrum of the *N*-oxyl-4',4'-dimethyloxazolidine derivative of 5 α -androstan-3-one appears to have a low-field full-width at a half-height of about 5.0 G, which corresponds to a δ of 3.1 G.⁸ (Note that the motional broadening can easily double the widths of the outer extrema when the separation of the hyperfine extrema is essentially unchanged from the rigid limit value (*i.e.*, $S > 0.95$).

Thus we observe that very near the rigid limit, where δ may be determined from the rigid limit extrema widths, two independent determinations of τ_R can be made from Figure 2.

The major contributions to the Δ_i^r are electron nuclear hyperfine interaction between the electron and the protons of the spin label and host. Heterogeneity of the environment also contributes to the rigid limit line width, because the nitroxide magnetic parameters depend on the details of the environment.¹² Unfortunately, these interactions will be quickly averaged with the onset of molecular motion, resulting in a decrease in the appropriate δ . When this is the case, it becomes necessary to estimate a δ , such that the rotational correlation times obtained from the plots of W_i vs. τ_R for both the low- and high-field extrema are equal within experimental error. For this process we may define effective inhomogeneous widths Δ_i^{er} which obey eq 1 and which generally obey $\Delta_i^{er} \leq \Delta_i^r$. Then we may rewrite eq 2 as

$$W_i \equiv \Delta_i / \Delta_i^{er} \quad (2')$$

This method then permits an accurate determination of both τ_R and δ .

As we have noted, the uncertainty in δ can result in serious errors when τ_R 's $> 3 \times 10^{-8}$ sec are determined from S . Once δ has been determined from the W_i , another estimate of τ_R may (when feasible) be obtained from S using either the analytical formulas of this paper and of I, or by linear interpolation of the graphs. This serves as a check on the results from the W_i . In other words τ_R and δ may often be obtained as a function of three experimental parameters, S , and the W_i .

The model-dependent studies shown in Figure 2 were performed for (1) Brownian diffusion where $\tau_R = (6R)^{-1}$ with R the rotational diffusion coefficient and (2) approximate free diffusion, in which $\tau_R = (6B_2R)^{-1}$ with $B_2^{-1} = \sqrt{7}$ yielding results equivalent to a moderate jump model with $|\langle \epsilon^2 \rangle_{av}|^{1/2} \approx 50^\circ$.⁷ These definitions are chosen so they yield model-independent results in the motional narrowing region for equal values of τ_R .⁷ The free diffusion model results in more nearly linear dependence (in a log-log plot) of $W - 1$ vs. τ_R in Figure 2 than the Brownian motion model. We have fit the plots in Figure 2 to the

form

$$\tau_R = \alpha(W - 1)^{-b} \quad (3)$$

for the region $(W - 1) > 0.01$ and the coefficients are given in Table I. W_3 also give the maximum variation between the curves and the results predicted from eq 3. It is clear that the use of eq 3 is a less accurate means of estimating τ_R than the curves. However, the fact that $b \approx 1$ (except for the anomalous curve F, which is presumably affected by overlap) is consistent with our interpretation of $(\Delta_i - \Delta_i^r)$ as a lifetime broadening. The curves in Figure 2 which differ only in the model of rotational diffusion are nearly identical for the region $(W - 1) > 0.03$. The more linear behavior for the free diffusion model probably reflects the fact that the picture of lifetime broadening by jumps out of the cone is a more accurate description when the root mean square jump angle $|\langle \epsilon^2 \rangle_{av}|^{1/2}$ is greater than Ω the cone angle. The Brownian motion model yields curves, which, at longer τ_R 's approach the rigid limit $(W - 1)$ values more rapidly than τ_R^{-1} , implying a breakdown of the simple picture.

An experimental check of this proposed method and its limitations is planned.

References and Notes

- (1) (a) Supported in part by a Grant from the National Science Foundation (Grant No. GP-13780) and the Cornell University Materials Science Center. (b) NIH Postdoctoral Fellow.
- (2) (a) S. A. Goldman, G. V. Bruno, and J. H. Freed, *J. Phys. Chem.*, **76**, 1858 (1972). Referred to as I in the text. (b) R. C. McCalley, E. J. Shimshick, and H. M. McConnell, *Chem. Phys. Lett.*, **13**, 115 (1972).
- (3) S. A. Goldman, G. V. Bruno, and J. H. Freed, *J. Chem. Phys.*, **59**, 3071 (1973).
- (4) J. S. Hyde and L. Dalton, *Chem. Phys. Lett.*, **16**, 568 (1972).
- (5) P. Jost, A. S. Waggoner, and O. H. Griffith in "The Structure and Function of Biological Membranes," Rothfield, Ed., Academic Press, New York, N. Y., 1971, suggest the use of an amplitude ratio in the central region of the nitroxide spectrum as a crude measure of relative motion. But such a ratio is too sensitive to the deviations of the nitroxide magnetic parameters from cylindrical symmetry (which vary considerably for different nitroxides and solvents) to be quantitatively useful.
- (6) In fact the naive analogy to the problem of chemical exchange between two lines (*cf.* P. W. Anderson, *J. Phys. Soc. Jap.*, **9**, 316 (1954); H. M. McConnell, *J. Chem. Phys.*, **28**, 430 (1958)) is a useful one. Thus, in this well-known case, in the slow-exchange limit, one has that the A th line with exchange-limited lifetime τ_A is broadened by τ_A^{-1} . Furthermore, the shift of the line, in a two line case, simply depends on the dimensionless product τ_S where $2s$ is the separation between the peaks, and $\tau^{-1} \equiv \tau_A^{-1} + \tau_B^{-1}$. In fact, when $\tau_A = \tau_B$, one has the simple result that for small τ^{-1} , the separation of the lines is decreased to $2s(1 - 2(\tau_S)^{-2})^{1/2} \approx 2s[1 - (\tau_S)^{-2}]$. The result of ref 2a that $S = S(\tau_R A_2)$ (*i.e.*, it scales as the product $\tau_R A_2$) is seen to be closely related to this well-known result.
- (7) S. A. Goldman, G. V. Bruno, C. F. Polnaszek, and J. H. Freed, *J. Chem. Phys.*, **56**, 716 (1972).
- (8) H. M. McConnell and B. G. McFarland, *Quart. Rev. Biophys.*, **3**, 91 (1970).
- (9) W. L. Hubbell and H. M. McConnell, *J. Amer. Chem. Soc.*, **93**, 314 (1971).
- (10) A. Abragam, "The Principles of Nuclear Magnetism," Oxford University Press, London, 1961.
- (11) One has for random rotational reorientation that the mean time τ required to reorient by an angle Ω is given by $\tau^{-1} = 6R/\Omega^2 = [B_2\tau_R\Omega^2]^{-1}$ (*cf.* ref 7 and references contained therein). But this expression does not appear to be completely applicable to the results obtained except that $\tau^{-1} \propto \tau_R^{-1}$.
- (12) R. P. Mason, J. Hwang, and J. H. Freed, to be submitted for publication.

Comments on the Interpretation of Electron Spin Resonance Spectra of Spin Labels Undergoing Very Anisotropic Rotational Reorientation^{1a}

Ronald Paul Mason,^{1b} Carl F. Polnaszek,^{1c} and Jack H. Freed*

Department of Chemistry, Cornell University, Ithaca, New York 14850 (Received January 21, 1974)

An analysis is given for motional effects on esr spectra of spin labels undergoing very anisotropic rotational relaxation in isotropic liquids. This analysis examines the spectral consequences for cases when the nitroxide is undergoing rapid rotation about a single bond, while the macromolecule to which it is attached is reorienting slowly. A simplified effective diffusion tensor R is employed such that R_{\parallel} refers to the bond motion and R_{\perp} to the effects of overall rotation. This approach is seen to be a useful approximation to developing the motional corrections to the effective time-independent S parameter approach of McConnell, *et al.* Our analysis including motional effects is found to be in good agreement with recent experiments of Wee and Miller on spin-labeled polymers. We show how motional effects may account for certain inconsistencies of results on polymer and membrane studies originally interpreted in terms of the effective time-independent approach, and how motional effects can influence the interpretation of the S parameter.

Wee and Miller² (WM) have recently studied esr spectra of solutions of spin-labeled polybenzylglutamate (PBLG) polymer in dimethylformamide (DMF). This system was found to have many of the spectral characteristics of spin label studies in membrane models and membranes.³⁻⁶ We have found their results both intriguing in their similarities to the other work as well as in the reduced ambiguities of the physical-chemical nature of their systems.

WM analyze their spectra in the manner of Hubbell, McFarland, and McConnell,³⁻⁶ who have utilized an effective time-independent spin Hamiltonian to account for rapid anisotropic motion. That is, the spin Hamiltonian for a nitroxide radical, whose motion is so slow as to yield rigid-limit spectra, is

$$\hbar \mathcal{H} = |\beta_e| \mathbf{S} \cdot \mathbf{g} \cdot \mathbf{B}_0 + h \mathbf{S} \cdot \mathbf{A} \cdot \mathbf{I} - g_N \beta_N \mathbf{I} \cdot \mathbf{B}_0 \quad (1)$$

where \mathbf{B}_0 is the applied dc field, \mathbf{g} and \mathbf{A} are the g and hyperfine tensors. However, a nitroxide spin label undergoing a complicated but very anisotropic motion is approximated by considering the motion about some molecular axis ν as being very fast while the motion perpendicular to that axis is very slow. This leads to an effective time-independent rigid-limit Hamiltonian

$$\hbar \mathcal{H} = |\beta_e| \mathbf{S} \cdot \mathbf{g}' \cdot \mathbf{B}_0 + h \mathbf{S} \cdot \mathbf{A}' \cdot \mathbf{I} - g_N \beta_N \mathbf{I} \cdot \mathbf{B}_0 \quad (2)$$

where the effective \mathbf{g}' and \mathbf{A}' tensors are axially symmetric about ν , so one need only specify g_{\parallel}' , g_{\perp}' , A_{\parallel}' , and A_{\perp}' in the usual notation. The use of such an effective Hamiltonian is based on the assumptions that (1) the motion about ν , which may be described by an effective rotational diffusion tensor component⁷ R_{\parallel} , is so fast that residual time-dependent effects of the averaging process, which could lead to line broadening, etc. are negligible and (2) the motion perpendicular to ν , described by an effective R_{\perp} , is so slow, its effects on the spectrum are negligible.

Thus the effective Hamiltonian of eq 2 corresponds to the limiting case in which $R_{\parallel}[\tau_{R_{\parallel}} = (6R_{\parallel})^{-1}]$ and $R_{\perp}[\tau_{R_{\perp}} = (6R_{\perp})^{-1}]$ are respectively too fast and too slow to appreciably affect the spectrum. The rotational correlation time, $\tau_R = (6R)^{-1}$ where $R = (R_{\perp} R_{\parallel})^{1/2}$ is undefined. It is an objective of this work to show that the results of WM as well as

much of the spin-labeled membrane work show unmistakable motional effects, contrary to their original interpretation in terms of eq 2.

One may relate the \mathbf{A}' of eq 2 and \mathbf{A} of eq 1 in terms of the direction cosines α_i , $i = x, y, \text{ or } z$ of ν in the molecular principal axis system. One takes the principal axes of \mathbf{A} (and of \mathbf{g}) such that the z axis is along the $2p-\pi$ orbital of nitrogen. The x axis is along the N-O bond, with the y axis perpendicular to the other two. Then one has

$$A_{\parallel}' = \sum_{i=x,y,z} \overline{\alpha_i^2} A_i \quad (3)$$

$$A_{\perp}' = \frac{1}{2} \sum_{i=x,y,z} (1 - \overline{\alpha_i^2}) A_i \quad (4)$$

where the superbars imply time averages. Similar equations hold for the elements of \mathbf{g} and \mathbf{g}' . In many nitroxides $A_x \approx A_y$, so eq 3 and 4 become

$$A_{\parallel}' = A_0 + 2/3(A_z - A_x)S \quad (5)$$

$$A_{\perp}' = \frac{1}{2}(3A_0 - A_{\parallel}') \quad (6)$$

where A_0 is the isotropic hyperfine term

$$A_0 = 1/3 \text{Tr}(\mathbf{A}) = 1/3 \text{Tr}(\mathbf{A}') = A_0' \quad (7)$$

and S (by analogy with liquid crystalline spectra) is known as the order parameter and is given by

$$S = \frac{1}{2}(3\overline{\alpha_z^2} - 1) = (A_{\parallel}' - A_{\perp}') / (A_z - A_x) \quad (8)$$

Thus S is a measure of the mean rotational amplitude leading to \mathcal{H}' , such that when $S = 1$, eq 2 becomes identical with eq 1 corresponding to the nitroxide exhibiting no motional averaging; while when $S = 0$, $A_{\parallel}' = A_{\perp}' = A_0$ corresponding to isotropic rotational motion with a correlation time less than about 1 nsec.⁶ Hubbell, *et al.*,³⁻⁶ have emphasized that for this interpretation in terms of the "pseudoaxial" rigid limit of eq 2 to be valid, one must have $\text{Tr} \mathbf{A} = \text{Tr} \mathbf{A}'$ according to eq 7, which follows directly from the rotational invariance of the trace of a tensor. We wish, in this work, however, to show that, while this condition is a necessary one, it is not, in general, sufficient as a result of motional effects. Before we consider our analysis in terms of motional effects we wish to review

some of the relevant experimental results and their original analysis.

Generally, A_0' as determined from spectra based upon the effective spin Hamiltonian of eq 2 have been found to fulfill the criterion of eq 7. However, A_0 for nitroxide radicals is weakly dependent upon solvent polarity, and this has sometimes resulted in uncertainty as to whether the criterion of eq 7 is fulfilled especially if the environment of the spin label is not known. Thus, in the work of Hubbell, *et al.*, variations in A_0' have been interpreted as changes in the polarity of the local environment of the nitroxide group, and a correction has been used to adjust the measured S for the polar-hydrophobic effect.⁵ Spectra of the dimethyl-*N*-oxyloxazolidine (DOXYL) long-chained spin labels in phospholipids and membranes are satisfactorily simulated with an effective \mathcal{H}' of eq 2 with one exception (*cf.* Figures 2-4 of ref 5). In this case, those computed spectra, which gave the best overall agreement with the observed spectra, still had outer hyperfine extrema that were narrower and of greater amplitude regardless of the line shape assumed. Although the principle source of this discrepancy may well be due to line broadening from heterogeneity of the fatty acid chains of the lecithin host, as suggested by Hubbell and McConnell,⁵ we note that the widths of outer hyperfine extrema can be markedly broadened by a rotational uncertainty-in-lifetime effect which can broaden these outer hyperfine extrema without significantly shifting their positions.⁸ So it is possible that a residual motion transverse to the symmetry axis ν is responsible for this discrepancy, although an orientation-dependent line width could also adequately account for this discrepancy. The fact that R_{\perp} may be fast enough that it affects the spectrum has been generally recognized. The rigorous theory of Freed, Bruno, and Polnaszek (FBP)⁹ has already been used to simulate spectra where the motion is anisotropic but the motional effects from both R_{\parallel} and R_{\perp} have direct observable effects on the spectrum.¹⁰

We give in Tables I-III some of the published experimental data for anisotropically immobilized spin labels. They include the results of ref 5 (Table I), ref 12 (Table II), and WM (Table III). These data have several trends in common. Hubbell, *et al.*, have noted that as A' approaches A_z , S approaches unity and the symmetry axis of \mathcal{H}' must approach the molecular z axis. $\cos^{-1}(\alpha_z^2)^{1/2}$ is referred to as the mean angular deviation between ν and z . In Tables I-III, an increase in A' and the resulting increase in S is accompanied by an increase in A_0' . Most, but not all, of the published data exhibit this phenomenon of an increase in A_0' with an increase in S .^{2,5,11,12} In the case of the DOXYL spin labels in aqueous dispersions of natural phospholipids this trend in A_0' is as noted explained as an increase in the polarity of the environment of the nitroxide as it is attached closer to the polar head group. The value of A_0' becomes as great as 15.2 G, which is the value of the isotropic hyperfine splitting of the radical in pure distilled water. Seelig, Limacher, and Bader have attributed this variation in terms of electrostatic interactions between the nitroxide dipole and the dipolar regions of the bilayer.¹³ The increase in S and its interpretation as a restriction in the motional amplitude of the DOXYL ring concomitant with an increase in the polarity of the environment as the DOXYL spin label is attached progressively closer to the polar head group is brought into question by our analysis below.

As already noted, the results of WM have characteristics similar to that of the DOXYL spin labels in membrane

TABLE I^a

Spin label	A_{\parallel}' , G	A_{\perp}' , G	A_0' , G	$g_{\parallel}' - g_{\perp}'$	S
IV(10,3)	27.8	9.0	15.2	-0.0036	0.695
IV(7,6)	26.0	9.5	15.0	-0.0033	0.62
IV(5,10)	21.8	10.3	14.1	-0.0026	0.46

^a Table I entitled "Resonance Data for Phospholipid Spin Labels IV(m,n) in Egg Lecithin-Cholesterol (2:1 Mole Ratio)" of ref 5.

TABLE II^a

Probe	T , °C	A_{\parallel}' , G	A_{\perp}' , G	A_0' , G	S
4 NS	22	26.6	9.3	15.1	0.65
4 NS	5	29.1	8.0	15.1	0.72
9 NS	5	25.0	9.7	14.8	0.58
12 NS	5	23.3	10.1	14.5	0.52

^a Table 3 entitled "Behavior of Spin-Probes Incorporated into Aqueous Dispersions of Lipids Extracted from Microsomal Preparations" of ref 12.

models and membranes in that an increase in A_{\perp}' results in an increase in S , which is concomitant with an increase in A_0' . However, in this case, the increase in A_0' is clearly not primarily due to solvent effects, because the PBLG polymer has a chemical composition similar to that of the DMF solvent. When we note that A_0 is found to be essentially independent of temperature for similar nitroxides,^{10,14} then the changes in the apparent A_0' with temperature in the results of WM appear to be definitely anomalous.

It is this anomaly, most unequivocal in the results of WM, which first prompted us to consider the possibilities that motional effects in these spectra are leading to inaccuracies, if not a break down, in their interpretation in terms of eq 2. That is, what happens when (1) R_{\parallel} is slow enough and/or (2) R_{\perp} is fast enough to lead to motional effects? It is already known, in the simpler case of isotropic rotation, that an increase in A' may be interpreted in terms of a slowing of the motion of the spin label.¹⁵ Thus, perhaps, in the case of "anisotropically immobilized" spectra, an increase in A_{\parallel}' may be due to a decrease in R_{\parallel} .¹⁶

We have developed, for problems of this sort, a slow motional computer program¹⁷ based on the rigorous theory of FBP.⁹ It allows the principal axes of \mathbf{R} (*i.e.*, x' , y' , and z') to be tilted relative to the principal axes of the magnetic tensors. The irreducible tensor components of \mathbf{A} and \mathbf{g} are then expressed in the x' , y' , z' coordinate system. We take θ to be the angle between z' and z . (Note that ν corresponds to z' .) In our analysis of the results of WM we tilted z' toward x (*i.e.*, the symmetry axis of \mathbf{R} lies in a plane formed by the $2p-\pi$ orbital and the N-O bond).¹⁸ Thus θ is the same as $\cos^{-1}(\alpha_z^2)^{1/2}$ of Hubbell, *et al.*, while $\cos^{-1}(\alpha_x^2)^{1/2}$ is $(\pi/2) - \theta$ and $\cos^{-1}(\alpha_y^2)^{1/2}$ is $\pi/2$.

We show in Figure 1 a set of simulated spectra designed for comparison with the results of WM, some of which are shown in Figure 2 with an illustration of their spin label in Figure 3. The series of spectra shown in Figure 1 (labeled A-I) were computed with a constant value of $R_{\perp} = 3.33 \times 10^6 \text{ sec}^{-1}$ or $\tau_{R_{\perp}} = (6R_{\perp})^{-1} = 5 \times 10^{-8} \text{ sec}$ but with $\tau_{R_{\parallel}}$ ranging from $6 \times 10^{-11} \text{ sec}$ through $5 \times 10^{-8} \text{ sec}$. Further, we have used a value of $\theta = 41.7^\circ$ corresponding to an $S = 0.336$, and this value of S remains unchanged for all the simulations. The spectra were calculated for spatially isotropic distribution of spin labels, *i.e.*, there is no true ordering. We have also prepared a table (*cf.* Table IV) in the manner of Tables I-III, in which the simulations have been analyzed as if they were from anisotropically immo-

TABLE III^a

Spectrum index	t_c^b	T, °C	$A_{ }'$, G	A_{\perp}' , G	$\Delta A'$, G	A_0'	S	$\cos^{-1}(\alpha_z^2)^{1/2}$, deg
F	0.42	Rt ^c	22.5	11.2	11.3	15.0	0.452	37.2
	0.30	Rt	21.3	11.2	10.1	14.6	0.40±	39.1
E	0.20	Rt	21.2	12.0	9.2	15.1	0.368	40.5
		4	22.8	11.6	11.2	15.3	0.448	37.3
	-43	Rt	25.8	10.8	15.0	15.8	0.600	31.1
		Rt	21.1	11.9	9.2	15.0	0.368	40.5
D	0.187	Rt	21.2	11.9	9.3	15.0	0.272	40.3
	0.148	-43	26.4	10.8	15.6	16.0	0.62±	30.1
		Rt	20.6	11.6	9.0	14.6	0.360	40.8
C	0.128	Rt	20.2	11.5	8.7	14.4	0.348	41.2
B	0.092	Rt	19.8	11.7	8.1	14.4	0.32±	42.2
A	0.008	Rt	25.8	10.9	14.9	15.9	0.596	31.2
		-43	25.8	10.9	14.9	15.9	0.596	31.2

^a Data from Table I of Wee and Miller (ref 1). ^b The polymer concentration (volume fraction) in DMF. ^c Rt denotes room temperature.

TABLE IV

Spectrum index	$R_{ } \times 10^4$, sec ⁻¹	$\tau_{R }$, nsec	$A_{ }'$, G	A_{\perp}' , G	$\Delta A'$, G	$A_0'^f$	$\cos^{-1}(\alpha_z^2)^{1/2}$, deg ^e	$g_{ }' - g_{\perp}'$	S^c	$g_{ }'$	g_{\perp}'	$g_0'^d$	$\cos^{-1}(\alpha_z^2)^{1/2}$, deg ^h
A ^a	27.8	0.06	18.9 ⁱ	11.5	7.4	14.0	43.2	-0.0008	0.296	2.0051	2.0059	2.0056	55 ⁱ
B ^a	16.7	0.10	18.9	11.3	7.6	13.8	42.9	-0.0008	0.304	2.0051	2.0059	2.0056	55
C ^a	8.33	0.20	19.2	11.1	8.1	13.8	42.2	-0.0010	0.324	2.0050	2.0060	2.0057	57
D ^a	4.17	0.40	20.2	10.7	9.5	13.9	40.0	-0.0014	0.380	2.0047	2.0061	2.0056	60
E ^a	2.50	0.67	22.6	10.35	12.25	14.4	35.7	-0.0025	0.490	2.0037	2.0062	2.0054	80
F ^a	1.67	1.00	24.1	10.9	13.2	15.3	34.1	-0.0017	0.528	2.0033	2.0058	2.0050	47
G ^a	0.278	6.00	27.3	c						2.0030	c		
H ^b	0.167	10.0	27.7	c						2.0028	c		
I ^b	0.033	50.0	29.75	c						2.0025	c		
J ^b	0 ^d	∞^d	30.8	c						2.0021	c		

^a A peak-to-peak residual derivative width of 1.0 G was used. ^b A peak-to-peak residual derivative width of 3.0 G was used. ^c The inner hyperfine extrema are not resolved. ^d $R_{||}$ and R_{\perp} are 0. ^e S and α_z are defined here by eq 8. ^f A_0' is defined by eq 7. ^g g_0' is defined as $1/2(g_x' + g_y' + g_z')$. ^h From construction $\cos^{-1}(\alpha_z^2)^{1/2} = \pi - 2\theta$. ⁱ If S = 0.336 is used $\cos^{-1}(\alpha_z^2)^{1/2}$ equals 50°, see text. ^j If (30.8 G - 29.75 G) is added to $A_{||}'$ then S = 0.338.²²

bilized spin labels, and we note it exhibits the typical aforementioned trends of the actual experimental results.

Our choice for $\tau_{R\perp}$ is somewhat arbitrary, but we note that τ_R values of about 1.5×10^{-5} and 7.5×10^{-8} sec were estimated by WM for relaxation of and about the helix axis, respectively, of their helical polypeptide (with a weight average molecular weight of 122,000 consisting of an average of 560 monomeric units) from standard equations given by Perrin.^{2,7,19} Note, however that even an isotropic τ_R of 7.5×10^{-8} sec will not significantly decrease the separation of the outer hyperfine extrema below that of the rigid limit (*i.e.*, $A_z \geq A' \geq 0.96A_z$).¹⁵ Thus a comparison of spectra I and J in Figure 1 for an isotropic $\tau_R = 5 \times 10^{-8}$ sec and the rigid limit, respectively, shows that the spectra are not substantially different except for a somewhat broader appearance for spectrum I. The simulation Figure 1I is in good agreement with spectrum Figure 2G of WM, which is for the solid end-labeled polymer near the rigid limit.

We note that the spectrum Figure 2B of WM closely resembles the computed spectra A and B of Figure 1. Apparently the rotational motion about the symmetry axis is very rapid and very unlikely attributable to the much slower motions of the polymer itself where $\tau_R \geq 10^{-7}$ sec. The rotational rate R is typical of that for motion about single covalent bonds (see below). WM have argued that the nitroxide spin label of this end-labeled polymer is only free to rotate about the single covalent bond joining the piperidine ring to the terminal peptide nitrogen (NH-CH bond), and these simulations support their arguments, because it is reasonable that R be taken as the rotational rate about this single bond (*e.g.*, Brevard, *et al.*, determined a correlation time of 1.1×10^{-10} sec for rotation

about a sterically hindered single bond²⁰). Although the internal motion of the nitroxide radical relative to the polymer was considered by WM, they did not appreciate that the changes in the progression of their spectra in Figure 2 were likely due to the slowing of the internal motion of the spin label.

The outer and inner pairs of extrema in Figures 1 and 2 are clearly not spaced about the same field position. This noticeable g factor asymmetry is consistent with a tilt toward the x axis; a corresponding tilt toward the y axis would result in noticeably less g factor asymmetry. The assignment of R to motion about the covalent bond linking the polymer to the piperidine ring is consistent with the rotational symmetry axis being in the xz plane (*i.e.*, in the plane formed by the N-O bond and the $2p-\pi$ orbital of the nitrogen in Figure 3).

As motion about the symmetry axis slows (*i.e.*, R decreases), an increase in the apparent ordering parameter S is seen in the data of Table IV. The increase in S results from an increase in A' , which is eventually not compensated for by a corresponding decrease in A_{\perp}' required by the rotational invariance of A_0' . An increase in the apparent A_0' parallels an increase in apparent S much as in the case of the investigations of membranes and membrane models with the DOXYL radicals (*cf.* Tables I and II). However, for the data of WM (*cf.* Table III), the increase in A_0' which accompanies the increase in S as the temperature is lowered can be taken as a clear indication that the limiting case of a fast τ_R is no longer applicable.

Hubbell, *et al.*, have implied that the first observable effect of incomplete averaging by motion about the symmetry axis is an overall broadening of the spectrum, and the interpretation in terms of \mathcal{H}' of eq 2 and the ordering

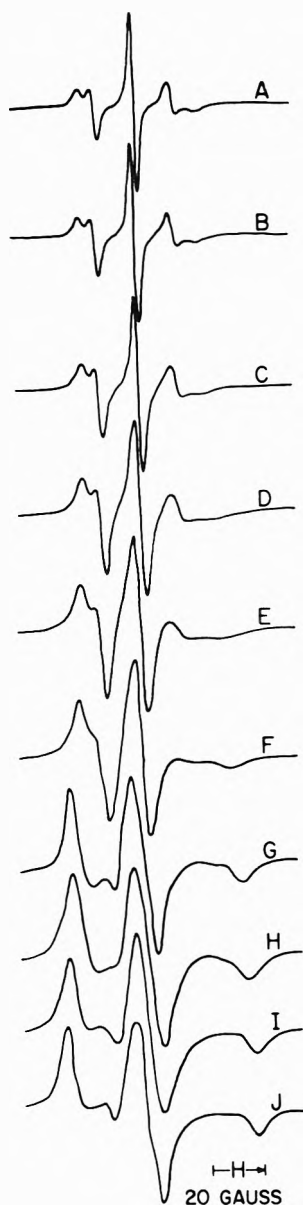


Figure 1. These simulations were computed with the magnetic parameters of the DOXYL spin label where $A_z = 30.8$ G, $A_x = A_y = 5.8$ G, $g_x = 2.0089$, $g_y = 2.0058$, and $g_z = 2.0021$.⁵ The symmetry axis of the rotational-diffusion tensor is defined in the molecular axis system by the angles $\cos^{-1}(\alpha_x^2)^{1/2} = 48.3^\circ$, $\cos^{-1}(\alpha_y^2)^{1/2} = 90.0^\circ$, and $\cos^{-1}(\alpha_z^2)^{1/2} = 41.7^\circ$. $\tau_{R\perp}$ is 5.0×10^{-8} sec and only $\tau_{R\parallel}$ was varied in this series of simulations. In these spectra the resonant magnetic field for $g = 2.0056$ occurs at 3235 G. See Table IV for values of τ_R and residual derivative width used in the simulations.

parameter remains unchanged.^{3b} It is clear from our series of stimulations, that, if τ_R is slow enough to broaden the spectrum, a change in the apparent S will also result. Note that given our analysis, the internal motion of the piperidine ring is only slightly dependent on the bulk viscosity η (or alternatively on polymer concentration). In the series of room temperature spectra Figure 2A through 2F of WM, η has increased considerably more than the order of magnitude that R has decreased, while the spectra at -43° are all quite similar.² The rotational rate R , if identified with the motion of the piperidine ring about the NH-CH bond, implies that θ be identified as the angle between the $2p-\pi$ orbital of nitrogen (molecular z axis) and the linking covalent bond. It appears that this

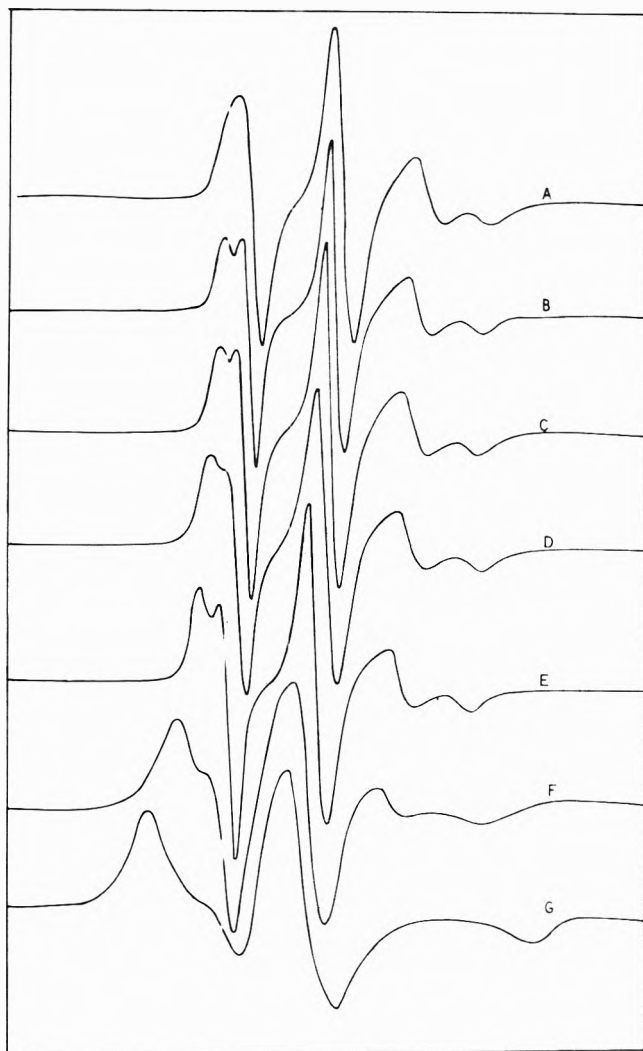


Figure 2. ESR spectra of polybenzylglutamate labeled with 2,2,6,6-tetramethyl-4-aminopiperidine 1-oxyl in dimethylformamide solutions of varying concentrations at room temperature. The polymer concentration (volume fraction) was (A) 0.008, (B) 0.0917, (C) 0.128, (D) 0.148, (E) 0.200, (F) 0.42 (0.5 weight fraction), and (G) 1.0 (solid polymer). (From ref 1, with permission).

tilt angle remains essentially unchanged, through the series of experiments of WM (as assumed in the simulations), which is expected if the tilt angle depends only on the geometry of the piperidine ring. This is supported by the absence of significant changes in the observed spectra due to phase transitions (*i.e.*, transitions between isotropic, biphasic, or liquid crystal phases), plus the fact that the overall motion of the polymer is slow enough so as not to affect the spectrum.

Spectra A and B of Figure 1 are representative of the case where R is large enough to completely average the "time-dependent" part of the Hamiltonian (*i.e.*, $\mathcal{H} - \mathcal{H}^0$) and R_{\perp} is too small to significantly shift the positions of the outer hyperfine extrema. Thus they effectively represent the limiting case of Hubbell, *et al.* One may confirm this by determining the pseudo-axial A' from the computer simulations of Figure 1A and 1B. One then obtains (in the manner of Seelig²¹) an order parameter in good agreement with the value of θ used in the simulations. The discrepancy of 1.5° between θ and the one obtained from S of our simulations probably results from our assumptions of motion due to R_{\perp} .²²

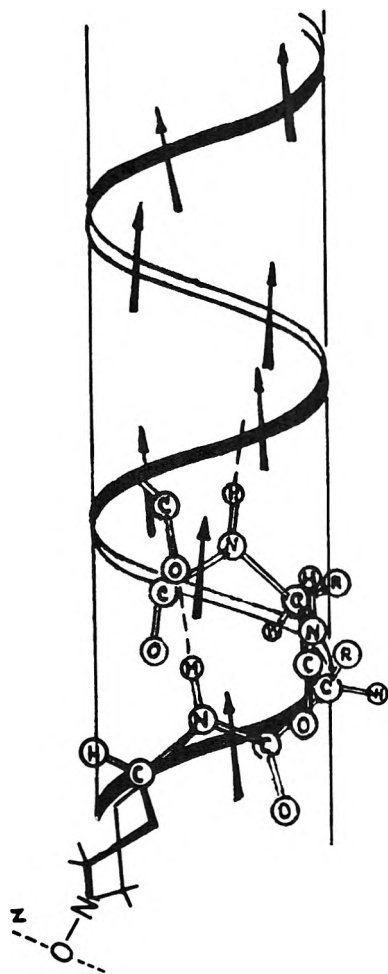


Figure 3. End-labeled polybenzylglutamate, right-handed α -helix. (From ref 1, with permission).

When R is no longer fast enough to average out the "time-dependent" part of \mathcal{H} , then an increase in the apparent S results, as well as eventually an increase in the apparent A_0' . This is clearly seen in Figure 1 and Table IV. This increase in the apparent A_0' is clearly observed in the work of WM. We again emphasize that θ , hence the true S , is unchanged in our simulations.

If R is the rotational rate of the piperidine ring about the covalent bond attaching the spin label to the polymer, an Arrhenius-type dependence of R is expected.^{23,24} The similarities between the spectrum of Figure 2B of WM and Figure 1B imply a R for the piperidine ring of about $1.67 \times 10^9 \text{ sec}^{-1}$ at room temperature and a volume fraction of 0.0917. Likewise, the similarities between Figure 2F of WM and Figure 1F imply a R of about $1.67 \times 10^8 \text{ sec}^{-1}$. Note that Figure 2F of WM resembles all their spectra at -43° .² Thus one may use the same value of R for -43° . One then estimates an activation energy of 1.9 kcal/mol from these results, which is a reasonable value for the rotational barrier about a single bond.²⁰ WM do not provide enough temperature-dependent data to otherwise confirm an Arrhenius-type behavior.

There is one aspect of our computer simulations which differs somewhat from the experimental spectra of WM. That is, our simulations show somewhat excessive width and related reduced amplitude of the outer hyperfine extrema. This clearly indicates that a $\tau_{R\perp}$ of $5.0 \times 10^{-8} \text{ sec}$ is too short; a longer value of τ_R would narrow these ex-

trima and improve agreement with observed amplitudes. Also, as already noted, the positions of the hyperfine extrema would not be significantly shifted. We have already called attention to the opposite discrepancy in comparison with results of Hubbell and McConnell, and this could mean a $\tau_{R\perp}$ on the order of $5.0 \times 10^{-8} \text{ sec}$ in their systems.

We wish to emphasize that from our above analysis, even if eq 7 is fulfilled, our simulations Figure 1A-E and Table IV show that substantial changes in apparent S can occur without a real change in θ as a result of a slowing of R . It is clear, then, that changes in apparent S can result from a slowing of the motion about ν as well as a change in $\cos^{-1}(\alpha_z^2)^{1/2}$ (*i.e.*, the mean angular deviation between ν and z). Therefore the invariance of $\text{Tr } A$ is a necessary, but not sufficient, condition that motion about ν be sufficiently rapid to permit the spectrum to be analyzed in terms of the effective static Hamiltonian of eq 2. It would appear that the rotational rates expected for covalent single bonds at room temperature are not, in general, fast enough to fulfill this condition.

Even in DOXYL spin label membrane systems where A_0' is independent of S^{13} and/or temperature,¹² the quantitative interpretation of the variations in S based upon eq 2-8 is uncertain, because the condition that trace (A) be invariant is a necessary, but not sufficient, condition. In any case, a change in S can arise from a real change in the angle between ν and z or a change in the rotational rate about ν as is the predominant phenomenon in the remaining spectra of WM. In general, these two phenomena cannot be distinguished unless the rotational rate about ν slows to where A_0' is clearly anomalous, and/or the slowed motion manifests itself in the other spectral characteristics illustrated in Figure 1. Note the difference in the spectra A and B of Figure 2 has been shown by computations to arise from a shorter $\tau_{R\perp}$ of about $3.0 \times 10^{-8} \text{ sec}$ for spectrum A. Apparently at infinite dilution the motion of the polymer is significant. Calculations of a statistical mechanical variety of S itself are not always fully justified, since, in general, it cannot be proved that changes in S did not arise from a change in the rotational rate about ν .²⁵ However, the alternative of careful analysis of the complete spectrum holds open the possibilities of obtaining considerable information of interest.

At this point it should be emphasized that the widely used interpretation of S as a qualitative indication of the viscosity or the "fluidity" of the environment of the spin label is not changed.

One should, of course, recognize that our above analysis in terms of a single R and R_\perp represents a considerable simplification of the complex dynamics of polymer motion as well as localized bond motions, including internal rotations. A somewhat more complete analysis would, for example, include the coupling of the internal rotation of the piperidine C-N bond to the overall anisotropic rotation of the helical polymer requiring the specification of R for the polymer, a τ_R for the bond rotation as well as the tilt angle θ .^{26,27} However, as long as the internal rotation is much faster than the overall motion, it can be treated as uncoupled from the latter. Also, to the extent that the overall motion is only showing marginal spectral effects, it would be difficult to obtain anything more precise than an effective R_\perp , as we have done above, as opposed to an actual R tensor. Of course, in principle, there are the helical flexing modes of motion, which are also slow, and which would be contributing to that quantity we refer to as an effective R_\perp . Finally, in this regard, we note the impor-

tance of localized cooperative modes of relaxation for the polymer motions even in isotropic polymer solutions of moderate concentration, and it becomes even more important in liquid-crystalline phases (*cf.* ref 17, 24, and 28). We also note that our analysis implies the internal rotation is Brownian, while a more complete analysis would include potential barriers and the possibilities of reorientation by jumps of substantial angle. Thus our analysis given above may be regarded as the first approximation to the motional corrections to the effective time-independent approach of Hubbell, *et al.*

In conclusion, we call attention to the fact that spectra of the "anisotropically immobilized" type do exhibit interesting dependencies on the molecular dynamics of the spin label, and phenomena related to motion about the symmetry axis of the rotational-diffusion tensor and even transverse to the symmetry axis have been observed experimentally but not generally recognized as such.

Acknowledgment. We wish to thank Professor Wilmer G. Miller for supplying his experimental figures and his permission to reproduce them and for helpful discussions concerning spin-labeled polypeptides.

References and Notes

- (1) (a) Supported in part by grants from the National Science Foundation (Grant No. GP-13780), The Petroleum Research Fund administered by The American Chemical Society, and by the Cornell University Materials Science Center. (b) NIH Postdoctoral Fellow. (c) NIH Predoctoral Fellow.
- (2) E. L. Wee and W. G. Miller, *J. Phys. Chem.*, **77**, 182 (1973).
- (3) (a) W. L. Hubbell and H. M. McConnell, *Proc. Nat. Acad. Sci. U.S.A.*, **63**, 16 (1969); (b) *ibid.*, **64**, 20 (1969).
- (4) H. M. McConnell and B. G. McFarland, *Quart. Rev. Biophys.*, **3**, 91 (1970).
- (5) W. L. Hubbell and H. M. McConnell, *J. Amer. Chem. Soc.*, **93**, 314 (1971).
- (6) B. G. McFarland and H. M. McConnell, *Proc. Nat. Acad. Sci. U.S.A.*, **68**, 1274 (1971).
- (7) J. H. Freed, *J. Chem. Phys.*, **41**, 2077 (1964).
- (8) R. P. Mason and J. H. Freed, *J. Phys. Chem.*, **78**, 1321 (1974).
- (9) J. H. Freed, G. V. Bruno, and C. F. Polnaszek, *J. Phys. Chem.*, **75**, 3385 (1971).
- (10) S. A. Goldman, G. V. Bruno, C. F. Polnaszek, and J. H. Freed, *J. Chem. Phys.*, **56**, 716 (1972).
- (11) J. Seelig and W. Hasselbach, *Eur. J. Biochem.*, **21**, 17 (1971).
- (12) S. Eletr, D. Zakim, and D. A. Vessey, *J. Mol. Biol.*, **78**, 351 (1973).
- (13) J. Seelig, H. Limacher, and P. Bader, *J. Amer. Chem. Soc.*, **94**, 6364 (1972).
- (14) R. P. Mason, J. Hwang, and J. H. Freed, submitted for publication.
- (15) S. A. Goldman, G. V. Bruno, and J. H. Freed, *J. Phys. Chem.*, **76**, 1858 (1972).
- (16) McConnell, *et al.*, note that the lower limit on R required for complete averaging depends markedly upon $\cos^{-1}(\alpha_z^2)^{1/2}$. If $v_{11}z$, then $\cos^{-1}(\alpha_z^2)^{1/2} = 0$, and for $A_x = A_y$, the only anisotropy to be averaged to produce axial symmetry is simply due to g . Thus $R_{11} \gg \hbar^{-1} \cdot (g_x - g_y)\beta|B_0 \sim 1.4 \times 10^7 \text{ sec}^{-1}$. While, if $v_{11}z$, then $\cos^{-1}(\alpha_z^2)^{1/2} = \pi/2$ and one requires $R \gg 7 \times 10^7 \text{ sec}^{-1}$.
- (17) C. F. Polnaszek, Thesis, Cornell University, 1974. One may take advantage of the large anisotropy in R to truncate the eigenfunction expansions for the simulations in the "quantum number K ." Truncation at $K = 2$ is nearly equivalent to treating the time-dependent fluctuations of $\{3C' - 3C\}$ by perturbation theory (see ref 6).
- (18) Although a tilt of R toward the x axis (*i.e.*, the N-O bond) can be distinguished from the tilt toward the y axis, in practice g_{\parallel}' and g_{\perp}' are not as useful as A_{\parallel}' and A_{\perp}' because the anisotropy is not as great for g .
- (19) F. Perrin, *J. Phys. Radium*, **7**, 497 (1934).
- (20) Ch. Brevard, J. P. Kintzinger, and J. M. Lehn, *Tetrahedron*, **28**, 2447 (1972).
- (21) J. Seelig, *J. Amer. Chem. Soc.*, **92**, 3881 (1970).
- (22) The apparent A_z (or A_{\parallel}') is reduced by 1.05 G from its rigid limit value by an isotropic $\tau_R = 5 \times 10^{-8} \text{ sec}$.¹⁴ If 1.05 G is added to A_{\parallel}' , the calculated S becomes 0.338 in near perfect agreement with the expected value of 0.336 for $\theta = 41.7^\circ$. Note, α_z^2 , and therefore S are most sensitive to changes in angles when $\cos^{-1}(\alpha_z^2)^{1/2}$ is near 45° .
- (23) W. Kominski and K. Mobius, *J. Magn. Resonance*, **5**, 182 (1971).
- (24) J. H. Freed, *Ann. Rev. Phys. Chem.*, **23**, 265 (1972).
- (25) Rotational diffusion of the DOXYL ring about the long (amphiphilic) molecular axis of the spin-labeled fatty acid need not be as rapid as in the case of the spin-labeled polymer to meet the condition that R_{\parallel} be appropriately rapid, because ν is generally closer to the direction of z about which the hyperfine tensor is already symmetric, and only the g anisotropy must be averaged to zero.
- (26) D. E. Woessner, B. S. Snowden, Jr., and G. H. Meyer, *J. Chem. Phys.*, **50**, 719 (1969).
- (27) D. Wallach, *J. Chem. Phys.*, **47**, 5258 (1967).
- (28) C. F. Polnaszek, G. V. Bruno, and J. H. Freed, *J. Chem. Phys.*, **58**, 3185 (1973).

Proton Magnetic Resonance Study of Molecular Interactions in Solutions of Fluoranthene in Carbon Tetrachloride and Cyclohexane

K. D. Bartle,

School of Chemistry, University of Leeds, Leeds LS2 9JT, England

R. B. Mallion,

Jesus College, Oxford, England

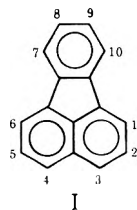
D. W. Jones,* and C. K. Pickles

School of Chemistry, University of Bradford, Bradford BD7 1DP, England (Received February 4, 1974)

The occurrence of solute-solute and solvent-solute interactions in solutions of fluoranthene (I) in carbon tetrachloride and cyclohexane has been investigated with the aid of 60- and 100-MHz high-resolution pmr and ultraviolet spectra. Pmr dilution shifts for the protons of I are large and closely similar for CCl₄ and cyclohexane solutions; plots of shift against concentration can be explained by self-association of I only if a large dimerization shift is assumed. Intermolecular π -electron "ring-current" shielding calculations for simple "staggered" and "eclipsed" parallel-orientation models for I molecules in CCl₄ and cyclohexane solutions favor eclipsed (or head-to-head) solute stacking. The postulation of this loose but specific time-averaged interaction correctly leads to the prediction that H-1 has the largest and H-8 the smallest pmr dilution shift. While the ultraviolet spectra of I and CCl₄ in cyclohexane are consistent with formation of a contact charge-transfer complex, a Scatchard plot of Δ_{obsd} (the pmr chemical shift in CCl₄-cyclohexane mixtures minus the shift in pure cyclohexane) leads to an equilibrium constant, K' , for "sociation" over and above this random interaction effect, close to zero.

Introduction

Differential proton magnetic resonance (pmr) dilution chemical shifts¹⁻⁶ in polynuclear aromatic hydrocarbons and heterocycles are well known and have been explained qualitatively, and in the case of benz[a]pyrene⁴ semi-quantitatively,⁵ by partial alignment of neighboring solute molecules in solution. Such loose associations have received little study in terms of more specific molecular interactions, and we now attempt to account in this way for the marked and different dilution shifts³ exhibited by the five proton types of fluoranthene (I), with its rather high solubility in some organic solvents.



Charge-transfer species have been reported in solutions of aromatic hydrocarbon electron donors in halogenomethanes;^{7,8} an investigation⁸ of complexes between polynuclear aromatic hydrocarbons and carbon tetrachloride did not include I. The spectroscopic measurements of I in solution reported here represent a contribution toward resolving the intriguing problems of weak interactions of planar molecules.

Experimental Section

Fluoranthene (Koch-Light Puriss grade) was recrystallized to constant melting point (382.5–383.2 K; lit.⁹ 382.5–383.5 K). Solutions were made up in spectroscopic-

grade carbon tetrachloride, cyclohexane, and *n*-hexane by weight/volume so that concentrations could be expressed in either mole fraction or molar. The composition of solvent mixtures after spectroscopy was checked by gas chromatography on a 1 m \times 5 mm column packed with 15% diisodecylphthalate on 60-80 mesh Chromosorb P. Solutions of acenaphthylene (II) and acenaphthene (III) (as in ref 10) were made up by weight in carbon tetrachloride.

Pmr spectra were recorded on Varian A-60 and HA-100 spectrometers; solutions contained 1% tetramethylsilane (TMS). A-60 spectra were calibrated against the separation between the resonances of a solution of 2% benzene-2% TMS in carbon tetrachloride checked against an Advance TC2 timer/counter. HA-100 spectra were calibrated by TMS sidebands, which also provided the lock signal; probe temperatures were measured from the separation between the resonances of methanol.¹¹ Intermolecular "ring-current" shieldings were calculated, with the program NPRC,^{5,12} on the Oxford University KDF 9 computer.

Ultraviolet (uv) spectra were recorded on Unicam SP 800 and Beckman DB recording spectrophotometers for 1-cm matched silica cells at room temperature. For reference, *n*-hexane or cyclohexane was generally used or, in some cases, a solution of carbon tetrachloride at the same concentration as that in the sample cell.

Results and Discussion

Solute-Solute Interaction. Chemical shifts^{3,13} in the pmr spectra of I were plotted against concentration (per cent w/w) in carbon tetrachloride. The dilution shifts (Table I) were confirmed by plotting peak positions from 100-MHz spectra (taken at 304 K) against the molarity of four solutions of I in carbon tetrachloride (Figure 1), a

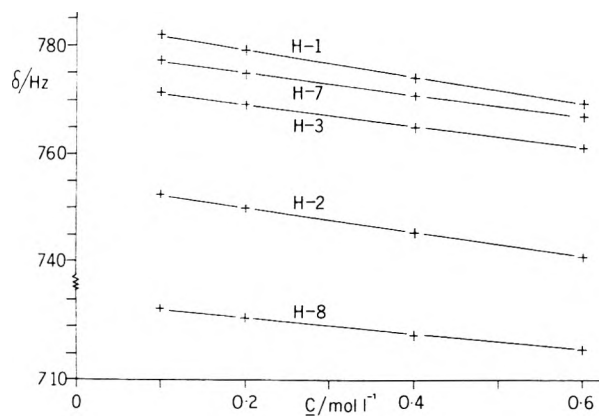


Figure 1. Graphs of positions (in Hz downfield from TMS) of 100-MHz H-1, H-2, H-3, H-7, and H-8 peaks of fluoranthene (I) vs. molarity in carbon tetrachloride solution at 304 K.

TABLE I: Dilution Shifts^a for the Protons of Fluoranthene

	Carbon tetrachloride solution			Cyclohexane solution (this work)	
	This work (Figure 1), Hz M ^{-1b}	Ratio	Ratio ^c (from data in ref 3 and 13)	Hz M ^{-1b}	Ratio
H-1	24.7	1.71	1.90	30.0	2.0
H-2	22.8	1.58	1.63	25.0	1.6
H-3	20.0	1.39	1.49	23.0	1.5
H-7	19.9	1.38	1.46	23.0	1.5
H-8	14.4	1	1	15.1	1

^a Positive sign denotes increased shielding with increasing concentration.

^b Based on peak positions. Least squares; correlation coefficient 0.999 in all cases. ^c Based on concentrations in per cent w/w; see text.

procedure which can give similar results when shifts deduced from complete, second-order spectral analyses are used; Table I includes the gradients of these apparently linear graphs. With cyclohexane as the solvent, poor solubility of I limited measurements to three concentrations up to 0.145 M (gradients are also given in Table I). In earlier work, assignment of chemical shifts in I was based³ in part on the assumption of there being a similar "ring current" in the five-membered ring to that of benzene. The very approximate nature¹⁴ of this assumption does not, however, appear to invalidate the original assignments; since the calculated Coulson bond order of C(2)-C(3) is larger than that for C(1)-C(2), it follows^{15,16} that $J_{23} > J_{12}$, so that, from the spectral analysis, $\delta_1 > \delta_3$; this assignment is supported by the spectra of 1- and 3-methylfluoranthenes (IV and V) in carbon disulfide solution. First-order analysis by Clar, *et al.*, from double-resonance experiments gives¹⁷ $\delta_2 = 7.18$, $\delta_3 = 7.51$ ppm for IV and $\delta_1 = 7.60$, $\delta_2 = 7.23$ ppm for V; if it is assumed that the *m*-methyl shielding is the same in both IV and V, these comparisons suggest that H-1 is at lower field in the "parent" hydrocarbon.

The influence of temperature (273-323 K) on peak positions of I (0.2 M) in carbon tetrachloride was also investigated. Small linear high-field shifts, only partly explicable^{18a} in terms of the change in volume of the solution, are observed for the protons in I, with decreasing temperature, as follows (shifts in Hz K⁻¹, at 100 MHz; least-squares correlation coefficients are in parentheses): H-1, 0.024 (0.987); H-2, 0.028 (0.998); H-3, 0.031 (0.997); H-7, 0.010 (0.974); and H-8, 0.026 (0.995).

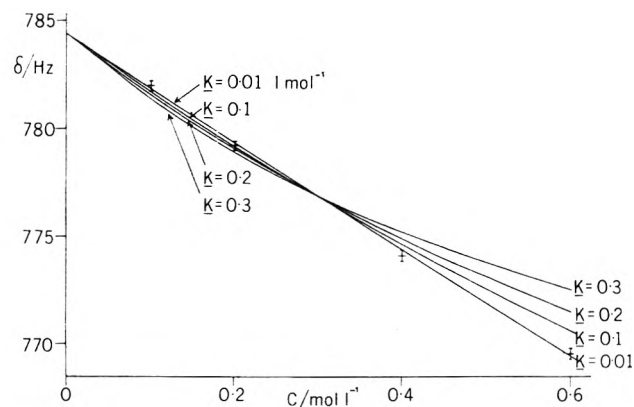


Figure 2. Comparison of experimental H-1 shifts (in Hz) at a series of concentrations (molar) of I in carbon tetrachloride, with dilution curves calculated for several pairs of values of equilibrium constant, K , and dimer shift, ν_d .

TABLE II: Maximum Values of Apparent Equilibrium Constants, K , for Dimerization of Fluoranthene in Carbon Tetrachloride Solution with the Range of Associated Values of Shift Difference, $(\nu_m - \nu_d)$, between Monomer and Dimer

Proton	K, M^{-1}	$(\nu_m - \nu_d)$, ppm
H-1	0.03 ± 0.01^a	3.3 - 6.4 ^a
H-2	0.02 ± 0.01	3.7 - 10.9
H-3	0.02 ± 0.01	3.4 - 10.1
H-7	0.03 ± 0.01	2.7 - 5.3
H-8	0.04 ± 0.01	1.5 - 2.5

^a Errors based on precision of ± 0.3 Hz in peak position measurements in spectra.

The pmr dilution shifts could be a consequence of association between fluoranthene molecules in solution. Of several methods available for determining association constants for monomer/dimer equilibria from pmr measurements, an approach analogous to that of Purcell, *et al.*,¹⁹ involves determination of the association constant, K , via eq 1; this is easily derived with the only (but necessary) assumption that the dilution shift is due exclusively to dimerization and that ν_{obsd} is a weighted average of the shifts at infinite dilution of monomer (ν_m) and dimer (ν_d) (which are constant throughout the concentration range)

$$\nu_{\text{obsd}} = (\nu_m + 2\nu_d K c_m)(1 + 2K c_m)^{-1} \quad (1)$$

where c and c_m are overall and monomer concentrations of I, respectively.

Equation 1 was used to generate pairs of values of K and ν_d from the mid-range value of c for CCl₄ solutions of I (0.3 M) and ν_m . Comparison of the full calculated dilution curve with experiment (*e.g.*, Figure 2) was then possible. Least-squares methods¹⁹⁻²¹ are unnecessary since the linear nature of our plot makes comparison of the full calculated dilution curve with experiment straightforward. While a number of combinations of K and ν_d fitted the observed curve, an upper limit of $0.03 \pm 0.01 M^{-1}$ could be fixed on K . Larger values of K gave substantially curved plots, outside the limits of experimental error.

While consistent, small (but finite) values of an association constant can thus be determined for both CCl₄ and cyclohexane solutions commensurate with the small influence of temperature, considerable doubt is thrown on their significance by the values of ν_d required in this model (Table II). Molecular-orbital calculations (*vide infra*) suggest that maximum intermolecular shielding values for the protons of dimers of I are smaller by at least an order of magnitude. Moreover, the fundamental as-

sumption in determining K by the pmr method that ν_m and ν_d are both independent of c may be in serious error for solutions of I, in which medium effects may intrude.²² Randomly distributed, but still strongly anisotropic, solute molecules are likely to shield the protons of both I monomer and dimer more strongly than those of the reference.

It was concluded, therefore, that the apparently linear dilution curves for I can be explained by a formal association model only if much too large an association shift is assumed, and if medium effects are taken into account. Accordingly, we sought an explanation based on a more loose structuring of solutions of I.

Molecular-Orbital Calculations of Intermolecular "Ring-Current" Effects. Intermolecular proton chemical shifts in I are likely to be dominated by effects arising from the simple (but essentially classical) concept of π -electron "ring currents,"^{23-25a} postulated to be induced in conjugated molecules in the presence of an external magnetic field which has a component perpendicular to the molecular planes. We attempt here to rationalize the rather striking pattern of observed³ dilution shifts in I solutions by means of a "ring-current" model in which, over a time average, solute-solute interactions are nonrandom, but fall short of actual complexing, so that association constants are not derived. Dilution shifts in azulene,¹ phenanthrene,² benz[*a*]pyrene,^{4,5} and dibenzothiophen⁶ have been accounted for by such a model, in which pairs of neighboring solute molecules are "stacked" symmetrically with their planes roughly parallel, an orientation which represents the cumulative effect of many encounters. There is some formal analogy with the interpretation of the aromatic-solvent-induced shift (ASIS) for protons of a polar solute in terms of a time-averaged cluster^{25b} of solvent molecules: in our case, increased concentration of the nonpolar solute I replaces addition of aromatic solvent. In neither case are specific complexes postulated.

Accordingly, in performing these calculations, we take the following crude model^{4,5} for the relative orientation of I solute molecules in CCl_4 and cyclohexane: we consider the instant when two neighboring molecules approach with their planes parallel; for simplicity, it is further assumed that the two molecules are orientated so that they are exactly superposed, when viewed along the normal to their molecular planes ("head-to-head" or "eclipsed" orientation). Then, with the molecules in this position, the shielding at each proton in one molecule by the ring-current anisotropy of the other molecule was calculated. The effects of previously calculated¹⁴ ring-current intensities for the various rings in one molecule of I on the proton chemical shifts of a neighboring I molecule were estimated by a procedure described elsewhere.^{12,26}

It is assumed⁵ that the process of dilution can be represented as an increase in the average separation, l , between the parallel molecular planes of neighboring solute molecules, and the above calculation was repeated for a different intermolecular separation; the process was continued for $l = 2.5$ – 8.0 C–C bond lengths. The calculated shieldings (expressed, as is conventional,^{5,12,25a} relative to the intramolecular ring-current shielding calculated to be experienced by a standard benzene proton) were then plotted against l^{-1} for each of the five chemically non-equivalent protons in the molecule. This procedure was repeated but with one of the molecules in the "dimer" pair rotated 180° before the "separating" process was begun (head-to-tail or staggered orientation).

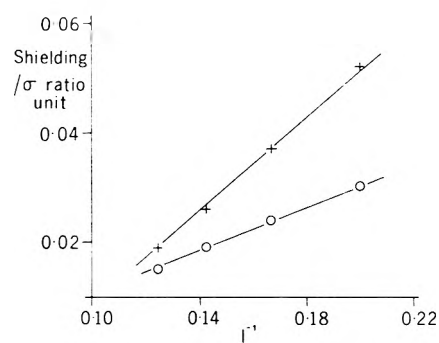


Figure 3. Graph of intermolecular shielding (in σ ratio units³³) for I (in eclipsed orientation) vs. reciprocal of intermolecular separation (l , C–C bond length units) for (i) H-1 (+), the proton most susceptible to dilution effects, and (ii) H-8 (O), the proton least susceptible.

TABLE III: Ratios of Gradients of Plots of Calculated Intermolecular Ring-Current Shielding against Reciprocal of Intermolecular Separation for Fluoranthene

Proton	Eclipsed orientation (i)	Staggered orientation (ii)
H-1	1.7	0.8
H-2	1.4	0.5
H-3	1.7	0.5
H-7	1.5	1.2
H-8	1	1

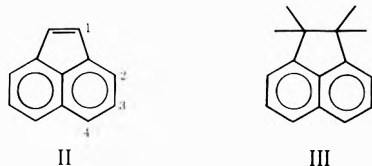
In confining attention to the increase in the average separation between the parallel molecular planes of the neighboring solute molecules,⁵ we are considering an l^{-1} dependence; dilution, of course, varies according to l^{-3} . In any case, even in the most concentrated I solution used in this work, the average intermolecular separation (22 C–C bond lengths) is much greater than that for which intermolecular ring-current shielding is significant (ca. 8 C–C bond lengths). Only a small proportion of (closer) intermolecular contacts would thus appear to influence shielding and, since the dependence of this fraction on the mean separation is unknown, no accurate representation seems possible of the relation between l and concentration. Thus we attempt to predict only the relative pattern of dilution shifts between the individual protons of this one particular molecule.

Figure 3 shows plots of calculated intermolecular shielding (eclipsed orientation) for the protons most (H-1) and least (H-8) susceptible to dilution effects (Table I). These graphs were very nearly straight lines; for the purpose of this calculation, their gradients (from correlation coefficients of >0.998) were taken to be some semi-quantitative measure of how the intermolecular ring-current effect on each proton might vary with dilution.⁵

In view of the very complex process of dilution and solute-solute interaction, our only extenuation for adopting this procedure is its convenience in providing at least a crude model for rationalizing quantitatively how the dependence of intermolecular shielding might vary from one proton to another within this one molecule. For the model with the molecules in both the eclipsed and staggered orientations, Table III lists these shielding ratios relative to such a "calculated dilution shift" for H-8. Comparison with Table I shows that, on the eclipsed model, H-1 is correctly predicted to have the largest and H-8 the smallest dilution shift, though Table III wrongly predicts that H-3 should be shifted as much as H-1. In view of the

marked influence which relative orientation has on the calculated intermolecular shieldings (columns i and ii of Table III), it is possible that a very small perturbation from the perfectly eclipsed i orientation may be enough to account for the H-1/H-3 discrepancy.

Qualitative support for model i for fluoranthene (I) is provided by dilution data for the similarly shaped II and III in carbon tetrachloride.¹⁰ In II, aromatic proton peaks



for H-2 to H-4 have dilution shifts between 0.46 and 0.57 Hz (per cent w/w)⁻¹ at 60 MHz, but for the olefinic H-1, more remote from the shielding influences of the aromatic rings in an eclipsed stacking arrangement, the shift is about half this, 0.24 Hz (per cent w/w)⁻¹. In III solutions, projections of an sp³ bonded H-1 below the ring plane expose it more to the "shielding cone"²⁶ of the aromatic rings of proximate stacked molecules than H-1 of II. Dilution shifts for III at 60 MHz are peaks H-2, H-3, H-4, 0.40–0.62 Hz (per cent w/w)⁻¹; H-1, 0.56 Hz (per cent w/w)⁻¹.

Solute-Solvent Interactions. Pmr and Uv Spectroscopy. Davis and Farmer⁸ interpreted uv spectral changes in alternant polynuclear hydrocarbons as evidence of specific interactions which have intrinsic interest. They found that, in high CCl₄ concentrations, the peak intensity of the strong polycyclic hydrocarbon band, designated β by Clar,²⁷ was reduced.

For a 3.2 × 10⁻⁵ M solution of I in *n*-hexane, addition of from 3.2 × 10⁻⁵ to 3.2 × 10⁻³ M carbon tetrachloride left the uv spectrum unchanged (except, of course, for the strong carbon tetrachloride absorption). In later experiments with a 2.4 × 10⁻⁵ M solution of I in cyclohexane and much higher (1.00–4.15 M) carbon tetrachloride concentration the p band (358 nm) was unchanged in position, intensity, and breadth. However, the β band (287.5 nm) and its neighbors were progressively broadened toward shorter wavelengths, as was observed for the β band in anthracene and other polynuclear hydrocarbons.⁸ Since the long-wavelength tail of the carbon tetrachloride absorption would mask any reduction in peak intensity, an equilibrium constant for association could not be derived. The absence in all solutions of any new charge-transfer band apparently rules out any true complex. The effects observed in the uv spectrum of I in the presence of carbon tetrachloride can be explained by encounter between free hydrocarbon and solvent molecules without specific interaction.²⁸

Pmr measurements can reveal the degree of "socialization"²⁹ of donor and acceptor: the excess association (with equilibrium constant *K'*) over that obtaining in a random mixture. Peak positions were therefore measured for six 0.145 M solutions of I in cyclohexane, containing different concentrations of carbon tetrachloride up to 100%. Then, if the mole fraction of carbon tetrachloride, *x*(CCl₄) ≫ *x*(fluoranthene), and if Δ_{obsd} is the chemical shift in CCl₄-cyclohexane mixture minus the shift in cyclohexane alone, then

$$\Delta_{\text{obsd}}/x(\text{CCl}_4) = -K'(\Delta_{\text{obsd}} - \Delta_c) \quad (2)$$

where Δ_c is the shift of pure complex relative to the unassociated state.

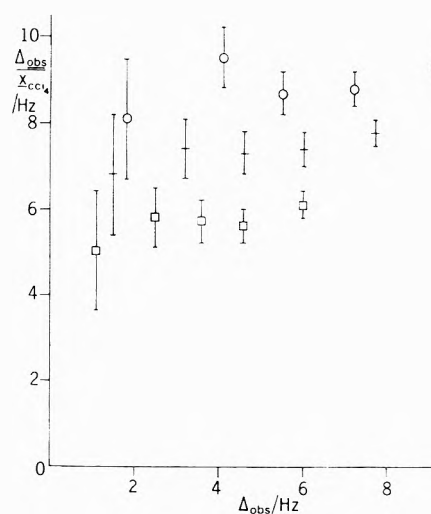


Figure 4. Scatchard graph $\Delta_{\text{obsd}}/x(\text{CCl}_4)$ vs. Δ_{obsd} for addition of carbon tetrachloride to 0.145 M I in cyclohexane. Δ_{obsd} is the chemical shift (in Hz) of H-1(O), H-3(+), and H-8(□) of I in carbon tetrachloride-cyclohexane mixture, minus the corresponding shift of cyclohexane; $x(\text{CCl}_4)$ is the mole fraction of carbon tetrachloride.

TABLE IV: Apparent Equilibrium Constants, *K'*, for Complex Formation between 0.145 M Fluoranthene and Carbon Tetrachloride in Cyclohexane Solution, Derived from Plots of Δ_{obsd} (Mole Fraction of CCl₄)⁻¹ against Shift, Δ_{obsd}

Proton	<i>K'</i> , mole fraction ⁻¹
H-1	0.02 (±0.13) ^a
H-2	-0.09 (±0.06)
H-3	-0.09 (±0.05)
H-7	0.06 (±0.16)
H-8	-0.08 (±0.09)

^a Standard errors in parentheses.

A Scatchard³⁰ plot (Figure 4) of $\Delta_{\text{obsd}}/x(\text{CCl}_4)$ against Δ_{obsd} yields $-K'$ as the slope.^{31,32} If the point corresponding to lowest *x*(CCl₄) is excluded, since the condition that *x*(CCl₄) ≫ *x*(fluoranthene) no longer holds, unweighted regression leads to effectively zero values of *K'* (Table IV). Thus pmr suggests no greater degree of association between CCl₄ and fluoranthene than the random interaction which gives rise to the effects observed in the uv spectrum.

Conclusions

Similarity of dilution shifts in the pmr spectra of I in carbon tetrachloride and cyclohexane solutions, as well as the actual pattern of differential solute dilution shifts among the various protons of I observed in each solvent, can be rationalized in terms of head-to-head (eclipsed) solute stacking during close intermolecular contact. Relative dilution shifts calculated, on the basis of such a model, as being due to intermolecular ring-current shieldings, are in fair agreement with experiment. However, reproducing the absolute values of such experimental shieldings via the present model is feasible only if it is assumed that very large shieldings are sensed during brief molecular encounters in which neighboring solute molecules are in much closer proximity than their time-averaged separation.

Interpretation of our experimental observations in terms of such partial alignment of neighboring solute molecules of I in carbon tetrachloride or cyclohexane solution thus

reinforces suggestions that some polynuclear hydrocarbons¹⁻⁵ and their heterocyclic analogs⁶ tend to orientate in solution with long axes parallel; this is somewhat analogous to explanations^{25b} of the ASIS in terms of a solvation model.

Although uv suggests a weak interaction, pmr affords no evidence of formal association of I with CCl₄.

Acknowledgments. We thank Dr. D. Shaw for recording the 100-MHz spectra, and acknowledge helpful discussions with Dr. P. A. Jones. R. B. M. is grateful to the late Professor C. A. Coulson for the hospitality of his Group at the Mathematical Institute, University of Oxford, and to the Science Research Council for a Research Fellowship.

References and Notes

- (1) W. Schneider, H. J. Bernstein, and J. A. Pople, *J. Amer. Chem. Soc.*, **80**, 3497 (1958).
- (2) K. D. Bartle and J. A. S. Smith, *Spectrochim. Acta, Sect. A*, **23**, 1689 (1967).
- (3) K. D. Bartle, D. W. Jones, and J. E. Pearson, *J. Mol. Spectrosc.*, **24**, 330 (1967).
- (4) C. W. Haigh and R. B. Mallion, *J. Mol. Spectrosc.*, **29**, 478 (1969).
- (5) R. B. Mallion, Ph.D. Thesis, University of Wales, 1969.
- (6) K. D. Bartle, D. W. Jones, and R. S. Matthews, *Tetrahedron*, **27**, 5177 (1971).
- (7) R. Anderson and J. M. Prausnitz, *J. Chem. Phys.*, **39**, 1225 (1963).
- (8) K. M. C. Davis and M. F. Farmer, *J. Chem. Soc. B*, 859 (1968).
- (9) I. Heilbron, Ed., "Dictionary of Organic Compounds," 4th ed., Eyre and Spottiswoode, London, 1965, p 144.
- (10) K. D. Bartle and D. W. Jones, *J. Mol. Spectrosc.*, **32**, 353 (1969).
- (11) A. L. Van Geet, *Anal. Chem.*, **40**, 2227 (1968).
- (12) C. W. Haigh and R. B. Mallion, *Mol. Phys.*, **22**, 955 (1971).
- (13) M. L. Heffernan, A. J. Jones, and P. J. Black, *Aust. J. Chem.*, **20**, 589 (1967).
- (14) R. B. Mallion, *J. Mol. Spectrosc.*, **35**, 491 (1970).
- (15) N. Jonathan, S. Gordon, and B. P. Dailey, *J. Chem. Phys.*, **36**, 2442 (1962).
- (16) K. D. Bartle, D. W. Jones, and R. S. Matthews, *J. Mol. Struct.*, **4**, 445 (1969).
- (17) E. Clar, A. Mullen, and U. Sanigök, *Tetrahedron*, **25**, 5639 (1969).
- (18) (a) The change in density^{18b} of CCl₄ between 273 and 323 K corresponds to the following shifts (Hz K⁻¹ at 100 MHz) H-1, 0.006; H-2, H-3, H-7, 0.005; H-8, 0.003. (b) J. Timmermans, "Physico-Chemical Constants of Pure Organic Compounds," Elsevier, New York, N. Y., 1950.
- (19) J. M. Purcell, H. Susi, and J. R. Cavanaugh, *Can. J. Chem.*, **47**, 3655 (1969).
- (20) L. F. Blackwell, P. D. Buckley, K. W. Jolley, and I. D. Watson, *Aust. J. Chem.*, **25**, 67 (1972).
- (21) S. J. Hu and S. I. Miller, *Org. Magn. Resonance*, **5**, 197 (1973).
- (22) F. Smith and I. Brown, *Aust. J. Chem.*, **26**, 705 (1973).
- (23) L. Pauling, *J. Chem. Phys.*, **4**, 673 (1936).
- (24) F. London, *C. R. Acad. Sci., Paris*, **28**, 205 (1937); *J. Phys. Radium*, **8**, 397 (1937); *J. Chem. Phys.*, **5**, 837 (1937).
- (25) (a) R. McWeeny, *Mol. Phys.*, **1**, 311 (1953); (b) E. M. Engler and P. Laszlo, *J. Amer. Chem. Soc.*, **93**, 1317 (1971).
- (26) C. W. Haigh and R. B. Mallion, *Org. Magn. Resonance*, **4**, 203 (1972).
- (27) E. Clar, "Polycyclic Hydrocarbons," Vol. 1, Academic Press, New York, N. Y., 1964, p 94.
- (28) J. E. Prue, *J. Chem. Soc.*, 7534 (1965).
- (29) R. L. Scott, *J. Phys. Chem.*, **75**, 3843 (1971).
- (30) G. Scatchard, *Ann. N. Y. Acad. Sci.*, **51**, 660 (1949).
- (31) R. Foster and C. A. Fyfe, *Trans. Faraday Soc.*, **61**, 1626 (1965).
- (32) G. R. Wiley and S. I. Miller, *J. Amer. Chem. Soc.*, **94**, 3287 (1972).
- (33) C. W. Haigh, R. B. Mallion, and E. A. G. Armour, *Mol. Phys.*, **18**, 751 (1970).

COMMUNICATIONS TO THE EDITOR

Singlet-Triplet Separation in Helium

Publication costs assisted by Brigham Young University

Sir: Recently several authors have discussed the energy separation between singlet and triplet excited states of the helium atom.¹ They show that the usual interpretation² is incorrect, since for accurate wave functions the average electronic repulsion is greater in the triplet states than in the corresponding singlet states. Messmer and Birss^{1b} give results for wave functions of the form

$$\Psi = [\phi_{1s}(1)\phi_{2p}(2) \pm \phi_{2p}(1)\phi_{1s}(2)]S^{\mp} \quad (1)$$

where the S^- spin function gives the 2^1P state and the S^+ spin functions give the 2^3P state. They compare two simple functions of type 1 with the accurate calculations of Pekeris.³ Their first pair of functions (Ψ_1 , in which ϕ_{1s} and ϕ_{2p} are Slater-type orbitals) give total energies which are very poor, and the repulsive energy of the triplet is less than that of the singlet. Their second pair of functions (Ψ_{11}) give results that agree with the accurate values given by Pekeris.³

The results for Ψ_1 given by Messmer and Birss are incorrect. Since Slater-type 1s and 2p orbitals are identical with the corresponding hydrogenic orbitals, Ψ_1 is the same pair of functions which Eckart⁴ used in his study of the

excited states of helium. When Eckart's functions are used correctly, they give the results shown in Table I. For comparison, we also give accurate results for 2^1P and 2^3P from Pekeris.³ It is evident that the two-parameter Eckart functions give values for $\langle 1/r_{12} \rangle$ that agree well with the accurate values.

The remarkable accuracy of these simple functions for the 2^1P and 2^3P states encouraged us to make similar calculations for the 2^1S and 2^3S states. We used a 2^3S function of the Eckart form

$$\Psi(2^3S) = [\phi_{1s}(1)\phi_{2s}(2) - \phi_{2s}(1)\phi_{1s}(2)]S^+$$

where

$$\phi_{2s} = N_{2s}e^{-\zeta' r}(A - \zeta' r)$$

$$\phi_{1s} = N_{1s}e^{-\zeta r}$$

and A is chosen to orthogonalize ϕ_{1s} and ϕ_{2s} .

Using the Hylleraas-Undheim theorem,⁵ we wrote the 2^1S function in the form

$$\Psi(2^1S) = [C_1\bar{\phi}_{1s}(1)\bar{\phi}_{1s}(2) + C_2(\phi_{1s}(1)\phi_{2s}(2) + \phi_{2s}(1)\phi_{1s}(2))]S^-$$

where the approximate energy of the 2^1S state is found by solving the second-order secular equation, the higher root

TABLE I: Orbital Exponents in This Work and Expectation Values Compared to Accurate Values in Atomic Units (1 au = 27.21 eV)

State	$\zeta(1s)$ $\zeta(2l)^a$	Expectation value	This work	Accurate value
2^1P	2.003	$\langle H \rangle$	-2.122	-2.124
	0.482	$\langle 1/r_{12} \rangle$	0.243	0.245
2^3P	1.991	$\langle H \rangle$	-2.131	-2.133
	0.545	$\langle 1/r_{12} \rangle$	0.266	0.267
2^1S^b	1.990	$\langle H \rangle$	-2.143	-2.146
	0.529	$\langle 1/r_{12} \rangle$	0.249	0.250
2^3S	2.009	$\langle H \rangle$	-2.172	-2.175
	0.694	$\langle 1/r_{12} \rangle$	0.272	0.268

^a $\zeta(2l)$ means $\zeta(2p)$ for P states and $\zeta(2s)$ for S states. ^b In $\psi(2^1S)$, $C_1 = 0.1207$ and $C_2 = 0.7071$.

being an upper bound for the 2^1S energy. The orbital exponent in $\bar{\phi}_{1s}$ was fixed at 1.6875⁶ and the exponents in ϕ_{1s} and ϕ_{2s} were varied to minimize the 2^1S energy. The results, given in Table I, are in excellent agreement with accurate values given by Kohl.^{1d}

References and Notes

- (1) (a) E. R. Davidson, *J. Chem. Phys.*, **41**, 656 (1964); **42**, 4199 (1965); (b) R. P. Messmer and F. W. Birss, *J. Phys. Chem.*, **73**, 2085 (1969); (c) J. Katriel, *Phys. Rev. A*, **5**, 1990 (1972); (d) D. Kohl, *J. Chem. Phys.*, **56**, 4236 (1972); (e) J. Killingbeck, *Mol. Phys.*, **25**, 455 (1973).
- (2) W. Kauzmann, "Quantum Chemistry," Academic Press, New York, N. Y., 1957, pp 319, 320.
- (3) B. Schiff, H. Lifson, C. L. Pekeris, and P. Rabinowitz, *Phys. Rev.*, **140**, A1104 (1965).
- (4) C. Eckart, *Phys. Rev.*, **36**, 878 (1930).
- (5) E. Hylleraas and B. Undheim, *Z. Phys.*, **65**, 759 (1930).
- (6) H. Eyring, J. Walter, and G. Kimball, "Quantum Chemistry," Wiley, New York, N. Y., 1944, p 106.

Department of Chemistry
Brigham Young University
Provo, Utah 84602

Richard L. Snow*
James L. Bills

Received October 11, 1973; Revised Manuscript Received May 9, 1974

Low-Temperature Studies of Photolyses of Transition-Metal Complexes. The Ferricyanide Ion

Publication costs assisted by Central Michigan University

Sir: At least three major modes of reaction of photoexcited transition-metal complexes can be distinguished: (i) electron ejection arising generally from irradiation within a CTTS absorption band; (ii) electron gain from solvent, arising after a charge-transfer process involving electron movement from the ligand to the metal (CTFL); and (iii) ligand loss, displacement, or rearrangement, arising frequently from d-d excitations, and depending upon differing ligand labilities in the ground and excited states. (In addition, localized absorption by ligands may be important but we are not concerned here with such processes.)

Process i has been studied by pulse photolysis methods for the liquid phase, which reveal the presence of "solvated" electrons and in the solid state, which gives trapped electrons. While ferrocyanide ions ($\text{Fe}(\text{CN})_6^{4-}$) readily lose electrons when exposed to light in the 200–250-nm range,¹ $\text{Fe}(\text{CN})_6^{3-}$ ions are not photoionized in this spectral region.



Figure 1. First derivative esr spectra for uv photolyzed $\text{Fe}(\text{CN})_6^{3-}$ in aqueous methanol at 77 K directly after photolysis showing features assigned to H_2COH (a) and HCO (b) radicals.

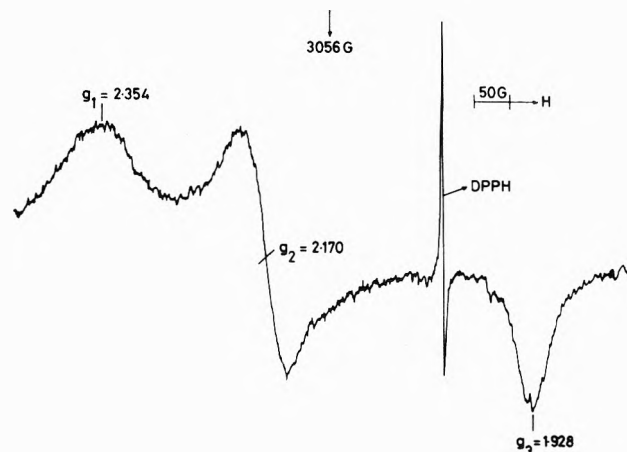
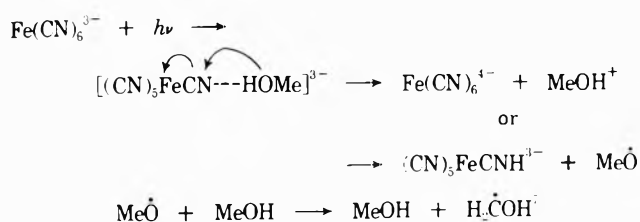


Figure 2. First derivative esr spectra for uv photolyzed $\text{Fe}(\text{CN})_6^{3-}$ in aqueous methanol at 77 K, after slight annealing above this temperature to remove signals from H_2COH and $\cdot\text{HCO}$ radicals, revealing features assigned to $\text{Fe}(\text{CN})_5\text{MeOH}^{2-}$.

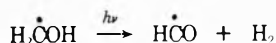
However, processes ii and iii have only been studied extensively in fluid solution, under which conditions the technique of esr spectroscopy is generally of little use. The great advantage of solid-state photolyses is that primary or secondary products are often detected, and subsequent complex processes are prevented.²

In the present work, ferricyanide ions in various solvents and a range of concentrations have been exposed to light from a high-pressure mercury arc (313 and 365 nm) at 77 K, and the products studied by esr spectroscopy. Under these conditions, both d-d and CTFL excitations occur,³ and products may be formed by either or both excitations. For methanolic and aqueous methanolic glasses, the esr spectra contain features that are unambiguously assignable to H_2COH (D_2COD) radicals⁴ and HCO (DCO)⁵ formed from the solvent, and also broad features for a nonaxial Fe^{II} complex in the spin-paired (d^5) configuration (Figures 1 and 2). In the absence of ferricyanide, no signals were detected. Also solutions of ferrocyanides treated similarly gave no solvent radicals.⁶

We suggest that the CH_2OH radicals stem from a CTFL process, the electron-deficient ligand extracting an electron (or possibly a hydrogen atom) from an adjacent solvent molecule during the lifetime of the excited state

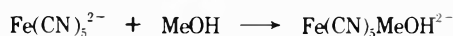
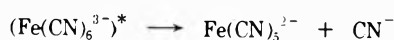


The HCO radicals, whose relative yield increases with time, are known⁵ to be formed by incidental photolysis of the resulting H₂COH radicals



though in this case they could also be formed from Fe(CN)₅MeOH²⁻.

The Fe^{III} species must be formed from the symmetrical parent Fe(CN)₆³⁻ ion by some sort of ligand modification. (The parent ions display no detectable resonance at 77 K because of their high symmetry and efficient spin relaxation.) Possible candidates are Fe(CN)₅³⁻, R-NCFe(CN)₅²⁻ (where R = H or solvent radical), and Fe(CN)₅MeOH²⁻. Clearly, departure from axial symmetry ($g_1 = 2.354$, $g_2 = 2.170$, $g_3 = 1.928$) rules out Fe(CN)₅³⁻, which has probably been detected in γ -irradiated alkali halide lattices containing the Fe(CN)₆⁴⁻ ion.⁸ This species was clearly axial, with $g_{\perp} 2.13$ and $g_{\parallel} 2.000$. It is difficult to see why a species of the type R-NCFe(CN)₅²⁻ should form on photoexcitation, and we are drawn to the conclusion that the nonaxial species is Fe(CN)₅MeOH²⁻. Since we were not able to detect Fe(CN)₅³⁻ radicals, it seems that, if the process is SN1 in type



then the second step must be extremely efficient even at 77 K.

These studies, which are clearly of significance to the study of reaction mechanisms, are being extended to other complexes.

References and Notes

- G. V. Buxton, F. S. Dainton, and J. Kalcinski, *Int. J. Radiat. Phys. Chem.*, **1**, 87 (1969).
- See, for example, U. Klaning and M. C. R. Symons, *J. Chem. Soc.*, 3239 (1959); 977 (1960).
- J. J. Alexander and H. B. Grey, *J. Amer. Chem. Soc.*, **90**, 4260 (1968).
- J. F. Gibson, M. C. R. Symons, and M. G. Townsend, *J. Chem. Soc.*, 269 (1959).
- J. A. Brivati, K. D. J. Root, M. C. R. Symons, and D. J. A. Tinling, *J. Chem. Soc. A*, 1942 (1969).
- K. DeArmond and W. Halper, (*J. Phys. Chem.*, **75**, 3230 (1971)), studied the photolysis of [Rh(phen)₃]³⁺ and related complex cations in glassy ethanolic solutions and detected a poorly resolved "free radical" signal in the $g = 2$ region which was tentatively assigned to a mixture of radicals (CH₃CHOH, CH₃CH₂, CH₃CO, and CH₃). However, their solvent gave the same esr spectrum on photolysis in the absence of the complex ions, and they were clearly studying a double absorption process. Since our reactions do not have the characteristics of a double photon process, there is no direct analogy.
- MeO radicals do not give detectable esr spectra under these conditions, but they are known to attack neighboring solvent molecules most efficiently to give H₂COH radicals.
- M. C. R. Symons and J. G. Wilkinson, *J. Chem. Soc., Dalton Trans.*, 14 (1973).
- On sabbatical leave from Central Michigan University, Mount Pleasant, Mich.

Department of Chemistry
The University
Leicester LE1 7RH, United Kingdom

Martyn C. R. Symons*
Douglas X. West⁹
James G. Wilkinson

Received October 18, 1973; Revised Manuscript Received April 1, 1974

Electron Spin Polarization Effects in a Study of Transient Hydrogen Atoms in Acidic Ices under Electron Irradiation

Publication costs assisted by the Faculty of Engineering,
University of Tokyo

Sir: The phenomenon of the chemically induced dynamic electron polarization (CIDEP) has recently attracted much attention,¹ since it presumably comes from some elementary process of the radical reaction. Its mechanism, however, is still far from complete understanding because of the scarcity of the experimental results. The phenomenon of CIDEP on hydrogen atoms (H atoms) in acidic aqueous solution was investigated by Fessenden, *et al.*,² and by Smaller, *et al.*³ As the phenomenon is considered to be sensitive to variation of the time scale of the events, measuring in different phases and at various temperatures seems helpful for its elucidation. It is known that H atoms are stably trapped at -196° in γ -irradiated acidic ices, and that they disappear rapidly above -165°. We have measured esr spectra of H atoms formed in acidic ices in the temperature range from -160 to -50°, and have observed the CIDEP phenomenon of H atoms in the higher temperature region (see below) together with the motional narrowing of their line width. The measurements were carried out during continuous electron irradiation from an accelerator.⁵ Here a preliminary account of the experimental results is given, which revealed rather different aspects of the CIDEP phenomenon of H atoms.

Solutions of sulfuric acid and hydrochloric acid were used. Since this seems to be the first observation of narrowing of H atom signals, the change of spectra with temperature is first described, taking 0.5 M sulfuric acid solution as an example. At -160°, the spectrum of transient H atoms was observed. It had the same characteristics as the so-called trapped H atoms at -196°. On elevating the temperature, the signals become less intense due to the increase in the detrapping rate. The narrowing of the line width begins at about -130°, where the signal intensities are extremely low. Above -110°, there appears an anomaly which is characteristic of the CIDEP phenomenon; the low-field line (LF line) is now in emission and the high-field line (HF line) in absorption. The apparent signal intensities in the derivative representation increase toward higher temperatures, with the line width showing further narrowing. With constant dose rate the HF line shows a minimum around -130°, while the LF line disappears around -130° and at higher temperature reappears as the emission line. Approximate line width at maximum slope is 3.8 G at -155°, 3.3 G at -139°, 1.6 G at -121°, 0.5 G at -96°, and 0.4 G at -74°. There is no phase transition in a usual hexagonal ice. Since the narrowing of the proton nmr line width begins above -60°, the narrowing of the esr line width observed here should be ascribed not to the tumbling motion of the water molecules surrounding the trapped H atoms, but to the translational diffusion of H atoms. This almost free diffusion of H atoms is considered to be a necessary condition for the observation of the CIDEP phenomenon.

It must be mentioned here that in the higher temperature region, namely, above -130°, the system may well be regarded to be in the steady state, since the accumulation of other radicals is very small.⁷ One important difference from CIDEP in the liquid phase was found in the dose rate dependence of the signal intensity in the higher tem-

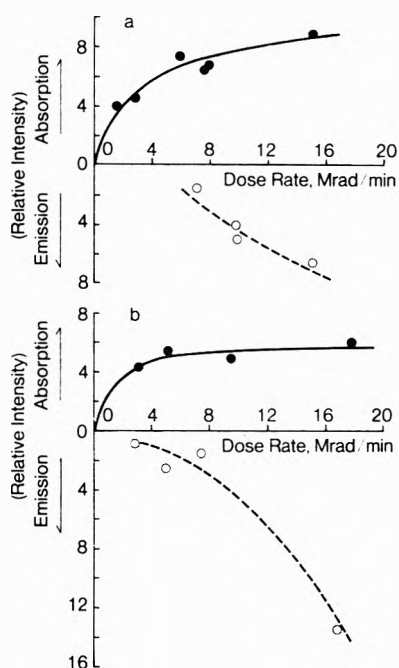


Figure 1. Dose rate dependence of H atom signals in (a) 0.5 M H_2SO_4 solution at -77° , (b) 1 M HCl solution at -78° : ●, high-field line; ○, low-field line.

perature region (Figure 1). Neither the HF line, nor the LF line is proportional to the dose rate in contrast to the observation by Fessenden, *et al.*² Still more important is the difference in dependence of the LF and HF line intensity upon the change of dose rate. In liquid-phase experiments, both lines are reported always to appear in about the same intensity.^{2,3} Increasing the dose rate results in a decrease of the life time of H atoms due to the increase of their concentration. Thus, the weakness of the LF line relative to the HF line at low dose rates is attributable to the relaxation process that effects significantly when the life time is long. On the other hand, the difference at the higher dose rate, or, more explicitly, the fact that the LF line far exceeds the HF line in the case of 1 M hydrochloric acid solution at high dose rates (Figure 1b) has an important implication to the theory of the phenomenon. This cannot be ascribed to a difference between the reaction schemes in the solid and liquid state, and must be due to the polarization process itself. Interpreted from the standpoint of the radical pair theory,¹ this phenomenon cannot be explained only by the mixing of singlet S and triplet T_0 , since it predicts equal polarization for both lines. As was proposed by Atkins, *et al.*,⁸ in the quite different case with radicals that have excited triplet precursors, the mechanism of mixing of triplet T_{-1} with S must be contributing at least to a comparable order, though it is difficult to explain at the present stage why the latter mechanism should be emphasized in the present experiment.

Further experiments and analysis are necessary to clarify the polarization mechanism, and we think this system is a good example for such study.

References and Notes

- (1) See for review P. W. Atkins and K. A. Mclauchlan in "Chemically Induced Magnetic Polarization," A. R. Lopley and G. L. Closs, Ed., Wiley, New York, N. Y., 1973, p 42.
- (2) (a) P. Neta, R. W. Fessenden, and R. H. Schuler, *J. Phys. Chem.*, **75**, 1654 (1971); (b) N. C. Verma and R. W. Fessenden, *J. Chem. Phys.*, **58**, 2501 (1973).

- (3) B. Smaller, E. C. Avery, and J. R. Remko, *J. Chem. Phys.*, **55**, 2414 (1971).
- (4) See for review, L. Kevan in "Radiation Chemistry of Aqueous Systems," G. Stein, Ed., Weizman Science Press of Israel, Jerusalem, 1968, p 21.
- (5) For the experimental setup see, H. Shiraishi, H. Kadoi, K. Hasegawa, Y. Tabata, and K. Oshima, *Bull. Chem. Soc. Jap.*, **47**, 1400 (1974).
- (6) K. Kume, *J. Phys. Soc. Jap.*, **15**, 1493 (1960).
- (7) At the higher temperature, OH and SO_4^- radicals which accumulate at -196° decay so rapidly that they give hardly any spectra. There remain some unknown species whose G value is very small. The situation is similar for HCl solution. In fact, the intensity of H atom signal changed very little during the course of irradiation.
- (8) P. W. Atkins, R. C. Gurd, K. A. Mclauchlan, and A. F. Simpson, *Chem. Phys. Lett.*, **8**, 55 (1971).
- (9) Department of Polymer Technology, The Royal Institute of Technology, Stockholm, Sweden, on leave from the University of Tokyo.
- (10) Address correspondence to the Nuclear Research Laboratory, Faculty of Engineering, University of Tokyo 7-3-1, Hongo, Bunkyo-ku, Tokyo, Japan.

Department of Nuclear Engineering
University of Tokyo
Tokyo, Japan

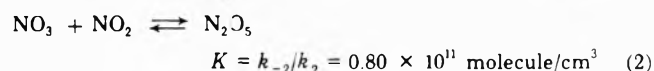
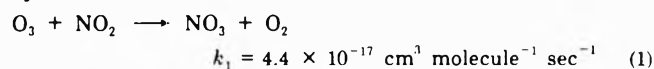
Hirotsugu Shiraishi⁹
Hajime Kadoi
Yosuke Katsumura
Yoneho Tabata*¹⁰
Keichi Oshima

Received October 29, 1973; Revised Manuscript Received April 29, 1974

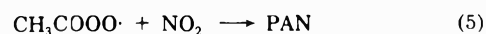
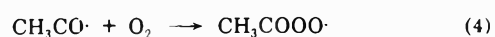
Reaction of the Nitrate Radical with Acetaldehyde and Propylene

Publication costs assisted by the Ford Motor Company

Sir: Acetaldehyde is known to react rapidly¹ with a mixture of O_3 and NO_2 but rather slowly² with O_3 or NO_2 alone. N_2O_5 and NO_3 are produced in the O_3 - NO_2 system by the reactions^{3,4}



It has also been reported⁵ that a mixture of N_2O_5 and CH_3CHO gives a high yield of peroxyacetylnitrate (PAN). Thus either N_2O_5 or NO_3 is reacting with acetaldehyde. Stephens¹ has observed that the PAN yield in the $\text{O}_3 + \text{NO}_2 + \text{CH}_3\text{CHO}$ system falls off sharply when $[\text{NO}_2]/[\text{O}_3] > 2$. Since reactions 1 and 2 require a stoichiometry of two molecules NO_2 per molecule of O_3 , excess NO_2 reduces the NO_3 concentration by shifting reaction 2 toward N_2O_5 . Hanst⁶ has analyzed these data and calculated the NO_3 concentration using reactions 1 and 2. From the linear relation between PAN yields and NO_3 concentrations, he concludes NO_3 is involved in PAN formation. As suggested by various authors,⁷ a plausible mechanism for PAN formation is given by



In view of the potential role of these reactions in photochemical smog formation, the kinetics and mechanism of the $\text{N}_2\text{O}_5 + \text{CH}_3\text{CHO}$ system have been studied in some detail. Since the reaction of propylene with NO_2 - O_3 mixtures also yields PAN as a product, the N_2O_5 - C_3H_6 system has also been investigated.

The concentrations of reactants and products were determined using a 40-m path length infrared cell. A de-

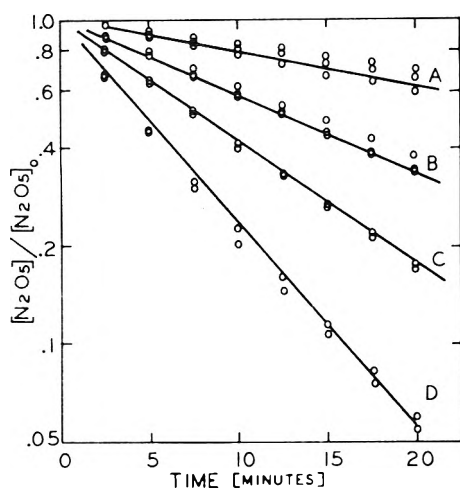


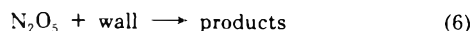
Figure 1. Time/concentration plot of N_2O_5 as a function of CH_3CHO and NO_2 . Solid lines are calculated, points are experimental data $[N_2O_5]_0 = 3.1$ mTorr: curve A, N_2O_5 alone; curve B, $[CH_3CHO]_0 = 28$ mTorr, $[NO_2]_0 = 4.6$ mTorr; curve C, $[CH_3CHO]_0 = 28$ mTorr, $[NO_2]_0 = 2.3$ mTorr; curve D, $[CH_3CHO]_0 = 14$ mTorr, $[NO_2]_0 = 0.57$ mTorr (calculated, see text).

tailed description of this apparatus has been given previously.⁸ PAN was analyzed both by infrared absorption and by electron capture gas chromatography. Most experiments were carried out using 400 Torr of O_2 and 350 Torr of argon as diluent, at 300°K.

Kinetic data were obtained by measuring the rate of N_2O_5 decay in the presence of various concentrations of CH_3CHO and NO_2 . The results are shown in Figure 1. The points are experimental data, while the lines are calculated based on reactions 2-6 as explained later. Curve D in this figure shows that the decay of N_2O_5 increases significantly over the background rate (curve A) when acetaldehyde is added. The first-order decay of N_2O_5 was found to be proportional to CH_3CHO concentration. The addition of NO_2 reduces the rate of reaction as shown by curves B and C. The addition of ozone (not shown) increases the decay rate of N_2O_5 . This is consistent with the occurrence of reaction 3 since the addition of O_3 increases the NO_3 concentration. Several experiments carried out at a low partial pressure of oxygen (<1 Torr) resulted in non-first-order decay of N_2O_5 . A change in mechanism is expected under these conditions since the other reactions can compete with reaction 4.

During the course of the reaction, infrared absorptions due to PAN and HNO_3 were observed. Using the published⁹ extinction coefficient for PAN at 1160 cm^{-1} , the yield of PAN per N_2O_5 consumed was found to be greater than 0.8. The HNO_3 yield was difficult to measure accurately because of rapid absorption on vessel walls. However, its yield was at least 50% of the amount of N_2O_5 reacted. Formation of some NO_2 was observed. For example, the data in curve D showed 0.5 ± 0.15 mTorr of NO_2 at the end of the run. A part of this NO_2 was impurity present in the N_2O_5 sample.

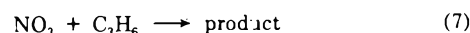
The experimental data described above can be used to derive a rate constant for reaction 3 by a numerical integration of reactions 2-6



where k_6 is the heterogeneous N_2O_5 background decay and was typically $5 \times 10^{-4} \text{ sec}^{-1}$. The rate of k_3 used in

this calculation was adjusted until the calculated N_2O_5 decay matched that observed experimentally. The exact values used for k_4 and k_5 do not affect the calculated N_2O_5 decay since no competing paths are allowed for reactions 4 and 5. Since there was some net formation of NO_2 , not all of the $CH_3CO\cdot$ reacts with NO_2 to form PAN. As mentioned earlier, small concentrations of NO_2 present as an impurity in N_2O_5 samples and also as a product have a pronounced effect on the reaction rate because of a shift in the NO_3 - N_2O_5 equilibrium. To obtain more reliable data, most experiments were run by adding sufficiently high concentrations of NO_2 to the reaction system to shift this equilibrium to a less sensitive region. As shown in Figure 1, all of the data with added NO_2 can be fitted by the calculated curves. The experimental data together with this mechanism lead to $k_3 = 1.2 \times 10^{-15} \text{ cm}^3 \text{ molecule}^{-1} \text{ sec}^{-1}$. The estimated uncertainty in the experimentally determined values of $d \ln [N_2O_5]/dt$ is $\pm 25\%$. The accuracy of the rate constant k_3 is also linearly dependent on the value of k_{-2}/k_2 .

In the N_2O_5 - C_3H_6 system, the decay of N_2O_5 was similarly monitored as a function of C_3H_6 and NO_2 concentration. In this system, NO_2 was a major product. Another product was observed in the region of 1670 cm^{-1} which was tentatively identified as a nitrite. PAN was not observed when N_2O_5 was used as a source of NO_3 . Thus the PAN observed in the reaction of C_3H_6 with NO_2 - O_3 mixtures probably results from the ozonolysis of propylene which produces acetaldehyde. The acetaldehyde thus formed can undergo subsequent reaction with NO_3 to form PAN. The kinetic behavior of N_2O_5 in propylene was determined at several initial NO_2 concentrations ranging from 0.5 to 10 mTorr. The effect of the added NO_2 on the N_2O_5 decay rates was consistent with the mechanism 2, 6, and 7



The calculated N_2O_5 decays gave the best fit to the data when a value of $3 \times 10^{-15} \text{ cm}^3 \text{ molecule}^{-1} \text{ sec}^{-1}$ was used for k_7 . The uncertainty in k_7 is similar to that discussed for k_3 .

In summary, NO_3 has been shown to undergo reaction with CH_3CHO and C_3H_6 at a rate much faster than the corresponding ozonolysis reactions (3.4×10^{-20} and 1.2×10^{-17} , respectively).^{2,10} Further work to determine the kinetics and mechanism of the reactions of NO_3 with other organic compounds and the implication to photochemical smog are underway.

References and Notes

- (1) E. R. Stephens, *Advan. Environ. Sci.*, **1**, 119 (1969).
- (2) D. H. Stedman and H. Niki, *Environ. Lett.*, **4**, 303 (1973).
- (3) E. D. Morris, Jr., C. H. Wu, and H. Niki, *J. Phys. Chem.*, **77**, 2507 (1973).
- (4) P. A. Leighton, "Photochemistry of Air Pollution," Academic Press, New York, N. Y., 1961, p 188.
- (5) C. S. Tuesday in "Chemical Reactions of the Lower and Upper Atmosphere," Interscience, New York, N. Y., 1961, p 15.
- (6) P. L. Hanst, *J. Air Pollut. Contr. Ass.*, **21**, 269 (1971).
- (7) See, for example, R. Louw, J. van Ham, and H. Nieboer, *J. Air Pollut. Contr. Ass.*, **23**, 716 (1973).
- (8) E. D. Morris, Jr., and H. Niki, *J. Phys. Chem.*, **77**, 1929 (1973).
- (9) E. R. Stephens and M. A. Price, *J. Chem. Educ.*, **50**, 351 (1973).
- (10) D. H. Stedman, C. H. Wu, and H. Niki, *J. Phys. Chem.*, **77**, 2511 (1973).

Scientific Research Staff
Ford Motor Company
Dearborn, Michigan 48121

E. D. Morris, Jr.
H. Niki*

Received February 4, 1974

INVALUABLE INFORMATIVE IN DEMAND

these internationally
respected, basic
research journals of
The American
Chemical Society

The Journal of Physical Chemistry

*ACS Members: U.S. \$20.00 Canada, PUAS \$25.00 Other Nations \$26.00	Nonmembers: U.S. \$60.00 Canada, PUAS \$65.00 Other Nations \$66.00
---	---

The Journal of Chemical and Engineering Data

*ACS Members: U.S. \$15.00 Canada, PUAS \$18.00 Other Nations \$18.50	Nonmembers: U.S. \$45.00 Canada, PUAS \$48.00 Other Nations \$48.50
---	---

Biochemistry

*ACS Members: U.S. \$20.00 Canada, PUAS \$25.00 Other Nations \$26.00	Nonmembers: U.S. \$60.00 Canada, PUAS \$65.00 Other Nations \$66.00
---	---

Inorganic Chemistry

*ACS Members: U.S. \$18.00 Canada, PUAS \$22.00 Other Nations \$23.00	Nonmembers: U.S. \$54.00 Canada, PUAS \$58.00 Other Nations \$59.00
---	---

The Journal of the American Chemical Society

*ACS Members: U.S. \$22.00 Canada, PUAS \$27.00 Other Nations \$28.00	Nonmembers: U.S. \$66.00 Canada, PUAS \$71.00 Other Nations \$72.00
---	---

The Journal of Agricultural and Food Chemistry

*ACS Members: U.S. \$10.00 Canada, PUAS \$13.50 Other Nations \$14.00	Nonmembers: U.S. \$30.00 Canada, PUAS \$33.50 Other Nations \$34.00
---	---

Macromolecules

*ACS Members: U.S. \$12.00 Canada, PUAS \$15.50 Other Nations \$16.00	Nonmembers: U.S. \$36.00 Canada, PUAS \$39.50 Other Nations \$40.00
---	---

The Journal of Organic Chemistry

*ACS Members: U.S. \$20.00 Canada, PUAS \$25.00 Other Nations \$26.00	Nonmembers: U.S. \$60.00 Canada, PUAS \$65.00 Other Nations \$66.00
---	---

The Journal of Medicinal Chemistry

*ACS Members: U.S. \$15.00 Canada, PUAS \$19.00 Other Nations \$20.00	Nonmembers: U.S. \$45.00 Canada, PUAS \$49.00 Other Nations \$50.00
---	---

Analytical Chemistry

*ACS Members: U.S. \$5.00 Canada, PUAS \$9.00 Other Nations \$10.00	Nonmembers: U.S. \$7.00 Canada, \$11.00 PUAS \$19.00 Other Nations \$20.00
---	---

American Chemical Society

1155 Sixteenth Street, N.W. Washington, D.C. 20036

name _____ position _____

address _____

city _____ state/country _____ zip _____

your company _____ nature of company's business _____

*NOTE Subscriptions at ACS member rates are for personal use only

I am an ACS member I am not an ACS member Bill me for \$ _____

Payment enclosed (payable to American Chemical Society) in the amount of

\$ _____ Payment must be made in U.S. currency by international

money order, UNESCO coupons, or U.S. bank draft, or order through your book dealer

Please enter a one year subscription for the
following journals:

- The Journal of the American Chemical Society
- The Journal of Organic Chemistry
- The Journal of Physical Chemistry
- Biochemistry
- The Journal of Agricultural and Food Chemistry
- The Journal of Medicinal Chemistry
- The Journal of Chemical and Engineering Data
- Inorganic Chemistry
- Macromolecules
- Analytical Chemistry

**AMERICAN
CHEMICAL
SOCIETY
PUBLICATIONS
IN
MICROFORM**



- Well over a million pages of chemistry's premier publications
- Back volumes and current subscriptions available in 35- or 16-mm microfilm and various cartridges
- Unlimited copying privileges built into microfilm subscriptions
- Current availability of nonprint materials in microfiche
- For full details of the ACS microform program, write or call:

Mr. Kenneth Phillips
Special Issues Sales
American Chemical Society
1155 16th St., N.W.
Washington, D. C. 20036
Tel: (202) 872-4364

and ask for your free copy of the informative booklet on the "Information Implosion!"

